University of Denver

Digital Commons @ DU

Electronic Theses and Dissertations

Graduate Studies

1-1-2017

Improved Characterization and Analysis Strategies for UV-LIF Bioaerosol Instrumentation: Lab and Field Application

Nicole Justine Savage
University of Denver

Recommended Citation

Improved Characterization and Analysis Strategies for UV-LIF Bioaerosol Instrumentation: Lab and Field Application

Abstract

Atmospheric particles of biological origin, also referred to as bioaerosols or primary biological aerosol particles (PBAP), are important to various human health and environmental systems. There has been a recent steep increase in the frequency of published studies utilizing commercial instrumentation based on ultraviolet laser/light-induced fluorescence (UV-LIF), such as the WIBS (wideband integrated bioaerosol sensor), for bioaerosol detection both outdoors and in the built environment. Significant work over several decades supported the development of these technologies, but efforts to systematically characterize the operation of new commercial sensors has remained lacking. Specifically, there are gaps in the understanding of how different classes of biological and non-biological particles can influence the detection ability of LIF-instrumentation.

In Chapter 2 we present the most comprehensive laboratory study of UV-LIF instrumentation ever reported, using 69 types of aerosol materials, including a representative list of pollen, fungal spores, and bacteria as well as the most important groups of non-biological materials reported to exhibit interfering fluorescent properties. Broad separation can be seen between biological and non-biological particles using the 5 data parameters delivered from the instrument. We highlight the importance that particle size plays on observed fluorescence properties and thus in the classification of particles. We also discuss several particle analysis strategies, including the use of different fluorescence thresholds. We conclude that raising the standard fluorescence baseline threshold can significantly reduce interference from mineral dust and other non-biological aerosols while contributing little to the reduction in signal from biological particles.

Preliminary work on a follow-up study (Chapter 3) utilized clustering techniques available in standard analysis software to investigate a method for improved discrimination between particle materials. This laboratory study focused on the separation of biological and interfering materials using an unsupervised method known as hierarchical agglomerative clustering (HAC). Previous studies have primarily focused on the separation (1) between standard particles types and (2) between particle types within ambient data sets. Little work has been done to understand the clustering process applied to controlled laboratory data or looking at the grouping efficiency of data preparation scenarios for biological and non-biological materials. Clustering results were optimized by inputting data in logarithmically-spaced bins and fluorescence intensity was not normalized to particle size, as had been done in previously published work. The clustering algorithm (Trial 1) successfully separated particles of *Aspergillus niger* (fungal spores) and diesel soot, which is a known interfering material due to its similar fluorescence characteristics as biological particles. *Aspergillus niger* and California sand, which was used as a surrogate for commonly observed, weakly fluorescent soil dust, showed relatively poor separation, which may have occurred as a result of the significant number of nonfluorescent particles involved in the analysis. The information gained from this study can help train data sets for supervised clustering methods with the hopes of better discrimination between particle materials.

Both studies were designed to propose analysis strategies that may be useful to the broader community of UV-LIF instrumentation users in order to promote deeper discussions about how best to continue improving UV-LIF instrumentation and analysis strategies.

Document Type
Thesis

Degree Name
M.S.

Department
Chemistry and Biochemistry

First Advisor
John A. Huffman, Ph.D.

Second Advisor
Bryan J. Cowen

Third Advisor
Brian J. Majestic

Keywords
Bioaerosol, Characterization, Fluorescence Threshold, Fluorescent Particles, UV-LIF, ultraviolet light induced fluorescence, WIBS, Wideband integrated bioaerosol sensor

Subject Categories
Atmospheric Sciences | Chemistry | Environmental Sciences

Publication Statement

Improved Characterization and Analysis Strategies for UV-LIF Bioaerosol

Instrumentation: Lab and Field Application

_____

A Thesis

Presented to

the Faculty of Natural Sciences and Mathematics

University of Denver

_____

In Partial Fulfillment

of the Requirements for the Degree

Master of Science

_____

By

Nicole J. Savage

August 2017

Advisor: J. Alex Huffman

Author: Nicole J. Savage
Title: Improved Characterization and Analysis Strategies for UV-LIF Bioaerosol
Instrumentation: Lab and Field Application
Advisor: J. Alex Huffman
Degree Date: August 2017

Abstract

Atmospheric particles of biological origin, also referred to as bioaerosols or primary

biological aerosol particles (PBAP), are important to various human health and

environmental systems. There has been a recent steep increase in the frequency of

published studies utilizing commercial instrumentation based on ultraviolet laser/light-

induced fluorescence (UV-LIF), such as the WIBS (wideband integrated bioaerosol

sensor), for bioaerosol detection both outdoors and in the built environment. Significant

work over several decades supported the development of these technologies, but efforts

to systematically characterize the operation of new commercial sensors has remained

lacking. Specifically, there are gaps in the understanding of how different classes of

biological and non-biological particles can influence the detection ability of LIF-

instrumentation.

In Chapter 2 we present the most comprehensive laboratory study of UV-LIF

instrumentation ever reported, using 69 types of aerosol materials, including a

representative list of pollen, fungal spores, and bacteria as well as the most important

groups of non-biological materials reported to exhibit interfering fluorescent properties.

Broad separation can be seen between biological and non-biological particles using the 5

data parameters delivered from the instrument. We highlight the importance that particle

size plays on observed fluorescence properties and thus in the classification of particles.

We also discuss several particle analysis strategies, including the use of different fluorescence thresholds. We conclude that raising the standard fluorescence baseline threshold can significantly reduce interference from mineral dust and other non-biological aerosols while contributing little to the reduction in signal from biological particles.

Preliminary work on a follow-up study (Chapter 3) utilized clustering techniques available in standard analysis software to investigate a method for improved discrimination between particle materials. This laboratory study focused on the separation of biological and interfering materials using an unsupervised method known as hierarchical agglomerative clustering (HAC). Previous studies have primarily focused on the separation (1) between standard particles types and (2) between particle types within ambient data sets. Little work has been done to understand the clustering process applied to controlled laboratory data or looking at the grouping efficiency of data preparation scenarios for biological and non-biological materials. Clustering results were optimized by inputting data in logarithmically-spaced bins and fluorescence intensity was not normalized to particle size, as had been done in previously published work. The clustering algorithm (Trial 1) successfully separated particles of *Aspergillus niger* (fungal spores) and diesel soot, which is a known interfering material due to its similar fluorescence characteristics as biological particles. *Aspergillus niger* and California sand, which was used as a surrogate for commonly observed, weakly fluorescent soil dust, showed relatively poor separation, which may have occurred as a result of the significant

number of nonfluorescent particles involved in the analysis. The information gained from this study can help train data sets for supervised clustering methods with the hopes of better discrimination between particle materials.

Both studies were designed to propose analysis strategies that may be useful to the broader community of UV-LIF instrumentation users in order to promote deeper discussions about how best to continue improving UV-LIF instrumentation and analysis strategies.

Acknowledgements

My most sincere thanks go to my research advisor and mentor, Dr. Alex Huffman. I thank him for introducing me to the wonders of atmospheric research with immense enthusiasm. His endless support and faith in my work has helped shape who I am today. I appreciate the constructive criticism and the motivation he has given me to keep me focused on my educational and personal goals. I would also like to acknowledge the Huffman group for their helpful discussions and collaboration. I am sincerely grateful for collaborators at the Max Planck Institute for Chemistry in Mainz, Germany, and the Cyprus Institute for the travel and research opportunities they have provided me. Tobias Könemann and Christopher Pöhlker are gratefully acknowledged for their helpful discussions and continuous support. I am especially thankful to the Department of Chemistry and Biochemistry at the University of Denver for providing me with financial support from the Phillipson Graduate Fellowship.

On a personal note, I would like to thank the Quattrini family for their love and guidance throughout my high school, undergraduate and graduate careers. There are no words to convey the gratitude I have for this family for their acceptance and infinite support they have given me. My deepest appreciation and respect goes to Jake Quattrini for showing me unconditional love and support for over 10 years.

Table of Contents

List of Tables

List of Figures

Appendix B

Chapter One: Introduction

1.1 Overview: What are Primary Biological Particles (PBAPs)

Atmospheric aerosols are defined as solid and/or liquid particles suspended in the air. Primary biological aerosol particles (PBAPs) or bioaerosols, are a subset of atmospheric aerosols and can be defined as the suspension of biological particulate matter released from the biosphere into the atmosphere. There are a number of biological particle types, including whole microorganisms (e.g. mold spores, bacteria, pollen) and their fragments, biopolymers, and reproductive entities (Després et al., 2012). Bioaerosols make up a substantial fraction of atmospheric aerosols. Coarse biological particles with a diameter of 1 µm or larger can comprise up to 30% by mass of aerosol in urban and rural environments and up to 80% in pristine environments (Després et al., 2012; Frohlich-Nowoisky et al., 2016; Huffman et al., 2013; Huffman et al., 2010; Matthias-Maser et al., 2000a; Matthias-Maser et al., 2000b; Schumacher et al., 2013). Bioaerosols can represent viable, non-viable, pathogenic, and allergenic particles. They are ubiquitous in the atmosphere, and many species can cause significant human and environmental health effects.

1.1.1 Physical Characteristics of PBAPs

Biological particles can range in size from several nanometers to hundreds of micrometers (Cox and Wathes, 1995; Jaenicke, 2005; Pöschl, 2005). They have different mechanisms of transport, deposition and light scattering properties, which are all important factors for their effects on health and detection. Other important factors for the characterization of biological particles include shape and density. The shape of bioaerosols can be defined as varying degrees of spherical or elongated shapes. The density of a biological particle is typically $1.0 – 1.5$ g/cm^3, however biological particles are often present in the air mixed with matter of different densities (Löndahl, 2014). Three common categories of bioaerosols include pollen, fungal spores, and bacteria, which will be discussed in more detail. These classes of biological particles were chosen for the studies presented, because they are typically 0.5 µm and greater in diameter, surpassing the lower particle size limit of instrumentation used.

1.1.2 Pollen

Pollen are microscopic grains discharged from the stamen of a plant and represent common aeroallergens. They are among the largest biological particle in physical size, ranging from $10 – 100$ µm in diameter (Löndahl, 2014; Miguel et al., 2006; Taylor et al., 2002). They are not only present as whole structures but as fragmented pieces as well. Pollen grains typically have a hard shell that prevents the disruption of genetic material due to environmental stress. The shell can rupture at high humidity into smaller fragments, typically in the range of 0.1 µm – 5 µm (Taylor et al., 2002). The morphology

characteristics can vary for different species. The concentration of pollen in the air

follows a seasonal cycle and the dispersal and transport of pollen is greatly dependent on

meteorological conditions (Harrison et al., 2005; Löndahl, 2014; Manninen et al., 2014).

Kuparinen et al. (2009) showed wind driven dispersal of pollen is promoted by the

increase of air temperature. Characteristic magnitudes of number concentrations in air

over vegetated regions are ~10-10^3 grains m^{-3} (Fröhlich -Nowoisky et al., 2009; Sofiev et

al., 2006)

1.1.3 Fungal Spores

Fungi are among the most common microorganisms worldwide, and they play the key

role of decomposers in most ecosystems. They can be allergenic to humans and infectious

to both human and environmental health. Fungal spores can be released into the

atmosphere by both passive and wet discharge mechanisms. Passive processes include

wind or external forces and wet spore ejection is due to the increase in surface tension or

osmotic pressure, highly dependent on relative humidity (Gosselin et al., 2016; Löndahl,

2014). Spores can range in size from ~1- 50 μm in diameter, but are typically in the 2-10

μm range (Elbert et al., 2007; Fröhlich -Nowoisky et al., 2009; Huffman et al., 2010;

Wang et al., 2008). Characteristic number concentrations for fungal spores over vegetated

regions range from 10^3-10^4 spores m^{-3} (Elbert et al., 2007; Fröhlich -Nowoisky et al.,

2009).

3

1.1.4 Bacteria

Bacteria are unicellular, prokaryotic, and are present in almost all environments on Earth and in the air. This type of particle represent a smaller subset of bioaerosols where individual bacteria are typically ~ 1 μm in size. Bacteria can often agglomerate or attach to the surfaces of other particles, however, therefore increasing the size of the particle in which they are associated (Bovallius et al., 1978; Lighthart, 1997; Shaffer and Lighthart, 1997; Tong and Lighthart, 1999; Wang et al., 2007). Some bacteria can form endospores, which are more dormant and resistant to environmental stresses than vegetative cells. Endospore formation is initiated by nutrient deprivation and allows the bacterium to produce a dormant, highly resistant cell. They can be highly resistant to heat, UV irradiation, and chemical damage (Nicholson et al., 2000). Characteristic number concentrations over vegetated areas are ~10^4 bacteria m^{-3} (Bauer et al., 2002; Burrows et al., 2009).

1.2 Why Do We Care About PBAPs?

1.2.1 Impact on Atmospheric Processes

The presence of bioaerosols in our atmosphere and the roles they play have been known for many decades (Andreae and Crutzen, 1997; Després et al., 2012; Jaenicke, 2005; Jaenicke and Matthais, 1988; MatthiasMaser and Jaenicke, 1995; Pöschl, 2005; Schnell and Vali, 1972). Bioaerosols have been proposed to influence several important environmental and Earth systems, especially including the formation and evolution of certain types of clouds.

Clouds contribute to the Earth's energy budget by adding both positive and negative effects to global radiative forcing estimates (Herring and Simmon, 2002). At any given time, clouds cover approximately 60% of the earth, but can exist in many different forms and at various magnitudes of lifetime (Herring and Simmon, 2002). They play a major role in both global and regional climate (i.e. influcing how much sunlight reaches the surface of the earth, how much heat escapes the atmosphere, the amount of light that is reflected back into space) and in the process of precipitation formation and in the hydrological cycle. Because clouds play a significant role in the Earth's energy balance, cloud formation is a crucial factor to understand. The Intergovernmental Panel on Climate Change (IPCC) has stated that cloud effects contribute the largest uncertainty to radiative forcing and climate change (Field et al., 2014).

When water vapor interacts with an aerosol particle, condensation can occur on the surface of the particle resulting in the formation of liquid cloud droplets. Depending on the surface properties of an aerosol particle, they can serve as nuclei for cloud droplets (giant cloud condensation nuclei; GCCN) and ice crystals (ice nuclei; IN) in the atmosphere, and thus have an effect on cloud formation and precipitation (Andreae and Rosenfeld, 2008; Pöschl et al., 2010). Depending on the surface properties of biological aerosol particles, they can serve as nuclei for cloud droplets and ice crystals in the atmosphere (Andreae and Rosenfeld, 2008; Pöschl et al., 2010). Figure 1.1 provides an overview for the roles bioaerosols play in both the biosphere and atmosphere.
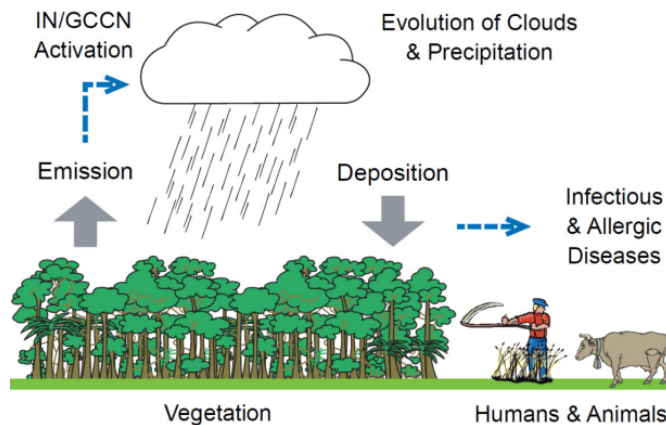
<u>Figure 1.1.</u> Schematic outlining the roles bioaerosols play in both the biosphere and atmosphere (Huffman et al., 2010).

Homogeneous ice nucleation can occur at temperatures below -37 °C, however biological particles are capable of lowering the energy barrier of ice nucleation, allowing adsorbed water vapor to freeze at temperatures as high as -2°C (Mason et al., 2015a). Types of bioaerosols, such as certain bacteria, more efficiently nucleate ice growth and may heavily influence precipitation patterns and hydrological cycles downwind of plants harboring ice-active bioaerosols (Morris et al., 2014). Removal of biological particles from the atmosphere happens via wet deposition (precipitation) or dry deposition (agglomeration/sedimentation). Dry deposition is less interesting on a global scale, but important in regards to local air quality and human health. Depending on bioaerosol properties and meteorological conditions, residence times can range from hours to weeks.

After the deposition of PBAP, biological particles can then interact with aquatic or terrestrial ecosystems, thus promoting PBAP growth and reproduction, eventually

resulting in re-emission. Terrestrial environments are the main source of biogenic

particles. Bioaerosol formation and emission can be influenced by climate and habitat

conditions, for example agriculture and construction. Compared to terrestrial emission of

bioaerosols, less is known about aquatic sources of biological particles. Oceans cover

approximately 70% of the earth's surface, however bioaerosol diversity over oceans is

heavily influenced by terrestrial sources as well as long transport (Frohlich-Nowoisky et

al., 2016; Wilson et al., 2015).

1.2.2 Impact on Human and Environmental Health

With every human breathe is the inevitable intake of particulate matter, with a

fraction of particles that are inhaled being biological in nature. Bioaerosols have the

potential to be pathogenic, allergenic, infectious, or toxic in both viable, non-viable,

whole and fragmented forms. They have been shown to travel long distances and

therefore have the potential to negatively affect ecosystems and human health (Echigo et

al., 2005; Griffin, 2007; Hervas et al., 2009; Ichinose et al., 2008; Kellogg and Griffin,

2006; Yukimura et al., 2009). Microorganisms can be transported via dust storms and

play a role in the biogeographical distribution, shifting concentrations of some species

and changing the biodiversity of environments (Griffin, 2007). Anthropogenic activities,

including, but not limited to composting can also lead to the emission of biological

particles. Within the past 5 years, for example, *Saccharopolyspora rectivirgula*, a

bacterial species known to cause farmer's lung disease when aerosolized, has been shown

to be prevalent at composting facilities, detected at 85% of the 31 different composting

facilities studied (Schafer et al., 2013). Due to their ubiquitous existence in nature, the

presence of bioaerosols is unavoidable in most enclosed environments and can originate

from indoor or outdoor sources (Jo and Seo, 2005; Jones and Harrison, 2004; Ren et al.,

1999).

1.3 Techniques for PBAP Detection

1.3.1 Traditional Techniques of PBAP Analysis

Until recently, most airborne sampling of bioaerosols utilized offline techniques such

as microscopy or cultivation-based methods (Després et al., 2012). Both are time-

consuming and relatively costly. Sampling directly into agar cultures can provide

information about properties of the viable or culturable fraction of the aerosol, but can

greatly underestimate the diversity of bioaerosols, because any one media type can only

facilitate a small fraction of organism types to grow. For example, it has been estimated

that approximately 17% of fungal spores are culturable (Bridge and Spooner, 2001) and

that an even lower fraction of approximately 10% of bacteria may be culturable (Chi and

Li, 2007; Heidelberg et al., 1997; Lighthart, 1997). The identification of bioaerosols

using light microscopy techniques can have errors when collected particles are small or

highly translucent, and both quantification and differentiation are somewhat subjective

because particles are counted by eye. Due to environmental stresses, some particles may

be morphologically indistinguishable and as a result can be mistaken for another particle

type or miscounted (Després et al., 2012; Pitt and Hocking, 1997). The majority of living

microorganisms are not detectable by these methods, and nonviable bioaerosols can also

contribute significantly to human and environmental health. As a result, the use of instrumentation that can detect bioparticles in real-time with high time and size resolution is ideal for the accurate detection of bioaerosols.

1.3.2 Ultra-Violet Light-Induced Fluorescence (UV-LIF) Instrumentation

The development of ultraviolet light-induced fluorescence instrumentation (UV-LIF) began in the 1980's and was led by military research groups for the detection of biological warfare agents (BWAs) (Hill et al., 1999; Ho, 2014; Primmerman, 2000). The goal of these military based instruments was to identify the presence of BWAs, rather than characterize the type of ambient particle present.

Single particle fluorescence spectroscopy is one of the most common real-time detection and characterization techniques of bioaerosols (Huffman and Santarpia, 2017). The detection principle of real-time, UV-LIF instrumentation is based on the assumption that biological particles are comprised of characteristic, intrinsic fluorophores that differ from those in non-biological particles. Some common target biofluorophores include riboflavin, tryptophan, and NAD(P)H. Amino acids (i.e. tryptophan) are the building blocks of proteins present in all organisms, and NAD(P)H and riboflavin are molecules produced through metabolic pathways (Pöhlker et al., 2012).

Today, several commercial UV-LIF bioaerosol detection systems are commercially available that each use a similar detection strategy of counting particles that exhibit intrinsic fluorescence when excited with light pulses at characteristic wavelengths (λ_{ex}). A couple of the most popular instruments include the : Ultraviolet Aerodynamic Particle

Sizer (UV-APS; licensed to TSI, Shoreview, MN, USA, λ_{ex} 355 nm, $\lambda_{emission}$ 420-575 nm) and Wideband integrated bioaerosol sensor (WIBS; Droplet Measurement Technologies, Longmont, CO, USA; λ_{ex} 280 and 370nm, $\lambda_{emission}$ 310-400 and 420-650 nm) (Jonsson and Kullander, 2014). Examples of indoor and outdoor studies using the UV-APS and/or the WIBS in several different environments will be presented in Chapter 2.

1.4 Research Aim

Until recently the understanding of physical and chemical processes involved with bioaerosols has been limited due to a lack of instrumentation capable of characterizing the particles precisely (e.g. with sufficient time and size resolution). Bioaerosols make up a fraction of atmospheric aerosols, substantial in some environments and limited in others, and therefore an instrument's sensitivity and selectivity to the detection of biological particles is crucial. Real-time UV-LIF instrumentation, such as the WIBS, is able to detect both viable and non-viable microorganisms and can help enhance the understanding of bioaerosol dispersal, biodiversity within different environments, and interactions within human and environmental systems.

One major weakness of UV-LIF instrumentation is the ability to accurately detect bioaerosol particles when present in a complex matrix of other particle types. Several types of non-biological particles, such as soot and smoke, dust, and HULIS, are weakly fluorescent and may act as interferences for UV-LIF detection (Pöhlker et al., 2012). The main aims of this thesis are:

10

- To create a comprehensive overview of fluorescent, size, and asymmetry properties of both biological and non-biological particles detected using a WIBS-4A (Chapter 2).

- To suggest improved thresholding strategies to eliminate weakly fluorescent, non-biological particles without underestimating the number of biological particles (Chapter 2).

- Present initial results from clustering algorithms on laboratory data of both biological and interfering non-biological particles to see if separation of clusters between these two groups is possible (Chapter 3).

The results presented here may provide users of commercial UV-LIF instrumentation a variety of analysis strategies with the goal of better detecting and characterizing biological particles. By reducing mis-identification and mis-characterization of bioaerosols the scientific community can better understand the roles bioparticles have in important environmental systems and possibly even reduce the negative impact bioparticles play in human and environmental health.

Chapter Two: Systematic Characterization and Fluorescence Threshold Strategies for the Wideband Integrated Bioaerosol Sensor (Wibs) Using Size-Resolved Biological and Interfering Particles

2.1 Abstract

Here we present a systematic characterization of the WIBS-4A instrument using 69 types of aerosol materials, including a representative list of pollen, fungal spores, and bacteria as well as the most important groups of non-biological materials reported to exhibit interfering fluorescent properties. Broad separation can be seen between the biological and non-biological particles directly using the five WIBS output parameters and by taking advantage of the particle classification analysis introduced by Perring et al. (2015). We highlight the importance that particle size plays on observed fluorescence properties and thus in the Perring-style particle classification. We also discuss several particle analysis strategies, including the commonly used fluorescence threshold defined as the mean instrument background (forced trigger; FT) plus 3 standard deviations (σ) of the measurement. Changing the particle fluorescence threshold was shown to have a significant impact on fluorescence fraction and particle type classification. We conclude that raising the fluorescence threshold from FT + 3σ to FT + 9σ does little to reduce the relative fraction of biological material considered fluorescent, but can significantly

reduce the interference from mineral dust and other non-biological aerosols. We discuss examples of highly fluorescent interfering particles, such as brown carbon, diesel soot, and cotton fibers, and how these may impact WIBS analysis and data interpretation in various indoor and outdoor environments. A comprehensive online supplement is provided, which includes size distributions broken down by fluorescent particle type for all 69 aerosol materials and comparing two threshold strategies. Lastly, the study was designed to propose analysis strategies that may be useful to the broader community of UV-LIF instrumentation users in order to promote deeper discussions about how best to continue improving UV-LIF instrumentation and analysis strategies.

2.2 Introduction

Biological material emitted into the atmosphere from biogenic sources on terrestrial and marine surfaces can play important roles in the health of many living systems and may influence diverse environmental processes (Cox and Wathes, 1995; Després et al., 2012; Frohlich-Nowoisky et al., 2016; Pöschl, 2005). Bioaerosol exposure has been an increasingly important component of recent interest, motivated by studies linking airborne biological agents and adverse health effects in both indoor and occupational environments (Douwes et al., 2003). Bioaerosols may also impact the environment by acting as giant cloud condensation nuclei (GCCN) or ice nuclei (IN), having an effect on cloud formation and precipitation (Ariya et al., 2009; Delort et al., 2010; Möhler et al., 2007; Morris et al., 2004). Biological material emitted into the atmosphere is commonly referred to as Primary Biological Aerosol Particles (PBAP) or bioaerosols. PBAP can

include whole microorganisms, such as bacteria and viruses, reproductive entities (fungal spores and pollen) and small fragments of any larger biological material, such as leaves, vegetative detritus, fungal hyphae, or biopolymers, and can represent living, dead, dormant, pathogenic, allergenic, or biologically inert material (Després et al., 2012). PBAP often represent a large fraction of supermicron aerosol, for example up to 65% by mass in pristine tropical forests, and may also be present in high enough concentrations at submicron sizes to influence aerosol properties (Jaenicke, 2005; Penner, 1994; Pöschl et al., 2010).

Until recently the understanding of physical and chemical processes involving bioaerosols has been limited due to a lack of instrumentation capable of characterizing particles with sufficient time and size resolution (Huffman and Santarpia, 2017). The majority of bioaerosol analysis historically utilized microscopy or cultivation-based techniques. Both are time-consuming, relatively costly and cannot be utilized for real-time analysis (Agranovski et al., 2004; Griffiths and Decosemo, 1994). Cultivation techniques can provide information about properties of the culturable fraction of the aerosol (e.g. bacterial and fungal spores), but can greatly underestimate the diversity and abundance of bioaerosols because the vast majority of microorganism species are not culturable (Amann et al., 1995; Chi and Li, 2007; Heidelberg et al., 1997). Further, because culture-based methods cannot detect non-viable bioaerosols, information about their chemical properties and allergenicity has been poorly understood.

In recent years, advancements in the chemical and physical detection of bioaerosols have enabled the development of rapid and cost-effective techniques for the real-time characterization and quantification of airborne biological particles (Hairston et al., 1997; Ho, 2002; Huffman and Santarpia, 2017; Sodeau and O'Connor, 2016). One important technique is based on ultraviolet laser/light-induced fluorescence (UV-LIF), originally developed by military research communities for the rapid detection of bio-warfare agents (BWA) (e.g. Hill et al., 2001; Hill et al., 1999; Pinnick et al., 1995). More recently, UV-LIF instrumentation has been commercialized for application toward civilian research in fields related to atmospheric and exposure science. The two most commonly applied commercial UV-LIF bioaerosol sensors are the wideband integrated bioaerosol sensor (WIBS; University of Hertfordshire, Hertfordshire, UK, now licensed to Droplet Measurement Technologies, Longmont, CO, USA), and the ultraviolet aerodynamic particle sizer (UV-APS; licensed to TSI, Shoreview, MN, USA). Both sensors utilize pulsed ultraviolet light to excite fluorescence from individual particles in a real-time system. The wavelengths of excitation and emission were originally chosen to detect biological fluorophores assumed to be widely present in airborne microorganisms (e.g. tryptophan-containing proteins, NAD(P)H co-enzymes, or riboflavin) (Pöhlker et al., 2012). Significant work was done by military groups to optimize pre-commercial sensor performance toward the goal of alerting for the presence of biological warfare agents such as anthrax spores. The primary objective from this perspective is to positively identify BWAs without being distracted by false-positive signals from fluorescent

15

particles in the surrounding natural environment (Primmerman, 2000). From the perspective of basic atmospheric science, however, the measurement goal is often to quantify bioaerosol concentrations in a given environment. So, to a coarse level of discrimination, BWA-detection communities aim to ignore most of what the atmospheric science community seeks to detect. Researchers on such military-funded teams also have often not been able to publish their work in formats openly accessible to civilian researchers, so scientific literature is lean on information that can help UV-LIF users operate and interpret their results effectively. Early UV-LIF bioaerosol instruments have been in use for two decades and commercial instruments built on similar concepts are emerging and becoming widely used by scientists in many disciplines. In some cases, however, papers are published with minimal consideration of complexities of the UV-LIF data. This study presents a detailed discussion of several important variables specific to WIBS data interpretation, but that can apply broadly to operation and analysis of many similar UV-LIF instruments.

The commercially available WIBS instrument has become one of the most commonly applied instrument toward the detection and characterization of bioaerosol particles in both outdoor and indoor environments. As will be discussed in more detail, the instrument utilizes two wavelengths of excitation (280 nm and 370 nm), the second of which is close to the one wavelength utilized by the UV-APS (355 nm). Both the WIBS and UV-APS, in various version updates, have been applied to many types of studies regarding outdoor aerosol characterization. For example they have been important

instruments: in the study of ice nuclei (Huffman et al., 2013; Mason et al., 2015b; Twohy et al., 2016), toward the understanding of outdoor fungal spore concentrations (Gosselin et al., 2016; O'Connor et al., 2015b; Saari et al., 2015a), to investigate the concentration and properties of bioaerosols from long-range transport (Hallar et al., 2011), in tropical aerosol (Gabey et al., 2010; Huffman et al., 2012; Valsan et al., 2016; Whitehead et al., 2016; Whitehead et al., 2010), in urban aerosol (Huffman et al., 2010; Saari et al., 2015b; Yu et al., 2016), from composting centers (O'Connor et al., 2015), at high altitude (Crawford et al., 2016; Gabey et al., 2013; Perring et al., 2015; Ziemba et al., 2016), and in many other environments (Healy et al., 2014; Li et al., 2016; O'Connor et al., 2015a). The same instrumentation has been utilized for a number of studies involving the built, or indoor, environment as well (Wu et al., 2016). As a limited set of examples, these instruments have been critical components in the study of bioaerosols in the hospital environment (Handorean et al., 2015; Lavoie et al., 2015) and to study the emission rates of biological particles directly from humans (Bhangar et al., 2016) in school classrooms (Bhangar et al., 2014), and in offices (Xie et al., 2017).

Despite the numerous and continually growing list of studies that utilize commercial UV-LIF instrumentation, only a handful of studies have published results from laboratory work characterizing the operation or analysis of the instruments in detail. For example, Kanaani et al. (2007, 2009; 2008) and Agranovski et al. (2003; 2005; 2004) presented several examples of UV-APS operation with respect to bio-fluorophores and biological particles. Healy et al. (2012) provided an overview of fifteen spore and pollen species

17

analyzed by the WIBS, and Toprak and Schnaiter (2013) discussed the separation of dust from ambient fluorescent aerosol by applying a simple screen of any particles that exhibited fluorescence in one specific fluorescent channel. Hernandez et al. (2016) presented a summary of more than 50 pure cultures of bacteria, fungal spores, and pollen species analyzed by the WIBS and with respect to fluorescent particle type. Fluorescent particles observed in the atmosphere have frequently been used as a lower-limit proxy for biological particles (e.g. Huffman et al., 2010), however it is well known that a number of key particle types of non-biological origin can fluoresce. For example, certain examples of soot, humic and fulvic acids, mineral dusts, and aged organic aerosols can exhibit fluorescent properties, and the effects that these play in the interpretation of WIBS data is unclear (Bones et al., 2010; Gabey et al., 2011; Lee et al., 2013; Pöhlker et al., 2012; Sivaprakasam et al., 2004).

The simplest level of analysis of WIBS data is to provide the number of particles that exceed the minimum detectable threshold in each of the three fluorescence categories. Many papers on ambient particle observations have been written using this data analysis strategy with both the WIBS and UV-APS data. Such analyses are useful and can provide an important first layer of discrimination by fluorescence. To provide more complicated discrimination as a function of observed fluorescence intensity, however, brings associated analysis and computing challenges, i.e. users often must write data analysis code themselves and processing large data sets can push the limits of standard laboratory computers. Discriminating based on fluorescence intensity also requires more detailed

investigations into the strategy by which fluorescent thresholds can be applied to define whether a particle is considered fluorescent. Additionally, relatively little attention has been given to the optical properties of non-biological particles interrogated by the WIBS and to optimize how best to systematically discriminate between biological aerosol of interest and materials interfering with those measurements.

Here we present a comprehensive and systematic laboratory study of WIBS data in order to aid the operation and data interpretation of commercially available UV-LIF instrumentation. This work presents 69 types of aerosol materials, including key biological and non-biological particles, interrogated by the WIBS-4A and shows the relationship of fluorescent intensity and resultant particle type as a function of particle size and asymmetry. A discussion of thresholding strategy is given, with emphasis on how varying strategies can influence characterization of fluorescent properties and either under- or over-prediction of fluorescent biological particle concentration.

2.3 WIBS Instrumentation

2.3.1 Instrument Design and Operation

The WIBS (Droplet Measurement Technologies; Longmont, Colorado) uses light scattering and fluorescence spectroscopy to detect, size, and characterize the properties of interrogated aerosols on a single particle basis (instrument model 4A utilized here). Air is drawn into the instrument at a flow rate of 0.3 L/min and surrounded by a filtered sheath flow of 2.2 L/min. The aerosol sample flow is then directed through an intersecting a 635 nm, continuous wave (cw) diode laser, which produces elastic scattering measured in

both the forward and side directions. Particle sizing in the range of approximately 0.5 µm to 20 µm is detected by the magnitude of the electrical pulse detected by a photomultiplier tube (PMT) located at 90 degrees from the laser beam. Particles whose measured cw laser-scattering intensity (particle size) exceed user-determined trigger thresholds will trigger two xenon flash lamps (Xe1 and Xe2) to fire in sequence, approximately 10 microseconds apart. The two pulses are optically filtered to emit at 280 nm and 370 nm, respectively. Fluorescence emitted by a given particle after each excitation pulse is detected simultaneously using two PMT detectors. The first PMT is optically filtered to detect the total intensity of fluorescence in the range 310-400 nm and the second PMT in the range 420-650 nm. So for every particle that triggers xenon lamp flashes, Xe1 produces a signal in the FL1 (310-400 nm) and FL2 (420-650 nm) channels, whereas the Xe2 produces only a signal in the FL3 (420-650 nm) channel because elastic scatter from the Xe2 flash saturates the first PMT. The WIBS-4A has two user defined trigger thresholds, T1 and T2 that define which data will be recorded. Particles producing a scattering pulse from the cw laser that is below the T1 threshold will not be recorded. This enables the user to reduce data collection during experiments with high concentrations of small particles. Particles whose scattering pulse exceeds the T2 threshold will trigger xenon flash lamp pulses for interrogation of fluorescence. Note that the triggering thresholds mentioned here are fundamentally different from the analysis thresholds that will be discussed in detail later.

Forward-scattered light is detected using a quadrant PMT. The detected light intensity in each quadrant are combined using Equation 1 into an asymmetry factor (AF), where k is an instrument defined constant, E is the mean intensity measured over the entire PMT, and E_i is the intensity measured at the ith quadrant (Gabey et al., 2010).

$$AF = \frac{k\left(\sum_{i=1}^{n}(E-E_i)^2\right)^{1/2}}{E} \quad (1)$$

This parameter relates to a rough estimate of the sphericity of an individual particle by measuring the difference of light intensity scattered into each of the four quadrants. A perfectly spherical particle would theoretically exhibit an AF value of 0, whereas larger AF values greater than 0 and less than 100, indicate rod-like particles (Gabey et al., 2010; Kaye et al., 1991; Kaye et al., 2005). It is important to note that this parameter is not rigorously a shape factor like used in other aerosol calculations (DeCarlo et al., 2004; Zelenyuk et al., 2006) and only very roughly relates a measure of particle sphericity.

2.3.2 WIBS Calibration

Particle sizing within the instrument was calibrated periodically by aerosolizing several sizes of nonfluorescent polystyrene latex spheres (PSLs; Polysciences, Inc., Pennsylvania), including 0.51 μm (part number 07307), 0.99 μm. (07310), 1.93 μm (19814), 3.0 μm (17134), and 4.52 μm (17135). A histogram of signal intensity was plotted separately for each PSL, and the peak of a Gaussian fit to those data was then plotted versus the physical diameter of the PSL. A second degree polynomial fit was used to generate an equation in order to calibrate side scatter values into size.

Fluorescence intensity in each WIBS channel was calibrated using 2.0 µm Green (G0200), 2.1 µm Blue (B0200), and 2.0 µm Red (R0200) fluorescent PSLs (Thermo-Scientific, Sunnyvale, California). For each particle type, a histogram of the fluorescence intensity signal in each channel was fitted with a Gaussian function, and the median intensity was recorded. Periodic checks were performed using the same stock bottles of the PSLs in order to verify that mean fluorescence intensity of each had not shifted more than one standard deviation between particle sample types (Table 2.1). The particle fluorescence standards used present limitations due to variations in fluorescence intensity between stocks of particles and due to fluorophore degradation over time. To improve reliability between instruments, stable fluorescence standards and calibration procedures (e.g. Robinson et al., 2017) will be important.

Voltage gain settings for the three PMTs that produce sizing, fluorescence, and AF values, respectively, significantly impact measured intensity values and are recorded here for rough comparison of calibrations and analyses to other instruments. The voltage settings used for all data presented here were set according to manufacturer specifications and are as follows: PMT_1 (AF) 400 V, PMT_2 (particle sizing and FL1 emission) 450 mV, and PMT_3 (FL2, FL3 emission) 732 mV.

Table 2.1. Fluorescence values of standard PSLs, with proprietary fluorescent dye color listed, determined as the peak (mean) of a Gaussian fit applied to a histogram of the fluorescence signal in each channel. Uncertainties are one standard deviation from the Gaussian mean.

	FL1	FL2	FL3
2 μm Green	69 ± 49	1115 ± 57	214 ± 29
2 μm Red	44 ± 30	160 ± 18	28 ± 13
2.1 μm Blue	724± 111	1904 ± 123	2045 ± 6

2.2.3 WIBS Data Analysis

An individual particle is considered to be fluorescent in any one of the three fluorescence channels (FL1, FL2, or FL3) when its fluorescence emission intensity exceeds a given baseline threshold. The baseline fluorescence can be determined by a number of strategies, but commonly has been determined by measuring the observed fluorescence in each channel when the xenon lamps are fired into the optical chamber when devoid of particles. This is referred to as the "forced trigger" (FT) process, because the xenon lamp firing is not triggered by the presence of a particle. The instrument background is also dependent on the intensity and orientation of Xe lamps, voltage gains of PMTs, quality of PMTs based on production batch, orientation of optical components i.e. mirrors in the optical chamber, etc. As a result of these factors, the background or baseline of a given instrument is unique and cannot been used as a universal threshold. All threshold values used in this study can are listed in supplementary Table S1. Fluorescence intensity in each channel is recorded at an approximate FT rate of one value per second for a user-defined time period, typically 30-120 seconds. The baseline threshold in each channel has typically been determined as the average plus 3x the

23

standard deviation (σ) of forced trigger fluorescence intensity measurement (Gabey et al., 2010), however alternative applications of the fluorescence threshold will be discussed. Particles exhibiting fluorescence intensity lower than the threshold value in each of the three channels are considered to be nonfluorescent. The emission of fluorescence from any one channel is essentially independent of the emission in the other two channels. The pattern of fluorescence measured allows particles to be categorized into 7 fluorescent particle types (A, B, C, AB, AC, BC, or ABC) as depicted in Figure 2.1, or as completely nonfluorescent (Perring et al., 2015).

Other threshold strategies have also been proposed and will be discussed. For example, Wright et al. (2014) used set fluorescence intensity value boundaries rather than using the standard Gabey et al. (2010) definition that applies a threshold as a function of observed background fluorescence. The Wright et al. (2014) study proposed five separate categories of fluorescent particles (FP1 through FP5). Each definition was determined by selecting criteria for excitation-emission boundaries and observing the empirical distribution of particles in a 3-dimensional space (FL1 vs. FL2 vs. FL3). For the study reported here, only the FP3 definition was used for comparison, because Wright et al. (2014) postulated the category as being enriched with fungal spores during their ambient study and because they observed that these particles scaled more tightly with observed ice nucleating particles. The authors classified a particle in the FP3 category if the fluorescence intensity in FL1 > 1900 arbitrary units (a.u) and between 0-500 a.u for each FL2 and FL3.
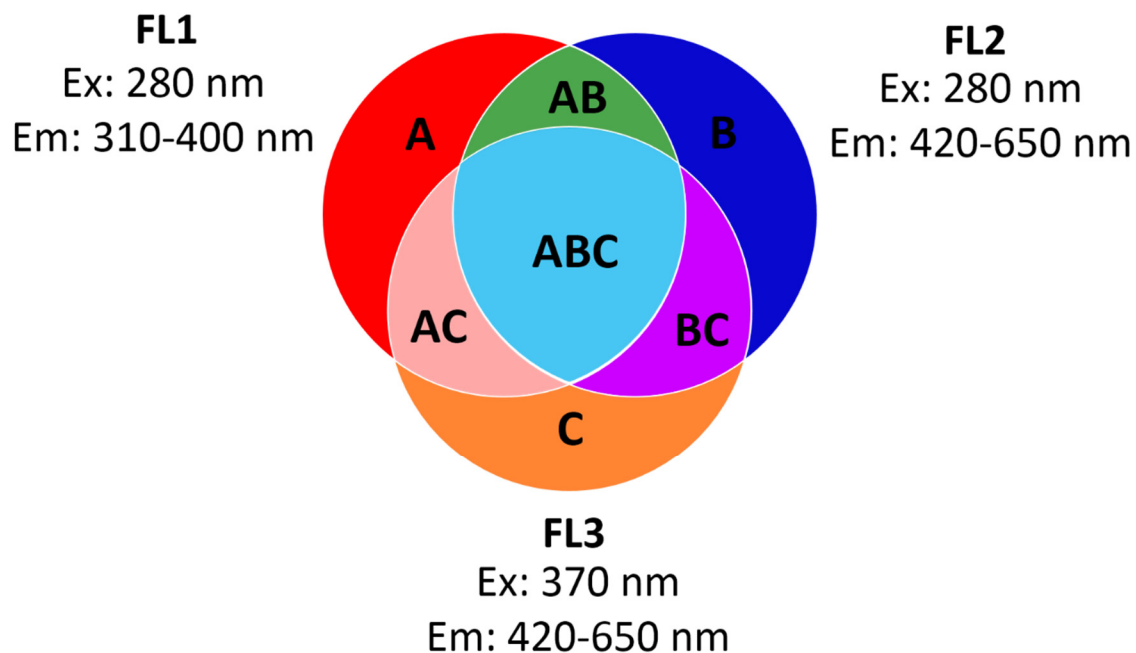
Figure 2.1. Particle type classification, as introduced by introduced by Perring et al. (2015). Large circles each represent one fluorescence channel (FL1, FL2, FL3). Colored zones represent particle types that each exhibit fluorescence in one, two, or three channels.

2.3 Materials

2.3.1 Table of materials

All materials utilized, including the vendors and sources from where they were acquired, have been listed in supplemental Table S1, organized into broad particle type groups: biological material (fungal spores, pollen, bacteria, and biofluorophores) and non-biological material (dust, humic-like substances or HULIS, polycyclic aromatic hydrocarbons or PAHs, combustion soot and smoke, and miscellaneous non-biological

materials). Combustion soot and smoke are grouped into one set of particles analyzed and are hereafter referred to as "soot" samples.

2.3.2 Brown Carbon Synthesis

Three different brown carbon solutions were synthesized using procedures described by Powelson et al. (2014): (Rxn 1) methylglyoxal + glycine, (Rxn 2) glycolaldehyde + methylamine, and (Rxn 3) glyoxal + ammonium sulfate. Reactions conditions were reported previously, so only specific concentration and volumes used here are described. All solutions described are aqueous and were dissolved into 18.2 MΩ water (Millipore Sigma; Denver, CO). For reaction 1, 25.0 mL of 0.5 M methylglyoxal solution was mixed with 25 mL of 0.5 M glycine solution. For reaction 2, 5.0 mL of 0.5 M glyoxal trimer dihydrate solution was mixed with 5.0 mL of 0.5 M ammonium sulfate solution. For reaction 3, 10.0 mL of 0.5 M glycolaldehyde solution was mixed with 10.0 mL of 0.5 M methylamine solution. The pH of the solutions was adjusted to approximately pH 4 by adding 1 M oxalic acid in order for the reaction to follow the appropriate chemical mechanism (Powelson et al., 2014). The solutions were covered with aluminum foil and stirred at room temperature for 8 days, 4 days, and 4 days, for reactions 1, 2, and 3, respectively. Solutions were aerosolized via the liquid aerosolization method described in Section 3.2.4.

2.4 Aerosolization Methods

2.4.1 Fungal Spore Growth and Aerosolization

Fungal cultures were inoculated onto sterile, disposable polystyrene plates (Carolina, Charlotte, NC) filled with agar growth media consisting of malt extract medium mixed with 0.04 M of streptomycin sulfate salt (S6501, Sigma-Aldrich) to suppress bacterial colony growth. Inoculated plates were allowed to mature and were kept in a sealed Plexiglas box for 3-5 weeks until aerosolized. Air conditions in the box were monitored periodically and were consistently 25-27 ºC and 70% relative humidity.

Fungal cultures were aerosolized inside an environmental chamber constructed from a re-purposed home fish tank (Aqueon Glass Aquarium, 5237965). The chamber has glass panels with dimensions 20.5 L x 10.25 H x 12.5 W in (supplemental Fig. A.1). Soft rubber beading seals the top panel to the walls, allowing isolation of air and particles within the chamber. Two tubes are connected to the lid. The first delivers pressurized and particle-free air through a bulkhead connection, oriented by plastic tubing (Loc-Line Coolant Hose, 0.64 inch outer diameter) and a flat nozzle. The second tube connects 0.75 inch internal diameter conductive tubing (Simolex Rubber Corp., Plymouth, MI) for aspiration of fungal aerosol, passing it through a bulkhead fitting and into tubing directed toward the WIBS. Aspiration tubing is oriented such that a gentle 90-degree bend brings aerosol up vertically through the top panel.

For each experiment, an agar plate with a mature fungal colony was sealed inside the chamber. The air delivery nozzle was positioned so that a blade of air was allowed to

27

approach the top of the spore colony at a shallow angle in order to eject spores into an approximately horizontal trajectory. The sample collection tube was positioned immediately past the fungal plate to aspirate aerosolized fungal particles. Filtered room air was delivered by a pump through the aerosolizing flow at approximately 9 – 15 L/min, varied within each experiment to optimize measured spore concentration. Sample flow was 0.3 L/min into the WIBS and excess input flow was balanced by outlet through a particle filter connected through a bulkhead on the top plate.

Two additional rubber septa in the top plate allow the user to manipulate two narrow metal rods to move the agar plate once spores were depleted from a given region of the colony. After each spore experiment, the chamber and tubing was evacuated by pumping for 15 minutes, and all interior surfaces were cleaned with isopropanol to avoid contamination between samples.

2.4.2 Bacterial Growth and Aerosolization

All bacteria were cultured in nutrient broth (Becton, Dickinson and Company, Sparks, MD) for 18 hours in a shaking incubator at 30°C for *Bacillus atrophaeus* (ATCC 49337, American Type Culture Collection, MD), 37°C for *Escherichia coli* (ATCC 15597), and 26°C *Pseudomonas fluorescens* (ATCC 13525). Bacterial cells were harvested by centrifugation at 7000 rpm (6140 g) for 5 min at 4°C (BR4, Jouan Inc., Winchester, VA) and washed 4 times with autoclave-sterilized deionized water (Millipore Corp., Billerica, MA) to remove growth media. The final liquid suspension was diluted with sterile deionized water, transferred to a polycarbonate jar and aerosolized using a three jet

Collison nebulizer (BGI Inc., Waltham, MA) operated at 5 L/min (pressure of 12 psi).

The polycarbonate jar was used to minimize damage to bacteria during aerosolization

(Zhen et al., 2014) . The tested airborne cell concentration was about ~10^5 cells/Liter as

determined by an optical particle counter (model 1.108, Grimm Technologies Inc.,

Douglasville, GA). Bacterial aerosolization took place in an experimental system

containing a flow control system, a particle generation system, and an air-particle mixing

system introducing filtered air at 61 L/min as described by Han et al. (2015).

2.4.3 Powder Aerosolization

Dry powders were aerosolized by mechanically agitating material by one of several

methods mentioned below and passing filtered air across a vial containing the powder.

For each method, approximately 2.5-5.0 g of sample was placed in a 10 mL glass vial.

For most samples (method P1), a stir bar was added, and the vial was placed on a

magnetic stir plate. Two tubes were connected through the lid of the vial. The first tube

connected a filter, allowing particle-free air to enter the vessel. The second tube

connected the vial through approximately 33 cm of conductive tubing (0.25 in inner

diam.) to the WIBS for sample collection.

The setup was modified (method P2) for a small subset of samples whose solid

powder was sufficiently fine to produce high number concentrations of submicron

aerosol particles that could risk coating the internal flow path and damaging optical

components of the instrument. In this case, the same small vial with powder and stir bar

was placed in a larger reservoir (~0.5 L), but without vial lid. The lid of the larger

29

reservoir was connected to filtered air input and an output connection to the instrument. The additional container volume allowed for greater dilution of aerosol before sampling into the instrument.

Some powder samples produced consistent aerosol number concentration even without stirring. For these samples, 2.5 – 5.0 g of material was placed in a small glass vial and set under a laboratory fume hood (method P3). Conductive tubing was held in place at the opening of the vial using a clamp, and the opposite end was connected to the instrument with a flow rate of 0.3 L/min. The vial was tapped by hand or with a hand tool, physically agitating the material and aerosolizing the powder.

2.4.4 Liquid Aerosolization

Disposable, plastic medical nebulizers (Allied Healthcare, St. Louis, MO) were used to aerosolize liquid solutions and suspensions. Each nebulizer contains a reservoir where the solution is held. Pressurized air is delivered through a capillary opening on the side, reducing static pressure and, as a result, drawing fluid into the tube. The fluid is broken up by the air jet into a dispersion of droplets, where most of the droplets are blown onto the internal wall of the reservoir, and droplets remaining aloft are entrained into the sample stream. Output from the medical nebulizer was connected to a dilution chamber (aluminum enclosure, 0.5 L), allowing the droplets to evaporate in the system before particles enter the instrument for detection.

2.4.5 Smoke Generation

Wood and cigarette smoke samples were aerosolized through combustion. Each sample was ignited separately using a personal butane lighter while held underneath a laboratory fume hood. Once the flame from the combusting sample was naturally extinguished, the smoldering sample was waved at a height ~5 cm above the WIBS inlet for 3– 5 minutes during sampling.

2.5 Pollen Microscopy

Pollen samples were aerosolized using the dry powder vial (P1, P2) and tapping (P3) methods detailed above. Samples were also collected by impaction onto a glass microscope slide for visual analysis using a home-built, single-stage impactor with D_{50} cut ~0.5 μm at flow-rate 1.2 L min^{-1}. Pollen were analyzed using an optical microscope (VWR model 89404-886) with a 40x objective lens. Images were collected with an AmScope complementary metal-oxide semiconductor camera (model MU800, 8 megapixels).

2.6 Results

2.6.1 Broad Separation of Particle Types

The WIBS is routinely used as an optical particle counter applied to the detection and characterization of fluorescent biological aerosol particles (FBAP). Each interrogated particle provides five discreet pieces of information: fluorescence emission intensity in each of the 3 detection channels (FL1, FL2, and FL3), particle size, and particle asymmetry. Thus, a thorough summary of data from aerosolized particles would require the ability to

31

show statistical distributions in five dimensions. As a simple, first-order representation of the most basic summary of the 69 particle types analyzed, Figure 2.2 and Table 2.2 show median values for each of the five data parameters plotted in three plot styles (columns of panels in Fig. 2.2).
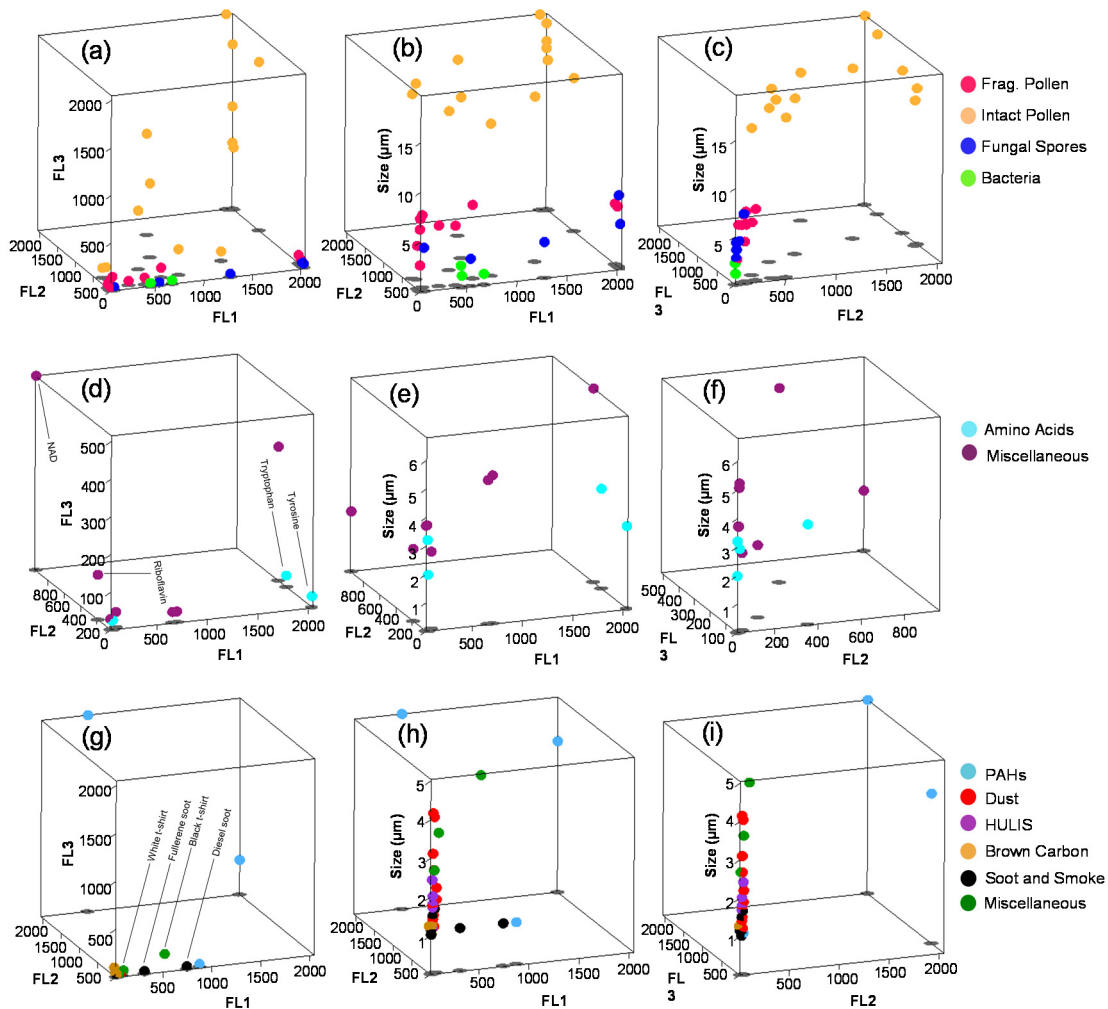
Figure 2.2. Representations including 4 of the 5 parameters recorded by the WIBS: FL1, FL2, FL3, and particle size. Biological material types (a-c), bio-fluorophores (d-f), and non-biological 1141 particle types (g-i). Data points represent median values. Gray ovals are shadows (cast directly downward onto the bottom plane) included to help reader with 3-D representation. Tags in (d) and (g) used to differentiate particles of specific importance within text.

Table 2.2. Median values for each of the five data parameters, along with percent of particles that saturate fluorescence detector in each fluorescence channel. Uncertainty (as one standard deviation, σ) listed for particle size and asymmetry factor (AF). Only a sub-selection of pollen are characterized as fragmented pollen because not all pollen presented the smaller size fraction or fluorescence characteristics that represent fragments.

Materials		FL1	FL1 Sat %	FL2	FL2 Sat %	FL3	FL3 Sat %	Size (µm)	AF	Aerosolization method
BIOLOGICAL MATERIALS										
Pollen										
Intact Pollen										
1	*Urtica diocia (Stinging Nettle)*	2047.0	99.2	2047.0	99.4	1072.0	9.9	16.9 ± 2.2	18.5 ± 8.3	Powder (P1)
2	*Artemisia vulgaris (Common Mugwort)*	1980.0	48.3	2047.0	99.7	2047.0	90.3	19.7 ± 1.0	14.2 ± 7.6	Powder (P1)
3	*Castanea sativa (European Chestnut)*	830.0	19.3	258.0	2.9	269.0	0.8	15.3 ± 1.7	17.0 ± 9.5	Powder (P1)
4	*Corylus avellana (Hazel)*	1371.0	44.4	532.0	5.6	99.0	2.8	16.6 ± 2.1	24.2 ± 12.6	Powder (P1)
5	*Taxus baccata (Common Yew)*	525.0	0.4	561.0	0.2	615.0	0.0	16.0 ± 1.3	22.2 ± 10.0	Powder (P1)
6	*Rumex acetosella (Sheep Sorrel)*	2047.0	73.5	2047.0	55.1	693.0	2.7	16.2 ± 2.0	21.7 ± 10.8	Powder (P1)
7	*Olea europaea (European Olive Tree)*	131.0	1.1	395.0	0.4	119.0	0.0	19.7 ± 1.2	17.7 ± 7.6	Powder (P1)
8	*Alnus glutinosa (Black Alder)*	109.0	3.3	432.0	1.2	102.0	0.9	18.6 ± 1.7	15.8 ± 8.5	Powder (P1)
9	*Phleum pratense (Timothy Grass)*	2047.0	100.0	2012.0	49.8	651.0	1.9	15.1 ± 1.7	24.1 ± 12.2	Powder (P1)
10	*Populus alba (White Poplar)*	2047.0	95.9	2047.0	92.2	1723.0	39.2	18.7 ± 1.9	21.2 ± 10.4	Powder (P1)
11	*Taraxacum officinale (Common Dandelion)*	2047.0	99.1	1309.0	21.8	1767.0	44.2	15.4 ± 1.8	22.2 ± 11.9	Powder (P1)
12	*Amaranthus retroflexus (Redroot Amaranth)*	980.0	36.7	1553.0	36.7	1061.0	18.0	17.7 ± 2.2	19.4 ± 12.1	Powder (P1)
13	*Aesculus hippocastanum (Horse-chestnut)*	762.0	23.5	876.0	23.5	776.0	23.5	16.2 ± 2.0	22.2 ± 13.4	Powder (P1)
14	*Lycopodium (Clubmoss)*	40.0	0.1	32.0	0.0	27.0	0.0	3.9 ± 1.86	24.5 ± 15.9	Powder (P1)
Fragment Pollen										
3	*Castanea sativa (European Chestnut)*	74.0	11.0	113.0	0.4	84.0	0.1	7.0 ± 3.1	24.6 ± 13.7	Powder (P1)
4	*Corylus avellana (Hazel)*	263.0	28.8	119.0	0.5	46.0	0.2	6.1 ± 3.7	20.4 ± 13.7	Powder (P1)
5	*Taxus baccata (Common Yew)*	40.0	0.2	28.0	0.1	34.0	0.0	2.6 ± 2.2	16.0 ± 12.2	Powder (P1)
6	*Rumex acetosella (Sheep Sorrel)*	417.0	87.1	88.0	0.4	71.0	0.1	6.0 ± 2.5	24.4 ± 12.4	Powder (P1)

33

#	Name									
7	*Olea europaea (European Olive Tree)*	40.0	1.9	22.0	0.1	33.0	0.0	2.6 ± 1.6	10.4 ± 9.3	Powder (P1)
8	*Alnus glutinosa (Black Alder)*	46.0	4.6	46.0	0.3	44.0	0.2	6.1 ± 3.2	25.2 ± 14.6	Powder (P1)
9	*Phleum pratense (Timothy Grass)*	2047.0	85.5	129.0	1.2	63.0	0.1	6.0 ± 3.2	23.1 ± 13.4	Powder (P1)
10	*Populus alba (White Poplar)*	642.0	35.2	237.0	8.6	103.0	0.5	7.4 ± 4.0	24.7 ± 14.2	Powder (P1)
11	*Taraxacum officinale (Common Dandelion)*	2047.0	71.9	195.0	0.4	88.0	0.8	6.1 ± 3.1	23.7 ± 13.5	Powder (P1)
12	*Amaranthus retroflexus (Redroot Amaranth)*	104.0	15.6	138.0	5.6	101.0	3.4	7.3 ± 2.8	27.7 ± 14.6	Powder (P1)
13	*Aesculus hippocastanum (Horse-chestnut)*	43.0	6.0	106.0	0.2	42.0	0.2	4.3 ± 3.1	19.7 ± 13.4	Powder (P1)
Fungal spores										
1	*Aspergillus brasiliensis*	1279.0	38.5	22.0	0.0	33.0	0.0	3.6 ± 1.8	20.8 ± 10.3	Fungal
2	*Aspergillus niger; WB 326*	543.0	6.2	18.0	0.0	29.0	0.0	2.7 ± 0.9	17.1 ± 10.7	Fungal
3	*Rhizopus stolonifera (Black Bread Mold); UNB-1*	78.0	11.2	20.0	0.1	34.0	0.1	4.4 ± 2.3	21.4 ± 14.4	Fungal
4	*Saccharomyces cerevisiae (Brewer's Yeast)*	2047.0	96.6	97.0	0.3	41.0	0.1	7.2 ± 3.7	28.7 ± 16.8	Fungal
5	*Aspergillus versicolor; NRRL 238*	2047.0	78.2	55.0	0.0	40.0	0.0	4.5 ± 2.5	24.5 ± 16.9	Fungal
Bacteria										
1	*Bacillus atrophaeus*	443.0	1.0	10.0	0.0	36.0	0.0	2.2 ± 0.4	17.4 ± 4.1	Bacterial
2	*Escherichia coli*	454.0	1.4	12.0	0.0	33.0	0.0	1.2 ± 0.3	19.3 ± 2.8	Bacterial
3	*Pseudomonas Stutzeri*	675.0	0.4	16.0	0.0	36.0	0.0	1.1 ± 0.3	19.2 ± 2.8	Bacterial
Biofluorophores										
1	Riboflavin	41.0	0.0	190.0	2.5	119.0	1.3	2.5 ± 2.5	13.2 ± 12.2	Powder (P1)
2	Chitin	116.5	6.2	61.0	0.1	40.0	0.0	2.7 ± 2.1	16.1 ± 13.5	Powder (P1)
3	NAD	49.0	0.2	962.0	26.7	515.0	15.0	2.1 ± 2.2	12.2 ± 10.1	Powder (P1)
4	Folic Acid	41.0	0.0	34.0	0.1	28.0	0.1	3.7 ± 3.4	18.6 ± 13.6	Powder (P1)
5	Cellulose, fibrous medium	54.0	0.2	37.0	0.1	27.0	0.0	3.7 ± 2.5	20.4 ± 15.7	Powder (P1)
6	Ergosterol	2047.0	81.8	457.0	2.6	355.0	11.6	6.8 ± 4.0	22.6 ± 12.9	Powder (P1)
7	Pyrdoxine	661.0		39.0		28.0		1.0 ± 0.2	20.0 ± 13.0	Powder (P1)
8	Pyridoxamine	706.0	10.7	40.0	0.0	28.0	0.0	5.2 ± 2.5	20.2 ± 12.7	Powder (P1)

9	Tyrosine	2047.0	59.7	42.0	0.0	29.0	0.0	2.9 ± 3.4	15.4 ± 11.6	Powder (P1)
10	Phenylalanine	53.0	0.0	29.0	0.0	24.0	0.0	3.2 ± 2.0	21.1 ± 15.4	Powder (P1)
11	Tryptophan	2047.0	78.0	357.0	9.0	30.0	0.0	3.5 ± 2.9	20.9 ± 17.0	Powder (P1)
12	Histidine	59.0	0.2	29.0	0.0	25.0	0.0	2.0 ± 1.7	11.6 ± 10.0	Powder (P1)
NON-BIOLOGICAL MATERIALS										
Dust										
1	Arabic Sand	48.0	0.1	37.0	0.0	29.0	0.0	3.1 ± 2.2	16.1 ± 15.7	Powder (P3)
2	California Sand	66.0	1.1	42.0	0.0	31.0	0.0	4.0v1.9	18.8 ± 14.6	Powder (P2)
3	Africa Sand	88.0	0.0	48.0	0.0	26.0	0.0	2.2 ± 1.4	15.3 ± 11.0	Powder (P2)
4	Murkee-Murkee Australian Sand	88.0	0.7	47.0	0.0	26.0	0.0	1.9 ± 1.1	10.9 ± 9.2	Powder (P2)
5	Manua Key Summit Hawaii Sand	54.0	0.1	33.0	0.0	25.0	0.0	1.5 ± 0.7	10.8 ± 13.4	Powder (P2)
6	Quartz	66.0	0.0	38.0	0.0	24.0	0.0	1.7 ± 0.8	11.2 ± 12.7	Powder (P2)
7	Kakadu Dust	58.0	0.0	35.0	0.0	25.0	0.0	2.7 ± 1.4	15.0 ± 12.0	Powder (P2)
8	Feldspar	60.0	0.0	36.0	0.0	25.0	0.0	1.2 ± 0.6	10.2 ± 10.6	Powder (P2)
9	Hematite	51.0	0.0	32.0	0.0	25.0	0.0	1.8 ± 1.0	10.8 ± 11.9	Powder (P2)
10	Gypsum	49.0	0.0	30.0	0.0	26.0	0.0	4.1 ± 3.0	19.3 ± 12.2	Powder (P2)
11	Bani AMMA	48.0	0.2	31.0	0.0	26.0	0.0	3.1 ± 2.1	15.8 ± 13.7	Powder (P2)
12	Arizona Test Dest	46.0	0.0	29.0	0.0	25.0	0.0	1.4 ± 0.7	10.5 ± 10.5	Powder (P2)
13	Kaolinite	46.0	0.0	29.0	0.0	25.0	0.0	1.5 ± 0.8	9.9 ± 10.3	Powder (P2)
HULIS										
1	Waskish Peat Humic Acid Reference	46.0	0.0	29.0	0.0	25.0	0.0	1.7 ± 0.8	10.9 ± 9.8	Powder (P1)
2	Suwannee River Humic Acid Standard II	46.0	0.0	30.0	0.0	26.0	0.0	2.0 ± 1.2	13.2 ± 16.5	Powder (P2)
3	Suwannee River Fulvic Acid Standard I	46.0	0.0	34.0	0.0	28.0	0.0	1.7 ± 1.0	12.0 ± 10.1	Powder (P2)
4	Elliott Soil Humic Acid Standard	47.0	0.0	29.0	0.0	25.0	0.0	1.2 ± 0.6	10.5 ± 10.2	Powder (P1)
5	Pony Lake (Antarctica) Fulvic Acid Reference	46.0	0.0	49.0	0.0	37.0	0.0	2.4 ± 1.8	14.0 ± 13.3	Powder (P2)
6	Nordic Aquatic Fulvic Acid Reference	48.0	0.1	32.0	0.0	27.0	0.0	1.8 ± 1.4	11.6 ± 9.6	Powder (P2)
Polycyclic Hydrocarbons										

1	Pyrene	490.0	7.4	2047.0	91.5	2047.0	81.8	5.0 ± 3.5	17.4 ± 12.6	Powder (P1)
2	Phenanthrene	2047.0	81.9	2047.0	66.3	360.0	22.4	3.9 ± 3.5	14.5 ± 13.6	Powder (P1)
3	Naphthalene	886.0	11.6	45.0	2.1	30.0	0.7	1.1 ± 1.0	10.6 ± 9.5	Powder (P1)
Combustion Soot and Smoke										
1	Aquadag	22.0	0.0	14.0	0.0	29.0	0.0	1.2 ± 0.6	10.5 ± 6.6	Liquid
2	Ash	48.0	0.2	31.0	0.0	23.0	0.0	1.7 ± 1.3	12.6 ± 11.9	Powder (P1)
3	Fullerene Soot	318.0	0.0	30.0	0.0	26.0	0.0	1.1 ± 0.5	17.0 ± 10.6	Powder (P2)
4	Diesel Soot	750.5	0.2	30.0	0.0	26.0	0.0	1.1 ± 0.4	21.2 ± 10.1	Powder (P1)
5	Cigarette Smoke	28.0	0.6	30.0	0.1	36.0	0.0	1.0 ± 0.8	9.5 ± 4.5	Smoke
6	Wood Smoke (*Pinus Nigra ,Black Pine*)	32.0	0.1	30.0	0.0	36.0	0.0	1.0 ± 0.7	9.5 ± 4.3	Smoke
7	Fire Ash	42.0	0.2	33.0	0.0	28.0	0.0	1.8 ± 1.2	14.0 ± 16.7	Powder (P1)
Brown Carbon										
1	Methylglyoxal + Glycine	17.0	0.0	53.0	0.0	88.0	0.0	1.2 ± 0.4	18.4 ± 3.1	Liquid
2	Glycolaldehyde + Methylamine	15.0	0.0	19.0	0.0	47.0	0.0	1.2 ± 0.4	17.9 ± 2.4	Liquid
3	Glyoxal + Ammonium Sulfate	30.0	0.0	9.0	0.0	35.0	0.0	1.3 ± 0.6	14.1 ± 3.5	Liquid
Miscellaneous non-biological										
1	Laboratory wipes	112.0	30.6	54.0	15.2	47.0	15.4	3.6v5.7	16.4 ± 14.4	Rubbed material over inlet
2	Cotton t-shirt (white)	567.0	34.9	145.0	16.1	139.0	16.4	4.9 ± 4.7	23.5 ± 16.2	
3	Cotton t-shirt (black)	56.0	13.5	22.0	1.7	34.0	1.5	2.7 ± 4.0	17.6 ± 14.8	

For the sake of WIBS analysis, each pollen type was broken into two size categories, because it was observed that most pollen species exhibited two distinct size modes. The largest size mode peaked above 10 μm in all cases and often saturated the sizing detector (see also fraction of particles that saturated particle detector for each fluorescence channel in Table 2). This was interpreted to be intact pollen. A broad mode also usually appeared at smaller particle diameters for some pollen species, suggesting that pollen grains had ruptured during dry storage or through the mechanical agitation process. This hypothesis was supported by optical microscopy through which a mixture of intact pollen grains and ruptured fragments were observed (Fig. A.2). For the purposes of this investigation, the two modes were separated at the minimum point between modes in order to observe optical properties of the intact pollen and pollen fragments separately. The list number for each pollen (Tables 2, S1) is consistent for the intact and fragmented species, though not all pollen exhibited obvious pollen fragments.

The WIBS was developed primarily to discriminate biological from non-biological particles, and the three fluorescence channels broadly facilitate this separation. Biological particles, i.e. pollen, fungal spores, and bacteria (top row of Fig. 2.2), each show strong median fluorescence signal in at least one of the three channels. In general, all fungal spores sampled (blue dots) show fluorescence in the FL1 channel with lower median emission in FL2 and FL3 channels. Both the fragmented (pink dots) and intact (orange dots) size fractions of pollen particles showed high median fluorescence emission intensity in all channels, varying by species and strongly as a function of particle size.

37

The three bacterial species sampled (green dots) showed intermediate median

fluorescence emission in the FL1 channel and very low median intensity in either of the

other two channels. To support the understanding of whole biological particles, pure

molecular components common to biological material were aerosolized separately and

are shown as the second row of Figure 2.2. Each of the biofluorophores chosen shows

relatively high median fluorescence intensity, again varying as a function of size. Key

biofluorophores such as NAD, riboflavin, tryptophan, and tyrosine are individually

labeled in Figure 2.2d. Supermicron particles of these pure materials would not be

expected in a real-world environment, but are present as dilute components of complex

biological material and are useful here for comparison. In general, the spectral properties

summarized here match well with fluorescence excitation emission matrices (EEMs)

presented by Pöhlker et al. (2013; 2012)

In contrast to the particles of biological origin, a variety of non-biological particles

were aerosolized in order to elucidate important trends and possible interferences. The

majority of non-biological particles shown in the bottom row of Figure 2.2 show little to

no median fluorescence in each channel and are therefore difficult to differentiate from

one another in the figure. For example, Figure 2.2g (lower left) shows the median

fluorescence intensity of 6 different groups of particle types (33 total dots), but almost all

overlap at the same point at the graph origin. The exceptions to this trend include the

PAHs (blue dots), miscellaneous particles (green) and several types of combustion soot

(black dots). The fluorescent properties of PAHs are well-known in both basic chemical

literature and as observed in the atmosphere (Finlayson-Pitts and Pitts, November 1999; Niessner and Krupp, 1991; Panne et al., 2000; Slowik et al., 2007). PAHs can be produced by a number of anthropogenic sources and are emitted in the exhaust from vehicles and other combustion sources as well as from biomass burning (Abdel-Shafy and Mansour, 2016; Aizawa and Kosaka, 2008, 2010; Lv et al., 2016). PAHs alone exhibit high fluorescence quantum yields (Mercier et al., 2013; Pöhlker et al., 2012), but as pure materials are not usually present in high concentrations at sizes large enough (>0.8 μm) to be detected by the WIBS. Highly fluorescent PAH molecules are also common constituents of other complex particles, including soot particle agglomerates. It has been observed that the fluorescent emission of PAH constituents on soot particles can be weak due to quenching from the bulk material (Panne et al., 2000). Several examples of soot particles shown in Figure 2.2g are fluorescent in FL1 and indeed should be considered as interfering particle types, as will be discussed. Three miscellaneous particles (laboratory wipes and two colors of cotton t-shirts) were also interrogated by rubbing samples over the WIBS inlet, because of their relevance to indoor aerosol investigation (e.g. Bhangar et al., 2016; e.g. Bhangar et al., 2014; Handorean et al., 2015). These particles (dark blue dots, Fig. 2.2 bottom row) show varying median intensity in FL1, suggesting that sources such as tissues, cleaning wipes, and cotton clothing could be sources of fluorescent particles within certain built environments.

Another interesting point from the observations of median fluorescence intensity is that the three viable bacteria aerosolized in this study each shows moderately fluorescent

characteristics in FL1 and low fluorescent characteristics in FL2 and FL3 (Fig. 2.2a-c). A study by Hernandez et al. (2016) also focused on analysis strategies using the WIBS and shows similar results regarding bacteria. Of the 14 bacteria samples observed in the Hernandez et al. study, 13 were categorized as predominantly A-type particles, thus meaning they exhibited fluorescent properties in FL1 and only a very small fraction of particles showed fluorescence above the applied threshold (FT + 3σ) in either FL2 or FL3. The FL3 channel in the WIBS-4A has an excitation of 370 nm and emission band of 420-650 nm, similar to that of the UV-APS with an excitation of 355 nm and emission band of 420-575 nm. Previous studies have suggested that viable microorganisms (i.e. bacteria) show fluorescence characteristics in the UV-APS due to the excitation source of 355 nm that was originally designed to excite NAD(P)H and riboflavin molecules present in actively metabolizing organisms (Agranovski et al., 2004; Hairston et al., 1997; Ho et al., 1999; Pöhlker et al., 2012). Previous studies with the UV-APS and other UV-LIF instruments using approximately similar excitation wavelengths have shown a strong sensitivity to the detection of "viable" bacteria (Brosseau et al., 2000; Hairston et al., 1997; Hill et al., 1999; Pan et al., 1999). Because the bacteria here were aerosolized and detected immediately after washing from growth media, we expect that a high fraction of the bacterial signal was a result of living vegetative bacterial cells. The results presented here and from other studies using WIBS instruments, in contrast to reports using other UV-LIF instruments, suggest that the WIBS-4A is highly sensitive to the detection of bacteria using 280 nm excitation (only FL1 emission), but less so using the 370 nm

40

excitation (FL3 emission) (e.g. Hernandez et al., 2016; Perring et al., 2015). A study by

Agranovski et al. (2003) also demonstrated that the UV-APS was limited in its ability to

detect endospores (reproductive bacterial cells from spore-forming species with little or

no metabolic activity and thus low NAD(P)H concentration). The lack of FL3 emission

observed from bacteria in the WIBS may also suggest a weaker excitation intensity in

Xe2 with respect to Xe1, manifesting in lower overall FL3 emission intensity (Könemann

et al., In Prep.). Gain voltages applied differently to PMT2 and PMT3 could also impact

differences in relative intensity observed. Lastly, it has been proposed that the rapid

sequence of Xe1 and Xe2 excitation could lead to quenching of fluorescence from the

first excitation flash, leading to overall reduced fluorescence in the FL3 channel

(Sivaprakasam et al., 2011). These factors may similarly affect all WIBS instruments and

should be kept in mind when comparing results here with other UV-LIF instrument types.

2.6.2 Fluorescence Type Varies With Particle Size

The purpose of Figure 2.2 is to distill complex distributions of the five data

parameters into a single value for each in order to show broad trends that differentiate

biological and non-biological particles. By representing the complex data in such a

simple way, however, many relationships are averaged away and lost. For example, the

histogram of FL1 intensity for fungal spore *Aspergillus niger* (Fig. A.3) shows a broad

distribution with long tail at high fluorescence intensity, including ca. ~ 6% of particles

that saturate the FL1 detector (Table S2). If a given distribution were perfectly Gaussian

and symmetric, the mean and standard deviation values would be sufficient to fully

describe the distribution. However, given that asymmetric distributions often include detector-saturating particles, no single statistical fit characterizes data for all particle types well. Median values were chosen for Figure 2.2 knowing that the resultant values can reduce the physical meaning in some cases. For example, the same *Aspergillus niger* particles show a broad FL1 peak at ~150 a.u. and another peak at 2047 a.u. (detector saturated), whereas the median FL1 intensity is 543 a.u., at which point there is no specific peak. In this way, the median value only broadly represents the data by weighting both the broad distribution and saturating peak. To complement the median values, however, Table 2.2 also shows the fraction of particles that were observed to saturate the fluorescence detector in each channel.

The representation of median values for each of the five parameters (Fig. 2.2) shows broad separation between particle classes, but discriminating more finely between particle types with similar properties by this analysis method can be practically challenging. Rather than investigating the intensity of fluorescence emission in each channel, however, a common method of analyzing field data is to apply binary categorization for each particle in each fluorescence channel. For example, by this process, a particle is either fluorescent in a given FL channel (above emission intensity threshold) or nonfluorescent (below threshold). In this way, many of the challenges of separation introduced above are significantly reduced, though others are introduced. Perring et al. (2015) introduced a WIBS classification strategy by organizing particles

sampled by the WIBS as either nonfluorescent or into one of seven fluorescence types (e.g. Fig. 2.1).

Complementing the perspective from Figure 2.2, stacked particle type plots (Fig. 2.3) show qualitative differences in fluorescence emission by representing different fluorescence types as different colors. The most important observation here is that almost all individual biological particles aerosolized (top two rows of Fig. 2.3) are fluorescent, meaning that they exhibit fluorescence emission intensity above the standard threshold (FT baseline $+ 3\sigma$) in at least one fluorescence channel and are depicted with a non-gray color. Figure A.4 shows the stacked particle type plots for all 69 materials analyzed in this study as a comprehensive library. In contrast to the biological particles, most particles from non-biological origin were observed not to show fluorescence emission above the threshold in any of the fluorescence channels and are thus colored gray. For example, 11 of the 15 samples of dust aerosolized show <15% of particles to be fluorescent at particle sizes <4 μm. Similarly, 4 of 5 samples of HULIS aerosolized show <7% of particles to be fluorescent at particle sizes <4 μm. The size cut-point here was chosen arbitrarily to summarize the distributions. Two examples shown in Figure 2.3 (Dust 10 and HULIS 3) are representative of average dust and HULIS types analyzed, respectively, and are relatively nonfluorescent. Of the four dust types that exhibit a higher fraction of fluorescence, two (Dust 3 and Dust 4) are relatively similar and show ~75% fluorescent particles <4 μm, with particle type divided nearly equally across the A, B, and AB particle types (Fig. A.4I). The two others (Dust 2 and Dust 6) show very few

43

similarities between one another, where Dust 2 shows size-dependent fluorescence and Dust 6 shows particle type A and B at all particle sizes (Fig. A.4I). As seen by the median fluorescence intensity representation (Fig. 2.2, Table 2.2), however, the relative intensity in each channel for all dusts is either below or only marginally above the fluorescence threshold. Thus, the threshold value becomes critically important and can dramatically impact the classification process, as will be discussed in a following section. Similarly, HULIS 5 (Fig. A.4K) is the one HULIS type that shows an anomalously high fraction of fluorescence, and is represented by B, C, BC particle types, but at intensity only marginally above the threshold value and at 0% detector saturation in each channel.
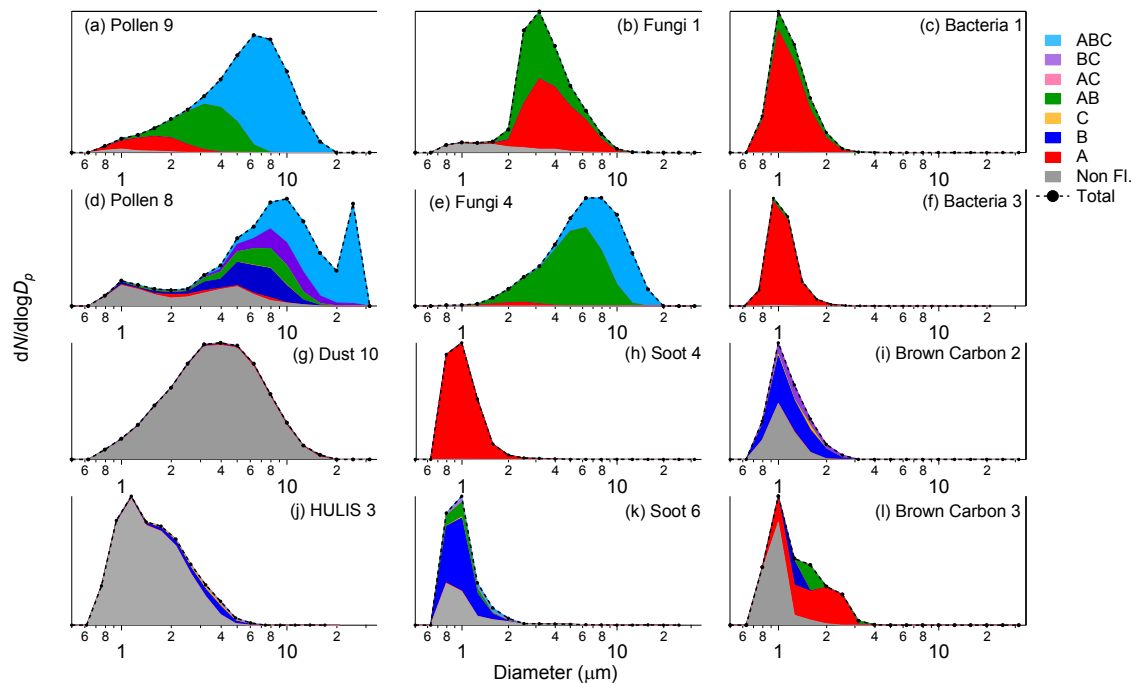
Figure 2.3. Stacked particle type size distributions including particle type classification, as introduced by Perring et al. (2015) using FT + 3σ threshold definition. Examples of each material type were selected to show general trends from larger pool of samples. Soot 4 (h) as an example of combustion soot and Soot 6 (wood smoke) as an example of smoke aerosol.

Several types of non-biological particles, specifically brown carbon and combustion soot and smoke, exhibited higher relative fractions of fluorescent particles compared to other non-biological particles. Two of the three types of brown carbon sampled show >50% of particles to be fluorescent at sizes >4 μm (Figs. 3i, l), though their median fluorescence is relatively low and neither shows saturation in any of the three fluorescent channels. Out of six soot samples analyzed, four showed >69% of particles to be fluorescent at sizes >4 μm, most of which are dominated by B particle types. Two samples of combustion soot are notably more highly fluorescent, both in fraction and intensity. Soot 3 (fullerene soot) and Soot 4 (diesel soot) show FL1 intensity of 318 a.u. and 751 a.u., respectively, and are almost completely represented as A particle type. The fullerene soot is not likely a good representative of most atmospherically relevant soot types, however diesel soot is ubiquitous in anthropogenically-influenced areas around the world. The fact that it exhibits high median fluorescence intensity implies that increasing the baseline threshold slightly will not appreciably reduce the fraction of particles categorized as fluorescent, and these particles will thus be counted as fluorescent in many instances. The one type of wood smoke analyzed (Soot 6) shows ca. 70% fluorescent at >4 μm, mostly in the B category, with moderate to low FL2 signal, and also presents similarly as cigarette smoke. Additionally, the two smoke samples in this study (Soot 5, cigarette smoke and Soot 6, wood smoke) share similar fluorescent particle type features with two of the brown carbon samples BrC 1 and BrC2. The smoke samples are categorized predominantly as B-type particles, whereas samples more purely comprised

of soot exhibit predominantly A-type fluorescence. This distinction between smoke and soot may arise partially because the smoke particles are complex mixtures of amorphous soot with condensed organic liquids, indicating that compounds similar to the brown carbon analyzed here could heavily influence the smoke particle signal.

Biological particle types were chosen for Figure 2.3 to show the most important trends among all particle types analyzed. Two pollen are shown here to highlight two common types of fluorescence properties observed. Pollen 9 (Fig. 2.3a) shows particle type transitioning between A, AB, and ABC as particle size gets larger. Pollen 9 (*Phleum pretense*) has a physical diameter of ~35 μm, so the mode seen in Figure 2.3a may be a result of fragmented pollen and due to the upper particle size limit of WIBS detection, intact pollen cannot be detected (Pöhlker et al., 2013). Pollen 8 (Fig. 2.3d) shows a mode peaking at ~10 μm in diameter and comprised of a mixture of B, AB, BC, and ABC particles as well as a larger particle mode comprised of ABC particles. The large particle mode appears almost monodisperse, but this is due to the WIBS ability to sample only the tail of the distribution due to the upper size limit of particle collection (~20 μm as operated). It is important to note that excitation pulses from the Xe flash lamps are not likely to penetrate the entirety of large pollen particles, and so emission information is likely limited to outer layers of each pollen grain. Excitation pulses can penetrate a relatively larger fraction of the smaller pollen fragments, however, meaning that the differences in observed fluorescence may arise from differences the layers of material interrogated. Fungi 1 (Fig. 2.3b) was chosen because it depicts the most commonly

47

observed fluorescence pattern among the fungal spore types analyzed (~3 μm mode mixed with A and AB particles). Fungi 4 (Fig. 2.3e) represents a second common pattern (particle size peaking at larger diameter, minimal A-type, and dominated by AB, ABC particle types). All three bacteria types analyzed were dominated by A-type fluorescence. One gram-positive (Bacteria 1) and one gram-negative bacteria (Bacteria 3) types are shown in Figure 2.3c, f, respectively.

2.6.3 Fluorescence Intensity Varies Strongly With Particle Size

An extension of observation from the many particle classes analyzed is that particle type (A, AB, ABC, etc.) varies strongly as a function of particle size. This is not surprising, given that it has been frequently observed and reported that particle size significantly impacts fluorescence emission intensity (e.g. Hill et al., 2001; Sivaprakasam et al., 2011). The higher the fluorescent quantum yield of a given fluorophore, the more likely it is to fluoresce. For example, pure biofluorophores (middle row of Fig. 2.2) and PAHs (bottom row of Fig. 2.2) have high quantum yields and thus exhibit relatively intense fluorescence emission, even for particles <1 μm. In contrast, more complex particles comprised of a wide mixture of molecular components are typically less fluorescent per volume of material. At small sizes the relative fraction of these particles that fluoresce is small, but as particles increase in size they are more likely to contain enough fluorophores to emit a sufficient number of photons to record an integrated light intensity signal above a given fluorescence threshold. Thus, the observed fluorescence

48

intensity scales approximately between the 2nd and 3rd power of the particle diameter (Hill et al., 2015; Sivaprakasam et al., 2011; Taketani et al., 2013).

The general trend of fluorescence dependence on size is less pronounced for FL1 than for FL2 and FL3. This can be seen by the fact that the scatter of points along the FL1 axis in Figure 2.2b is not clearly size-dependent and is strongly influenced by particle type (i.e. composition dependent). In Figure 2.2c, however, the median points cluster near the vertical (size) axis and both FL2 and FL3 values increase as particle size increases. It is important to note, however, that the method chosen for particle generation in the laboratory strongly impacts the size distribution of aerosolized particles. For example, higher concentrations of an aqueous suspension of particle material generally produce larger particles, and the mechanical force used to agitate powders or aerosolize bacteria can have strong influences on particle viability and physical agglomeration or fragmentation of the aerosol (Mainelis et al., 2005). So, while the absolute size of particles shown here is not a key message, the relative fluorescence at a given size can be informative.

As discussed, each individual particle shows increased probability of exhibiting fluorescence emission above a given fluorescence threshold as size increases. Using Pollen 9 (*Phleum pratense*, Fig. 2.3a) as an example, most particles <3 μm show fluorescence in only the FL1 channel and are thus classified as A-type particles. For the same pollen, however, particles ca. 2-6 μm in diameter are more likely to be recorded as AB-type particles, indicating that they have retained sufficient FL1 intensity, but have

exceeded the FL2 threshold to add B-type fluorescence character. Particles larger still (>4 μm) are increasingly likely to exhibit ABC character, meaning that the emission intensity in the FL3 channel has increased to cross the fluorescence threshold. Thus, for a given particle type and a constant threshold as a function of particle size, the relative breakdown of fluorescence type changes significantly as particle size increases. The same general trend can be seen in many other particle types, for example Pollen 8 (*Alnus glutinosa*, Fig. 2.3d), Fungi 1 (*Aspergillus brasiliensis*, Fig. 2.3b), and to a lesser degree HULIS 3 (Suwannee fulvic acid, Fig. 2.3j) and Brown Carbon 2 (Fig. 2.3i). The "pathway" of change, for Pollen 9, starts as A-type at small particle size and adds B and eventually ABC (A→AB→ABC), whereas Pollen 8 starts primarily with B-type at small particle size and separately adds either B or C en route to ABC (B→AB or BC→ABC). In this way, not only is the breakdown of fluorescence type useful in discriminating particle distributions, but the pathway of fluorescence change with particle size can also be instructive.

To further highlight the relationship between particle size and fluorescence, four kinds of particles (Dust 2, HULIS 5, Fungi 4, and Pollen 9) were each binned into 4 different size ranges, and the relative number fraction was plotted versus fluorescence intensity signal for each channel (Fig. 2.4). In each case, the fluorescence intensity distribution shifts to the right (increases) as the particle size bin increases. This trend is strongest in the FL2 and FL3 (middle and right columns of Fig. 2.4) for most particle types, as discussed above.

50
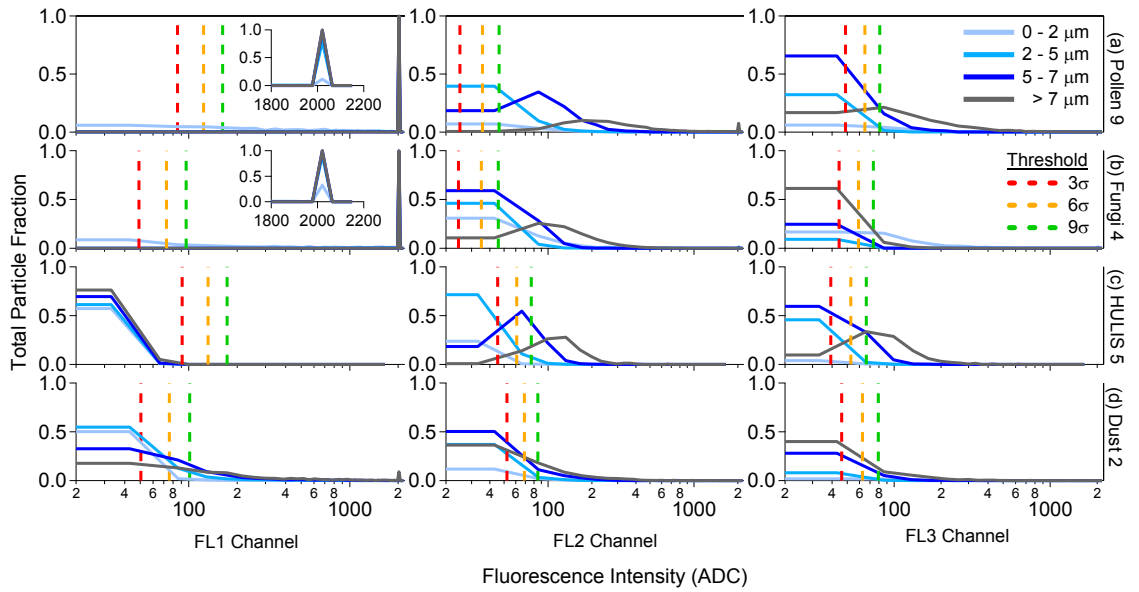
Figure 2.4. Relative fraction of fluorescent particles versus fluorescence intensity in analog-to-1152 digital counts (ADC) for each channel. Particles are binned into 4 different size ranges (trace colors). Vertical lines indicate three thresholding definitions. Insets shown for particles that 1154 exhibit fluorescence saturation characteristics.

51

The fact that particle fluorescence type can change so dramatically with increasing particle size becomes critically important when the Perring-style particle type classification is utilized for laboratory or field investigation. For example Hernandez et al. (2016) aerosolized a variety of species of pollen, fungal spores, and bacteria in the laboratory and presented the break-down of particle types for each aerosolized species. This first comprehensive overview summarized how different types of biological material (e.g. pollen and bacteria) might be separated based on their fluorescence properties when presented with a population of relatively monodisperse particles. This was an important first step, however, differentiation becomes more challenging when broad size distributions of particles are mixed in an unknown environment. In such a case, understanding how the particle type may change as a function of particle size may become an important aspect of analysis.

2.6.4 Fluorescence Threshold Defines Particle Type

Particle type analysis is not only critically affected by size, but also by the threshold definition chosen. Figure 2.5 represents the same matrix of particle types as in Figure 2.3, but shows the fluorescence intensity distribution in each channel (at a given narrow range of sizes in order to minimize the sizing effect on fluorescence). Figure 2.5 can help explain the breakdown of particle type (and associated colors) shown in Figure 2.3. For example, in Figure 2.5a, the median fluorescence intensity in FL1 for Pollen 9 (2046 a.u., detector saturated) in the size range 3.5-4.0 μm far exceeds the 3σ threshold (51 a.u.), and so essentially all particles exhibit FL1 character. Approximately 90% of particles of

Pollen 9 are above the 3σ FL2 threshold (25 a.u.), and approximately 63% of particles are above the 3σ FL3 threshold (49 a.u). These three channels of information together describe the distribution of particle type at the same range of sizes: 9% A, 26% AB, 63% ABC, and 2% other categories. Since essentially all particles are above the threshold for FL1, particles are thus assigned as A type particles (if < FL2 and FL3 thresholds), AB (if >FL2 threshold and <FL3 threshold), or ABC (if > FL2 and FL3 thresholds). Thus, the distribution of particles at each fluorescence intensity and in relation to a given thresholding strategy defines the fluorescence type breakdown and the pathway of fluorescence change with particle size. It is important to note differences in this pathway for biofluorophores (Figs. S4G and S4H). For example Biofluorophore 1 (riboflavin) follows the pathway B→C→BC while Biofluorophore 11 (tryptophan) follows the pathway A→BC→ABC.
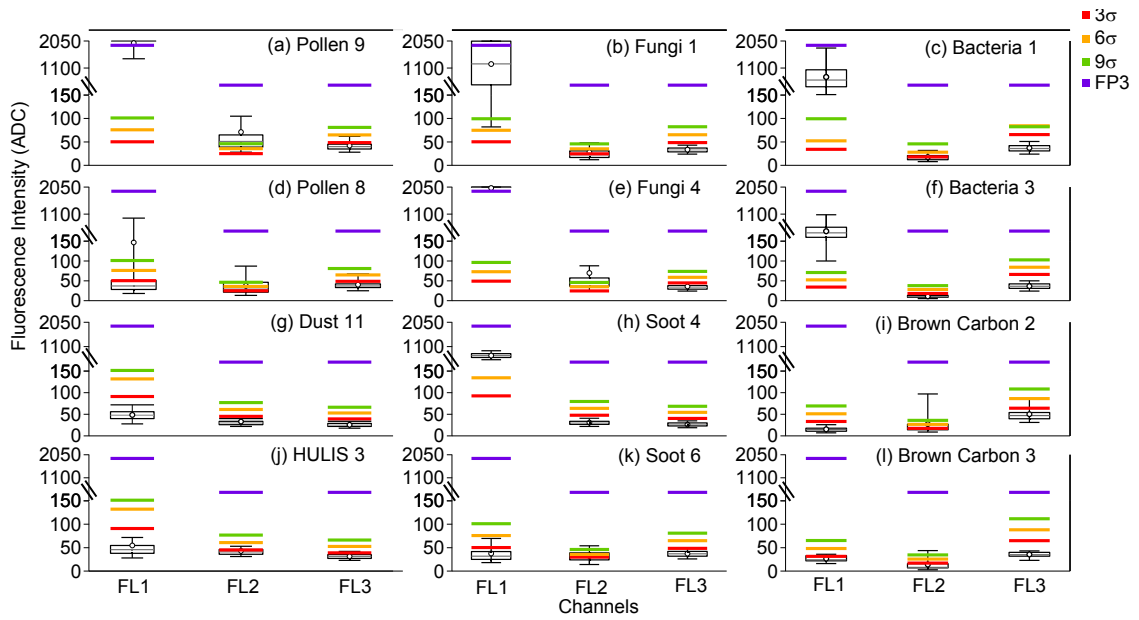
Figure 2.5. Box whisker plots showing statistical distributions of fluorescence intensity in analog-to-digital counts (ADC) in each channel. Averages are limited to particles in the size range 3.5- 1159 4.0 μm for pollen, fungal spore, HULIS, and dust samples and in the range 1.0-1.5 μm for 1160 bacteria, brown carbon, and soot samples. Horizontal bars associated with each box-whisker 1161 show four separate threshold levels.

54

By extension, the choice of threshold bears heavily on how a given particle breakdown appears and thus how a given instrument may be used to discriminate between biological and non-biological particles. A commonly made assumption is that particles exhibiting fluorescence by the WIBS (or UV-APS) can be used as a lower limit proxy to the concentration of biological particles, though it is known that interfering particle types confound this simple assumption (Huffman et al., 2010). Increasing the fluorescence threshold can reduce categorizing weakly fluorescent particles as biological, but can also remove weakly fluorescing biological particles of interest (Huffman et al., 2012). Figure 2.6 provides an analysis of 8 representative particle types (3 biological, 5 non-biological) in order to estimate the trade-offs of increasing fluorescence threshold separately in each channel. Once again, the examples chosen here represent general trends and outliers, as discussed previously for Figure 2.3. Four threshold strategies are presented: three as the instrument fluorescence baseline plus increasing uncertainty on that signal (FT + 3σ, FT + 6σ, and FT + 9σ), as well as the FP3 strategy suggested by Wright et al. (2014). Using Dust 4 as an example (Fig. 2.6d), by increasing the threshold from 3σ (red traces) to 6σ (orange traces), the fraction of dust particles fluorescent in FL1 decreases from approximately 50% to 10%. Increasing the fluorescence threshold even higher to 9σ, reduces the fraction of fluorescence to approximately 1%, thus eliminating nearly all interfering particles of Dust 3. In contrast, for biological particles such as Pollen 9 (Fig. 2.6b), increasing the threshold from 3σ to 9σ does very little to impact the relative breakdown of fluorescence category or the fraction of particles considered

fluorescent in at least one channel. Changing threshold from 3σ to 9σ decreases the FL1

fraction minimally (98.3% to 97.9%), and for FL2 and FL3 the fluorescence fraction

decreases from 90% to 50% and from 60% to 42%, respectively. Figure 2.6 also

underscores how increasing particle size affects fluorescence fraction, as several particle

types (e.g. Pollen 9 and HULIS 5) show sigmoidal curves that proceed toward the right

(lower fraction at a given size) as the threshold applied increases and thus removes more

weakly fluorescent particles.
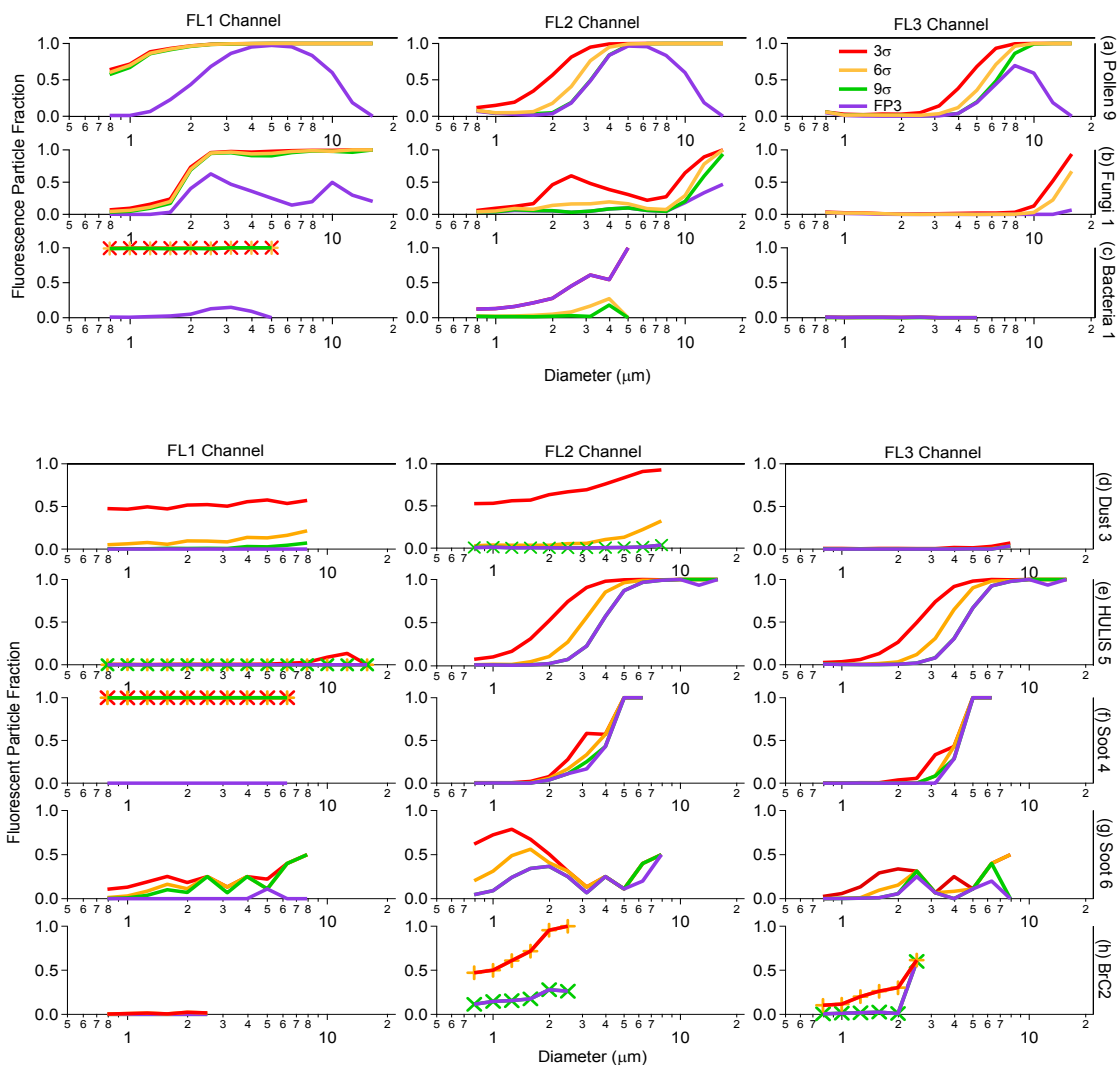
Figure 2.6. Fraction of particle number exhibiting fluorescent in a given channel versus particle diameter for various material types for four different thresholds definitions. Data markers shown only when disambiguation of traces is necessary. Brown carbon sample denoted by BrC.

To better understand how the different thresholding strategies qualitatively change the distribution of particle fluorescence type, Figure 2.7 shows stacked fluorescence type distributions for each of the four thresholds analyzed. Looking first at Dust 3 (Fig. 2.7d),

the standard threshold definition of 3σ shows approximately 80% of particles to be fluorescent in at least one channel, resulting in a distribution of predominantly A, B, and AB-type particles. As the threshold is increased, however, the total percentage of fluorescent particles decreases dramatically to 1% at 9σ and the particle type of the few remaining particles shifts to A-type particles. A similar trend of fluorescent fraction can also be seen for Soot 6 (wood smoke) and Brown Carbon 2, where almost no particle (10% and 16%, respectively) remain fluorescent using the 9σ threshold. Soot 4 (diesel soot), in contrast, exhibits the same fraction and breakdown of fluorescent particles whether using the 3σ or 9σ threshold. Using the FP3 threshold (which employs very high FL1 threshold), however, the fluorescent properties of the diesel soot change dramatically to nonfluorescent. As a 'worst case' scenario, HULIS 5 shows ca. 60% of particles to be fluorescent using the 3σ threshold. In this case, increasing the threshold from 6σ to 9σ only marginally decreases the fraction of fluorescent particles to ca. 35% and 22%, respectively, and the break-down remains relatively constant in B, C, and BC types. Changing the threshold definition to FP3 in this case also does not significantly change the particle type break-down, since the high FP3 threshold applies only to FL1.
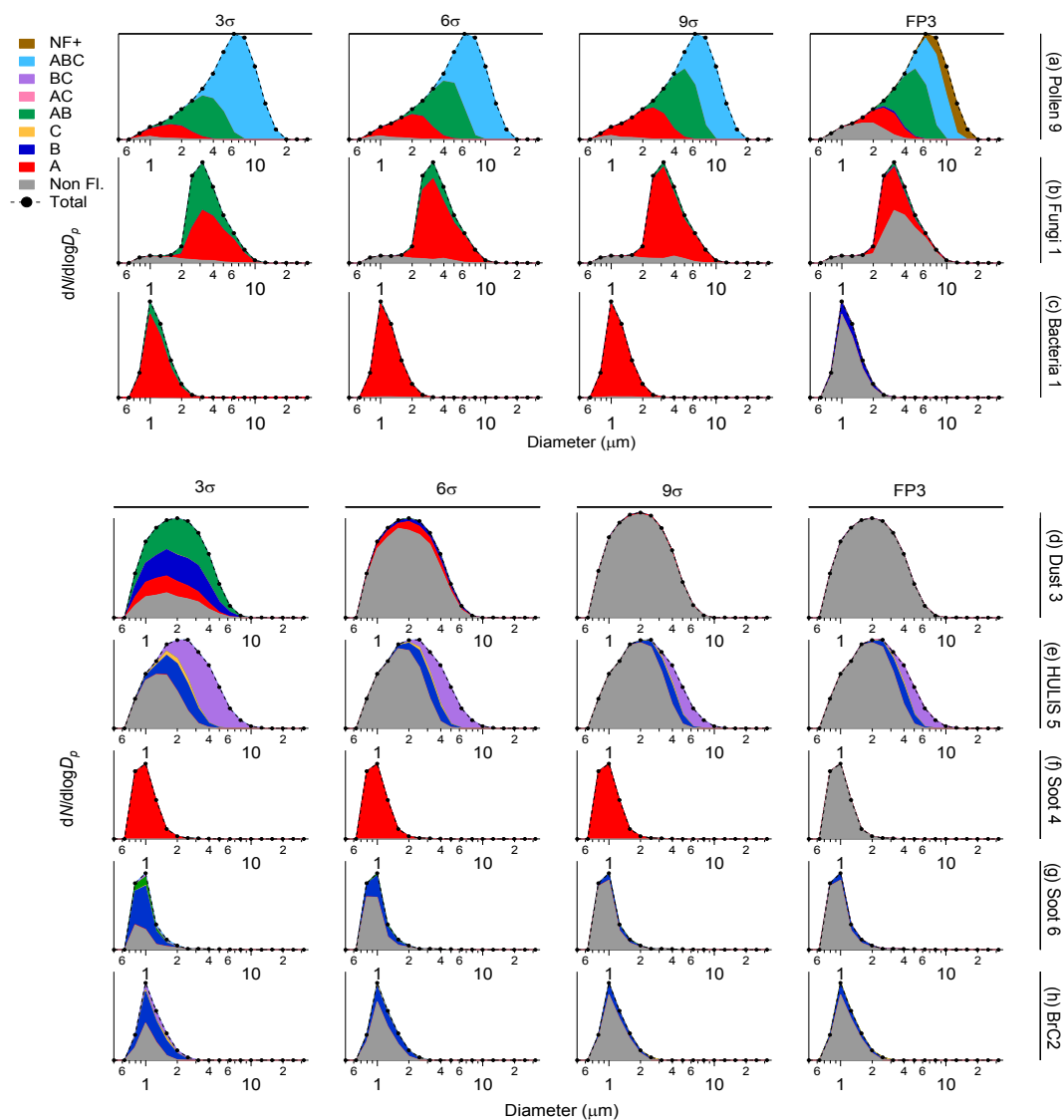
Figure 2.7. Stacked particle type size distributions for representative particle classes shown using four separate thresholding strategies. NF+ particle type (right-most column) represents particles that exceed the FL2 and/or FL3 upper bound of the Wright et al. (2014) FP3 definition and that are therefore considered as one set of "non-fluorescent" particles by that definition. Legend above top rows indicate threshold definition used.

As stated, the WIBS is mostly often applied toward the detection and characterization of biological aerosol particles. For the biological particles analyzed (Fig. 2.7, top rows), increasing the threshold from 3σ to 9σ shows only a marginal decrease in the total fluorescent fraction for Pollen 9, Fungal Spore 1, and Bacteria 1, and only a slight shift in fluorescence type as a function of size. Using the FP3 threshold, however, for each of the three biological species the nonfluorescent fraction increases substantially. Wright et al. (2014) found that the FP3 threshold definition showed a strong correlation with ice nucleating particles and the authors suggested these particles with high FL1 intensity were likely to be fungal spores. This may have been the case, but given the analysis here, the FP3 threshold is also likely to significantly underestimate fungal spore number by missing weakly or marginally fluorescent spores.

Based on the threshold analysis results shown in Figure 2.7, marginally increasing the threshold in each case may help eliminate non-biological, interfering particles without significantly impacting the number of biological particles considered fluorescent. Each threshold strategy brings trade-offs, and individual users must understand these factors to make appropriate decisions for a given scenario. These data suggest that using a threshold definition of FT baseline $+ 9\sigma$ is likely to reduce interferences from most non-biological particles without significantly impacting most biological particles.

2.6.5 Particle Asymmetry Varies With Particle Size

As a part of the comprehensive WIBS study, particle asymmetry (AF) was analyzed as a function of particle size for all particles. As described in Section 2.1, AF in the

WIBS-4A is determined by comparing the symmetry of the forward elastic scattering response of each particle, measured at the quadrant PMT. Many factors are related to the accuracy of the asymmetry parameter, including the spatial alignment of the collection optics, signal-to-noise and dynamic range of the detector, agglomeration of particles with different refractive indices, and the angle at which a non-symmetrical particle hits the laser (Gabey et al., 2010; Kaye et al., 2007). Figure 2.8 shows a summary of the relationship between AF and particle size for all material types analyzed in Table 2.2. Soot particles are known to frequently cluster into chains or rings depending on the number of carbon atoms (Von Helden et al., 1993) and, as a result, can have long aspect ratios that would be expected to manifest as large AF values. The bacteria species chosen have rod-like shape features and thus would also exhibit large AF values. These properties were observed by the WIBS, as two types of soot (diesel and fullerene) and all three bacteria showed higher AF values than other particles at approximately the same particle diameter. For an unknown reason, all three brown carbon samples also showed relatively high AF values given that the individual particles of liquid organic aerosol would be expected to be spherical with low AF. Similarly, the intact pollen showed anomalously low AF, because a substantial fraction of each was shown to saturate the WIBS sizing detector, even if the median particle size (shown) is lower than the saturating value. For this reason we postulate that the side-scattering detector may not be able to reliably estimate either particle size or AF when particles are near the sizing limits. Intact pollen, soot samples (diesel and fullerene soot), bacteria and brown carbon

61

samples were excluded from the linear regression fit, because they appeared visually as

outliers to the trend. All remaining particle groups of material types (7 in total) are

represented by blue in Figure 2.8. A linear regression R^2 value of 0.87 indicates a high

degree of correlation between particle AF and size across the remaining particles. The

strong correlation between these two factors across a wide range of particle types, mixed

with the confounding anomaly of brown carbon, raises a question about the degree to

which the asymmetry factor parameter from the WIBS-4A can be useful or, conversely,

to what degree the uncertainty in AF is dominated by instrumental factors, including

those listed above.
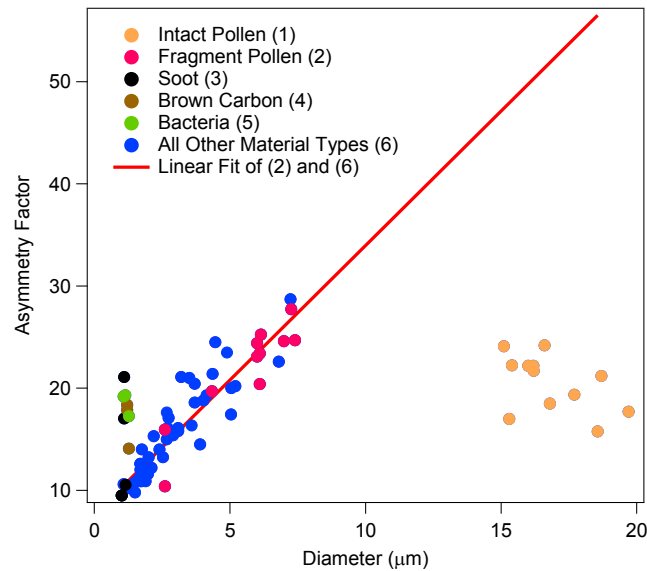
Figure 2.8. Median values of particle asymmetry factor versus particle size for all particle types analyzed. Fitted linear regression shown, with equation y = 2.63x +7.64 and R2 = 0.87. Linear regression analysis was done for samples pooled from the categories of Fragmented Pollen (2) 1184 and All Other Material Types (6).

2.7 Summary and Conclusions

UV-LIF instruments, including the WIBS, are common tools for the detection and characterization of biological aerosol particles. The number of commercially available instruments regularly deployed for ambient monitoring of environmental particle properties is rising steeply, yet critical laboratory work has been needed to better understand how the instruments categorize a variety of both biological and non-biological particles. In particular, the differentiation between weakly fluorescent, interfering particles of non-biological origin and weakly fluorescing biological particles is very challenging. Here we have aerosolized a representative list of pollen, fungal spores, and bacteria along with key aerosol types from the groups of fluorescing non-biological materials expected to be most problematic for UV-LIF instrumentation.

By analyzing the five WIBS data parameter outputs for each interrogated particle, we have summarized trends within each class of particles and demonstrated the ability of the instrument to broadly differentiate populations of particles. The trend of particle fluorescence intensity and changing particle fluorescence type as a function of particle size was shown in detail. This is critically important for WIBS and other UV-LIF instrumentation users to keep in mind when analyzing populations of unknown, ambient particles. In particular, we show that the pathway of fluorescence particle type change (e.g. A → AB → ABC or B → BC → ABC) with increasing particle size can be one characteristic feature of unique populations of particles. When comparing the fluorescence break-down of individual aerosol material types, care should be taken to

limit comparison within a narrow range of particle sizes in order to reduce complexity due to differing composition or fluorescence intensity effects.

The fluorescence threshold applied toward binary categorization of fluorescence or nonfluorescent in each channel is absolutely critical to the conceptual strategy that a given user applies to ambient particle analysis. A standard WIBS threshold definition of instrument background (FT baseline) + 3σ is commonly applied to discriminate between particles with or without fluorescence. As has been shown previously, however, any single threshold confounds simple discrimination of biological and non-biological particles by mixing poorly fluorescent biological material into nonfluorescent categories, and highly fluorescent non-biological material into fluorescent categories. Previously introduced thresholding strategies were also used for comparison. The Wright et al. (2014) definition was shown to aid in removing non-biological particles such as soot, but that it can also lead to the dramatic underestimation of the biological fraction. The strategy utilized by Toprak and Schnaiter (2013) was to define fluorescent biological particles as those with fluorescent characteristics in FL1 and FL3, ignoring any particles with fluorescence in FL2. They proposed this because FL1 shows excitation and emission characteristics well suited for the detection of tryptophan, and FL3 for the detection of NAD(P)H and riboflavin. However, the study here, along with studies by Hernandez et al. (2016) and Perring et al. (2015), have shown that FL2 fluorescence characteristics (B, AB, BC, and ABC type) are common for many types of biological particles and so

64

removing particles with FL2 fluorescence is likely to remove many bioparticles from characterization.

Any one threshold has associated trade-offs and is likely to create some fraction of both false positive and false negative signals. Here we have shown a systematic analysis of four different fluorescence thresholding strategies, concluding that by raising the threshold to FT + 9σ, the reduction in biological material counted as fluorescent is likely to be only minimally effected, while the fraction of interfering material is likely to be reduced almost to zero for most particle types. Several materials exhibiting outlier behavior (e.g. HULIS 5, diesel soot) could present as false positive counts using almost any characterization scheme. It is important to note that HULIS 5 was one of a large number of analyzed particle types and in the minority of HULIS types, however, and it is unclear how likely these highly fluorescent materials are to occur in any given ambient air mass. More studies may be required to sample dusts, HULIS types, soot and smoke, brown organic carbon materials, and various coatings in different real-world settings to better understand how specific aerosol types may contribute to UV-LIF interpretation at a given study location. We also included a comprehensive supplemental document including size distributions for all 69 aerosol materials, stacked by fluorescent particle type and comparing the FT + 3σ and FT + 9σ threshold strategies. These figures are included as a qualitative reference for other instrument users when comparing against laboratory-generated particles or for use in ambient particle interpretation.

It should be noted, however, that the presented assessment is not intended to be exhaustive, but has the potential to guide users of commercial UV-LIF instrumentation through a variety of analysis strategies toward the goal of better detecting and characterizing biological particles. One important note is that the information presented here is strongly instrument dependent due to fluorescence PMT voltages and gains, specific fluorescence calibrations applied, and other instrument parameters (Robinson et al., 2017). For example, the suggested particle type classification introduced by Perring et al. (2015), will vary somewhat between instruments, though more work will be necessary to determine the magnitude of these changes. Thus, we do not introduce these data primarily as a library to which all other WIBS instrument should be compared rigorously, but rather as general trends that are expected to hold broadly true.

Several examples of strongly fluorescing particles of specific importance to the built environment (e.g. cellulose fibers, particles from cotton t-shirts, and laboratory wipes) show that these particle types could be very important sources of fluorescent particles indoors (i.e. Figs. S4S and S4T). This will also require further study, but should be taken seriously by researchers who utilize UV-LIF instrumentation to estimate concentrations and properties of biological material within homes, indoor occupational environments, or hospitals.

The study presented here is meant broadly to achieve two aims. The first aim is to present a summary of fluorescent properties of the most important particle types expected in a given sample and to suggest thresholding strategies (i.e. FT $+ 9\sigma$) that may be widely

useful for improving analysis quality. The second aim is to suggest key analysis and

plotting strategies that other UV-LIF, especially WIBS, instrumentation users can utilize

to interrogate particles using their own instruments. By proposing several analysis

strategies we aim to introduce concepts to the broader atmospheric community in order to

promote deeper discussions about how best to continue improving UV-LIF

instrumentation and analyses.

Chapter Three: Cluster Analysis of Laboratory Data Including Biological and Interfering Non-Biological Particles

3.1. Aim

Presented here are initial results of a clustering study of laboratory data, more comprehensive than any reported or published study, with the goal to improve characterization and differentiation of different biological types. Previous studies have been published using laboratory-generated PSLs, ambient data, or a small set of laboratory data which includes pollen, fungal spores, bacteria, and dust (Crawford et al., 2016; Crawford et al., 2014; Crawford et al., 2015; Gosselin et al., 2016; Robinson et al., 2013; Ruske et al., 2017). Presented is a unique data set of both biological and non-biological particles, where the unbiased separation of these particles will help train data sets for supervised learning methods, resulting in more accurate clustering and classification of particles. The short-term goal for this study is to input both biological and interfering non-biological data into the clustering algorithm to provide insight on the classification of particles. A longer-term goal is the application of these results to improve ambient data clustering and analysis. Several clustering scenarios were explored. Figure 3.1 outlines the procedure used to generate the cluster product from raw data. The

68

use of the fluorescence particle type classification analysis introduced by Perring et al. (2015) will be used a visual representation for the different clusters generated.
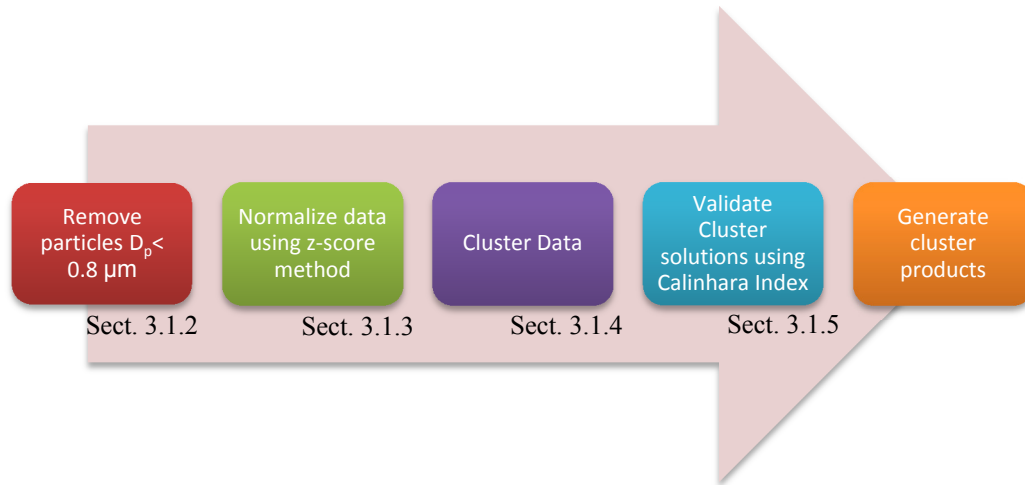
Figure 3.1. Schematic showing the data preparation process resulting in the generated clustering products.

3.2 Chapter Overview

Bioaerosols make up a substantial fraction of atmospheric aerosol and have the potential to negatively impact human and environmental health. In order to predict and improve the impact bioaerosols play on various systems, it is important to identify and characterize these biological particles with more detail. One common method for the detection of bioaerosols is UV-LIF instrumentation, because it can provide detection in near real-time and high size resolution. There are many ways to improve discrimination between particle types by optimizing physical and optical parameters of the instruments. By applying improved data

filtering and particle classification techniques (i.e. fluorescence thresholds; Chapter 2), particle characterization can be further improved. A number of multivariate analysis techniques have also been applied to ambient particle analysis, including principle component analysis (PCA) and several factor and cluster analysis strategies. Recent generations of UV-LIF instruments provide multiple dimensions of data for all particles sampled and secondary analyses such as clustering techniques may provide unbiased insights to the classification of bioaerosols.

This study will focus on one type of unsupervised learning method, which has previously been applied to characterize biological particles. These previous studies, however, primarily focused on the (a) separation of fluorescence particle standards and (b) clustering of ambient data sets (Crawford et al., 2016; Crawford et al., 2014; Crawford et al., 2015; Gosselin et al., 2016; Robinson et al., 2013; Ruske et al., 2017). In previous studies, there has been a limited number of attempts to separate biological particles from interfering particles by clustering methods using controlled laboratory UV-LIF data, or to separate different kinds of biological particles from one another. Presented here are initial clustering results applied to data from a comprehensive WIBS laboratory study, which analyzed a large set of biological and interferring, non-biological particles (see Chapter 2).

3.3 Clustering Introduction

Cluster analysis is a data mining process in which data objects placed in the same group (or cluster) are more similar to one another than to those objects placed in other groups. Clustering techniques can be divided into two central models: (1) supervised and (2) unsupervised learning. Both models have associated advantages and disadvantages. Supervised learning methods allow the "training" of data and grouping to better reflect the data observations (Eick et al., 2004; Ruske et al., 2017). This type of method enhances or "trains" the clustering algorithm in that the output cluster classes are pre-determined rather than discovered, as is the case for unsupervised methods. Supervision requires the user to have appropriate starting conditions to put into the model, which are often difficult or impossible to determine. Supervised training methods are also much more time-efficient compared to unsupervised methods, which is important when analyzing ambient datasets where particle counts (individual objects) can be greater than 10^6 (Ruske et al., 2017). In contrast, unsupervised training methods present less bias and can adapt to unique situations, because the resultant clusters are based on models that have not been previously trained. Supervised methods have certain advantages, however, it is critical to first apply unsupervised models to laboratory data of known particle types in order to gain insight on how these models interpret data input and to learn how we can best train datasets (Ruske et al., 2017).

71

Hierarchical agglomerative clustering (HAC) is an unsupervised learning method and is among the most popular models used for bioaerosol related studies (Crawford et al., 2016; Crawford et al., 2015; Pan et al., 2009; Pan et al., 2007; Pinnick et al., 2013; Pinnick et al., 2004; Robinson et al., 2013; Ruske et al., 2017). Other unsupervised clustering techniques such as k-means, which is not considered a HAC technique, is not ideal for ambient data sets because they rely on user input of the number of clusters used to represent the data, which is not usually known prior to analysis (Ruske et al., 2017). There are several different HAC methods or "linkages" including: Single, Complete, Average, Weighted, Ward's, Centroid, and Median. A brief description of each linkage follows (Crawford et al., 2015; Mullner, 2013) :

- **Single**: The distance between two clusters is the minimum distance between any single data point in cluster A and any single data point in cluster B.

- **Complete**: Same as Single linkage except uses the maximum distance.

- **Average**: The distance between two clusters is the average distance between all data points in cluster A and all data points in cluster B. Each cluster is weighted proportional to cluster size.

- **Weighted**: Same as Average linkage except each cluster is weighted equally, regardless of the size of the cluster.

- **Ward's**: The pair of clusters which yield the minimum in total within cluster variance after merging.

- **Centroid**: The distance between clusters is defined as the distance between the two mean vectors (centers) of the clusters, regardless of the size of the clusters.

- **Median**: Same as Centroid clustering except equal weighting is used to define the centroid of the newly formed cluster.

Several studies have analyzed the clustering efficiency of the linkage strategies described above and have determined that Ward's method performed the best with respect to assignment of aerosol particles into different clusters, and, as a result, this clustering model will be used in the work presented (Crawford et al., 2015; Ruske et al., 2017).

3.3.1 Ward's Clustering Analysis

Ward's method for clustering is among the most popular approaches for HAC and is the only method based on a classical sum-of-squares criterion, minimizing the within-group sum of squares (or variance). The clustering scheme for HAC can be seen in Equation (1) (Mullner, 2013),

$$(1) \qquad \frac{\sqrt{(n_I+n_K)d(I,K)^2+(n_J+n_K)d(J,K)^2-n_Kd(I,J)^2}}{n_I+n_J+n_K}$$

where n_x denotes the size of the clusters, I and J represent two clusters joined into a new cluster, and K represents any other cluster. The input data is given as

vectors in Euclidean space. The detection instrument used in this study is the WIBS-4A, which delivers 5 parameters of information for each individual particle detected (3 fluorescence channels, size and AF), resulting in 5 dimensions of data.

3.3.2 Data Preparation

A particle is considered nonfluorescent in a given channel if its fluorescence intensity does not exceed the threshold applied for that channels. The threshold utilized here is determined using baseline + 3σ and will be discussed further in Section 3.4.2. Fluorescence saturation occurs at 2047 ADC, at which point the PMT reaches its upper limit of detection. A study by Ruske et al. (2017) investigated whether nonfluorescent and/or saturating data points included in the clustering analysis hinders the efficiency of the cluster output. The authors determined that taking out both saturating and nonfluorescent particles of the HAC analysis resulted in a better clustering performance in terms of correctly classifying ambient particles into their assigned groups. Their conclusions were not based on laboratory data using known particles, however, and so in the work presented here, both saturating and nonfluorescent particles were retained. As shown in Chapter 2, many biological particles present a large fraction of particles that saturate the fluorescence detectors or present as nonfluorescent. We decided to keep saturating and nonfluorescent data points in this analysis to limit the underestimation of particles assigned to a given cluster. The lower size detection

limit of the WIBS-4A is ~ 0.8 μm and therefore all particles smaller than this size were removed from clustering.

3.3.3 Data Normalization

Normalization of the raw data is necessary before performing the clustering algorithm, because data parameters delivered from the instrument are measured on different scales. For example, fluorescent intensity values range from 0 to 2050 ADC, size 0 to ~ 20 μm, and AF 0 to 100 units. Crawford et al. (2015) performed Ward's clustering analysis on PSLs using several different normalization techniques, concluding that z-score normalization is the best technique when looking at cluster performance using Ward's linkage for the separation of PSLs. As a result, we utilize the z-score normalization of Ward's linkage HAC for the presented study. In this type of normalization, the mean value of all data points is subtracted from each individual data point, and then each data point is divided by the standard deviation of all points. Standarization using the z-score method compares results to a normal (Gaussian) population, and it therefore relies on the assumption that iput data can be described by a normal distribution (Gordon, 2006).

3.3.4 HAC Scenarios

The WIBS is a fluorescence-based instrument, used for the detection and characterization of PBAPs. However, the instrument can misidentify biological particles due to weakly fluorescing, non-biological interfering particles. To

75

achieve optimal results from the clustering analysis, data must be input into the clustering algorithm with a careful understanding that data preparation can significantly change results. To aide in choosing the most appropriate set of input conditions, a total of 6 clustering scenarios were explored in this study, with conditions summarized in Table 3.1. The scenarios vary in regards to (i) whether fluorescence is normalized by size and (ii) whether the data were input in logarithmically spaced bins to produce a normal distribution. Hierarchical agglomerative clustering gives the best results if (1) all variables are independent of one another and (2) variables result in a normal (Gaussian) distribution (Norusis, 2011).

Ambient particle distributions are well known to exhibit lognormal distributions. Further, fluorescence intensity has been shown to scale with particle size (Hill et al., 2001; Sivaprakasam et al., 2011). Several previous studies attempted to utilize HAC for ambient data log-distributed particle size data (Crawford et al., 2014; Crawford et al., 2015; Robinson et al., 2013), but applied the assumption that particle fluorescence is normally distributed. If this assumption does not hold correct, however, weakly fluorescing particles will likely be grouped into a single cluster, based on the high abundance of these particles (Robinson et al., 2013). The study presented here uses known laboratory samples as inputs, and not an ambient data, and therefore many weakly fluorescing, interfering particles are expected to have lognormal distribution for

the fluorescence parameters. Ambient data sets have both fluorescent and

nonfluorescent particles, however, a laboratory sample of dust would primarily

have nonfluorescent characterisitics, resulting in a log-normal distribution of

fluorescence intensities. Scenarios C, D, and E normalize fluorescence to size to

explore this concept. Scenarios B and D take into account the normal distribution

data of all variables (AF, size, 3 channels of fluorescence information). In

comparison, scenarios E and F look at the log-spaced distributions of size and AF

and keeping the assumption that the fluorescence output is normally distributed.

Table 3.1. Six scenarios varying in fluorescence normalization and variables
logged to produce a normal distribution.

Parameters	A	B	C	D	E	F
1. Fluorescence Normalization 2. Variables Logged	1.No 2.No	1. No 2. Yes	1. Yes 2. No	1. Yes 2. Yes	1. Yes 2. Yes, only AF/Size variables	1. No 2. Yes, only AF/Size variables

3.3.5 Cluster Validation

To determine the optimal number of clusters, the Calinski-Harabasz criterion

(CH; Calinhara index) was used. This validation method measures how well-

separated a cluster is from other clusters based on the overall between-cluster

variance versus the overall within-cluster variance. The CH index is calculated

using Equation (2) (Liu et al., 2010).

$$(2) \qquad \sum_i \frac{n_i d^2(c_i c)/(NC-1)}{\sum_i \sum_{x \, E \, C_i} d^2(x,c_i)/(n-NC)}$$

77

where n represents the number of objects in data set, c the center of data set, NC the number of clusters, c_i is center if the ith cluster, and d is distance between x and y. For each clustering output the Calinhara index was calculated for cluster solutions with one through ten clusters, and the solution with the highest CH value was generally determined to be the optimal number of clusters.

3.4 Materials and Methods

All materials utilized, including the vendors and sources from where they were acquired, have been listed in Appendix A, Table A.1. Details of size and fluorescence properties of particles utilized for this chapter are also shown in Table 2.2. Aerosolization procedures follow the same experimental design for fungal spores and powder in Chapter 2, Section 2.2.1. The clustering analysis was done using the open-source software R package fastercluster (Mullner, 2013; R Core Team, 2011). The WIBS-4A is a commonly used UV-LIF based instrument for the detection and characterization of biological particles. This instrument was used to collect 3 channels of fluorescence information (FL1, FL2, and FL3), particle size, and particle asymmetry for each interrogated particle. For more information on the design, operation and calibration of this instrument see Chapter 2, Section 2.1.

3.4.1 WIBS Data Analysis

The fluorescence threshold of the 3 channels (FL1, FL2 and FL3) is calculated using baseline + 3σ, where the baseline is determined by measuring the

fluorescence in the 3 channels when there are no particles present in the optical chamber (see Chapter 2, Section 2.4.1 for more details). The fluorescence characteristics of a particle in a given channel can be classified into 7 different particle types (Perring et al., 2015) as depicted in Figure 2.1.

3.5 Cluster Products

3.5.1 Overview of Clustering Process

Hierarchical clustering methods work by grouping objects from the bottom up, meaning that each object starts as its own "cluster," and clusters are merged together based on similarities until a greatly reduced number of clusters are presented as a final solution. Presented here are three different clustering trials: (1) *Aspergillus niger* (Fungi 2) vs. diesel soot (Soot 4), (2) *Aspergillus niger* vs. *Saccharomyces Cerevisiae* (Fungi 4)*, (3) *Aspergillus niger* vs. California sand (Dust 2). During each trial, a given number of particles from each material type was placed into a conceptual pool before running through the algorithm to organize clusters. The output of the algorithm also reports the group each particle was input from in order to evaluate the accuracy of the clustering. Trial 1 was chosen to summarize the clustering process of the six scenarios described in Table 3.1. The clustering process includes (i) the determination of the optimal number of clusters for each scenario, (ii) evaluation of cluster performance based on particle assignment and cluster composition, and (iii) visual representations of cluster ouputs using particle type classification introduced by Perring et al.

79

(2015). The next two clustering trials were chosen to demonstrate the ability of the HAC method to separate particle types that could be misinterpreted as the same type of ambient particle type. Eventually, the comprehensive lab data discussed in Chapter 2 will be run more systematically through the clustering algorithm. These trials represent the initial steps in this process.

3.5.2 Clustering Process, Trial 1: *Aspergillus niger* vs. Diesel Soot Particle Cluster Input Properties

The clustering process is demonstrated here first using an input mixture of 27,759 *Aspergillus niger* (Fungi 2) particles and 5,657 diesel soot (soot) particles. Diesel soot is commonly observed in almost all atmospheric samples that have some level of anthropogenic influence, and because it has fluorescence characteristics similar to small biological particles, when excited by photons with a wavelength of 280 nm, diesel soot can be misinterpreted as being biological in nature using WIBS data (Pöhlker et al., 2012). Particle size distributions representing the distributions input into the clustering trial, stacked by fluorescent particle type, are shown in Figure 3.2 for both Fungi 2 and diesel soot. It can be seen that both particle materials have predominantly particle type A characteristics, meaning that they are fluorescent in only channel FL1 (Figure 2.1). The fungi material also presents a small amount of both AB and non-fluorescent characteristics. The size distribution of Fungi 2 peaks at ~ 3 µm, whereas soot peaks at ~ 1 µm in size. Fungi 2 exhibits moderately higher FL1

channel fluorescence, with a median of 523 ADC, whereas soot exhibits a median

of 751 ADC in this channel. Both particles show almost no fluorescent

characteristics in either FL2 or FL3 (see Table 2.2). In summary, the particle

distributions are relatively similar in fluorescence particle type and their

differences are largely related to particle size, so separation of these particles

through Trial 1 was originally thought to represent a relatively challenging initial

exercise.
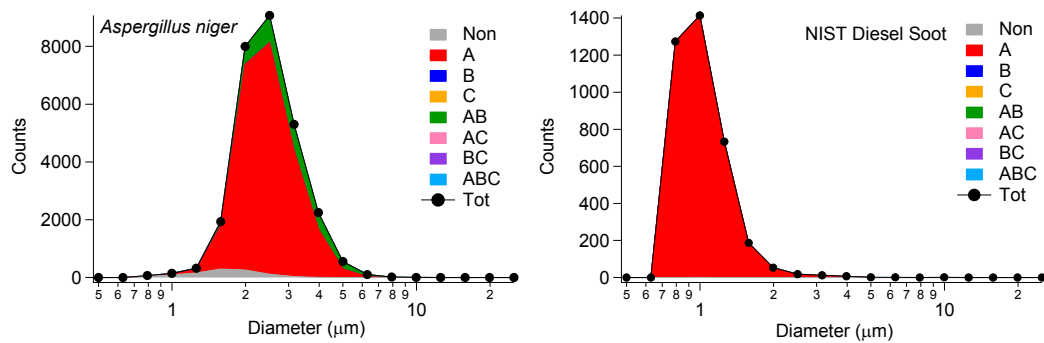
Figure 3.2. Trial 1: Particle type stacked size distributions for *Aspergillus niger* and diesel soot using FT + 3σ threshold. These data represent a summary of input parameters to the HAC.

Optimizing number of output clusters

An important feature of HAC is that it provides clusters in an unsupervised

manner, and the user must determine the number of clusters that makes physical

sense. One useful tool to systematically determine the optimal number of final

clusters is the Calinhara (CH) index, which uses the interclass-intraclass distance

ratio. A set of clustering solutions that have been solved rationally will typically

show a generally negative slope of CH index versus the number of clusters (e.g. Fig. 3.3). The negative slope is a result of clustering performance increasing as the number of cluster solutions decreases. The optimal cluster solution is defined by the highest CH value present. In this trial, two different populations of essentially homogeneous particle materials were input into the clustering algorithm, and as a result a higher number of cluster solutions is not as desirable for this trial. Scenario A and F each show a solution for which the CH index suggests the optimal number of cluster to be greater than 6, which suggests these trials did not perform well using the input data. These two scenarios also present positive slopes for the CH cluster validation (Figure 3.3), indicating that intercluster-intracluster variance ratio is high for a small number of cluster solutions.

While the CH index is an important tool to estimate the ideal number of clusters, it only does so approximately and therefore, complimentary tools of investigation must be applied to determine the best cluster solution. In particular, here we have analyzed the properties of each cluster and compared them with input properties in order to qualitatively test the clusters. This type of secondary analysis was done on 4, 3, and 2 cluster solutions for each scenario, because the CH index estimated the optimal number to be 2 or 3 clusters for all scenarios, disregarding scenario A and F, as discussed above.

Figure 3.3. Trial 1: Calinhara index to determine the optimal number of clusters for each scenario, where the highest value indicates the best solution.
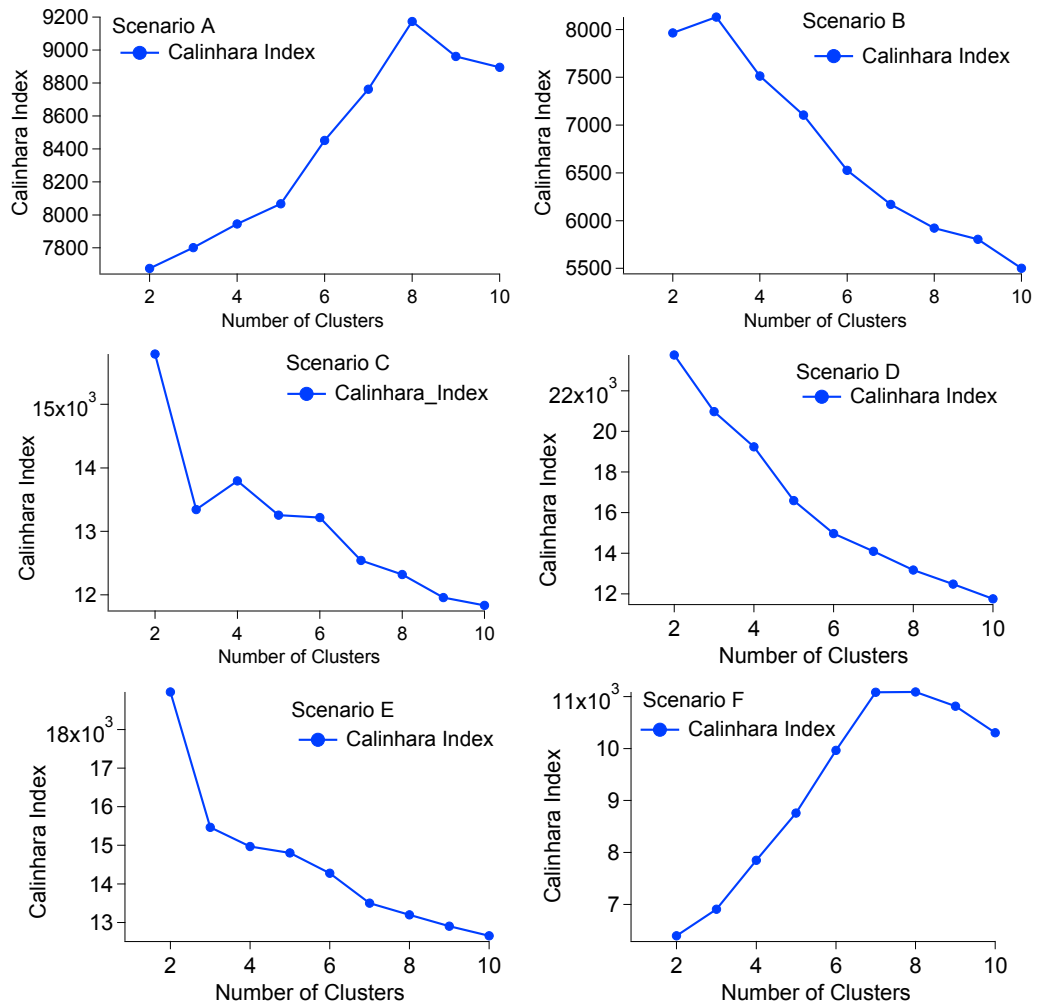
Optimal cluster solution

As a way of visualizing the quality of clustering solutions, Figures 3.4 (2-cluster solution), 3.5 (3-cluster), and 3.6 (4-cluster) summarize two important pieces of information for each scenario (Table 3.1). At the bottom of each panel shows the total input particles for a given trial and scenario, with individual particle populations separated by color. For each cluster the total number of particles is shown by the size of the horizontal bar and the percentage of particles in that clustering belonging to a given input population is listed as a number. Scenarios A and F provide similar output clusters and do a poor job of accurately separating the input populations, as was expected given the discussion above about CH index results. This can be seen in the 2- and 3-cluster solutions in that cluster 1 for each mixes ~80% fungal spores with ~20% soot. In the A, B, and F scenarios, fluorescence is not normalized by size. For scenario A, no variables are logged, whereas in scenario B all variables are logged, and in scenario F only AF and size parameters are logged to produce a normal distribution.

Scenarios A and F were determined to be suboptimal, because both scenarios suggest the number of clusters to be 7 or greater. Scenarios B, C, D and E were explored further to determine which performed the best in terms of clustering efficiency. Raw counts for each particle material for this trial for 2, 3 and 4-cluster solutions can be seen in Appendix B, Table B.1. By comparing solutions from the 3- and 4-cluster solutions for scenario B (Figure 3.6 and 3.5,

84

respectively), the results are generally similar. Cluster 2 is 99.5% diesel soot in both cases, and the othe clusters are dominated by fungal particles. As the number of clusters is reduced from the 4-cluster to 3-cluster solutions, cluster 3 (4-cluster) is merged into cluster 1. The composition of cluster 1 changes only slightly from 99.9% fungi (4-cluster) to 99.5% fungi (3-cluster). This trend for the merging of clusters can also be seen from the 3-cluster to the 2-cluster solutions, where clusters 3 and 1 in the 3-cluster solution (Figure 3.5) combine to form the cluster 1 in the cluster 2-solution (Figure 3.4). Looking further into the 2-cluster solution, the two particle types were sufficiently separated, with cluster 1 comprised of 99.3% fungi particles and cluster 2 comprised of 95.5% of diesel particles. In general, the 2-cluster solutions perform best, in that the final cluster compositions are relatively pure. It is important to note, however, that while two materials were aerosolized and input into the clustering algorithm, it is possible that one or both types of material could present additional populations of particles (i.e. fungal spores, hyphae, etc.). In this case it is possible that a 3-cluster solution may make more sense, because the two different kinds of fungi particles would not be conflated into one cluster. In order to explore this idea, a secondary analysis would need to be done to determine the number of different populations in each particle material, therefore, we present a summry of results using the assumption that only two broad populations of particle exist as inputs.

85

Scenario B, 2-cluster solution presented optimal results. Cluster 1 was comprised predominantly of fungi particles and presented qualitative traits similar to the input fungal particles, whereas cluster 2 was comprised predominantly of soot particles. Looking at particle type stacked size distributions of the cluster output (Figure 3.7), the fluorescence and size characteristics of cluster 1 are similar to that of *Aspergillus niger* in Figure 3.2. Cluster 1 also shows AB characteristics and presents nonfluorescence characteristics. Cluster 2 is in the size range of diesel soot (Figure 3.2) and shows mainly A type characteristics. There are some AB characteristics present in cluster 2 at ~1.8 μm in size and greater, these particles are most likely the missed assigned fungi particles, because diesel soot doesn't have AB characteristics. Scenario B results will be presented for the remainder of the trials, because of its out-performance compared to the other scenarios in regards to particle assignment and cluster composition.
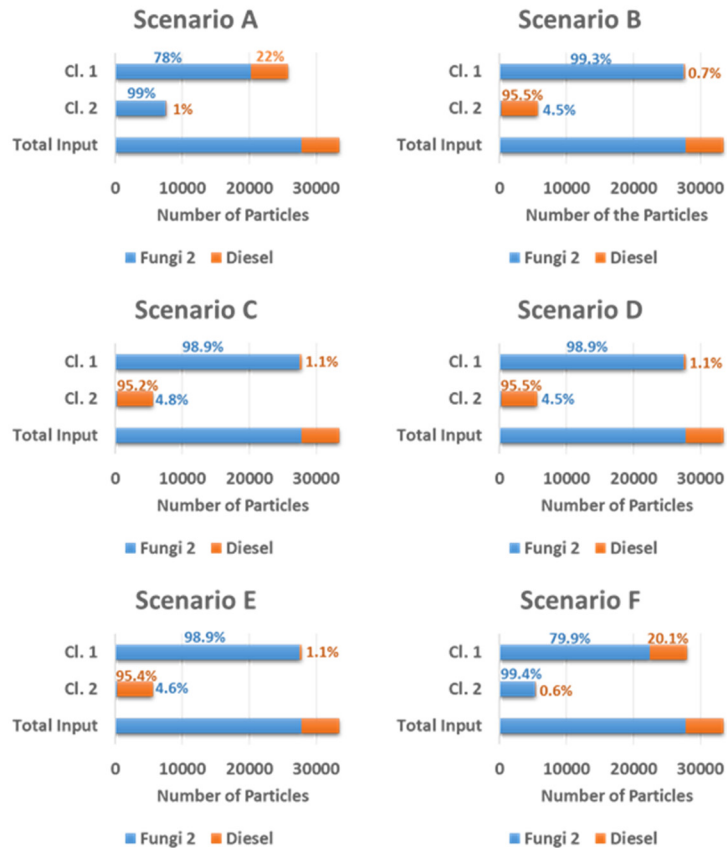
Figure 3.4. Trial 1, 2-Cluster solution: Particle counts and percent cluster composition for 2-cluster solution for each scenario to qualitatively determine the best performing scenario. The length of the bar gives information on particle counts and the percentage listed gives the cluster composition.
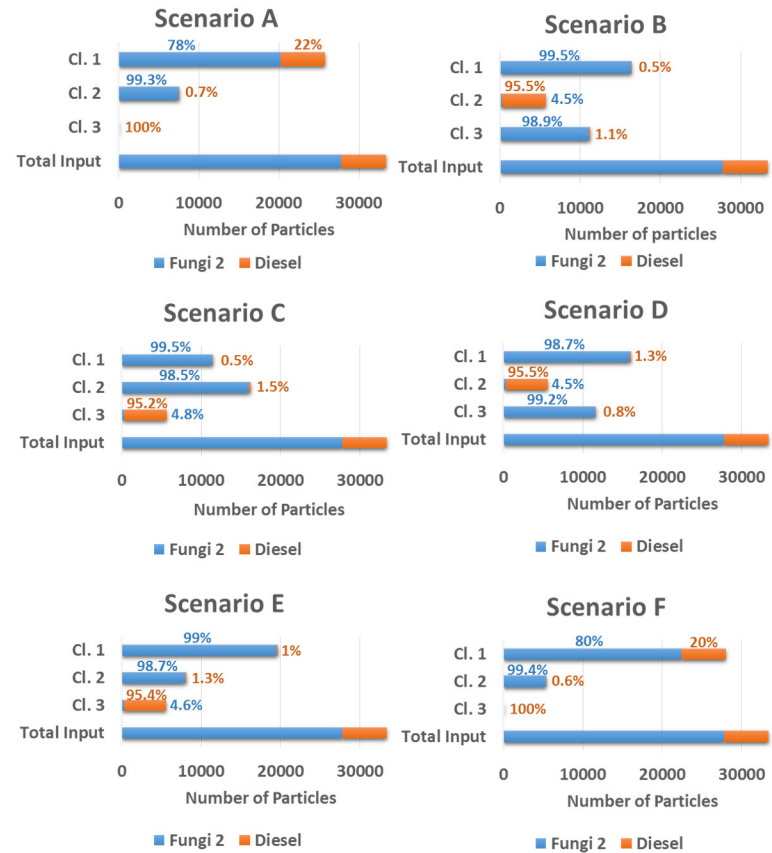
Figure 3.5. Trial 1, 3-Cluster solution: Particle counts and percent cluster composition for 3-cluster solution for each scenario to qualitatively determine the best performing scenario. The length of the bar gives information on particle counts and the percentage listed gives the cluster composition
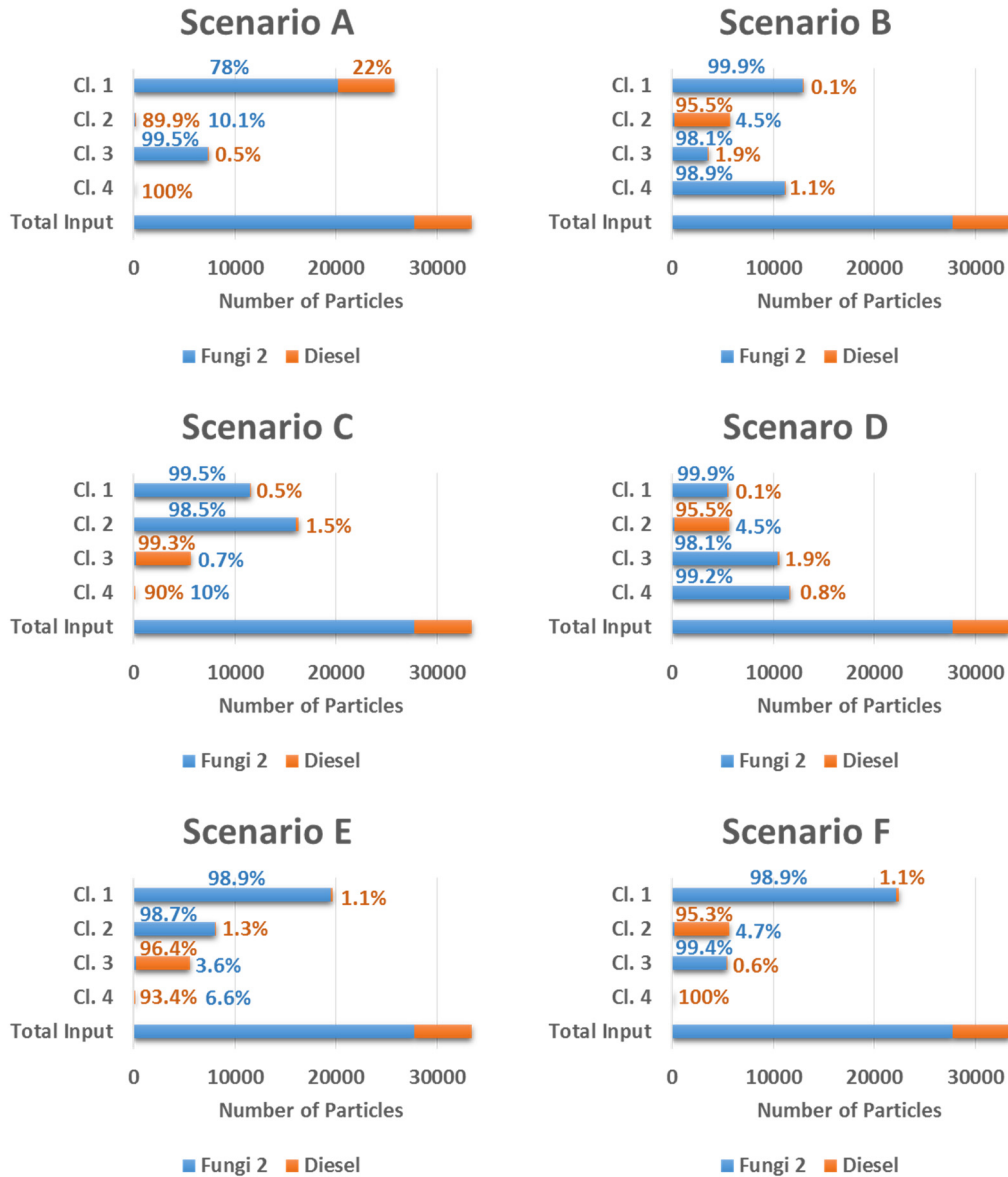
Figure 3.6. Trial 1, 4-Cluster solution: Particle counts and percent cluster composition for 4-cluster solution for each scenario to qualitatively determine the best performing scenario. The length of the bar gives information on particle counts and the percentage listed gives the cluster composition
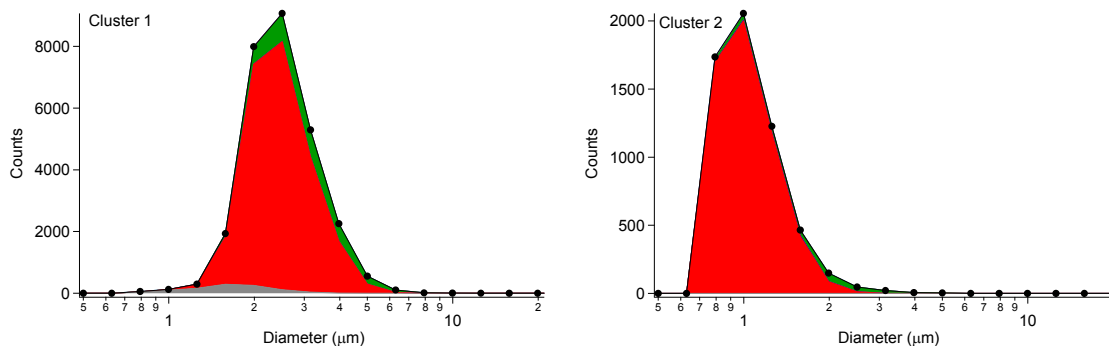
Figure 3.7. Trial 1: Particle type stacked size distributions for the 2-cluster solution for scenario B, using FT + 3σ threshold.

3.5.3 Trial 2: *Aspergillus niger* vs. *Saccharomyces cerevisiae*

Using Trial 1, scenario B was shown to optimally separate one biological particle type from an exemplary interfering non-biological particle type that showed similar fluorescing properties. Given the success of that trial and the justification for using scenario B, therefore, the subsequent analyses was simplified and only the results from scenario B are shown (logged variables, no fluorescence normalization, Table 3.1). Trial 2 was designed to separate two different types of biological particles (both fungal spores) using the HAC algorithm.

The two biological particles chosen were *Aspergillus niger* (Fungi 2) nd *Sacchoromyces niger* (Fungi 4). Particle type stacked category plots for each particle material can be seen in Figure 3.8. These represent one visualization of the input data for clustering Trial 2.
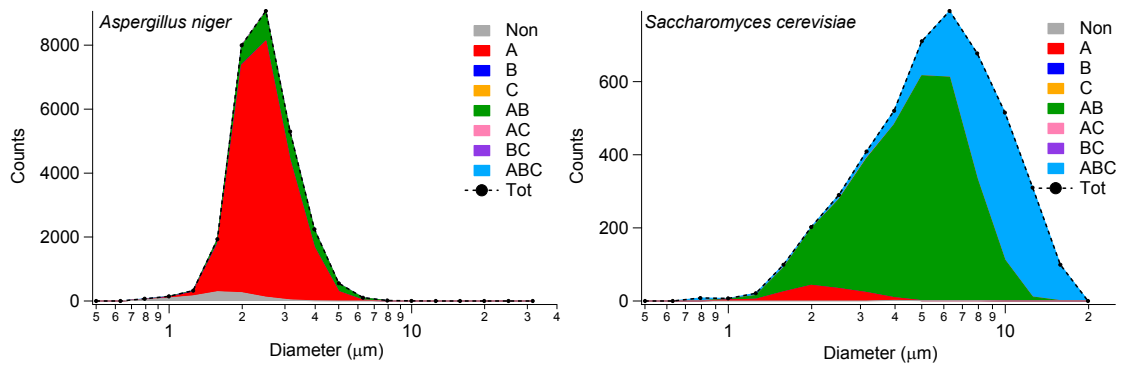
Figure 3.8. Trial 2: Particle type stacked size distributions for *Aspergillus niger* and *Saccharomyces cerevisae* using FT + 3σ threshold. These data represent a summary of input parameters to the HAC.

Fungi 4 has a broad size distribution, ranging from ~ 1.2 µm to 20 µm and peaking at ~ 7 µm in size. The particle type fluorescence characteristics present in Fungi 4 are A, AB, and ABC. As described in Trial 1, the size distribution of Fungi 2 peaks at ~ 3 µm and shows predominantly A type particles with some AB fluorescence characteristics.

The Calinhara index estimated the optimal number of cluster solutions for scenario B to be 2 (shown in Appendix B, Figure B.1). Particle count and percent cluster composition can be seen in Figure 3.9 for the 2-cluster solution. Raw particle counts for Cluster 2, 3 and 4 solutions can be seen in Appendix B, Figure B.2.

90
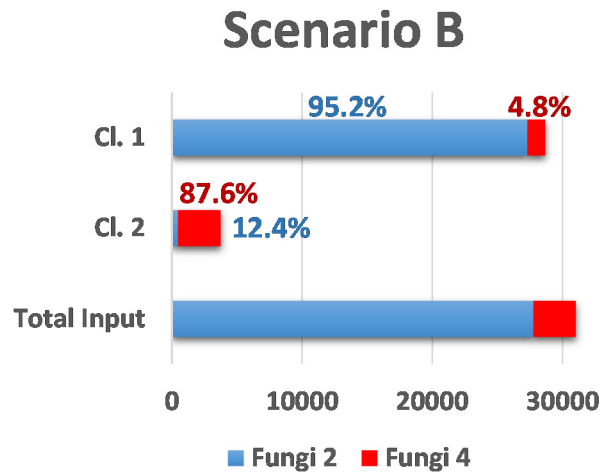
Scenario B

Figure 3.9. Trial 2: Particle counts and cluster composition of scenario B, 2-cluster solution. The length of the bar gives information on particle counts and the percentage gives the cluster composition.

Cluster 1 is predominantly Fungi 2, comprising 95.2% of the cluster, while cluster 2 is comprised of 87.6% of Fungi 4. The particle type stacked size distribution of the cluster output data (Figure 3.10) shows that cluster 2 has similar fluorescence characteristics as *Saccharomyces Cerevisiae* (Fungi 4) (Figure 3.8), however size characteristics differ in that the raw data has a wide size range whereas, cluster 2 has a limited particle population below 3 µm. Cluster 1 stacked size distribution (Figure 3.10) shows similar fluorescence and size characteristics to the raw distribution of *Aspergillus niger* (Fungi 2) (Figure 3.8) and even has the nonfluorescent population represented.
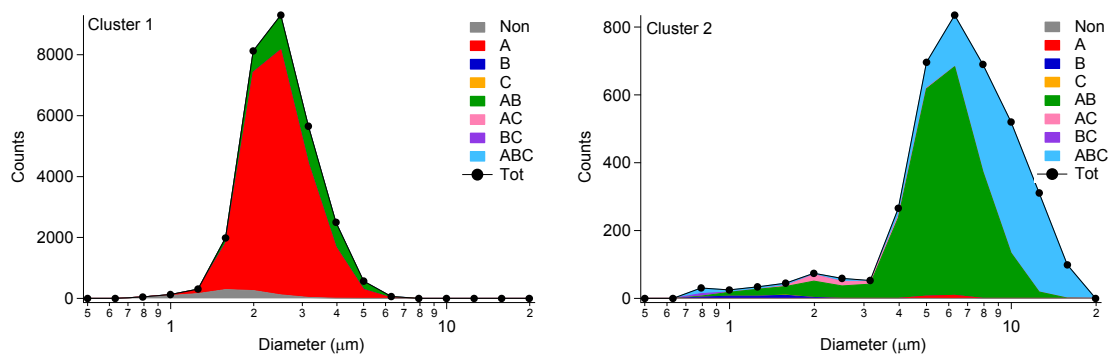
Figure 3.10. Particle type stacked size distributions for cluster 1 and cluster 2 outputs for the 2-cluster solution, scenario B using FT + 3σ threshold.

Scenario B, cluster 2 solutions performed well in terms of separating two different fungal materials. Size plays a significant role in the clustering efficiency, as this trial clustering result shows discrepancies from the cluster output data in comparison to the raw data.

3.5.4 Trial 3: *Aspergillus niger* fungal spores vs. California sand

After testing the clustering algorithm's ability to separate (1) a biological and non-biological particle with similar fluorescence and size characteristics and (2) two biological particles with different fluorescence and size characteristics, the next scenario was to test the separation ability of a fluorescence biological particle and non-fluorescence, non-biological particle. From the study presented in Chapter 2, California sand was shown to have predominantly non-fluorescence characteristics and a broad size distribution, as seen in Figure 3.11.
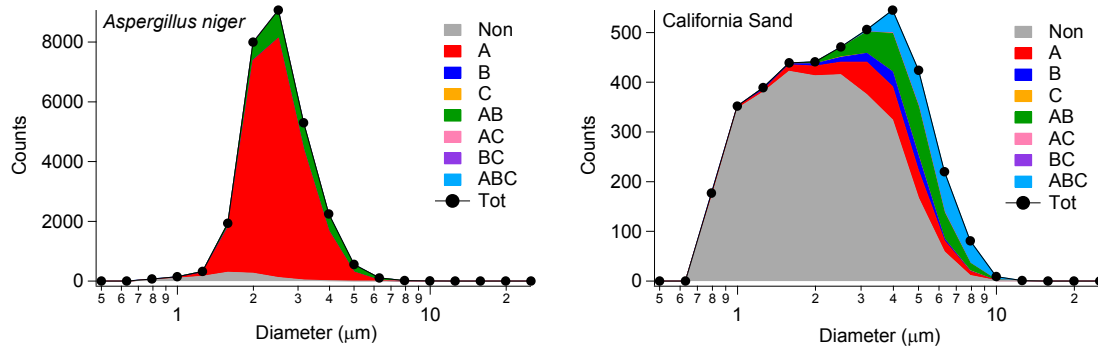
Figure 3.11. Trial 3-Particle type stacked size distributions for *Aspergillus niger* and California sand, using FT + 3σ threshold.

The Calinhara index determined the best cluster solution to be 2 for scenario B (Appendix B, Figure B.2). However, looking at the particle counts and percent composition of each cluster of the 2-cluster solution in Figure 3.12a, cluster 1 and cluster 2 are both dominated by fungi particles, but with 13% influence from dust, resulting in poor overall separation between the two particles materials. Therefore, this type of composition analysis was done for the cluster 3 solution to see if the two particle materials could be separated (Figure 3.12b). For the 3-cluster solution, cluster 1 and 3 were dominated by fungi particles, comprising 87.2% and 99.9% of the clusters. Cluster 2 was dominated by dust particles, comprising 82.4% of the cluster. Raw particle counts for 2, 3, and 4 cluster solutions for each scenario can be seen in Appendix B, Table B.3.
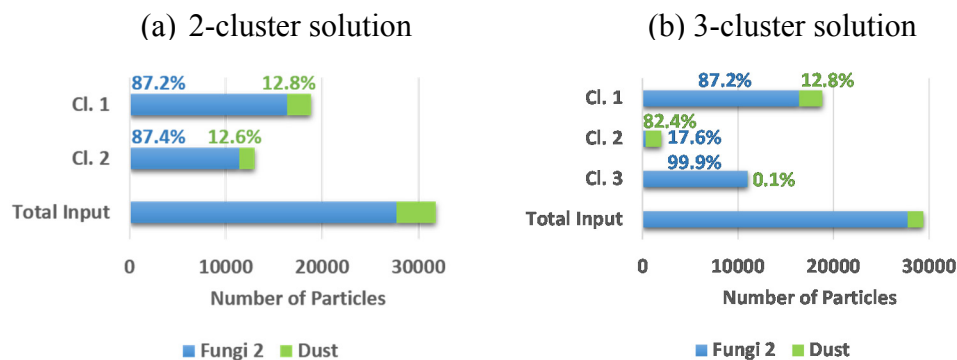
Figure 3.12 Trial 3- Particle counts and cluster composition of scenario B, 2-cluster solution (left) and 3-cluster solution (right). The length of the bar gives information on particle counts and the percentage gives the cluster composition.

Particle type stacked size distributions for the output clusters generated and are present in Figure 3.13. Cluster 1 and 2 have similar size and fluorescence characteristics as *Aspergillus niger* (Fungi 2) (Figure 3.11). Cluster 2 has similar fluorescence characteristics as California dust (Figure 3.11), however, the size distribution is not as broad as the raw data distribution and shows a limited number of particles under ~ 2 μm in size. The nonfluorescent fraction of particles that were suppose to be present in cluster 2, were misassigned and placed in cluster 1.
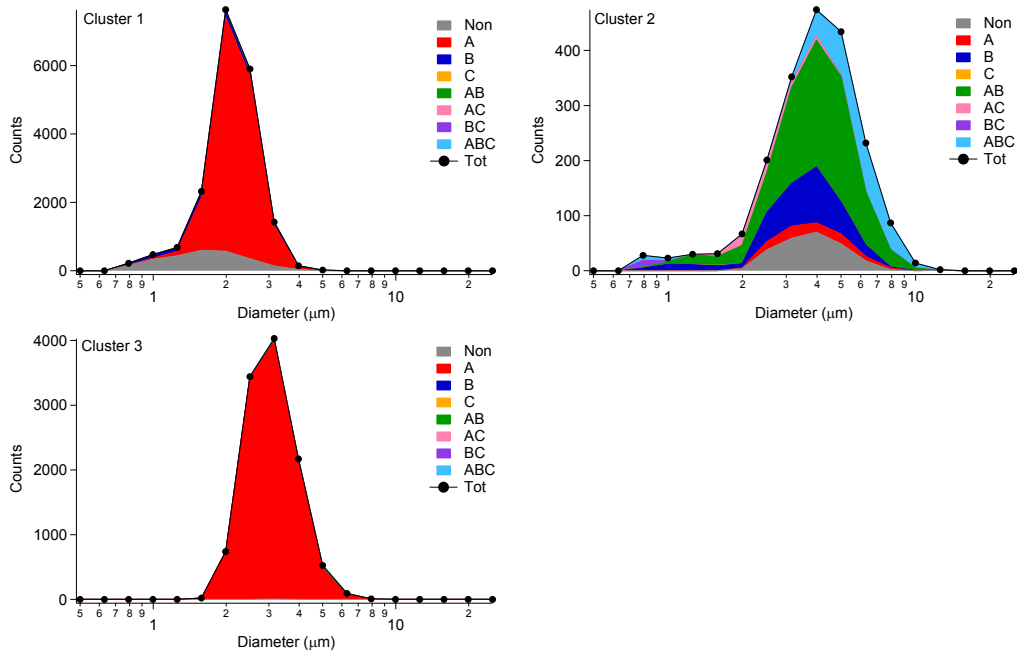
Figure 3.13. Trial 3: Particle type stacked size distributions for cluster 1, 2 and 3 outputs for scenario B, using FT + 3σ threshold.

The separation trial of *Aspergillus niger* vs. California sand performed the worst of the three trials in terms of percent cluster composition and particle counts. Previous bioaerosol clustering studies have found that taking out both saturating and nonfluorescent particles before clustering improved the separation output (Crawford et al., 2015; Ruske et al., 2017). Table 3.2 shows median values for each of the five parameters observed from the WIBS. It can be seen in the table that California sand has little fluorescence characteristics in any of the three channels and has similar size and fluorescence signatures as cluster 2 product. *Aspergillus niger* has a smaller median diameter compared to California sand, and has a higher FL1 fluorescence signature, which is also presented by cluster 1 and cluster 3. Median values are presented in Table

95

3.2, however, *Aspergillus niger* has fluorescence characteristics ranging from

nonfluorescing particles to saturating particles in the FL1 channel. The highly fluorescent

particles in FL1 have been assigned to cluster 3, increasing the median value. Looking at

the 3-cluster solution for Figure 3.12, most of the California sand particles were assigned

to cluster 2, however, ~13% of the particles were assigned to cluster 1, where weakly

fluorescent fungi particles were assigned. The significant amount of nonfluorescing

particles may have negatively impacted the separation ability of the clustering algorithm.

In the future, to test this hypothesis, all nonfluorescent particles that don't exceed the

standard FT + 3σ threshold for fluorescence for any of the three channels will be

excluded from the analysis.

Table 3.2. Trial 3: Median values for each of the five input data parameters for *Aspergillus niger*, California sand, and the output data parameters for the cluster products.

	Diameter (µm)	AF (a.u.)	FL1 (ADC)	FL2 (ADC)	FL3 (ADC)
Asper. Niger	2.7 ± 0.9	17.1 ± 10.7	543	18	29
Cali Sand	4.0 ± 1.9	18.1 ± 14.6	66	42	31
Cl. 1	2.4 ± 0.6	11.75 ± 7.0	301	18	29
Cl. 2	4.6 ± 1.8	22.9 ± 12.0	87	52	35
Cl. 3	3.4 ± 0.8	25.4 ± 9.3	860	19	29

3.6 Summary and Conclusions

UV-LIF instrumentation, including the WIBS, are common tools for the detection of

bioaerosols. These commercially available instruments have been used to study various

environments, including in indoor and outdoor settings. However, more work needs to be

done to better understand how the UV-LIF community can categorize both biological and

non-biological particles. Hierarchical agglomerative clustering techniques can provide

the unbiased separation of particles based on similarities between data observations.

Previous studies have used HAC to determine the separation efficiency mainly

focusing on (i) PSLs with different size and fluorescence properties and (ii) ambient data

sets. Studies have also used HAC methods for the clustering of ambient data sets using

finely resolved fluorescence bins (Pan et al., 2009; Pan et al., 2007; Pinnick et al., 2013;

Pinnick et al., 2004). Here, we presented the initial results of a comprehensive laboratory

clustering study, looking at several data preparation scenarios for trials involving the

separation of (1) a biological particle and non-biological particle with similar fluorescent

properties (2) two biological particles with different fluorescence characteristics and (3) a biological particle and nonfluorescent, non-biological particle.

Scenario B (all data variables logged, fluorescence not normalized to size) was shown to optimally separate one biological particle type from an interfering non-biological particle type that showed similar fluorescing properties, and therefore was used for the remainder of the clustering trials. The optimal clustering solution was determined for each trial using the Calinhara Index.

Of all trials that were explored throughout this study, trial 1 had the best separation efficiency, with an optimal cluster solution of 2, resulting in cluster 1 comprising of 99.3% of Fungi 2 particles and 95.5% of cluster 2 being diesel particles.

Since trial 1 efficiently separated two particles with similar fluorescent properties, the next trial chosen also involved two fluorescent particle materials, but with different fluorescing properties. The two biological materials were discriminated from one another with 95.2% of the particles in cluster 1 predominantly being Fungi 2 and 87.6% of the particles in cluster 2 being Fungi 4. The misassignment of particles to clusters seemed to be due to size, where cluster 1 consisted of particles with a smaller size distribution in comparison to cluster 2.

Trial 3 involved the separation of a fluorescent biological material and a nonfluorescent, non-biological material. This trial performed the worst in terms of separation efficiency between the two particle types, with the optimal number of clusters being 3. Studies suggested taking out both saturating and nonfluorescent particles

98

resulted in better clustering performance (Crawford et al., 2015; Ruske et al., 2017). However, some biological particles have both particles that saturate the detector or have nonfluorescent properties, and to prevent underestimating the presence of bioparticles, both characteristics were kept in this clustering study.

Future work may include removing nonfluorescent and/or saturating particles and determining how efficient the algorithm was on discrimination between particles. The Calinhara Index is a useful tool in helping determine the optimal number of cluster solutions to use for a given clustering trial. However, this process may be somewhat subjective and it's difficult to know whether a further cluster split is a result of a "new" and fundamentally different cluster, or if it is just splitting one set of particles into two groups somewhat arbitrarily, therefore, more work needs to be done to understand how to systematically chose the optimum number of cluster solutions, reducing subjectivity.

Chapter Four: Conclusions

4.1 Thesis Summary

Bioaerosols can make up a substantial fraction of atmospheric aerosol mass and present a diverse population. They have the potential to be pathogenic, allergenic, infectious, or toxic in both viable, non-viable, whole, and fragmented forms. Bioparticles can travel long distances from their point of origin, and thus can negatively impact human and environmental health. The detection and identification of these biological particles is important to help investigate complex processes within many environmental systems and to alert against potentially harmful aerosols. Previous detection methods used offline techniques and can greatly underestimate the concentration of biological particles. The benefits of using UV-LIF instrumentation include the real-time detection of fluorescent particles with high time- and size- resolution. One of the most commonly explored UV-LIF instrumentation is the WIBS, which has been applied in various indoor, outdoor, and occupational environments as described in Section 2.1. This instrument delivers 5 data parameters including both physical and chemical information that can be used for the characterization of biological particles. There are many potential interfering, non-biological particles with similar fluorescing characteristics that can greatly impact the detection of bioaerosols. The overall goal for this thesis was to suggest different

analysis and thresholding strategies for UV-LIF users in the hopes to better detect and characterize biological particles.

4.2 Particle Type Category Analysis and Thresholding Strategies

This thesis presents the first comprehensive and systematic laboratory study of WIBS-4A data, intended to help the data interpretation of commercial available UV-LIF instrumentation. Presented here was a detailed analysis of 69 particle materials, including (1) biological: fungi, pollen and bacteria and related biofluorophores and (2) non-biological particles: dust, HULIS, brown carbon, PAHs, combustion soot and smoke. We demonstrated that the WIBS can broadly separate different particle materials based on raw data outputs. We also showed a detail analysis of changing fluorescence intensity and particle type as a function of size, which is important to be aware of when looking at ambient data sets.

The threshold used to define the particle type categorization is crucial, with the default threshold being $FT + 3\sigma$, and has been commonly used as a threshold to discriminate between biological and non-biological particles. This work presents a detailed thresholding analysis of $FT + 3, +6$, and $+9\sigma$ and how the threshold impacts the fluorescence fraction of biological and non-biological materials as well as particle type classification. We concluded that $FT + 9\sigma$ may be useful to discriminate between bio- and non-biological particles, because the influence on the fluorescence fraction of bioparticles is relatively small and the reduction in interference from some types of non-biological particles can be significant.

101

One important issue currently facing the UV-LIF instrumentation community is the difficulty of comparing between WIBS instruments due to subtle variations in detector sensitivity, which is a function of PMT voltage. Polystyrene spheres are commonly used as standard particles for fluorescent analysis, but their use can be problematic because the fluorescence characteristics of PSLs can vary between batches and also degrade over time. This makes it difficult to know how results from an individual instrument compare to results from the same instrument after some time or to another, identical instrument. Recently, a new fluorescence calibration technique introduced by Robinson et al. (2017) uses mixed tryptophan–ammonium sulfate particles to calibrate FL1 and pure quinine particles to calibrate FL2. However, to our knowledge there is still no fluorescence calibration method for the FL3 channel of the WIBS and further work needs to apply this method to two WIBS instruments, ensuring an absolute value for each channel can be obtained to allow for comparison.

Specifically, here we suggest using FT + 9σ to help better discriminate between bio- and interfering, non-biological particles. However, applying one threshold may not be the final answer to this detection goal. For example, not all thresholds for the three output channels need to follow the FT + 9σ algorithm. A size dependent threshold may also be useful in helping to filter out large non-biological particles. It is well known that fluorescence is strongly influenced on particle size, however, there is no commonly applied fluorescence calibration technique that take this into consideration.

Lastly, the analysis strategies presented may be biased in that an individual applies a threshold and qualitatively determined the particle material. However, data mining techniques such as clustering algorithms can eliminate this issue by grouping data observations together based on similarities.

4.3 Clustering Analysis

Hierarchical agglomerative clustering techniques provide unbiased methods for the separation and characterization of different particle materials. The characterization of biological particles using UV-LIF instrumentation is an on-going scientific goal of the atmospheric community. UV-LIF instrumentation provides multiple parameters of data for each interrogated particle, making it difficult for a user to interpret large data sets of unknown data. Presented in this thesis were initial results of a comprehensive laboratory clustering study looking at the separation ability of both biological and interfering particles, with the hopes to learn how to best prepare data before inputting into the algorithm.

Six scenarios were explored throughout this detailed clustering analysis, all varying with whether fluorescence was normalized to size and if/what data variables were logged to produce a normal distribution. Scenario B (all data variables logged, fluorescence not normalized to size), was determined to be the best performing in terms of cluster composition. The optimal number of cluster solutions for each scenario and trial was determined using the Calinhara Index, based on the intercluster-intracluster variance ratio.

We demonstrated that the clustering algorithm can efficiently discriminate between a biological particle and a non-biological particle (trial 1) with similar fluorescence and size properties. Diesel soot is a known interfering particle due to its fluorescence characteristics similar to that of biological particles when excited by 280 nm. Visual representations using particle type stacked category size distributions showed qualitative fluorescence information for each generated cluster that could then be compared to input data. However, the worst performing trial was the separation of a biological particle and a predominantly nonfluorescent, non-biological particle. Both having drastic differences in fluorescence and size characteristics, this poor separation performance was surprising. The significant amount of nonfluorescent particles present in this trial may have resulted in the poor discriminability between the two particle materials, where nonfluorescent, non-biological particles and lowly fluorescent, biological particle merged into a cluster.

Clustering methods eliminate subjectivity when it comes to the characterization of data, because the data is characterized into a cluster based on an algorithm and not an individual. However, determining the optimal number of clusters for each separation trial can be somewhat biased as the Calinhara Index only gives an approximation and cluster composition reveals complimentary information.

Data preparation before the analysis is also extremely important in that results will differ depending on whether (a) particles that have saturating or nonfluorescent properties are filtered out (b) if the data is normally or log-normally distributed (c) whether the data

is normalized so that all the observations are on the same scale and (d) to ensure all variables are independent of one another.

The clustering algorithm provides groups based on similarities between data observations, however, it is still up to the user to define what that data means. There is no defined answer to what particle material is assigned to a cluster, therefore, it is important to carry out laboratory studies with known data to better understand outputs. Given some of the disadvantages of this clustering study, the results can still provide useful insight on how HAC unsupervised clustering algorithms work. A better understanding of unsupervised learning methods and the merging of multi-dimension data, can help train data for supervised learning methods for a more accurate characterization of particles.

4.4 Perspectives and Future Directions

UV-LIF is useful to detect PBAP, but it has limitations. There are many weakly fluorescing, non-biological particles that can interfere with the detection of bioaerosols. In the atmospheric environment, biological particles in most cases will be complex mixtures, agglomerating with other biological material and non-biological material (Hill et al., 1999).

One inherent disadvantage of the WIBS is the broad bands of emission information it provides. Finely resolved fluorescence information, resulting in single particle fluorescence spectra, can provide more chemical information and thus aid the discrimination between particle materials. However, one disadvantage of having full particle spectra is the abundance of data, therefore, data mining analyses such as

clustering methods or principle component analysis are necessary in order to process information. Clusters generated from these methods are still unclassified, and it is up to the user to determine to what particle material best fits the chemical and physical characteristics of a generated cluster.

It is likely that fluorescence-based instruments alone cannot discriminate well against non-biological particle types. The work presented in this thesis is the next step toward providing analysis strategies and promoting discussion within the field on how to better discriminate between different particle materials. Offline techniques (e.g. molecular techniques) coupled to real-time fluorescence detection based methods can provide secondary information to help characterize generated clusters. These techniques can include chemical tracer and molecular genetic analyses and results can aid in the identification and quantification of both culturable and non-culturable organisms (Després et al., 2012; Despres et al., 2007). Future work would include the co-deployment of the WIBS and collection methods for offline analyses, such as discussed. A study by Gosselin et al. (2016) presented the first quantitative comparison of real-time aerosol UV-LIF instruments with molecular tracers and provides evidence for the successful clustering of fungal spore particles. However, in-depth WIBS analysis studies like the one presented in this thesis in combination with offline molecular techniques such as nucleic extraction can allow the detection of a diverse population of biological particles, both culturable and non-culturable.

106

Robinson et al. (2017) provided a method for the calibration of the FL1 and FL2 channel of the WIBS instrument using fluorescent stable solutions. However, still no method exists for the calibration of the FL3 channel. Future work should include a calibration technique for the FL3 channel and should also include the application of the calibration method Robinson et al. (2017) suggests to multiple WIBS instruments. The goal of this future work is to come up with a standard protocol for using this calibration procedure for the comparison of data across different WIBS instruments and previous collected data.

References

Abdel-Shafy, H. I., and Mansour, M. S. M.: A review on polycyclic aromatic hydrocarbons: Source, environmental impact, effect on human health and remediation, Egyptian Journal of Petroleum, 25, 107-123, http://dx.doi.org/10.1016/j.ejpe.2015.03.011, 2016.

Agranovski, V., Ristovski, Z., Hargreaves, M., Blackall, P. J., and Morawska, L.: Real-time measurement of bacterial aerosols with the UVAPS: performance evaluation, Journal of Aerosol Science, 34, 301-317, 10.1016/s0021-8502(02)00181-7, 2003.

Agranovski, V., Ristovski, Z. D., Ayoko, G. A., and Morawska, L.: Performance evaluation of the UVAPS in measuring biological aerosols: Fluorescence spectra from NAD(P)H coenzymes and riboflavin, Aerosol Science and Technology, 38, 354-364, 10.1080/02786820490437505, 2004.

Agranovski, V., and Ristovski, Z. D.: Real-time monitoring of viable bioaerosols: capability of the UVAPS to predict the amount of individual microorganisms in aerosol particles, Journal of Aerosol Science, 36, 665-676, 10.1016/j.jaerosci.2004.12.005, 2005.

Aizawa, T., and Kosaka, H.: Investigation of early soot formation process in a diesel spray flame via excitation-emission matrix using a multi-wavelength laser source, Int. J. Engine Res., 9, 79-96, 10.1243/14680874jer01407, 2008.

Aizawa, T., and Kosaka, H.: Effects of Fischer-Tropsch diesel fuel on soot formation processes in a diesel spray flame, Int. J. Engine Res., 11, 79-87, 10.1243/14680874jer04709, 2010.

Amann, R. I., Ludwig, W., and and Schleifer, K. H.: Phylogenetic identification and in-situ detection of individual microbial-cells without cultivation, Microbiol. Rev., 59, 143-169, 1995.

Andreae, M. O., and Crutzen, P. J.: Atmospheric aerosols: Biogeochemical sources and role in atmospheric chemistry, Science, 276, 1052-1058, 10.1126/science.276.5315.1052, 1997.

Andreae, M. O., and Rosenfeld, D.: Aerosol-cloud-precipitation interactions. Part 1. The nature and sources of cloud-active aerosols, Earth Sci. Rev., 89, 13-41, 2008.

Ariya, P. A., Sun, J., Eltouny, N. A., Hudson, E. D., and Hayes, C. T.: Physical and chemical characterization of bioaerosols implications for nucleation processes, Int. Rev. Phys. Chem., 28, 1-32, 2009.

Bauer, H., Kasper-Giebl, A., Loflund, M., Giebl, H., Hitzenberger, R., Zibuschka, F., and Puxbaum, H.: The contribution of bacteria and fungal spores to the organic carbon content of cloud water, precipitation and aerosols, Atmospheric Research, 64, 109-119, 10.1016/s0169-8095(02)00084-4, 2002.

Bhangar, S., Huffman, J. A., and Nazaroff, W. W.: Size-resolved fluorescent biological aerosol particle concentrations and occupant emissions in a university classroom, Indoor air, 24, 604-617, 10.1111/ina.12111, 2014.

Bhangar, S., Adams, R. I., Pasut, W., Huffman, J. A., Arens, E. A., Taylor, J. W., Bruns, T. D., and Nazaroff, W. W.: Chamber bioaerosol study: human emissions of size-resolved fluorescent biological aerosol particles, Indoor air, 26, 193-206, 10.1111/ina.12195, 2016.

Bovallius, A., Bucht, B., Roffey, R., and Anas, P.: LONG-RANGE AIR TRANSMISSION OF BACTERIA, Appl. Environ. Microbiol., 35, 1231-1232, 1978.

Bridge, P., and Spooner, B.: Soil fungi: diversity and detection., Plant Soil, 2001.

Brosseau, L. M., Vesley, D., Rice, N., Goodell, K., Nellis, M., and Hairston, P.: Differences in detected fluorescence among several bacterial species measured with a direct-reading particle sizer and fluorescence detector, Aerosol Science and Technology, 32, 545-558, 10.1080/027868200303461, 2000.

Burrows, S. M., Elbert, W., Lawrence, M. G., and Poschl, U.: Bacteria in the global atmosphere - Part 1: Review and synthesis of literature data for different ecosystems, Atmospheric Chemistry and Physics, 9, 9263-9280, 2009.

Chi, M. C., and Li, C. S.: Fluorochrome in monitoring atmospheric bioaerosols and correlations with meteoro ogical factors and air pollutants, Aerosol Sci. Tech., 41, 672-678, 2007.

Cox, C. S., and Wathes, C. M.: Bioaerosols Handbook, Book, Whole, CRC Press., Boca Raton, FL, 1995.

Crawford, I., Robinson, N. H., Flynn, M. J., Foot, V. E., Gallagher, M. W., Huffman, J. A., Stanley, W. R., and Kaye, P. H.: Characterisation of bioaerosol emissions from a Colorado pine forest: results from the BEACHON-RoMBAS experiment, Atmospheric Chemistry and Physics, 14, 8559-8578, 10.5194/acp-14-8559-2014, 2014.

Crawford, I., Ruske, S., Topping, D. O., and Gallagher, M. W.: Evaluation of hierarchical agglomerative cluster analysis methods for discrimination of primary biological

aerosol, Atmospheric Measurement Techniques, 8, 4979-4991, 10.5194/amt-8-4979-2015, 2015.

Crawford, I., Lloyd, G., Herrmann, E., Hoyle, C. R., Bower, K. N., Connolly, P. J., Flynn, M. J., Kaye, P. H., Choularton, T. W., and Gallagher, M. W.: Observations of fluorescent aerosol-cloud interactions in the free troposphere at the High-Altitude Research Station Jungfraujoch, Atmospheric Chemistry and Physics, 16, 2273-2284, 10.5194/acp-16-2273-2016, 2016.

DeCarlo, P. F., Slowik, J. G., Worsnop, D. R., Davidovits, P., and Jimenez, J. L.: Particle morphology and density characterization by combined mobility and aerodynamic diameter measurements. Part 1: Theory, Aerosol Science and Technology, 38, 1185-1205, 10.1080/027868290903907, 2004.

Delort, A. M., Vaitilingom, M., Amato, P., Sancelme, M., and Parazols, M.: A short overview of the microbial population in clouds: potential roles in atmospheric chemistry and nucleation processes, Atmos. Res., 98, 249-260, 2010.

Despres, V. R., Nowoisky, J. F., Klose, M., Conrad, R., Andreae, M. O., and Poschl, U.: Characterization of primary biogenic aerosol particles in urban, rural, and high-alpine air by DNA sequence and restriction fragment analysis of ribosomal RNA genes, Biogeosciences, 4, 1127-1141, 2007.

Després, V. R., Huffman, J. A., Burrows, S. M., Hoose, C., Safatov, A. S., Buryak, G., Froehlich-Nowoisky, J., Elbert, W., Andreae, M. O., Poeschl, U., and Jaenicke, R.: Primary biological aerosol particles in the atmosphere: a review, Tellus Series B-Chemical and Physical Meteorology, 64, 15598-15598, 10.3402/tellusb.v64i0.15598, 2012.

Douwes, J., Thorne, P., Pearce, N., and Heederik, D.: Bioaerosol health effects and exposure assessment: Progress and prospects, Annals of Occupational Hygiene, 47, 187-200, 10.1093/annhyg/meg032, 2003.

Echigo, A., Hino, M., Fukushima, T., Mizuki, T., Kamekura, M., and Usami, R.: Endospores of halophilic bacteria of the family *Bacillaceae* isolated from the non-saline Japanese soil may be transported by kosa event (Asian dust storm). Saline Systems, 2005.

Eick, C., Zeidat, N., and Zhao, Z.: Supervised Clustering- Algorithms and Benefits. International Conference on Tools with Artificial Intelligence, 2004.

Elbert, W., Taylor, P. E., Andreae, M. O., and Poeschl, U.: Contribution of fungi to primary biogenic aerosols in the atmosphere: wet and dry discharged spores,

carbohydrates, and inorganic ions, Atmospheric Chemistry and Physics, 7, 4569-4588, 2007.

Field, C. B., Barros, V. R., Dokken, D. J., Mach, K. J., Mastrandrea, M. D., Bilir, T. E., Chatterjee, M., Ebi, K. L., Estrada, Y. O., Genova, R. C., Girma, B., Kissel, E. S., Levy, A. N., MacCracken, S., Mastrandrea, P. R., and White, L. L.: IPCC, 2014: Summary for policymakers. In: Climate Change 2014: Impacts,Adaptation, and Vulnerability.
Part A: Global and Sectoral Aspects. Contribution of Working Group II to the Fifth Assessment Report of the
Intergovernmental Panel on Climate Change, Cambridge University Press, Cambridge, United Kingdom and New
York, NY, USA, 2014.

Finlayson-Pitts, B. J., and Pitts, J., James N.: Chemistry of the Upper and Lower Atmosphere : Theory, Experiments, and Applications (1), Academic Pres, San Diego, USA, 993 pp., November 1999.

Frohlich-Nowoisky, J., Kampf, C. J., Weber, B., Huffman, J. A., Pohlker, C., Andreae, M. O., Lang-Yona, N., Burrows, S. M., Gunthe, S. S., Elbert, W., Su, H., Hoor, P., Thines, E., Hoffmann, T., Despres, V. R., and Poschl, U.: Bioaerosols in the Earth system: Climate, health, and ecosystem interactions, Atmospheric Research, 182, 346-376, 10.1016/j.atmosres.2016.07.018, 2016.

Fröhlich -Nowoisky, J., Pickersgill, D. A., Despres, V. R., and Poschl, U.: High diversity of fungi in air particulate matter, Proc. Natl. Acad. Sci. U. S. A., 106, 12814-12819, 10.1073/pnas.0811003106, 2009.

Gabey, A. M., Gallagher, M. W., Whitehead, J., Dorsey, J. R., Kaye, P. H., and Stanley, W. R.: Measurements and comparison of primary biological aerosol above and below a tropical forest canopy using a dual channel fluorescence spectrometer, Atmospheric Chemistry and Physics, 10, 4453-4466, 10.5194/acp-10-4453-2010, 2010.

Gabey, A. M., Vaitilingom, M., Freney, E., Boulon, J., Sellegri, K., Gallagher, M. W., Crawford, I. P., Robinson, N. H., Stanley, W. R., and Kaye, P. H.: Observations of fluorescent and biological aerosol at a high-altitude site in central France, Atmospheric Chemistry and Physics, 13, 7415-7428, 10.5194/acp-13-7415-2013, 2013.

Gordon, S.: The Normal Distribution. University of Syndey, 2006.

Gosselin, M. I., Rathnayake, C. M., Crawford, I., Pohlker, C., Frohlich-Nowoisky, J., Schmer, B., Despres, V. R., Engling, G., Gallagher, M., Stone, E., Poschl, U., and Huffman, J. A.: Fluorescent bioaerosol particle, molecular tracer, and fungal spore

concentrations during dry and rainy periods in a semi-arid forest, Atmospheric Chemistry and Physics, 16, 15165-15184, 10.5194/acp-16-15165-2016, 2016.

Griffin, D. W.: Atmospheric movement of microorganisms in clouds of desert dust and implications for human health, Clin. Microbiol. Rev., 20, 459-477, 10.1128/cmr.00039-06, 2007.

Griffiths, W. D., and Decosemo, G. A. L.: THE ASSESSMENT OF BIOAEROSOLS - A CRITICAL-REVIEW, Journal of Aerosol Science, 25, 1425-1458, 10.1016/0021-8502(94)90218-6, 1994.

Hairston, P. P., Ho, J., and Quant, F. R.: Design of an instrument for real-time detection of bioaerosols using simultaneous measurement of particle aerodynamic size and intrinsic fluorescence, Journal of Aerosol Science, 28, 471-482, 10.1016/S0021-8502(96)00448-X, 1997.

Han, T., Zhen, H. J., Fennell, D. E., and Mainelis, G.: Design and Evaluation of the Field-Deployable Electrostatic Precipitator with Superhydrophobic Surface (FDEPSS) with High Concentration Rate, Aerosol and Air Quality Research, 15, 2397-2408, 10.4209/aaqr.2015.04.0206, 2015.

Handorean, A., Robertson, C. E., Harris, J. K., Frank, D., Hull, N., Kotter, C., Stevens, M. J., Baumgardner, D., Pace, N. R., and Hernandez, M.: Microbial aerosol liberation from soiled textiles isolated during routine residuals handling in a modern health care setting, Microbiome, 3, 72-72, 10.1186/s40168-015-0132-3, 2015.

Harrison, R. M., Jones, A. M., Biggins, P. D. E., Pomeroy, N., Cox, C. S., Kidd, S. P., Hobman, J. L., Brown, N. L., and Beswick, A.: Climate factors influencing bacterial count in background air samples, Int. J. Biometeorol., 49, 167-178, 10.1007/s00484-004-0225-3, 2005.

Healy, D. A., Huffman, J. A., O'Connor, D. J., Pohlker, C., Poschl, U., and Sodeau, J. R.: Ambient measurements of biological aerosol particles near Killarney, Ireland: a comparison between real-time fluorescence and microscopy techniques, Atmospheric Chemistry and Physics, 14, 8055-8069, 10.5194/acp-14-8055-2014, 2014.

Heidelberg, J. F., Shahamat, M., Levin, M., Rahman, I., Stelma, G., Grim, C., and and Colwell, R. R.: Effect of aerosolization on culturability and viability of gram-negative bacteria, Appl. Environ., 63, 3585-3588, 1997.

Hernandez, M., Perring, A. E., McCabe, K., Kok, G., Granger, G., and Baumgardner, D.: Chamber catalogues of optical and fluorescent signatures distinguish bioaerosol classes, Atmospheric Measurement Techniques, 9, 3283-3292, 10.5194/amt-9-3283-2016, 2016.

Arbiters of Energy, 2002.

Hervas, A., Camarero, L., Reche, I., and Casamayor, E. O.: Viability and potential for immigration of airborne bacteria from Africa that reach high mountain lakes in Europe, Environ. Microbiol., 11, 1612-1623, 10.1111/j.1462-2920.2009.01926.x, 2009.

Hill, S. C., Pinnick, R. G., Niles, S., Pan, Y. L., Holler, S., Chang, R. K., Bottiger, J., Chen, B. T., Orr, C. S., and and Feather, G.: Real-time measurement of fluorescence spectra from single airborne biological particles, Field Anal. Chem. Technol., 3, 221-239, 1999.

Hill, S. C., Pinnick, R. G., Niles, S., Fell, N. F., Pan, Y. L., Bottiger, J., Bronk, B. V., Holler, S., and Chang, R. K.: Fluorescence from Airborne Microparticles: Dependence on Size, Concentration of Fluorophores, and Illumination Intensity, Appl. Optics, 40, 3005-3013, 2001.

Hill, S. C., Williamson, C. C., Doughty, D. C., Pan, Y. L., Santarpia, J. L., and Hill, H. H.: Size-dependent fluorescence of bioaerosols: Mathematical model using fluorescing and absorbing molecules in bacteria, J. Quant. Spectrosc. Radiat. Transf., 157, 54-70, 10.1016/j.jqsrt.2015.01.011, 2015.

Ho, J., Spence, M., and Hairston, P.: Measurement of Biological Aerosol with a Fluorescent Aerodynamic Particle Sizer (FLAPS): Correlation of Optical Data with Biological Data. Aerobiologia, 1999.

Ho, J.: Future of biological aerosol detection, Advances in Biodetection, 457, 125-148, http://dx.doi.org/10.1016/S0003-2670(01)01592-6, 2002.

Ho, J.: History of the Early Biodetection Development, in, Bioaerosol Detection Technologies, 9-33, 2014.

Huffman, J. A., Treutlein, B., and Poeschl, U.: Fluorescent biological aerosol particle concentrations and size distributions measured with an Ultraviolet Aerodynamic Particle Sizer (UV-APS) in Central Europe, Atmospheric Chemistry and Physics, 10, 3215-3233, 2010.

Huffman, J. A., Sinha, B., Garland, R. M., Snee-Pollmann, A., Gunthe, S. S., Artaxo, P., Martin, S. T., Andreae, M. O., and Poschl, U.: Size distributions and temporal variations of biological aerosol particles in the Amazon rainforest characterized by microscopy and real-time UV-APS fluorescence techniques during AMAZE-08, Atmospheric Chemistry and Physics, 12, 11997-12019, 10.5194/acp-12-11997-2012, 2012.

Huffman, J. A., Prenni, A. J., DeMott, P. J., Pohlker, C., Mason, R. H., Robinson, N. H., Frohlich-Nowoisky, J., Tobo, Y., Despres, V. R., Garcia, E., Gochis, D. J., Harris, E., Mueller-Germann, I., Ruzene, C., Schmer, B., Sinha, B., Day, D. A., Andreae, M. O., Jimenez, J. L., Gallagher, M., Kreidenweis, S. M., Bertram, A. K., and Poschl, U.: High concentrations of biological aerosol particles and ice nuclei during and after rain, Atmospheric Chemistry and Physics, 13, 6151-6164, 10.5194/acp-13-6151-2013, 2013.

Huffman, J. A., and Santarpia, J. L.: Online techniques for quantification and characterization of biological aerosol, in: Microbiology of Aerosols, edited by: Delort, A. M., and Amato, P., Wiley (In Press), Hoboken, NJ, Chapter 4, 2017.

Ichinose, T., Yoshida, S., Hiyoshi, K., Sadakane, K., Takano, H., Nishikawa, M., Mori, I., Yanagisawa, R., Kawazato, H., Yasuda, A., and Shibamoto, T.: The effects of microbial materials adhered to Asian sand dust on allergic lung inflammation, Arch. Environ. Contam. Toxicol., 55, 348-357, 10.1007/s00244-007-9128-8, 2008.

Jaenicke, R., and Matthais, S.: The primary biogenic fraction of the atmospheric aerosol. In: Aerosols and Climate, Deepak Publishing, Hampton, VA, 1988.

Jaenicke, R.: Abundance of cellular material and proteins in the atmosphere, Science, 308, 73, 2005.

Jo, W. K., and Seo, Y. J.: Indoor and outdoor bioaerosol levels at recreation facilities, elementary schools, and homes, Chemosphere, 61, 1570-1579, 10.1016/j.chemosphere.2005.04.103, 2005.

Jones, A. M., and Harrison, R. M.: The effect of meteorological factors on atmospheric bioaerosols concentration - a review. Sci. Tot. Environ., 2004.

Jonsson, P., and Kullander, F.: Bioaerosol Detection and Fluorescence Spectroscopy, in, Bioaerosol Detection Technologies, 111-143, 2014.

Kanaani, H., Hargreaves, M., Ristovski, Z., and Morawska, L.: Performance assessment of UVAPS: Influence of fungal spore age and air exposure, Journal of Aerosol Science, 38, 83-96, 10.1016/j.jaerosci.2006.10.003, 2007.

Kanaani, H., Hargreaves, M., Smith, J., Ristovski, Z., Agranovski, V., and Morawska, L.: Performance of UVAPS with respect to detection of airborne fungi, Journal of Aerosol Science, 39, 175-189, 10.1016/j.jaerosci.2007.10.007, 2008.

Kanaani, H., Hargreaves, M., Ristovski, Z., and Morawska, L.: Fungal spore fragmentation as a function of airflow rates and fungal generation methods, Atmospheric Environment, 43, 3725-3735, 10.1016/j.atmosenv.2009.04.043, 2009.

114

Kaye, P., Aptowicz, K., Chang, R., Foot, V., and Videen, G.: Optics of Biological Particles. In: Angularly Resolved Elastic Scattering from Airborne Particles, 2007.

Kaye, P. H., Eyles, N. A., Ludlow, I. K., and Clark, J. M.: AN INSTRUMENT FOR THE CLASSIFICATION OF AIRBORNE PARTICLES ON THE BASIS OF SIZE, SHAPE, AND COUNT FREQUENCY, Atmospheric Environment Part a-General Topics, 25, 645-654, 10.1016/0960-1686(91)90062-c, 1991.

Kaye, P. H., Stanley, W. R., Hirst, E., Foot, E. V., Baxter, K. L., and Barrington, S. J.: Single particle multichannel bio-aerosol fluorescence sensor, Optics Express, 13, 3583-3593, 10.1364/opex.13.003583, 2005.

Kellogg, C. A., and Griffin, D. W.: Aerobiology and the global transport of desert dust, Trends Ecol. Evol., 21, 638-644, 10.1016/j.tree.2006.07.004, 2006.

Könemann, T., Savage, N., McMeeking, G., Su, H., Huffman, J. A., Pöhlker, C., and Pöschl, U.: Spectral Intensity Bioaerosol Sensor (SIBS): Technical Description and Laboratory Assessment of a Novel Instrument for Single Particle Detection. In Prep.

Kuparinen, A., Katul, G., Nathan, R., and Schurr, F. M.: Increases in air temperature can promote wind-driven dispersal and spread of plants, Proc. R. Soc. B-Biol. Sci., 276, 3081-3087, 10.1098/rspb.2009.0693, 2009.

Lavoie, J., Marchand, G. E., Cloutier, Y., Halle, S., Nadeau, S., Duchaine, C., and Pichette, G.: Evaluation of bioaerosol exposures during hospital bronchoscopy examinations, Environ. Sci.-Process Impacts, 17, 288-299, 10.1039/c4em00359d, 2015.

Li, J., Zhou, L., Zhang, X., Xu, C., Dong, L., and Yao, M.: Bioaerosol emissions and detection of airborne antibiotic resistance genes from a wastewater treatment plant, Atmospheric Environment, 124, 404-412, 10.1016/j.atmosenv.2015.06.030, 2016.

Lighthart, B.: The ecology of bacteria in the alfresco atmosphere, FEMS Microbiol. Ecol., 23, 263-274, 10.1016/s0168-6496(97)00036-6, 1997.

Liu, Y., Li, Z., Xiong, H., Gao, X., and Wu, J.: Understanding of Internal Clustering Validation Measures. IEEE Computer Society, 2010.

Löndahl, J.: Physical and Biological Properties of Bioaerosols, in, Springer, 33-49, 2014.

Lv, Y., Li, X., Xu, T. T., Cheng, T. T., Yang, X., Chen, J. M., Iinuma, Y., and Herrmann, H.: Size distributions of polycyclic aromatic hydrocarbons in urban atmosphere: sorption mechanism and source contributions to respiratory deposition, Atmospheric Chemistry and Physics, 16, 2971-2983, 10.5194/acp-16-2971-2016, 2016.

Mainelis, G., Berry, D., An, H. R., Yao, M. S., DeVoe, K., Fennell, D. E., and Jaeger, R.: Design and performance of a single-pass bubbling bioaerosol generator, Atmospheric Environment, 39, 3521-3533, 10.1016/j.atmosenv.2005.02.043, 2005.

Manninen, H. E., Back, J., Sihto-Nissila, S. L., Huffman, J. A., Pessi, A. M., Hiltunen, V., Aalto, P. P., Hidalgo, P. J., Hari, P., Saarto, A., Kulmala, M., and Petaja, T.: Patterns in airborne pollen and other primary biological aerosol particles (PBAP), and their contribution to aerosol mass and number in a boreal forest, Boreal Environ. Res., 19, 383-405, 2014.

Mason, R. H., Chou, C., McCluskey, C. S., Levin, E. J. T., Schiller, C. L., Hill, T. C. J., Huffman, J. A., DeMott, P. J., and Bertram, A. K.: The micro-orifice uniform deposit impactor-droplet freezing technique (MOUDI-DFT) for measuring concentrations of ice nucleating particles as a function of size: improvements and initial validation, Atmospheric Measurement Techniques, 8, 2449-2462, 10.5194/amt-8-2449-2015, 2015a.

Mason, R. H., Si, M., Li, J., Chou, C., Dickie, R., Toom-Sauntry, D., Poehlker, C., Yakobi-Hancock, J. D., Ladino, L. A., Jones, K., Leaitch, W. R., Schiller, C. L., Abbatt, J. P. D., Huffman, J. A., and Bertram, A. K.: Ice nucleating particles at a coastal marine boundary layer site: correlations with aerosol type and meteorological conditions, Atmospheric Chemistry and Physics, 15, 12547-12566, 10.5194/acp-15-12547-2015, 2015b.

Matthias-Maser, S., Bogs, B., and Jaenicke, R.: The size distribution of primary biological aerosol particles in cloud water on the mountain Kleiner Feldberg/Taunus(FRG), Atmospheric Research, 54, 1-13, 10.1016/s0169-8095(00)00039-9, 2000a.

Matthias-Maser, S., Obolkin, V., Khodzer, T., and Jaenicke, R.: Seasonal variation of primary biological aerosol particles in the remote continental region of Lake Baikal/Siberia, Atmospheric Environment, 34, 3805-3811, 10.1016/s1352-2310(00)00139-4, 2000b.

MatthiasMaser, S., and Jaenicke, R.: The size distribution of primary biological aerosol particles with radii >0.2 mu m in an urban rural influenced region, Atmospheric Research, 39, 279-286, 10.1016/0169-8095(95)00017-8, 1995.

Mercier, X., Faccinetto, A., and Desgroux, P.: Cleaner Combustion: Developing Detailed Chemical Kinetic Models, Green Energy and Technology, Springer, London, 2013.

Miguel, A. G., Taylor, P. E., House, J., Glovsky, M. M., and Flagan, R. C.: Meteorological influences on respirable fragment release from Chinese elm pollen, Aerosol Science and Technology, 40, 690-696, 10.1080/02786820600798869, 2006.

Möhler, O., DeMott, P. J., Vali, G., and Levin, Z.: Microbiology and atmospheric processes: the role of biological particles in cloud physics, Biogeosciencs, 4, 1059-1071, 2007.

Morris, C. E., Georgakopoulos, D. G., and Sands, D. C.: Ice nucleation active bacteria and their potential role in precipitation, Journal De Physique Iv, 121, 87-103, 10.1051/jp4:2004121004, 2004.

Morris, C. E., Conen, F., Huffman, J. A., Phillips, V., Poschl, U., and Sands, D. C.: Bioprecipitation: a feedback cycle linking Earth history, ecosystem dynamics and land use through biological ice nucleators in the atmosphere, Glob. Change Biol., 20, 341-351, 10.1111/gcb.12447, 2014.

Mullner, D.: fastcluster: Fast Hierarchical, Agglomerative Clustering Routines for R and Python, J. Stat. Softw., 53, 1-18, 2013.

Nicholson, W. L., Munakata, N., Horneck, G., Melosh, H. J., and Setlow, P.: Resistance of Bacillus endospores to extreme terrestrial and extraterrestrial environments, Microbiol. Mol. Biol. Rev., 64, 548-+, 10.1128/mmbr.64.3.548-572.2000, 2000.

Niessner, R., and Krupp, A.: DETECTION AND CHEMICAL CHARACTERIZATION OF POLYCYCLIC AROMATIC HYDROCARBON AEROSOLS BY MEANS OF LASER-INDUCED FLUORESCENCE, Part. Part. Syst. Charact., 8, 23-28, 10.1002/ppsc.19910080106, 1991.

Norusis, M.: Cluster Analysis, in: IBM SPSS Statistics 19 Guide to Data Analysis, Norusis & SPSS Inc., 2011.

O'Connor, D. J., Daly, S. M., and Sodeau, J. R.: On-line monitoring of airborne bioaerosols released from a composting/green waste site, Waste Management, 42, 23-30, 10.1016/j.wasman.2015.04.015, 2015a.

O'Connor, D. J., Healy, D. A., and Sodeau, J. R.: A 1-month online monitoring campaign of ambient fungal spore concentrations in the harbour region of Cork, Ireland, Aerobiologia, 31, 295-314, 10.1007/s10453-015-9365-7, 2015b.

Pan, Y. L., Holler, S., Chang, R. K., Hill, S. C., Pinnick, R. G., Niles, S., Bottiger, J. R., and Bronk, B. V.: Real-time detection and characterization of individual flowing airborne biological particles: fluorescence spectra and elastic scattering measurements, P. Soc. Photo-Opt. Ins., 3855, 117-125, 1999.

Pan, Y. L., Pinnick, R. G., Hill, S. C., Rosen, J. M., and Chang, R. K.: Single-particle laser-induced-fluorescence spectra of biological and other organic-carbon aerosols in the atmosphere: Measurements at New Haven, Connecticut, and Las Cruces, New

Mexico, Journal of Geophysical Research-Atmospheres, 112, 15, 10.1029/2007jd008741, 2007.

Pan, Y. L., Pinnick, R. G., Hill, S. C., and Chang, R. K.: Particle-Fluorescence Spectrometer for Real-Time Single-Particle Measurements of Atmospheric Organic Carbon and Biological Aerosol, Environmental Science & Technology, 43, 429-434, 10.1021/es801544y, 2009.

Panne, U., Knoller, A., Kotzick, R., and Niessner, R.: On-line and in-situ detection of polycyclic aromatic hydrocarbons (PAH) on aerosols via thermodesorption and laser-induced fluorescence spectroscopy, Fresenius J. Anal. Chem., 366, 408-414, 10.1007/s002160050083, 2000.

Penner, J. E.: Carbonaceous Aerosols Influencing Atmospheric Radiation: Black and Organic Carbon, 35, 1994.

Perring, A. E., Schwarz, J. P., Baumgardner, D., Hernandez, M. T., Spracklen, D. V., Heald, C. L., Gao, R. S., Kok, G., McMeeking, G. R., McQuaid, J. B., and Fahey, D. W.: Airborne observations of regional variation in fluorescent aerosol across the United States, Journal of Geophysical Research-Atmospheres, 120, 1153-1170, 10.1002/2014JD022495, 2015.

Pinnick, R. G., Hill, S. C., Nachman, P., Pendleton, J. D., Fernandez, G. L., Mayo, M. W., and Bruno, J. G.: Fluorescence Particle Counter for Detecting Airborne Bacteria and Other Biological Particles, Aerosol Science and Technology, 23, 653-664, 10.1080/02786829508965345, 1995.

Pinnick, R. G., Hill, S. C., Pan, Y. L., and Chang, R. K.: Fluorescence spectra of atmospheric aerosol at Adelphi, Maryland, USA: measurement and classification of single particles containing organic carbon, Atmospheric Environment, 38, 1657-1672, 10.1016/j.atmosenv.2003.11.017, 2004.

Pinnick, R. G., Fernandez, E., Rosen, J. M., Hill, S. C., Wang, Y., and Pan, Y. L.: Fluorescence spectra and elastic scattering characteristics of atmospheric aerosol in Las Cruces, New Mexico, USA: Variability of concentrations and possible constituents and sources of particles in various spectral clusters, Atmospheric Environment, 65, 195-204, 10.1016/j.atmosenv.2012.09.020, 2013.

Pitt, J. I., and Hocking, A. D.: Fungi and food spoilage. Springer, 1997.

Pöhlker, C., Huffman, J. A., and Poeschl, U.: Autofluorescence of atmospheric bioaerosols - fluorescent biomolecules and potential interferences, Atmospheric Measurement Techniques, 5, 37-71, 10.5194/amt-5-37-2012, 2012.

Pöhlker, C., Huffman, J. A., Foerster, J. D., and Poeschl, U.: Autofluorescence of atmospheric bioaerosols: spectral fingerprints and taxonomic trends of pollen, Atmospheric Measurement Techniques, 6, 3369-3392, 10.5194/amt-6-3369-2013, 2013.

Pöschl, U.: Atmospheric aerosols: composition, transformation, climate and health effects, Angewandte Chemie-International, 44, 7520-7540, 2005.

Pöschl, U., Martin, S. T., Sinha, B., Chen, Q., Gunthe, S. S., Huffman, J. A., Borrmann, S., Farmer, D. K., Garland, R. M., Helas, G., Jimenez, J. L., King, S. M., Manzi, A., Mikhailov, E., Pauliquevis, T., Petters, M. D., Prenni, A. J., Roldin, P., Rose, D., Schneider, J., Su, H., Zorn, S. R., Artaxo, P., and Andreae, M. O.: Rainforest Aerosols as Biogenic Nuclei of Clouds and Precipitation in the Amazon, Science, 329, 1513-1516, 10.1126/science.1191056, 2010.

Powelson, M. H., Espelien, B. M., Hawkins, L. N., Galloway, M. M., and De Haan, D. O.: Brown Carbon Formation by Aqueous-Phase Carbonyl Compound Reactions with Amines and Ammonium Sulfate, Environmental Science & Technology, 48, 985-993, 10.1021/es4038325, 2014.

Primmerman, C.: Detection of biological agents. Lincoln Laboratory Journal, 2000.

Prospero, J. M., and Mayol-Bracero, O. L.: UNDERSTANDING THE TRANSPORT AND IMPACT OF AFRICAN DUST ON THE CARIBBEAN BASIN, Bull. Amer. Meteorol. Soc., 94, 1329-1337, 10.1175/bams-d-12-00142.1, 2013.

Ren, P., Jankun, T. M., and Leaderer, B. P.: Comparisons of seasonal fungal prevalence in indoor and outdoor air and in house dusts of dwellings in one Northeast American county, J. Expo. Anal. Environ. Epidemiol., 9, 560-568, 10.1038/sj.jea.7500061, 1999.

Robinson, E., Gao, R.-S., Schwarz, J., Fahey, D., and Perring, A.: Fluorescence Calibration Method for Single Particle Aerosol Fluorescence Instruments. 2017.

Robinson, N. H., Allan, J. D., Huffman, J. A., Kaye, P. H., Foot, V. E., and Gallagher, M.: Cluster analysis of WIBS single-particle bioaerosol data, Atmospheric Measurement Techniques, 6, 337-347, 10.5194/amt-6-337-2013, 2013.

Ruske, S., Topping, D. O., Foot, V. E., Kaye, P. H., Stanley, W. R., Crawford, I., Morse, A. P., and Gallagher, M. W.: Evaluation of machine learning algorithms for classification of primary biological aerosol using a new UV-LIF spectrometer, Atmospheric Measurement Techniques, 10, 695-708, 10.5194/amt-10-695-2017, 2017.

119

Saari, S., Mensah-Attipoe, J., Reponen, T., Veijalainen, A. M., Salmela, A., Pasanen, P., and Keskinen, J.: Effects of fungal species, cultivation time, growth substrate, and air exposure velocity on the fluorescence properties of airborne fungal spores, Indoor air, 25, 653-661, 10.1111/ina.12166, 2015a.

Saari, S., Niemi, J. V., Ronkko, T., Kuuluvainen, H., Jarvinen, A., Pirjola, L., Aurela, M., Hillamo, R., and Keskinen, J.: Seasonal and Diurnal Variations of Fluorescent Bioaerosol Concentration and Size Distribution in the Urban Environment, Aerosol and Air Quality Research, 15, 572-581, 10.4209/aaqr.2014.10.0258, 2015b.

Schafer, J., Klug, K., Van Kampen, V., and Jackel, U.: Quantification of Saccharopolyspora rectivirgula in Composting Plants: Assessment of the Relevance of S-rectivirgula, Annals of Occupational Hygiene, 57, 875-883, 10.1093/annhyg/met010, 2013.

Schnell, R. C., and Vali, G.: ATMOSPHERIC ICE NUCLEI FROM DECOMPOSING VEGETATION, Nature, 236, 163-+, 10.1038/236163a0, 1972.

Schumacher, C. J., Poehlker, C., Aalto, P., Hiltunen, V., Petaja, T., Kulmala, M., Poeschl, U., and Huffman, J. A.: Seasonal cycles of fluorescent biological aerosol particles in boreal and semi-arid forests of Finland and Colorado, Atmospheric Chemistry and Physics, 13, 11987-12001, 10.5194/acp-13-11987-2013, 2013.

Science, P. E. C. o.: 14.4-Agglomerative Hierarchical Clustering, Stat 505, 2017.

Shaffer, B. T., and Lighthart, B.: Survey of culturable airborne bacteria at four diverse locations in Oregon: Urban, rural, forest, and coastal, Microb. Ecol., 34, 167-177, 10.1007/s002489900046, 1997.

Sivaprakasam, V., Lin, H. B., Huston, A. L., and Eversole, J. D.: Spectral characterization of biological aerosol particles using two-wavelength excited laser-induced fluorescence and elastic scattering measurements, Optics Express, 19, 6191-6208, 10.1364/oe.19.006191, 2011.

Slowik, J. G., Cross, E. S., Han, J. H., Kolucki, J., Davidovits, P., Williams, L. R., Onasch, T. B., Jayne, J. T., Kolb, C. E., and Worsnop, D. R.: Measurements of morphology changes of fractal soot particles using coating and denuding experiments: Implications for optical absorption and atmospheric lifetime, Aerosol Science and Technology, 41, 734-750, 10.1080/02786820701432632, 2007.

Sodeau, J. R., and O'Connor, D. J.: Chapter 16 - Bioaerosol Monitoring of the Atmosphere for Occupational and Environmental Purposes, in: Comprehensive Analytical Chemistry, The Quality of Air, Elsevier, 391-420, 2016.

Sofiev, M., Siljamo, P., Ranta, H., and Rantio-Lehtimaki, A.: Towards numerical forecasting of long-range air transport of birch pollen: theoretical considerations and a feasibility study, Int. J. Biometeorol., 50, 392-402, 10.1007/s00484-006-0027-x, 2006.

Taketani, F., Kanaya, Y., Nakamura, T., Koizumi, K., Moteki, N., and Takegawa, N.: Measurement of fluorescence spectra from atmospheric single submicron particle using laser-induced fluorescence technique, Journal of Aerosol Science, 58, 1-8, 10.1016/j.jaerosci.2012.12.002, 2013.

Taylor, P. E., Flagan, R. C., Valenta, R., and Glovsky, M. M.: Release of allergens as respirable aerosols: A link between grass pollen and asthma, J. Allergy Clin. Immunol., 109, 51-56, 10.1067/mai.2002.120759, 2002.

A language for statistical computing: http://www.R-project.org/. 2011.

Tong, Y. Y., and Lighthart, B.: Diurnal distribution of total and culturable atmospheric bacteria at a rural site, Aerosol Science and Technology, 30, 246-254, 10.1080/027868299304822, 1999.

Toprak, E., and Schnaiter, M.: Fluorescent biological aerosol particles measured with the Waveband Integrated Bioaerosol Sensor WIBS-4: laboratory tests combined with a one year field study, Atmospheric Chemistry and Physics, 13, 225-243, 10.5194/acp-13-225-2013, 2013.

Twohy, C. H., McMeeking, G. R., DeMott, P. J., McCluskey, C. S., Hill, T. C. J., Burrows, S. M., Kulkarni, G. R., Tanarhte, M., Kafle, D. N., and Toohey, D. W.: Abundance of fluorescent biological aerosol particles at temperatures conducive to the formation of mixed-phase and cirrus clouds, Atmospheric Chemistry and Physics, 16, 8205-8225, 10.5194/acp-16-8205-2016, 2016.

Valsan, A. E., Ravikrishna, R., Biju, C. V., Poehlker, C., Despres, V. R., Huffman, J. A., Poeschl, U., and Gunthe, S. S.: Fluorescent biological aerosol particle measurements at a tropical high-altitude site in southern India during the southwest monsoon season, Atmospheric Chemistry and Physics, 16, 9805-9830, 10.5194/acp-16-9805-2016, 2016.

Von Helden, G., Hsu, M. T., Gotts, N., and Bowers, M. T.: CARBON CLUSTER CATIONS WITH UP TO 84 ATOMS - STRUCTURES, FORMATION MECHANISM, AND REACTIVITY, J. Phys. Chem., 97, 8182-8192, 10.1021/j100133a011, 1993.

Wang, C. C., Fang, G. C., and Lee, L.: Bioaerosols study in central Taiwan during summer season, Toxicol. Ind. Health, 23, 133-139, 10.1177/0748233707078741, 2007.

Wang, C. C., Fang, G. C., and Lee, L. Y.: The study of ambient air bioaerosols during summer daytime and nighttime periods in Taichung, Central Taiwan, Environ. Forensics, 9, 6-14, 10.1080/15275920701729175, 2008.

Whitehead, J. D., Gallagher, M. W., Dorsey, J. R., Robinson, N., Gabey, A. M., Coe, H., McFiggans, G., Flynn, M. J., Ryder, J., Nemitz, E., and Davies, F.: Aerosol fluxes and dynamics within and above a tropical rainforest in South-East Asia, Atmospheric Chemistry and Physics, 10, 9369-9382, 10.5194/acp-10-9369-2010, 2010.

Whitehead, J. D., Darbyshire, E., Brito, J., Barbosa, H. M. J., Crawford, I., Stern, R., Gallagher, M. W., Kaye, P. H., Allan, J. D., Coe, H., Artaxo, P., and McFiggans, G.: Biogenic cloud nuclei in the central Amazon during the transition from wet to dry season, Atmospheric Chemistry and Physics, 16, 9727-9743, 10.5194/acp-16-9727-2016, 2016.

Wilson, T. W., Ladino, L. A., Alpert, P. A., Breckels, M. N., Brooks, I. M., Browse, J., Burrows, S. M., Carslaw, K. S., Huffman, J. A., Judd, C., Kilthau, W. P., Mason, R. H., McFiggans, G., Miller, L. A., Najera, J. J., Polishchuk, E., Rae, S., Schiller, C. L., Si, M., Temprado, J. V., Whale, T. F., Wong, J. P. S., Wurl, O., Yakobi-Hancock, J. D., Abbatt, J. P. D., Aller, J. Y., Bertram, A. K., Knopf, D. A., and Murray, B. J.: A marine biogenic source of atmospheric ice-nucleating particles, Nature, 525, 234-+, 10.1038/nature14986, 2015.

Wright, T. P., Hader, J. D., McMeeking, G. R., and Petters, M. D.: High Relative Humidity as a Trigger for Widespread Release of Ice Nuclei, Aerosol Science and Technology, 48, 5, 10.1080/02786826.2014.968244, 2014.

Wu, Y., Chen, A. L., Luhung, I., Gall, E. T., Cao, Q. L., Chang, V. W. C., and Nazaroff, W. W.: Bioaerosol deposition on an air-conditioning cooling coil, Atmospheric Environment, 144, 257-265, 10.1016/j.atmosenv.2016.09.004, 2016.

Xie, Y. Y., Fajardo, O. A., Yan, W. Z., Zhao, B., and Jiang, J. K.: Six-day measurement of size-resolved indoor fluorescent bioaerosols of outdoor origin in an office, Particuology, 31, 161-169, 10.1016/j.partic.2016.09.004, 2017.

Yu, X. W., Wang, Z. B., Zhang, M. H., Kuhn, U., Xie, Z. Q., Cheng, Y. F., Poschl, U., and Su, H.: Ambient measurement of fluorescent aerosol particles with a WIBS in the Yangtze River Delta of China: potential impacts of combustion-related aerosol particles, Atmospheric Chemistry and Physics, 16, 11337-11348, 10.5194/acp-16-11337-2016, 2016.

Yukimura, K., Nakai, R., Kohshima, S., Uetake, J., Kanda, H., and Naganuma, T.: Spore-forming halophilic bacteria isolated from Arctic terrains: Implications for long-range transportation of microorganisms, Polar Sci., 3, 163-169, 10.1016/j.polar.2009.07.002, 2009.

Zelenyuk, A., Cai, Y., and Imre, D.: From agglomerates of spheres to irregularly shaped particles: Determination of dynamic shape factors from measurements of mobility and vacuum aerodynamic diameters, Aerosol Science and Technology, 40, 197-217, 10.1080/02786820500529406, 2006.

Zhen, H., Han, T., Fennell, D., and Mainelis, G.: A systematic comparison of four bioaerosol generators: Effect on culturability and membrane integrity when aerosolizing *E. coli* bacteria., Journal of Aerosol Science, 2014

Ziemba, L. D., Beyersdorf, A. J., Chen, G., Corr, C. A., Crumeyrolle, S. N., Diskin, G., Hudgins, C., Martin, R., Mikoviny, T., Moore, R., Shook, M., Thornhill, K. L., Winstead, E. L., Wisthaler, A., and Anderson, B. E.: Airborne observations of bioaerosol over the Southeast United States using a Wideband Integrated Bioaerosol Sensor, Journal of Geophysical Research-Atmospheres, 121, 8506-8524, 10.1002/2015JD024669, 2016.

Appendix A: Chapter 2 Supplement

Appendix A was included as the online supplement in the reviewed version of Savage et

al. (2017), which was re-formatted here as Chapter 2.

Table A.1. Material types analyzed, including biological and non-biological. Table
includes threshold values for FT + 3σ and FT +9σ.

	Materials	Provider	Part Number	Aeroso-lization Method	3σ FL1	3σ FL2	3σ FL3	9σ FL1	9σ FL2	9σ FL3
BIOLOGICAL MATERIALS										
Pollen										
1	*Urtica diocia (Stinging Nettle)*	BONAPOL	-	Powder (P1)	49.0	24.3	44.4	96.5	45.6	73.5
2	*Artemisia vulgaris (Common Mugwort)*	BONAPOL	-	Powder (P1)	49.0	24.3	44.4	96.5	45.6	73.5
3	*Castanea sativa (European Chestnut)*	BONAPOL	-	Powder (P1)	48.2	24.1	46.1	95.2	45.2	77.6
4	*Corylus avellana (Hazel)*	BONAPOL	-	Powder (P1)	48.2	24.1	46.1	95.2	45.2	77.6
5	*Taxus baccata (Common Yew)*	BONAPOL	-	Powder (P1)	48.2	24.1	46.1	95.2	45.2	77.6
6	*Rumex acetosella (Sheep Sorrel)*	BONAPOL	-	Powder (P1)	48.2	24.1	46.1	95.2	45.2	77.6
7	*Olea europaea (European Olive Tree)*	BONAPOL	-	Powder (P1)	48.2	24.1	46.1	95.2	45.2	77.6
8	*Alnus glutinosa (Black Alder)*	BONAPOL	-	Powder (P1)	50.5	24.9	48.8	101.2	46.3	80.9
9	*Phleum pratense (Timothy Grass)*	BONAPOL	-	Powder (P1)	50.5	24.9	48.8	101.2	46.3	80.9
10	*Populus alba (White Poplar)*	BONAPOL	-	Powder (P1)	47.7	23.9	46.2	95.6	44.8	77.8
11	*Taraxacum officinale (Common Dandelion)*	BONAPOL	-	Powder (P1)	47.7	23.9	46.2	95.6	44.8	77.8
12	*Amaranthus retroflexus (Redroot Amaranth)*	BONAPOL	-	Powder (P1)	45.6	24.4	46.6	89.5	45.7	78.9

124

#	Name	Source	Catalog #	Form					
13	*Aesculus hippocastanum (Horse-chestnut)*	BONAPOL	-	Powder (P1)	45.6	24.4	46.6	89.5	45.7	78.9
14	*Lycopodium (Clubmoss)*	Polysci., Inc.	16867	Powder (P1)	85.1	52.3	46.1	162.5	85.2	79.2

Fungal spores										
1	*Aspergillus brasiliensis*	ATCC*	-	Fungal	50.3	24.7	48.5	99.5	45.9	82.4
2	*Aspergillus niger; WB 326*	ATCC	16888	Fungal	50.3	24.7	48.5	99.5	45.9	82.4
3	*Rhizopus stolonifera (Black Bread Mold); UNB-1*	ATCC	14037	Fungal	50.3	24.7	48.5	99.5	45.9	82.4
4	*Saccharomyces cerevisiae (Brewer's Yeast)*	ATCC	-	Fungal	49.0	24.3	44.5	96.5	45.6	73.5
5	*Aspergillus versicolor; NRRL 238*	ATCC	10106	Fungal	49.0	24.3	44.5	96.5	45.6	73.5

Bacteria										
1	*Bacillus atrophaeus*	ATCC	49337	Bacterial	34.1	18.1	65.8	70.8	38.1	103.0
2	*Escherichia coli*	ATCC	15597	Bacterial	34.1	18.1	65.8	70.8	38.1	103.0
3	*Pseudomonas stutzeri*	ATCC	13525	Bacterial	34.1	18.1	65.8	70.8	38.1	103.0

Biofluorophores										
1	Riboflavin	Sigma	R7649	Powder (P1)	87.3	56.2	49.1	166.8	92.4	84.3
2	Chitin	Sigma	C9752	Powder (P1)	87.3	56.2	49.1	166.8	92.4	84.3
3	NAD	Sigma	N8129	Powder (P1)	87.3	56.2	49.1	166.8	92.4	84.3
4	Folic Acid	Sigma	F7876	Powder (P1)	87.3	56.2	49.1	166.8	92.4	84.3
5	Cellulose, fibrous medium	Sigma	4352396	Powder (P1)	85.3	54.5	48.5	159.7	88.6	82.1
6	Ergosterol	Sigma	45480	Powder (P1)	92.8	48.0	40.5	176.1	79.7	68.8
7	Pyridoxine	Sigma	P5669	Powder (P1)	96.7	46.1	40.6	186.5	77.7	69.0
8	Pyridoxamine	Sigma	P9380	Powder (P1)	92.8	48.0	40.5	176.1	79.7	68.8

9	Tyrosine	Sigma	855456	Powder (P1)	87.1	52.3	44.8	166.4	86.8	75.8
10	Phenylalanine	Sigma	78019	Powder (P1)	85.3	54.5	48.5	159.7	88.6	82.1
11	Tryptophan	Sigma	93659	Powder (P1)	85.3	54.5	48.5	159.7	88.6	82.1
12	Histidine	Sigma	H8000	Powder (P1)	90.9	45.2	39.3	173.0	76.8	66.3
NON-BIOLOGICAL MATERIALS										
Dust										
1	Arabic Sand	UM-SEES **	-	Powder (P3)	85.1	52.3	46.1	162.5	85.2	79.2
2	California Sand	UM-SEES	-	Powder (P2)	85.1	52.3	46.1	162.5	85.2	79.2
3	Africa Sand	UM-SEES	-	Powder (P2)	87.9	45.7	39.4	166.4	77.8	66.8
4	Murkee-Murkee Australian Sand	UM-SEES	-	Powder (P2)	87.9	45.7	39.4	166.4	77.8	66.8
5	Manua Key Summit Hawaii Sand	UM-SEES	-	Powder (P2)	87.9	45.7	39.4	166.4	77.8	66.8
6	Quartz	UM-SEES	-	Powder (P2)	87.9	45.7	39.4	166.4	77.8	66.8
7	Kakadu Dust	UM-SEES	-	Powder (P2)	87.9	45.7	39.4	166.4	77.8	66.8
8	Feldspar	UM-SEES	-	Powder (P2)	87.9	45.7	39.4	166.4	77.8	66.8
9	Hematite	UM-SEES	-	Powder (P2)	87.9	45.7	39.4	166.4	77.8	66.8
10	Gypsum	UM-SEES	-	Powder (P2)	90.9	45.2	39.3	173.0	76.8	66.3
11	Bani AMMA	UM-SEES	-	Powder (P2)	90.9	45.2	39.3	173.0	76.8	66.3
12	Arizona Test Dest	UM-SEES	-	Powder (P2)	90.9	45.2	39.3	173.0	76.8	66.3
13	Kaolinite	Sigma		Powder (P2)	90.9	45.2	39.3	173.0	76.8	66.3
HULIS										
1	Waskish Peat Humic Acid Reference	IHSS***	1R107H	Powder (P1)	90.9	45.2	39.3	173.0	76.8	66.3
2	Suwannee River Humic Acid Standard II	IHSS	2S101H	Powder (P2)	90.9	45.2	39.3	173.0	76.8	66.3
3	Suwannee River Fulvic Acid Standard I	IHSS	1S101F	Powder (P2)	90.9	45.2	39.3	173.0	76.8	66.3

4	Elliott Soil Humic Acid Standard	IHSS	1S102H	Powder (P1)	90.9	45.2	39.3	173.0	76.8	66.3
5	Pony Lake (Antarctica) Fulvic Acid Reference	IHSS	1R109F	Powder (P2)	90.9	45.2	39.3	173.0	76.8	66.3
6	Nordic Aquatic Fulvic Acid Reference	IHSS	1R105F	Powder (P2)	90.9	45.2	39.3	173.0	76.8	66.3
Polycyclic Hydrocarbons										
1	Pyrene	Sigma	82648	Powder (P1)	92.8	48.0	40.5	176.1	79.7	68.8
2	Phenanthrene	Sigma	695114	Powder (P1)	92.8	48.0	40.5	176.1	79.7	68.8
3	Naphthalene	Sigma	84679	Powder (P1)	92.8	48.0	40.5	176.1	79.7	68.8
Combustion Soot and Smoke										
1	Aquadag	Synthesized in lab	-	Liquid	45.6	24.4	46.6	89.5	45.7	78.9
2	Ash	MPIC	-	Powder (P1)	96.7	46.1	40.6	186.5	77.7	69.0
3	Fullerene Soot	Alfa Aesar	40971	Powder (P2)	92.8	48.0	40.5	176.1	79.7	68.8
4	Diesel Soot	NIST	2975	Powder (P1)	92.8	48.0	40.5	176.1	79.7	68.8
5	Cigarette Smoke	Marlboro 83s	-	Smoke	50.5	24.9	48.8	101.2	46.3	80.9
6	Wood Smoke (*Pinus Nigra ,Black Pine*)	Local Sample	-	Smoke	50.5	24.9	48.8	101.2	46.3	80.9
7	Fire Ash	UM-SEES	-	Powder (P1)	85.1	52.3	46.1	162.5	85.2	79.2
Brown Carbon										
1	Methylglyoxal + Glycine	Synthesized in lab	-	Liquid	30.9	16.8	60.8	63.8	35.1	101.2
2	Glycolaldehyde + Methylamine	Synthesized	-	Liquid	33.5	17.6	64.0	69.4	36.1	108.5
3	Glyoxal + Ammonium Sulfate	Synthesized	-	Liquid	31.5	17.2	64.9	65.2	34.7	111.7
Miscellaneous non-biological										
1	Laboratory wipes	Kimberly Clark	-		46.4	23.7	43.9	92.7	44.5	73.9
2	Cotton t-shirt (white)	Hanes	-		46.4	23.7	43.9	92.7	44.5	73.9

3	Cotton t-shirt (black)	Hanes	-		46.4	23.7	43.9	92.7	44.5	73.9
4	2 µm Green	Thermo-Sci.	G0200	Liquid	-	-	-	-	-	-
5	2 µm Red	Thermo-Sci.	R0200	Liquid	-	-	-	-	-	-
6	2.1 µm Blue	Thermo-Sci.	B0200	Liquid	-	-	-	-	-	-
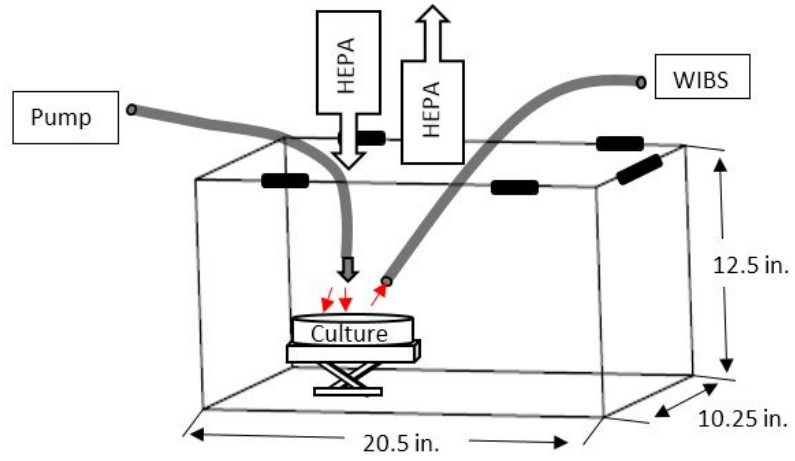
Figure A.1. Schematic diagram of home-built chamber for the aerosolization of fungal spores.
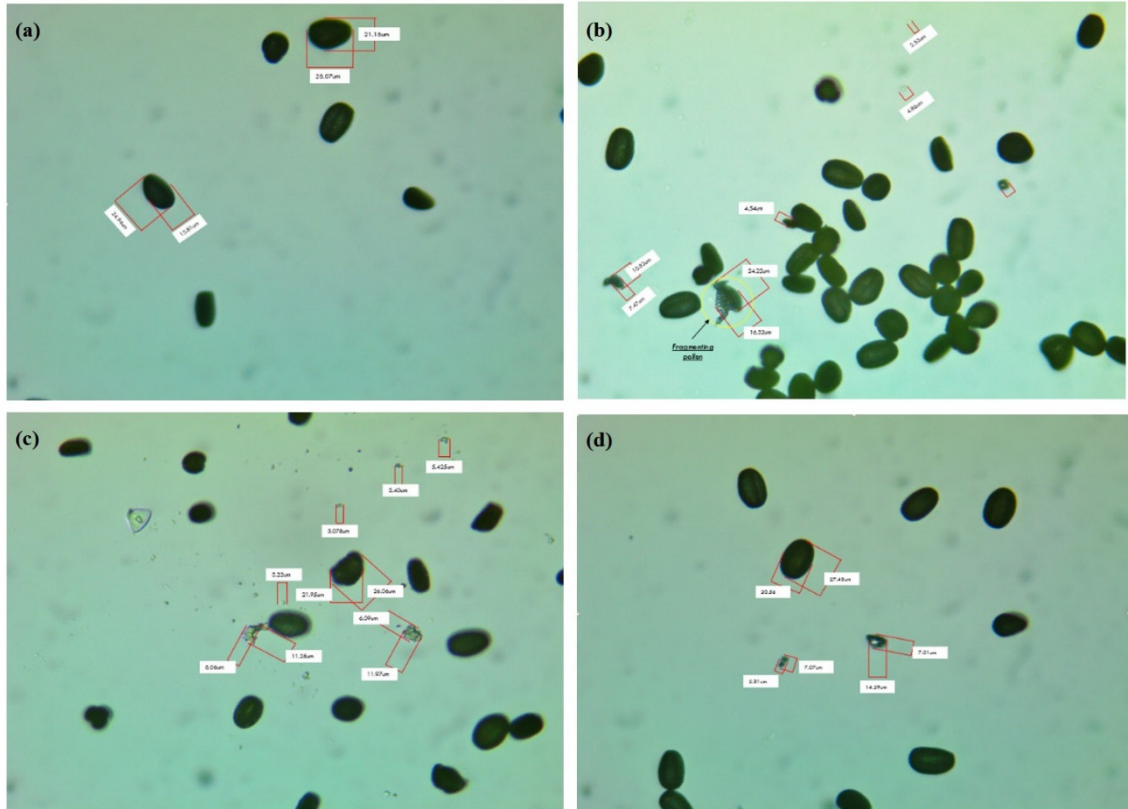
Figure A.2. Impacted pollen (*Olea europaea*) images collected with an AmScope camera (MU800, AmScope) with an objective lens with 40x magnification. (a) Not stirred (b-d) Stirred.
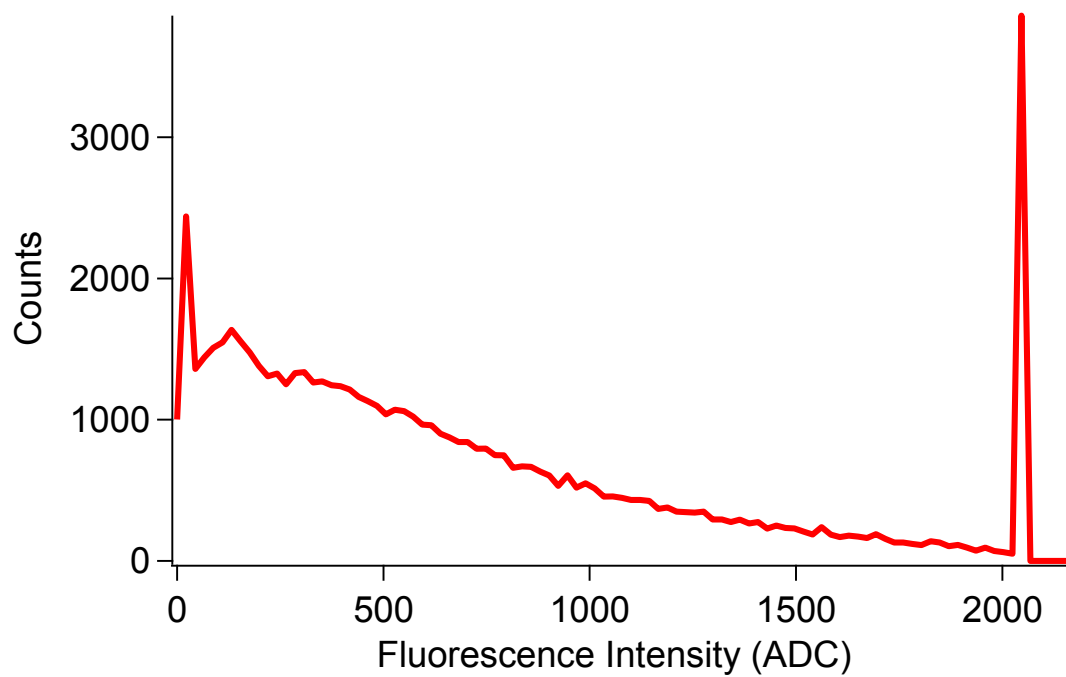
Figure A.3. Fluorescence intensity histogram of FL1 for *Aspergillus niger* (Fungi 2). One broad mode extending from 0-2000 analog-to-digital counts (ADC) and a second mode showing detector saturation at ~2047 ADC.
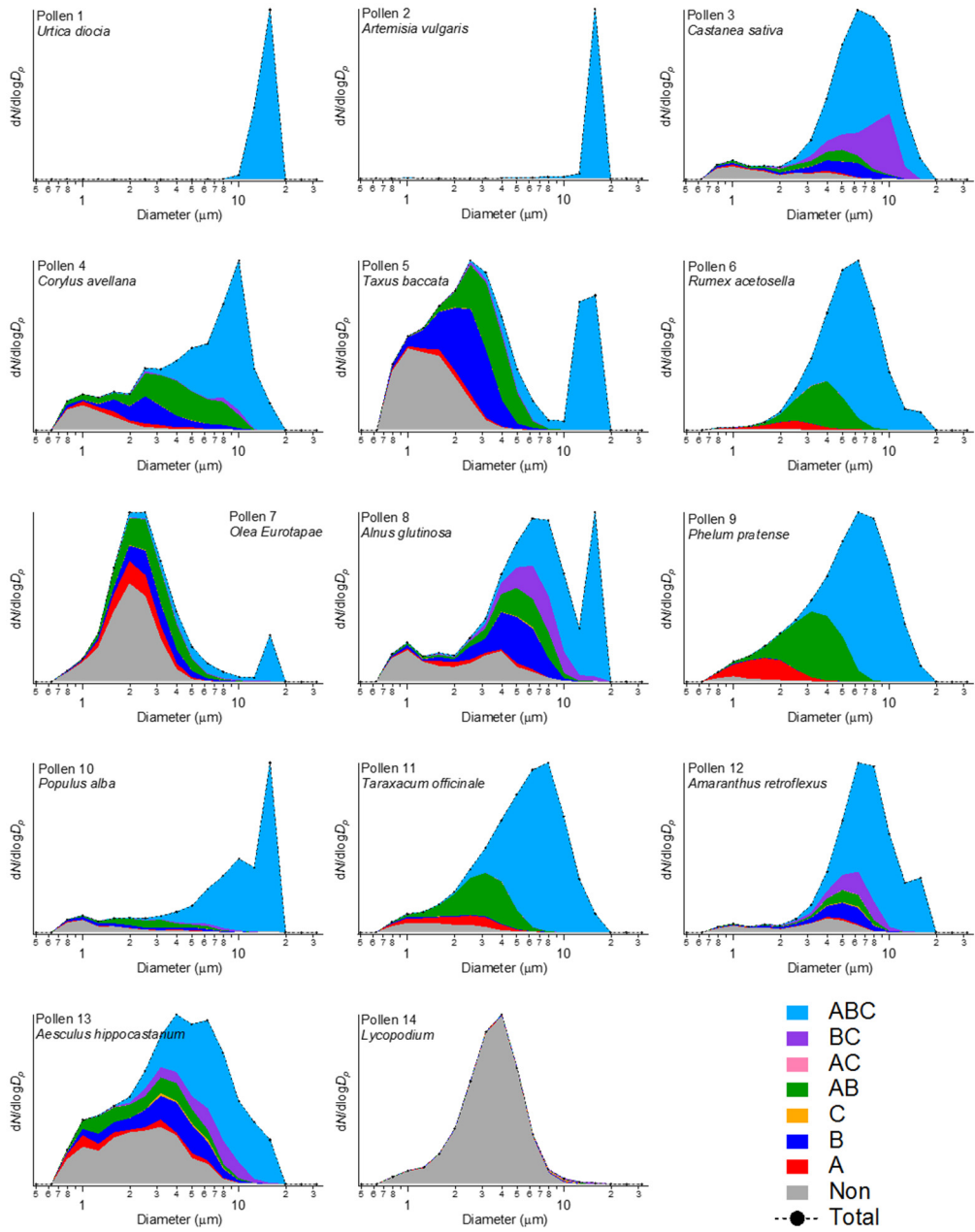
Figure A.4A. Stacked particle type size distributions of pollen using FT + 3σ threshold.
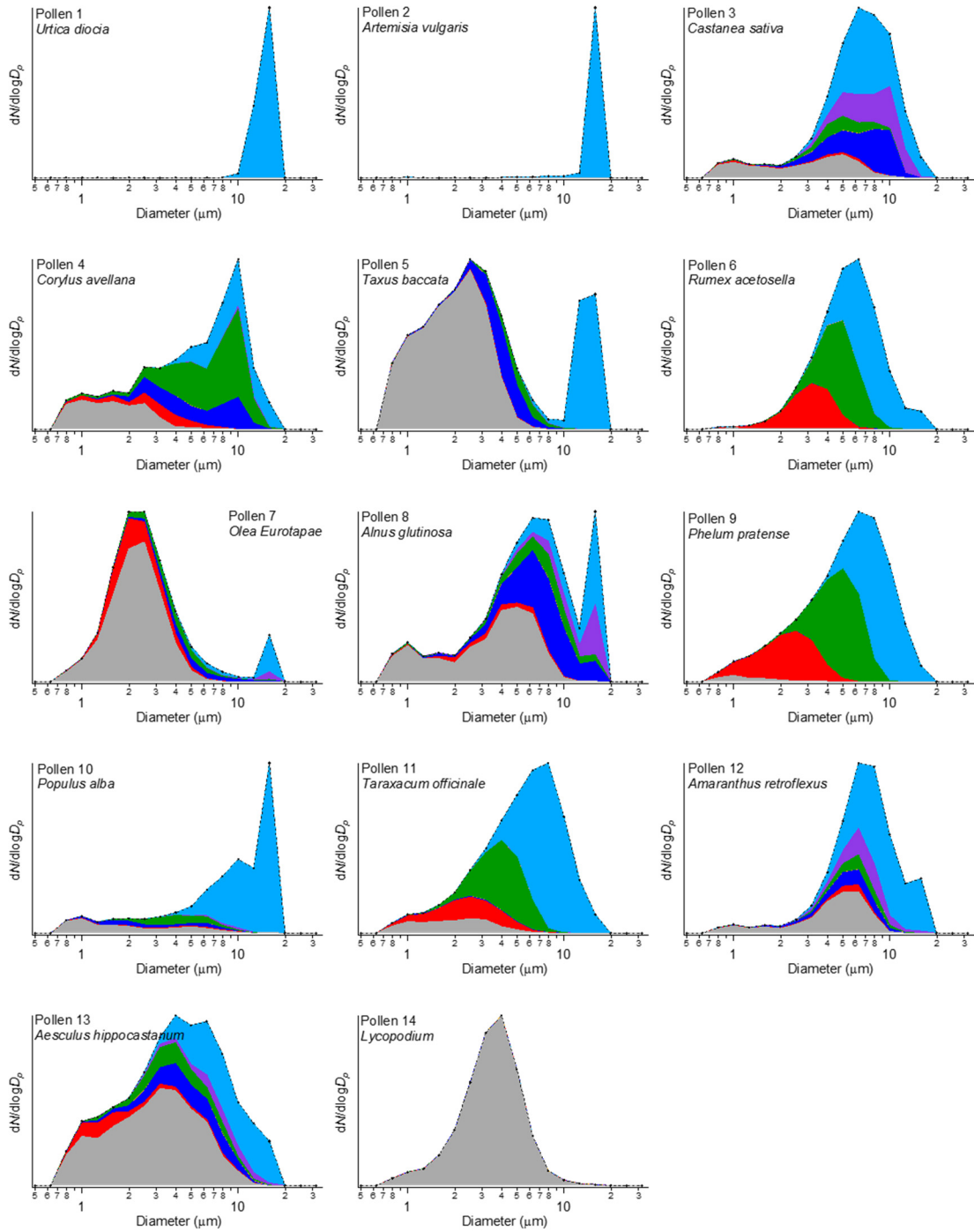
Figure A.4B. Stacked particle type size distributions of pollen using FT + 9σ threshold.
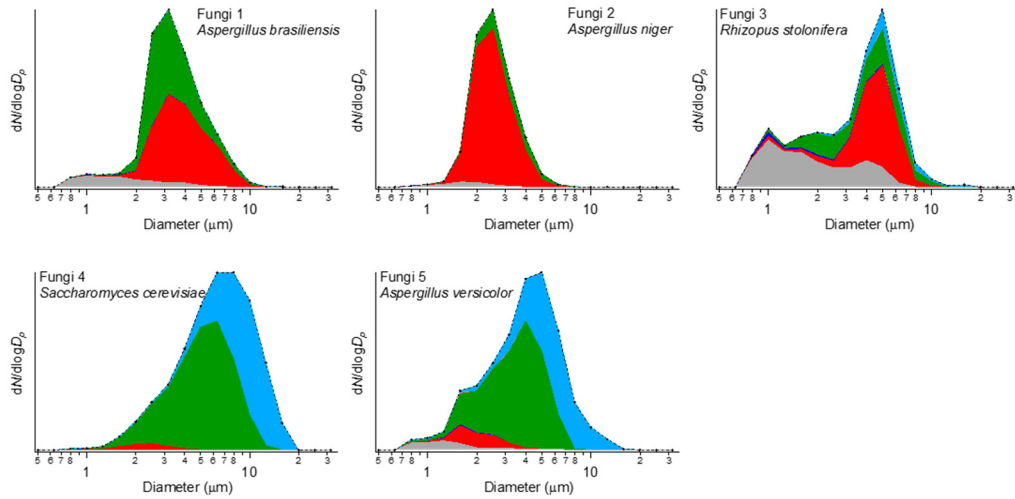
Figure A.4C. Stacked particle type size distributions of fungal spores using FT + 3σ threshold.
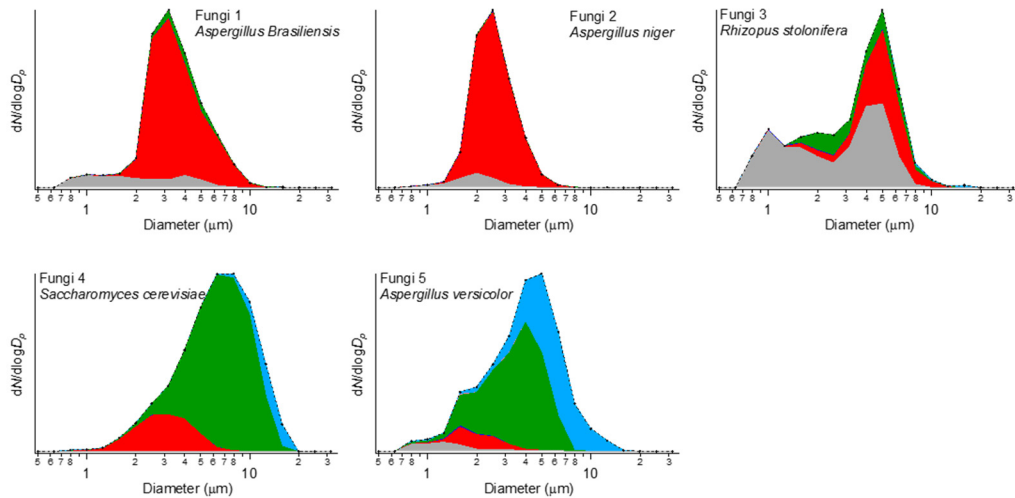
Figure A.4D. Stacked particle type size distributions of fungal spores using FT + 9σ threshold.
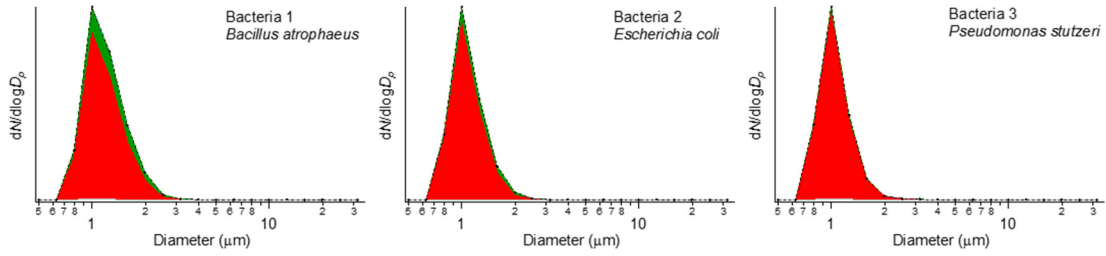
Figure A.4E. Stacked particle type size distributions of bacteria using FT + 3σ threshold.
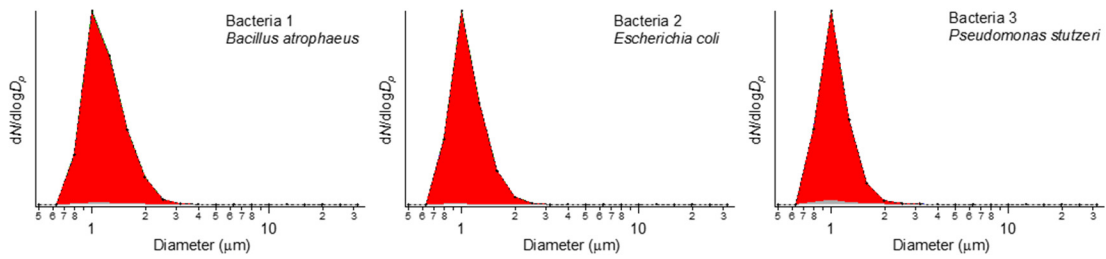
Figure A.4F. Stacked particle type size distributions of bacteria using FT + 9σ threshold.
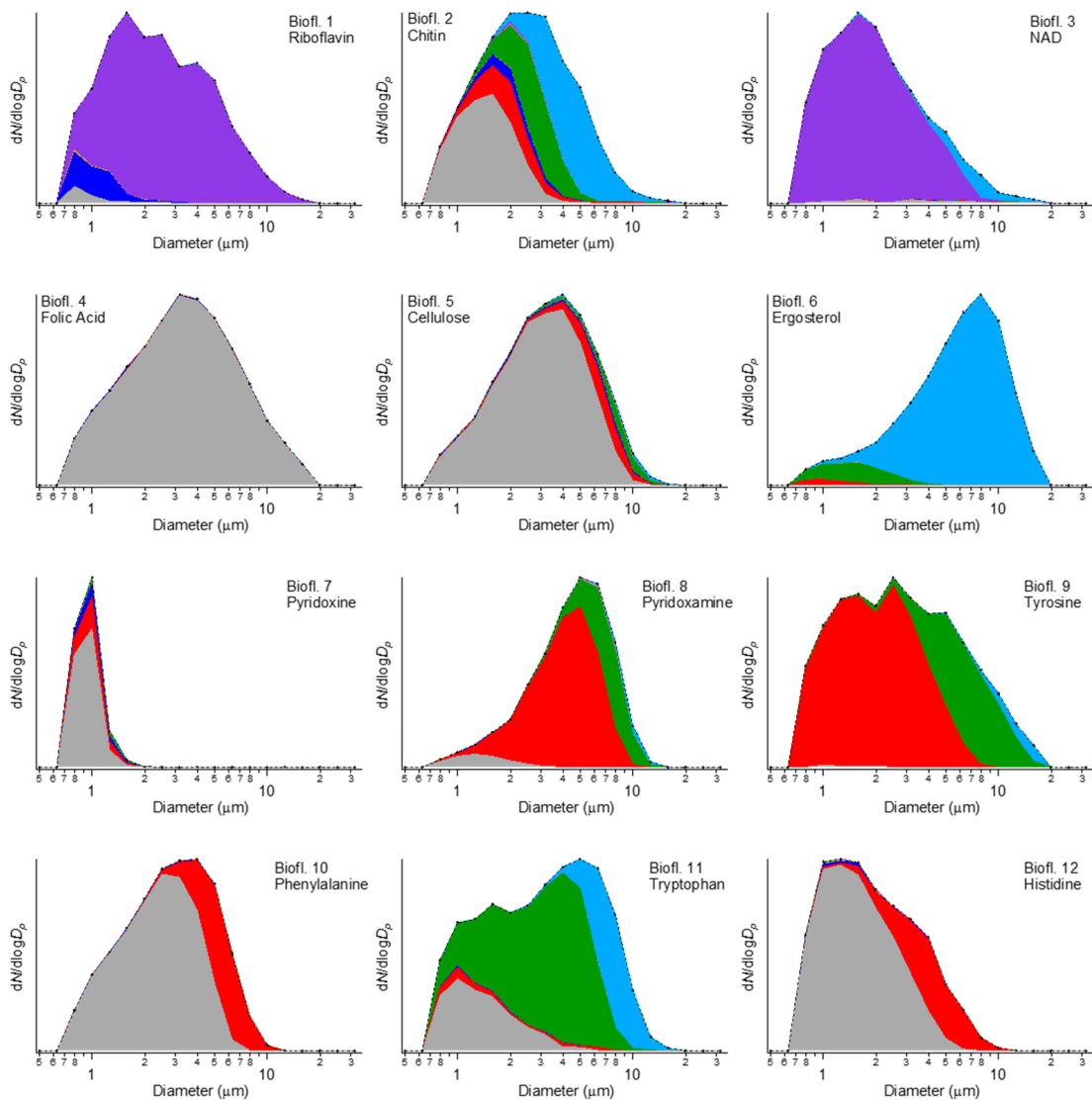
Figure A.4G. Stacked particle type size distributions of biofluorophores using FT + 3σ threshold.
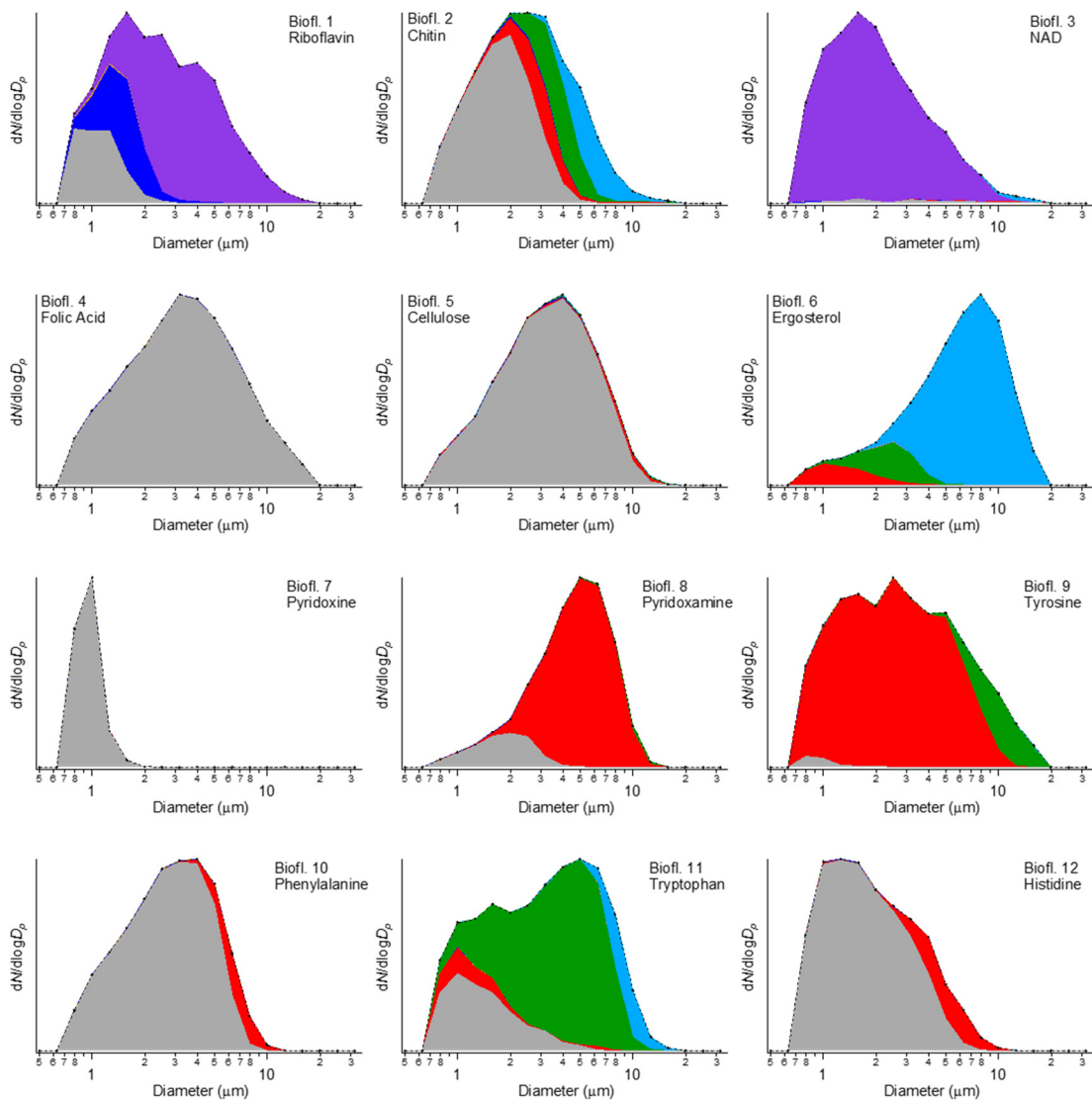
Figure A.4H. Stacked particle type size distributions of biofluorophores using FT + 9σ threshold.

137
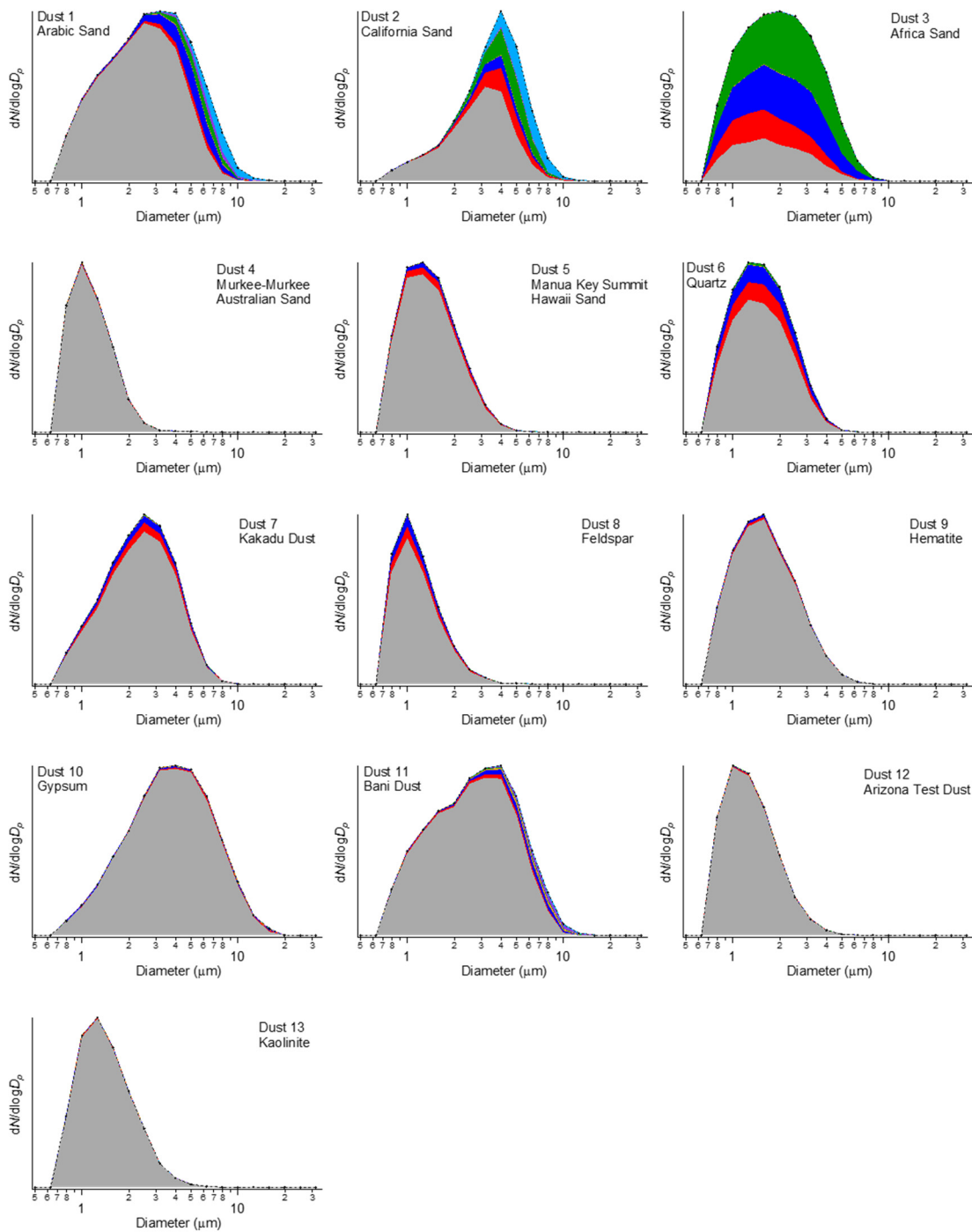
Figure A.4I. Stacked particle type size distributions of dust using FT + 3σ threshold.
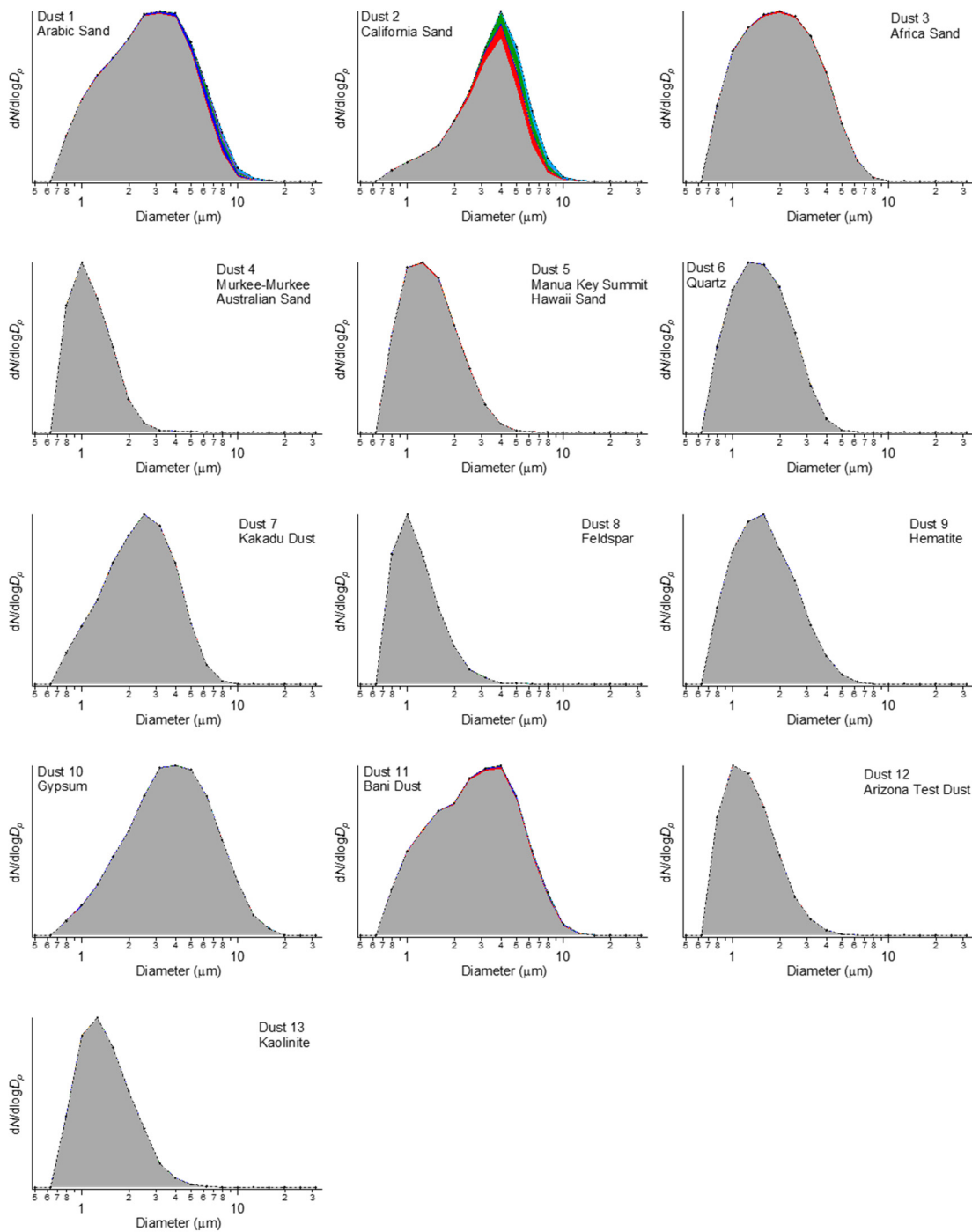
Figure A.4J. Stacked particle type size distributions of dust using FT + 9σ threshold.
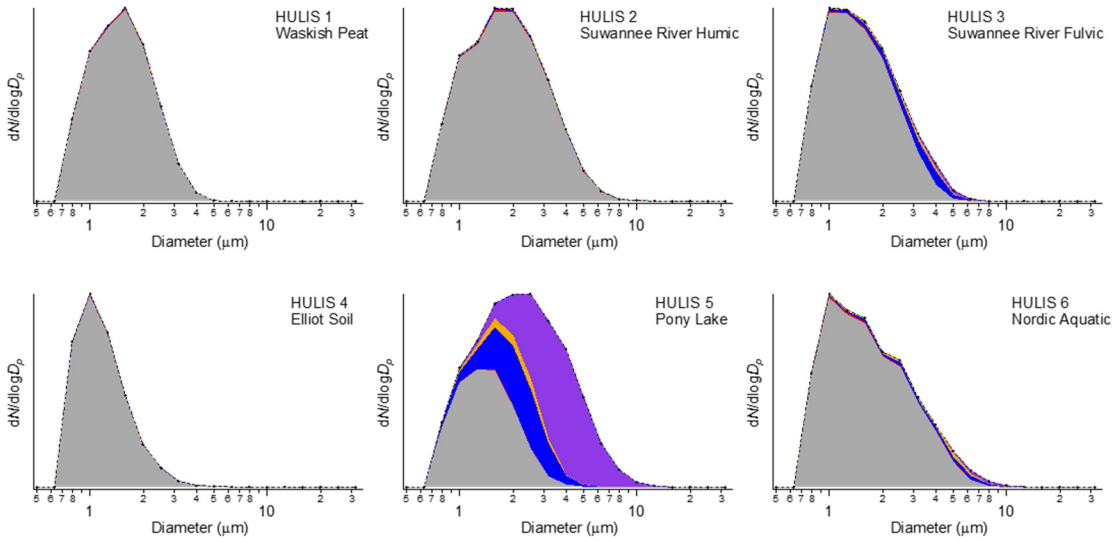
Figure A.4K. Stacked particle type size distributions of HULIS using FT + 3σ threshold.
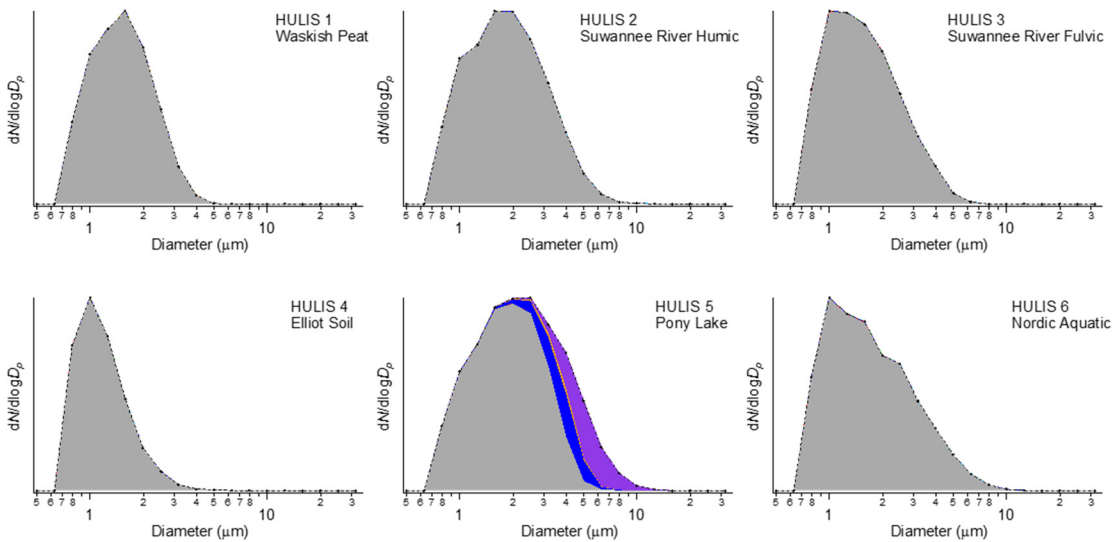
Figure A.4L. Stacked particle type size distributions of HULIS using FT + 9σ threshold.
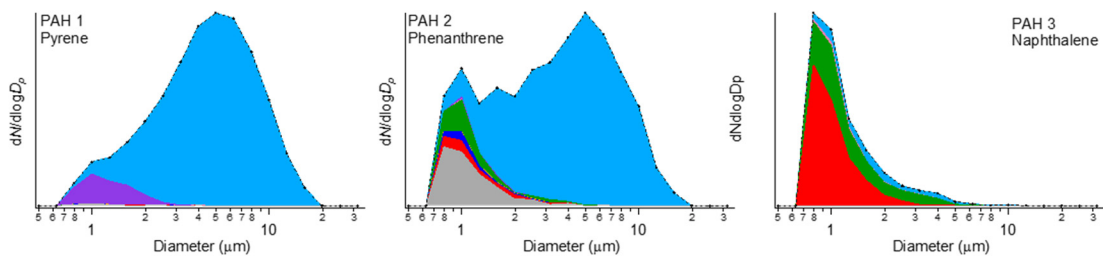
Figure A.4M. Stacked particle type size distributions of PAHs using FT + 3σ threshold.
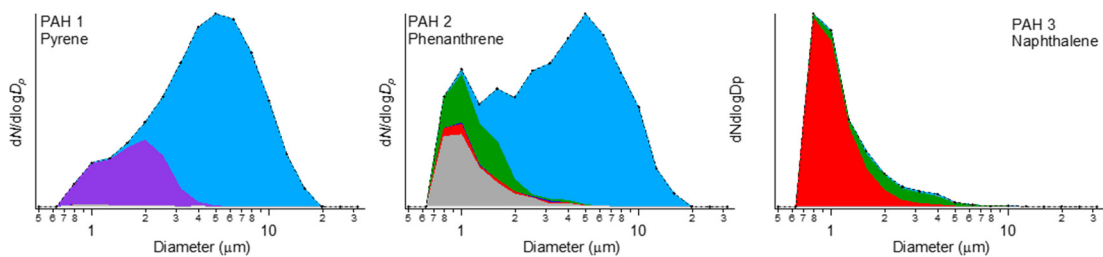
Figure A.4N. Stacked particle type size distributions of PAHs using FT + 9σ threshold.
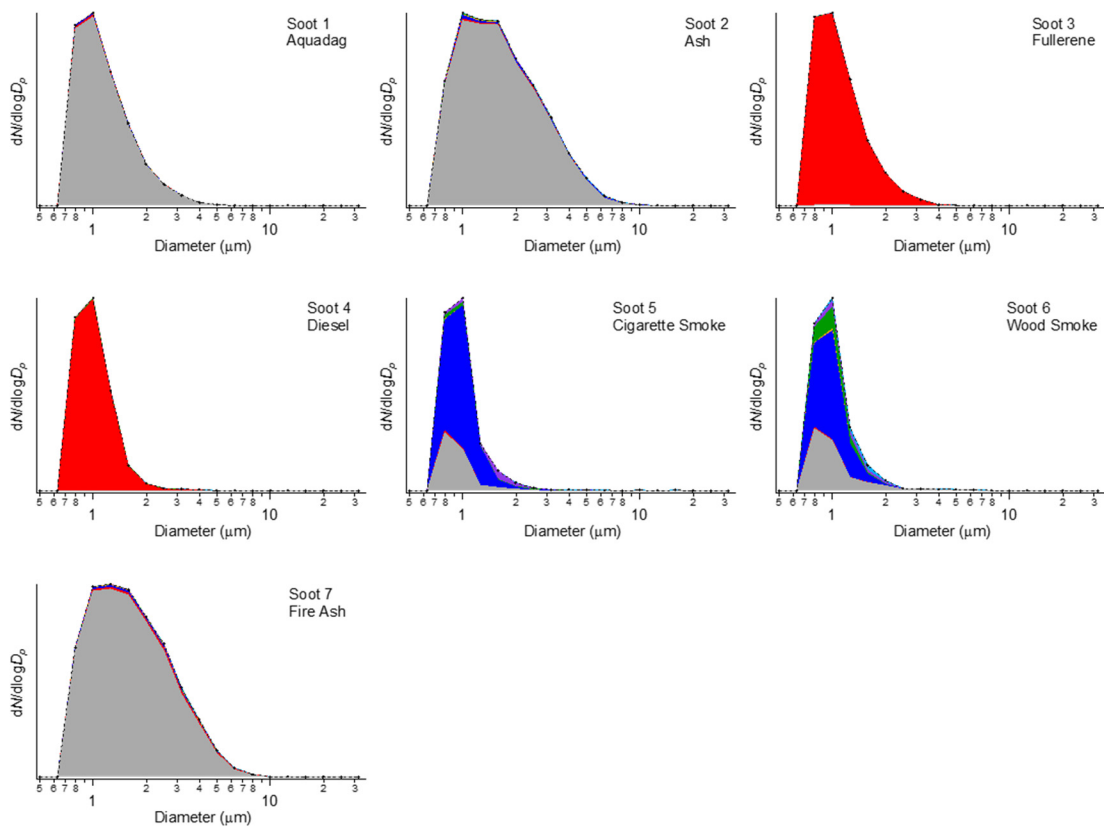
Figure A.4O. Stacked particle type size distributions of soot using FT + 3σ threshold.
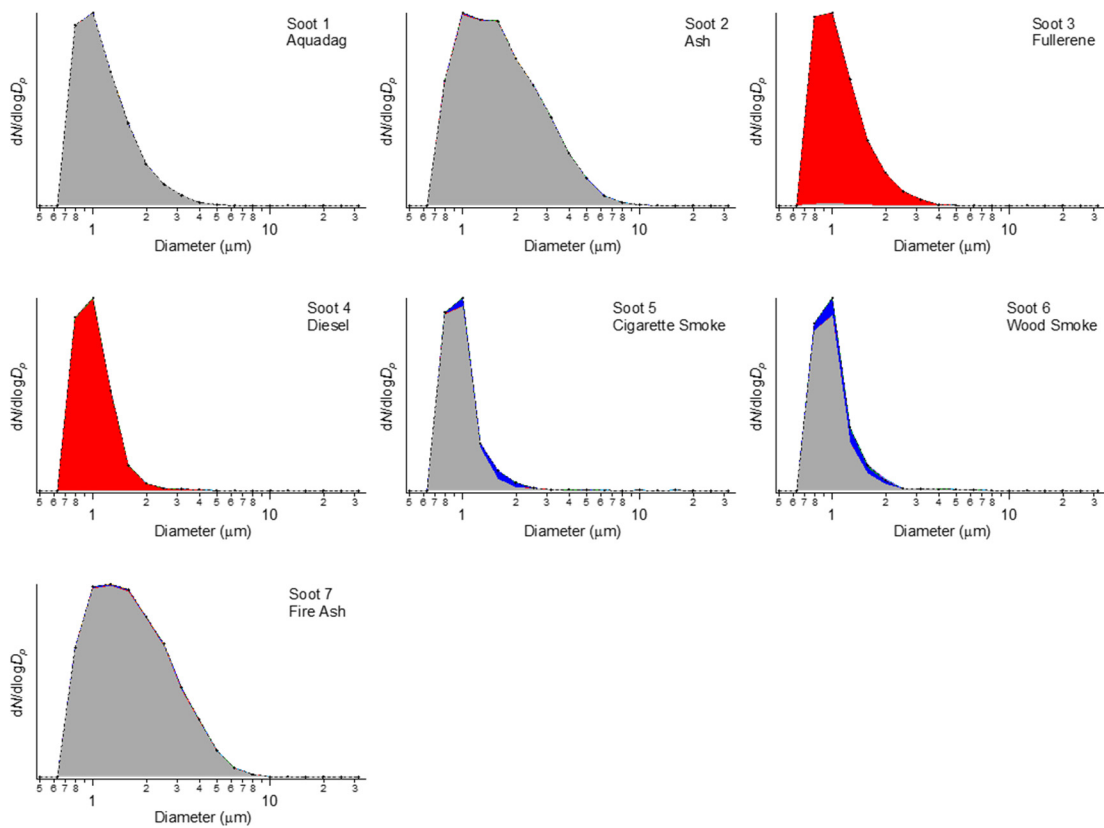
Figure A.4P. Stacked particle type size distributions of soot using FT + 9σ threshold.
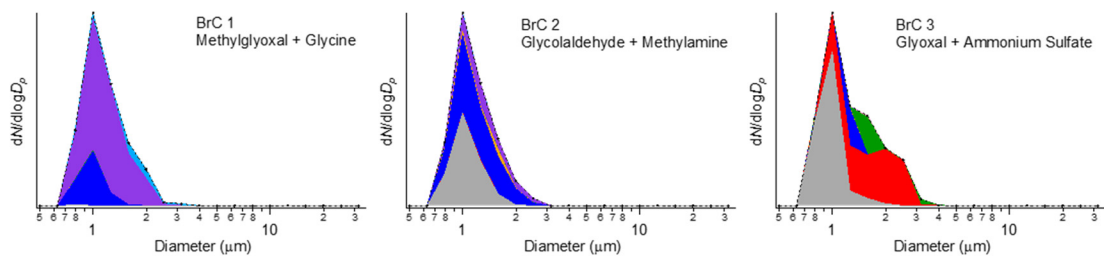
Figure A.4Q. Stacked particle type size distributions of brown carbon (BrC) using FT + 3σ threshold.
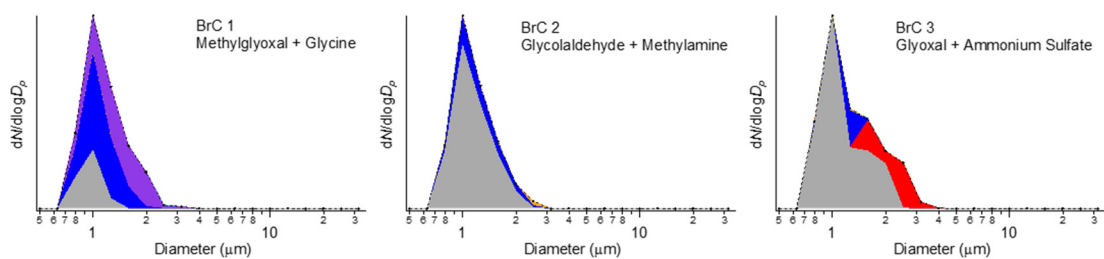
Figure A.4R. Stacked particle type size distributions of brown carbon (BrC) using FT + 9σ threshold.

144
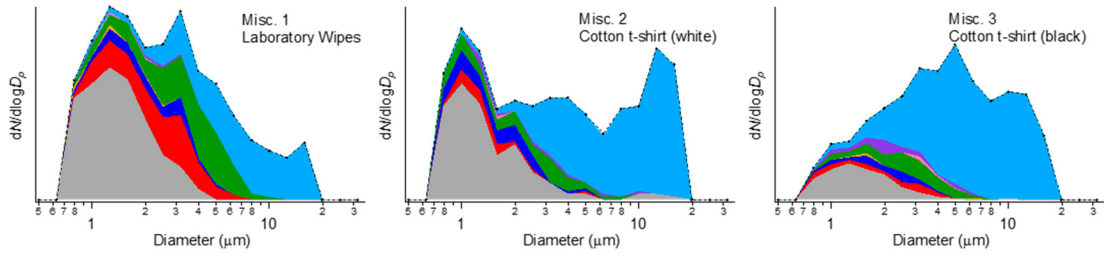
Figure A.4S. Stacked particle type size distributions of miscellaneous samples using FT + 3σ threshold.
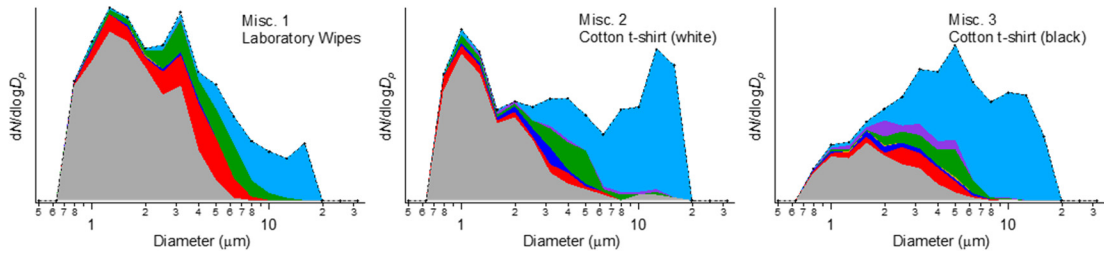
Figure A.4T. Stacked particle type size distributions of miscellaneous samples using FT + 9σ threshold.

Appendix B: Chapter 3 Supplement

Appendix B lists information supplemental to the clustering work presented in Chapter 3.

Table B.1. Trial 1: Particle counts for *Aspergillus niger* (Fungi 2) and diesel soot generated for each scenario for 2, 3 and 4-cluster solutions. Table values represent number of particles in each category.

	A		B		C		D		E		F	
Cl.	Fungi 2	Diesel	Fungi 2	Diesel	Fungi 2	Diesel	Fungi 2	Diesel	Fungi 2	Diesel	Fungi 2	Diesel
1	20222	5600	27502	204	27487	296	27505	298	27501	303	22396	5623
2	7537	57	257	5453	272	5361	254	5359	258	5354	5363	34

	A		B		C		D		E		F	
Cl.	Fungi 2	Diesel	Fungi 2	Diesel	Fungi 2	Diesel	Fungi 2	Diesel	Fungi 2	Diesel	Fungi 2	Diesel
1	20222	5600	16370	75	11460	53	15907	206	19495	200	22396	5623
2	7537	54	257	5453	16027	243	254	5359	8006	103	5363	31
3	0	3	11132	129	272	5361	11598	92	258	5354	0	3

	A		B		C		D		E		F	
Cl.	Fungi 2	Diesel	Fungi 2	Diesel	Fungi 2	Diesel	Fungi 2	Diesel	Fungi 2	Diesel	Fungi 2	Diesel
1	20222	5600	12887	7	11460	53	5471	5	19495	200	22131	234
2	170	19	257	5453	16027	243	254	5359	8006	103	265	5389
3	7367	35	3483	68	263	5360	10436	201	201	5350	5363	31
4	0	3	11132	129	9	1	11598	91	57	4	0	3
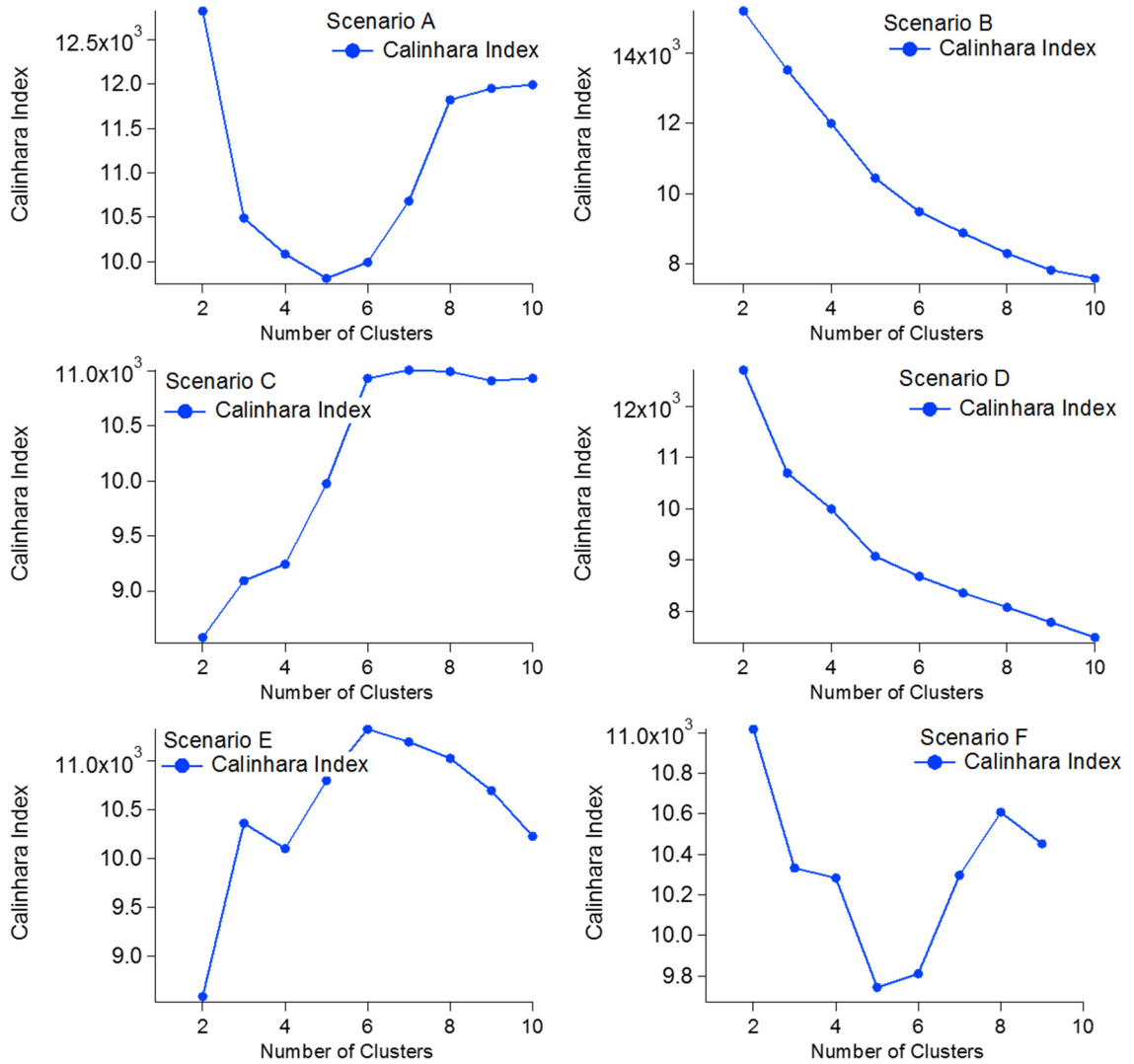
Figure B.1. Trial 2: Calinhara Index for *Aspergillus niger* and *Saccharomyces cerevisiae* trial.

Table B.2. Trial 2: Particle counts for *Aspergillus niger* (Fungi 2) and *Sacchoromyces cerevisiae* (Fungi 4) generated for each scenario for 2, 3 and 4-cluster solutions. Table values represent number of particles in each category.

	A		B		C		D		E		F	
Cl.	Fungi 2	Fungi 4	Fungi 2	Fungi 4	Fungi 2	Fungi 4	Fungi 2	Fungi 4	Fungi 2	Fungi 4	Fungi 2	Fungi 4
1	25709	777	27297	1384	27758	4655	24634	1663	27758	4655	9566	4529
2	2050	3883	462	3276	1	5	3125	2997	1	5	18193	131

	A		B		C		D		E		F	
Cl.	Fungi 2	Fungi 4	Fungi 2	Fungi 4	Fungi 2	Fungi 4	Fungi 2	Fungi 4	Fungi 2	Fungi 4	Fungi 2	Fungi 4
1	25709	777	17836	321	6165	3896	17507	1108	11639	4058	9466	2504
2	2048	3878	462	3276	21593	759	7127	555	16119	597	18193	131
3	2	5	9461	1063	1	5	3125	2997	1	5	100	2025

	A		B		C		D		E		F	
Cl.	Fungi 2	Fungi 4	Fungi 2	Fungi 4	Fungi 2	Fungi 4	Fungi 2	Fungi 4	Fungi 2	Fungi 4	Fungi 2	Fungi 4
1	25709	777	5448	9	6165	3896	9532	11	11639	4058	9466	2504
2	234	2181	462	3276	20189	186	7127	555	14726	77	18193	131
3	2	5	12388	312	1404	573	3125	2997	1393	520	64	13
4	1814	1697	9461	1063	1	5	7975	1097	1	5	36	2012
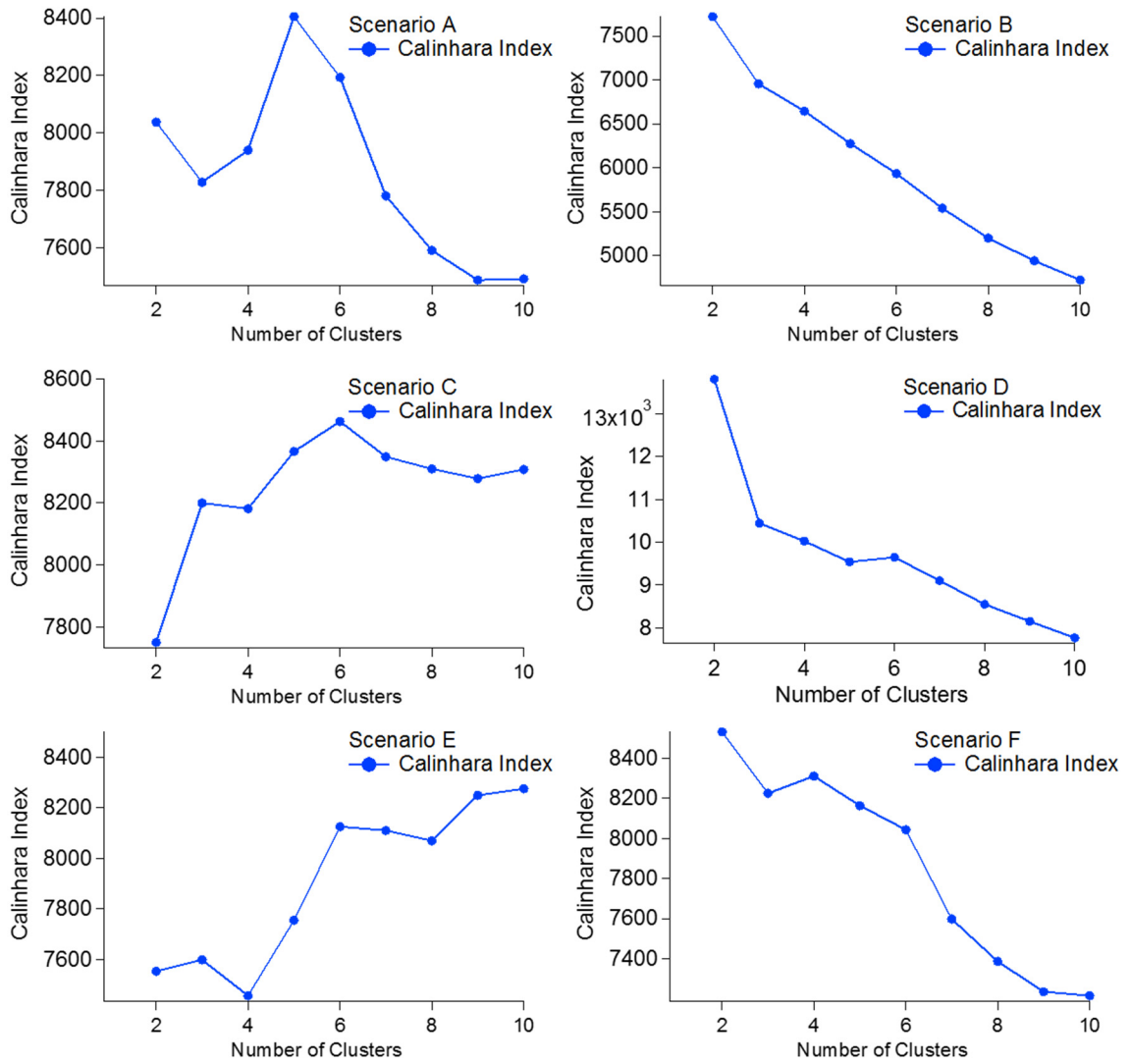
Figure B.2. Trial 3: Calinhara Index for *Aspergillus niger* and California dust trial.

Table B.3. Trial 2: Particle counts for *Aspergillus niger* (Fungi 2) and California dust generated for each scenario for 2, 3 and 4-cluster solutions. Table values represent number of particles in each category.

Cl.	A		B		C		D		E		F	
	Dust	Fungi 2	Dust	Fungi 2	Dust	Fungi 2	Dust	Fungi 2	Dust	Fungi 2	Dust	Fungi 2
1	2493	13685	2413	16401	2243	14564	1884	17302	2594	14438	2336	15524
2	1562	14074	1642	11358	1812	13195	2171	10457	1461	13321	1719	12235

Cl.	A		B		C		D		E		F	
	Dust	Fungi 2	Dust	Fungi 2	Dust	Fungi 2	Dust	Fungi 2	Dust	Fungi 2	Dust	Fungi 2
1	2493	13685	2413	16401	2231	14450	1868	4051	2592	14431	2336	15524
2	1558	14010	1627	348	1812	13195	2171	10457	1461	13321	1705	12076
3	4	64	15	11010	12	114	16	13251	2	7	14	159

Cl.	A		B		C		D		E		F	
	Dust	Fungi 2	Dust	Fungi 2	Dust	Fungi 2	Dust	Fungi 2	Dust	Fungi 2	Dust	Fungi 2
1	2493	13685	2403	6290	2226	11569	1868	4051	1512	13736	2336	15524
2	1551	13908	1627	348	1812	13195	1178	9867	1461	13321	1705	12076
3	7	102	10	10111	12	114	993	590	1080	695	7	95
4	4	64	15	11010	5	2881	16	13251	2	7	7	64

Appendix C: SIBS Instrument Characterization

Another project goal I worked on started in the summer of 2015. This project involved a lab characterization study to better understand some common biological particle types and also interfering (non-biological) species that could potentially make data interpretation more difficult. The characterization was to be done using real time instruments including a WIBS, Spectral Intensity Bioaerosol Sensor (SIBS) and an Ultraviolet Aerodynamic Particle Sizer (UVAPS). The SIBS is a newly developed instrument by DMT that improves upon the spectral resolution of the WIBS and other commercial bioaerosol sensors by providing higher resolution spectral information. The SIBS measures time-resolved fluorescence following sequential excitation at 280 and 370 nm over 16 emission channels spanning a range of approximately 288-734 nm. The instrument provides single particle fluorescence measurements, fluorescence lifetime, an asymmetry factor, and particle size for each interrogated particle. German collaborators who have recently bought the first unit have invited me to do a joint characterization study alongside our existing instruments. I began this initial comparison in the summer of 2015 at the Max Planck Institute of Chemistry (MPIC) in Mainz, Germany. During the initial study we realized that the prototype instrument required significant technical improvements before it was deployable. Since that point the instrument has received several major modifications and upgrades including the addition of a quadrant photomultiplier tube detector (PMT) for asymmetry analysis, a cooled PMT (Hamamatsu), and a modified control board to reduce electrical and thermal noise in

fluorescence detection. Since the summer of 2015, I have been continuously involved in the development of this instrument and have been in close contact with DMT to provide as much feedback and suggestions regarding the development of the SIBS. In September of 2015, I was able to communicate my findings in a poster session at the American Atmospheric Aerosol Research (AAAR) Conference in Minneapolis, Minnesota. I also presented updated work in Septemember of 2016 at AAAR in Portland, Oregon. I was given a student poster award for my work presented on the SIBS at the 2016 conference. A manuscript describing SIBS characterization work is in preparation.

Appendix D: Cyprus and Barbados Field Campaigns

In recent years, advancements in chemical and physical detection of bioaerosols have allowed the characterization of airborne biological particles much more quickly and cost effectively than by previous techniques. One such instrument is the WIBS, which uses single particle fluorescence spectroscopy to characterize biological particles. My aim was to use this instrument to investigate the properties of bioaerosols associated with dust events originating from various geographical locations on field campaigns.

Approximately 800 Tg of soil dust is emitted each year from North Africa and brought west over the Atlantic Ocean (Prospero and Mayol-Bracero, 2013). Satellite images often show dust plumes continuing from the coast of Africa to the Caribbean Basin. Dust concentrations are the highest in Barbados and have a strong seasonal cycle. Over a 48 year period of dust measurements in Barbados, seasonal dust concentrations have changed significantly (Prospero and Mayol-Bracero, 2013). The impact of dust on climate and human health is dependent on the concentration of dust as well as the chemical and physical properties of individual particles.

One sampling site was located in Barbados in Ragged Point, where a small research laboratory is facing the eastern coast of the island to sample air moving west onto the island. The information gained from this field campaign (Jun 2016-Aug 2016) could help in the understanding of how the properties of bioaerosols may affect the properties of cloud formation. Along with the WIBS, another instrument known as the MOUDI (Multiple Orifice Uniform Deposit Impactor) was collecting atmospheric samples, size

153

resolving the impacted particles onto various substrates in the range of 0.05 to 18 μm[4].

The results from this lab campaign will help give a better understanding on the physical and chemical properties of bioaerosols and how their ice nucleation properties may affect cloud formation and precipitation.

A separate campaign I attended in Agia Marina, Cyprus (April 2016) was to also look at dust events and pollution due to long range transport. Cyprus is at the crossroads of 3 continents and long range transported natural and anthropogenic sources. The origin of these sources include pollution from Western Europe, Eastern Europe, Middle East, sea salt from the Mediterranean Sea, as well as dust from Libya, Egypt and Saudi Arabia.

The results from the proposed Barbados campaign will be compared to data I collected in Cyprus, with the hopes that we can gain a better understanding of the differences in properties of bioaerosols originating from various geographical locations. The information gained from both these field campaigns could help in the understanding of how the properties of bioaerosols may affect the properties of cloud formation. Initial results of the impact of fluorescence thresholding on fluorescence particles in both campaigns were presented at a poster session at AAAR conference in October, 2016 in Portland, Oregon.

Appendix E: Cluster Code

E.1 Open-Source R Software

The following text represents computer code writtern for the open-source R software platform, using the Fastcluster package. The code can be put directly into the R platform for the purpose of clustering particles types to discriminate between different particle populations.

Clustering code printed on pages 155-157.

Important Notes about R:
- Before loading in data, save workspace in same folder as the data is saved in, close workspace and reopen before starting your analysis
- R is case sensitive
- The symbol "##" indicates comments regarding the code, however, all lines can be copied and pasted.

Description of code: The code provided uses Hierarchical agglomerative clustering: Ward's linkage method to unbaisly discriminate between different particle materials.

```
## Load data
dat<-read.csv("YourFileName.csv")

##View data in new table
View(dat)

## view data in window as strings, gives number of variables and obeservations in data loaded
str(dat)

##histogram of Fl. intensities not normalized
hist(dat$FL1_280)
hist(dat$FL2_280)
hist(dat$FL2_370)
hist(dat$AF)
hist(dat$Size_cal)

##log histogram
hist(log(dat$FL1_280))
hist(log(dat$FL2_280))
hist(log(dat$FL2_370))
hist(log(dat$Size))
hist(log(dat$AF))

## divide Fl. intensity by Fl2.SctPk
## will create a new columns in data file loaded into R
dat$FL1_norm<-dat$FL1_280/dat$FL2.SctPk
dat$FL2_norm<-dat$FL2_280/dat$FL2.SctPk
dat$FL3_norm<-dat$FL2_370/dat$FL2.SctPk

## View data with new columns of FL normalized by FL2.SctPk
View(dat)
```

```
##histogram of Fl. intensities normalized by Fl2SctPk
hist(dat$FL1_norm)
hist(dat$FL2_norm)
hist(dat$FL3_norm)

##log normalized FL. histogram
hist(log(dat$FL1_norm))
hist(log(dat$FL2_norm))
hist(log(dat$FL3_norm))

##log data to produce normal distrubution
dat$FL1_280<-log(dat$FL1_280)
dat$FL2_280<-log(dat$FL2_280)
dat$FL2_370<-log(dat$FL2_370)
dat$Size_cal<-log(dat$Size_cal)
dat$AF<-log(dat$AF)

##z-score data- centered and scaled
##columns are specified in brackets
dat.scale<-scale(dat[,1:5])
dat
dat.scale
str(dat)

##Install Cluster package-used by Crawford, same for R and Python
install.packages("fastcluster")
library(fastcluster)

## Install cluster stats package for calinhara function
install.packages ("fpc")
library (fpc)

##HAC using squared euclidean distance and average method
dat.clust<-hclust(dist(dat.scale),method="ward.D2")

##Dendogram
require(graphics)
plot(dat.clust)

##defining number of clusters
n<-4

##cutting tree/dendrogram into "n"=number clusters
## Cuts a tree, e.g., as resulting from hclust, into several groups either by specifying the desired number(s) of groups or the cut
height(s).
memb <- cutree(dat.clust, k = n)

##Calinhara Index
calinhara(dat.scale,memb)

##Returns the first or last parts of a vector, matrix, table, data frame
head(memb)

##creates column with particle by particle cluster number
dat$gp<-memb

## used to store data tables

##new temporary table with z-scaled data
dat.temp<-data.frame(dat.scale)

##add clustering assignment to data imported
dat.temp$gp<-memb
```

156

```
## View data in table with cluster assignment and particle type
table(dat$gp,dat$Type)

## Mean centered but since z-scaled then basically 0
center.all<-colMeans(dat.scale)

##Export data as .csv and will be saved in same folder at data
 write.csv(dat, file="FungiDust_B_4Clust.csv")
```

///

E.2 Igor Pro, Wavemetrics

The following text represents computer code writtern for the Igor Pro (version 6.36),
Wavemetrics platform. The code can be put directly into the Igor plateform for the
purpose of discriminating between different particle populations by created particle type
stacked size distributions for each cluster (i.e. using Perring-style analysis).

Igor code printed on pages 157 – 183

Important Notes about Igor Code:
- The symbol "##" indicates comments regarding the code, however, all lines can
  be copied and pasted into Igor.

Description of Igor code: The code provided is intended for the .csv file saved from the
clustering analysis done in R. Particles will be categorized by (i) cluster assignment and
(ii) particle type classification, introduced by Perring et al. (2015). The max number of
clusters this code deals with is 4.

///
Description of function: Extractdata() function takes the data from the raw .csv file from the R clustering analysis and extracts data
variable by cluster number.

```
Function ExtractData()
      wave Fl1_280, Fl2_280, Fl2_370, Size_cal, AF, gp

      ##extract data for cluster 1
      •Extract/o Fl1_280, Fl1_Clust1, gp==1
      •Extract/o Fl2_280, Fl2_Clust1, gp==1
      •Extract/o Fl2_370, Fl3_Clust1, gp==1
      •Extract/o Size_cal, Size_Clust1, gp==1
      •Extract/o AF, AF_Clust1, gp==1

      ##extract data for cluster 2
      •Extract/o Fl1_280, Fl1_Clust2, gp==2
      •Extract/o Fl2_280, Fl2_Clust2, gp==2
      •Extract/o Fl2_370, Fl3_Clust2, gp==2
      •Extract/o Size_cal, Size_Clust2, gp==2
      •Extract/o AF, AF_Clust2, gp==2

      ##extract data for cluster 3
      •Extract/o Fl1_280, Fl1_Clust3, gp==3
      •Extract/o Fl2_280, Fl2_Clust3, gp==3
      •Extract/o Fl2_370, Fl3_Clust3, gp==3
      •Extract/o Size_cal, Size_Clust3, gp==3
```

•Extract/o AF, AF_Clust3, gp==3
•Extract/o gp, gp3, gp==3

##extract data for cluster 4
•Extract/o Fl1_280, Fl1_Clust4, gp==4
•Extract/o Fl2_280, Fl2_Clust4, gp==4
•Extract/o Fl2_370, Fl3_Clust4, gp==4
•Extract/o Size_cal, Size_Clust4, gp==4
•Extract/o AF, AF_Clust4, gp==4
•Extract/o gp, gp4, gp==4

End
///
Description of function: Categories() function should be used after Extractdata() function, it categorizes clustering data into the Perring-style classifications (A, B, C, AB, AC, BC, ABC, Non, and Fl. particles)

Function Categories()
    wave size_cal, af, fl1_280, Fl2_280, Fl2_370, Fl1_thresh, Fl2_thresh, Fl3_thresh, gp,
    wibs_datetime, ft_midtime

    //Total Particles
    extract/o/d size_cal, TOT_sizeClust1, gp==1
    extract/o/d AF, TOT_AFClust1, gp==1
    extract/o/d fl1_280, TOT_Fl1Clust1,gp==1
    extract/o/d fl2_280, TOT_Fl2Clust1,gp==1
    extract/o/d fl2_370, TOT_Fl3Clust1, gp==1

    extract/o/d size_cal, TOT_sizeClust2, gp==2
    extract/o/d AF, TOT_AFClust2, gp==2
    extract/o/d fl1_280, TOT_Fl1Clust2,gp==2
    extract/o/d fl2_280, TOT_Fl2Clust2,gp==2
    extract/o/d fl2_370, TOT_Fl3Clust2, gp==2

    extract/o/d size_cal, TOT_sizeClust3, gp==3
    extract/o/d AF, TOT_AFClust3, gp==3
    extract/o/d fl1_280, TOT_Fl1Clust3,gp==3
    extract/o/d fl2_280, TOT_Fl2Clust3,gp==3
    extract/o/d fl2_370, TOT_Fl3Clust3, gp==3

    extract/o/d size_cal, TOT_sizeClust4, gp==4
    extract/o/d AF, TOT_AFClust4, gp==4
    extract/o/d fl1_280, TOT_Fl1Clust4,gp==4
    extract/o/d fl2_280, TOT_Fl2Clust4,gp==4
    extract/o/d fl2_370, TOT_Fl3Clust4, gp==4

    //NonFl
    extract/o/d size_cal, NON_sizeClust1, FL1_280 < interp(wibs_datetime[p],ft_midtime,FL1_thresh) && FL2_280 < interp(wibs_datetime[p],ft_midtime,FL2_thresh) && FL2_370 < interp(wibs_datetime[p],ft_midtime,FL3_thresh) && gp==1

    extract/o/d AF, NON_AFClust1,   FL1_280 < interp(wibs_datetime[p],ft_midtime,FL1_thresh) && FL2_280 < interp(wibs_datetime[p],ft_midtime,FL2_thresh) && FL2_370 < interp(wibs_datetime[p],ft_midtime,FL3_thresh) && gp==1

    extract/o/d fl1_280, Non_Fl1Clust1, FL1_280 < interp(wibs_datetime[p],ft_midtime,FL1_thresh) && FL2_280 < interp(wibs_datetime[p],ft_midtime,FL2_thresh) && FL2_370 < interp(wibs_datetime[p],ft_midtime,FL3_thresh) && gp==1

    extract/o/d fl2_280, Non_Fl2Clust1, FL1_280 < interp(wibs_datetime[p],ft_midtime,FL1_thresh) && FL2_280 < interp(wibs_datetime[p],ft_midtime,FL2_thresh) && FL2_370 < interp(wibs_datetime[p],ft_midtime,FL3_thresh) && gp==1

    extract/o/d fl2_370, Non_Fl3Clust1,   FL1_280 < interp(wibs_datetime[p],ft_midtime,FL1_thresh) && FL2_280 < interp(wibs_datetime[p],ft_midtime,FL2_thresh) && FL2_370 < interp(wibs_datetime[p],ft_midtime,FL3_thresh) && gp==1

    extract/o/d wibs_datetime, Non_datetimeClust1, FL1_280 < interp(wibs_datetime[p],ft_midtime,FL1_thresh) && FL2_280 < interp(wibs_datetime[p],ft_midtime,FL2_thresh) && FL2_370 < interp(wibs_datetime[p],ft_midtime,FL3_thresh) && gp==1

158

extract/o/d size_cal, NON_sizeClust2, FL1_280 < interp(wibs_datetime[p],ft_midtime,FL1_thresh) && FL2_280 < interp(wibs_datetime[p],ft_midtime,FL2_thresh) && FL2_370 < interp(wibs_datetime[p],ft_midtime,FL3_thresh)&& gp==2

extract/o/d AF, NON_AFClust2,   FL1_280 < interp(wibs_datetime[p],ft_midtime,FL1_thresh) && FL2_280 < interp(wibs_datetime[p],ft_midtime,FL2_thresh) && FL2_370 < interp(wibs_datetime[p],ft_midtime,FL3_thresh) && gp==2
extract/o/d fl1_280, Non_Fl1Clust2, FL1_280 < interp(wibs_datetime[p],ft_midtime,FL1_thresh) && FL2_280 < interp(wibs_datetime[p],ft_midtime,FL2_thresh) && FL2_370 < interp(wibs_datetime[p],ft_midtime,FL3_thresh) && gp==2

extract/o/d fl2_280, Non_Fl2Clust2, FL1_280 < interp(wibs_datetime[p],ft_midtime,FL1_thresh) && FL2_280 < interp(wibs_datetime[p],ft_midtime,FL2_thresh) && FL2_370 < interp(wibs_datetime[p],ft_midtime,FL3_thresh) && gp==2

extract/o/d fl2_370, Non_Fl3Clust2, FL1_280 < interp(wibs_datetime[p],ft_midtime,FL1_thresh) && FL2_280 < interp(wibs_datetime[p],ft_midtime,FL2_thresh) && FL2_370 < interp(wibs_datetime[p],ft_midtime,FL3_thresh) && gp==2

 extract/o/d wibs_datetime, Non_datetimeClust2, FL1_280 < interp(wibs_datetime[p],ft_midtime,FL1_thresh) && FL2_280 < interp(wibs_datetime[p],ft_midtime,FL2_thresh) && FL2_370 < interp(wibs_datetime[p],ft_midtime,FL3_thresh) && gp==2

extract/o/d size_cal, NON_sizeClust3, FL1_280 < interp(wibs_datetime[p],ft_midtime,FL1_thresh) && FL2_280 < interp(wibs_datetime[p],ft_midtime,FL2_thresh) && FL2_370 < interp(wibs_datetime[p],ft_midtime,FL3_thresh)&& gp==3

extract/o/d AF, NON_AFClust3, FL1_280 < interp(wibs_datetime[p],ft_midtime,FL1_thresh) && FL2_280 < interp(wibs_datetime[p],ft_midtime,FL2_thresh) && FL2_370 < interp(wibs_datetime[p],ft_midtime,FL3_thresh) && gp==3

extract/o/d fl1_280, Non_Fl1Clust3, FL1_280 < interp(wibs_datetime[p],ft_midtime,FL1_thresh) && FL2_280 < interp(wibs_datetime[p],ft_midtime,FL2_thresh) && FL2_370 < interp(wibs_datetime[p],ft_midtime,FL3_thresh) && gp==3

 extract/o/d fl2_280, Non_Fl2Clust3, FL1_280 < interp(wibs_datetime[p],ft_midtime,FL1_thresh) && FL2_280 < interp(wibs_datetime[p],ft_midtime,FL2_thresh) && FL2_370 < interp(wibs_datetime[p],ft_midtime,FL3_thresh)&& gp==3
extract/o/d fl2_370, Non_Fl3Clust3, FL1_280 < interp(wibs_datetime[p],ft_midtime,FL1_thresh) && FL2_280 < interp(wibs_datetime[p],ft_midtime,FL2_thresh) && FL2_370 < interp(wibs_datetime[p],ft_midtime,FL3_thresh) && gp==3

extract/o/d wibs_datetime, Non_datetimeClust3, FL1_280 < interp(wibs_datetime[p],ft_midtime,FL1_thresh) && FL2_280 < interp(wibs_datetime[p],ft_midtime,FL2_thresh) && FL2_370 < interp(wibs_datetime[p],ft_midtime,FL3_thresh) && gp==3

 extract/o/d size_cal, NON_sizeClust4, FL1_280 < interp(wibs_datetime[p],ft_midtime,FL1_thresh) && FL2_280 < interp(wibs_datetime[p],ft_midtime,FL2_thresh) && FL2_370 < interp(wibs_datetime[p],ft_midtime,FL3_thresh)&& gp==4

extract/o/d AF, NON_AFClust4, FL1_280 < interp(wibs_datetime[p],ft_midtime,FL1_thresh) && FL2_280 < interp(wibs_datetime[p],ft_midtime,FL2_thresh) && FL2_370 < interp(wibs_datetime[p],ft_midtime,FL3_thresh) && gp==4

extract/o/d fl1_280, Non_Fl1Clust4, FL1_280 < interp(wibs_datetime[p],ft_midtime,FL1_thresh) && FL2_280 < interp(wibs_datetime[p],ft_midtime,FL2_thresh) && FL2_370 < interp(wibs_datetime[p],ft_midtime,FL3_thresh) && gp==4

extract/o/d fl2_280, Non_Fl2Clust4, FL1_280 < interp(wibs_datetime[p],ft_midtime,FL1_thresh) && FL2_280 < interp(wibs_datetime[p],ft_midtime,FL2_thresh) && FL2_370 < interp(wibs_datetime[p],ft_midtime,FL3_thresh)&& gp==4

extract/o/d fl2_370, Non_Fl3Clust4, FL1_280 < interp(wibs_datetime[p],ft_midtime,FL1_thresh) && FL2_280 < interp(wibs_datetime[p],ft_midtime,FL2_thresh) && FL2_370 < interp(wibs_datetime[p],ft_midtime,FL3_thresh) && gp==4

extract/o/d wibs_datetime, Non_datetimeClust4, FL1_280 < interp(wibs_datetime[p],ft_midtime,FL1_thresh) && FL2_280 < interp(wibs_datetime[p],ft_midtime,FL2_thresh) && FL2_370 < interp(wibs_datetime[p],ft_midtime,FL3_thresh) && gp==4

//A

extract/o/d size_cal, A_sizeClust1,FL1_280 > interp(wibs_datetime[p],ft_midtime,FL1_thresh) && FL2_280 < interp(wibs_datetime[p],ft_midtime,FL2_thresh) && FL2_370 < interp(wibs_datetime[p],ft_midtime,FL3_thresh)&& gp==1

extract/o/d AF, A_AFClust1, FL1_280 > interp(wibs_datetime[p],ft_midtime,FL1_thresh) && FL2_280 < interp(wibs_datetime[p],ft_midtime,FL2_thresh) && FL2_370 < interp(wibs_datetime[p],ft_midtime,FL3_thresh) && gp==1

extract/o/d fl1_280, A_Fl1Clust1, FL1_280 > interp(wibs_datetime[p],ft_midtime,FL1_thresh) && FL2_280 < interp(wibs_datetime[p],ft_midtime,FL2_thresh) && FL2_370 < interp(wibs_datetime[p],ft_midtime,FL3_thresh) && gp==1

159

extract/o/d fl2_280, A_Fl2Clust1, FL1_280 > interp(wibs_datetime[p],ft_midtime,FL1_thresh) && FL2_280 < interp(wibs_datetime[p],ft_midtime,FL2_thresh) && FL2_370 < interp(wibs_datetime[p],ft_midtime,FL3_thresh)&& gp==1

extract/o/d fl2_370, A_Fl3Clust1, FL1_280 > interp(wibs_datetime[p],ft_midtime,FL1_thresh) && FL2_280 < interp(wibs_datetime[p],ft_midtime,FL2_thresh) && FL2_370 < interp(wibs_datetime[p],ft_midtime,FL3_thresh)&& gp==1

extract/o/d wibs_datetime, A_datetimeClust1, FL1_280 > interp(wibs_datetime[p],ft_midtime,FL1_thresh) && FL2_280 < interp(wibs_datetime[p],ft_midtime,FL2_thresh) && FL2_370 < interp(wibs_datetime[p],ft_midtime,FL3_thresh)&& gp==1

extract/o/d size_cal, A_sizeClust2,FL1_280 > interp(wibs_datetime[p],ft_midtime,FL1_thresh) && FL2_280 < interp(wibs_datetime[p],ft_midtime,FL2_thresh) && FL2_370 < interp(wibs_datetime[p],ft_midtime,FL3_thresh)&& gp==2

extract/o/d AF, A_AFClust2, FL1_280 > interp(wibs_datetime[p],ft_midtime,FL1_thresh) && FL2_280 < interp(wibs_datetime[p],ft_midtime,FL2_thresh) && FL2_370 < interp(wibs_datetime[p],ft_midtime,FL3_thresh)&& gp==2

extract/o/d fl1_280, A_Fl1Clust2, FL1_280 > interp(wibs_datetime[p],ft_midtime,FL1_thresh) && FL2_280 < interp(wibs_datetime[p],ft_midtime,FL2_thresh) && FL2_370 < interp(wibs_datetime[p],ft_midtime,FL3_thresh) && gp==2

extract/o/d fl2_280, A_Fl2Clust2, FL1_280 > interp(wibs_datetime[p],ft_midtime,FL1_thresh) && FL2_280 < interp(wibs_datetime[p],ft_midtime,FL2_thresh) && FL2_370 < interp(wibs_datetime[p],ft_midtime,FL3_thresh) && gp==2

extract/o/d fl2_370, A_Fl3Clust2, FL1_280 > interp(wibs_datetime[p],ft_midtime,FL1_thresh) && FL2_280 < interp(wibs_datetime[p],ft_midtime,FL2_thresh) && FL2_370 < interp(wibs_datetime[p],ft_midtime,FL3_thresh) && gp==2

 extract/o/d wibs_datetime, A_datetimeClust2, FL1_280 > interp(wibs_datetime[p],ft_midtime,FL1_thresh) && FL2_280 < interp(wibs_datetime[p],ft_midtime,FL2_thresh) && FL2_370 < interp(wibs_datetime[p],ft_midtime,FL3_thresh) && gp==2

extract/o/d size_cal, A_sizeClust3,FL1_280 > interp(wibs_datetime[p],ft_midtime,FL1_thresh) && FL2_280 < interp(wibs_datetime[p],ft_midtime,FL2_thresh) && FL2_370 < interp(wibs_datetime[p],ft_midtime,FL3_thresh) && gp==3

extract/o/d AF, A_AFClust3, FL1_280 > interp(wibs_datetime[p],ft_midtime,FL1_thresh) && FL2_280 < interp(wibs_datetime[p],ft_midtime,FL2_thresh) && FL2_370 < interp(wibs_datetime[p],ft_midtime,FL3_thresh) && gp==3

extract/o/d fl1_280, A_Fl1Clust3, FL1_280 > interp(wibs_datetime[p],ft_midtime,FL1_thresh) && FL2_280 < interp(wibs_datetime[p],ft_midtime,FL2_thresh) && FL2_370 < interp(wibs_datetime[p],ft_midtime,FL3_thresh) && gp==3

extract/o/d fl2_280, A_Fl2Clust3, FL1_280 > interp(wibs_datetime[p],ft_midtime,FL1_thresh) && FL2_280 < interp(wibs_datetime[p],ft_midtime,FL2_thresh) && FL2_370 < interp(wibs_datetime[p],ft_midtime,FL3_thresh)&& gp==3

extract/o/d fl2_370, A_Fl3Clust3, FL1_280 > interp(wibs_datetime[p],ft_midtime,FL1_thresh) && FL2_280 < interp(wibs_datetime[p],ft_midtime,FL2_thresh) && FL2_370 < interp(wibs_datetime[p],ft_midtime,FL3_thresh)&& gp==3

extract/o/d wibs_datetime, A_datetimeClust3, FL1_280 > interp(wibs_datetime[p],ft_midtime,FL1_thresh) && FL2_280 < interp(wibs_datetime[p],ft_midtime,FL2_thresh) && FL2_370 < interp(wibs_datetime[p],ft_midtime,FL3_thresh)&& gp==3

extract/o/d size_cal, A_sizeClust4,FL1_280 > interp(wibs_datetime[p],ft_midtime,FL1_thresh) && FL2_280 < interp(wibs_datetime[p],ft_midtime,FL2_thresh) && FL2_370 < interp(wibs_datetime[p],ft_midtime,FL3_thresh) && gp==4

extract/o/d AF, A_AFClust4, FL1_280 > interp(wibs_datetime[p],ft_midtime,FL1_thresh) && FL2_280 < interp(wibs_datetime[p],ft_midtime,FL2_thresh) && FL2_370 < interp(wibs_datetime[p],ft_midtime,FL3_thresh) && gp==4

extract/o/d fl1_280, A_Fl1Clust4, FL1_280 > interp(wibs_datetime[p],ft_midtime,FL1_thresh) && FL2_280 < interp(wibs_datetime[p],ft_midtime,FL2_thresh) && FL2_370 < interp(wibs_datetime[p],ft_midtime,FL3_thresh) && gp==4

extract/o/d fl2_280, A_Fl2Clust4, FL1_280 > interp(wibs_datetime[p],ft_midtime,FL1_thresh) && FL2_280 < interp(wibs_datetime[p],ft_midtime,FL2_thresh) && FL2_370 < interp(wibs_datetime[p],ft_midtime,FL3_thresh)&& gp==4

extract/o/d fl2_370, A_Fl3Clust4, FL1_280 > interp(wibs_datetime[p],ft_midtime,FL1_thresh) && FL2_280 < interp(wibs_datetime[p],ft_midtime,FL2_thresh) && FL2_370 < interp(wibs_datetime[p],ft_midtime,FL3_thresh)&& gp==4

extract/o/d wibs_datetime, A_datetimeClust4, FL1_280 > interp(wibs_datetime[p],ft_midtime,FL1_thresh) && FL2_280 < interp(wibs_datetime[p],ft_midtime,FL2_thresh) && FL2_370 < interp(wibs_datetime[p],ft_midtime,FL3_thresh)&& gp==4

 //B

extract/o/d size_cal, B_sizeClust1, FL2_280 > interp(wibs_datetime[p],ft_midtime,FL2_thresh) && FL1_280 < interp(wibs_datetime[p],ft_midtime,FL1_thresh) && FL2_370 < interp(wibs_datetime[p],ft_midtime,FL3_thresh)&& gp==1

extract/o/d AF, B_AFClust1, FL2_280 > interp(wibs_datetime[p],ft_midtime,FL2_thresh) && FL1_280 < interp(wibs_datetime[p],ft_midtime,FL1_thresh) && FL2_370 < interp(wibs_datetime[p],ft_midtime,FL3_thresh) && gp==1

extract/o/d fl1_280, B_Fl1Clust1, FL2_280 > interp(wibs_datetime[p],ft_midtime,FL2_thresh) && FL1_280 < interp(wibs_datetime[p],ft_midtime,FL1_thresh) && FL2_370 < interp(wibs_datetime[p],ft_midtime,FL3_thresh)&& gp==1

extract/o/d fl2_280, B_Fl2Clust1, FL2_280 > interp(wibs_datetime[p],ft_midtime,FL2_thresh) && FL1_280 < interp(wibs_datetime[p],ft_midtime,FL1_thresh) && FL2_370 < interp(wibs_datetime[p],ft_midtime,FL3_thresh) && gp==1

extract/o/d fl2_370, B_Fl3Clust1,FL2_280 > interp(wibs_datetime[p],ft_midtime,FL2_thresh) && FL1_280 < interp(wibs_datetime[p],ft_midtime,FL1_thresh) && FL2_370 < interp(wibs_datetime[p],ft_midtime,FL3_thresh) && gp==1

extract/o/d wibs_datetime, B_datetimeClust1,FL2_280 > interp(wibs_datetime[p],ft_midtime,FL2_thresh) && FL1_280 < interp(wibs_datetime[p],ft_midtime,FL1_thresh) && FL2_370 < interp(wibs_datetime[p],ft_midtime,FL3_thresh) && gp==1

extract/o/d size_cal, B_sizeClust2, FL2_280 > interp(wibs_datetime[p],ft_midtime,FL2_thresh) && FL1_280 < interp(wibs_datetime[p],ft_midtime,FL1_thresh) && FL2_370 < interp(wibs_datetime[p],ft_midtime,FL3_thresh)&& gp==2

extract/o/d AF, B_AFClust2, FL2_280 > interp(wibs_datetime[p],ft_midtime,FL2_thresh) && FL1_280 < interp(wibs_datetime[p],ft_midtime,FL1_thresh) && FL2_370 < interp(wibs_datetime[p],ft_midtime,FL3_thresh)&& gp==2

extract/o/d fl1_280, B_Fl1Clust2, FL2_280 > interp(wibs_datetime[p],ft_midtime,FL2_thresh) && FL1_280 < interp(wibs_datetime[p],ft_midtime,FL1_thresh) && FL2_370 < interp(wibs_datetime[p],ft_midtime,FL3_thresh) && gp==2

extract/o/d fl2_280, B_Fl2Clust2, FL2_280 > interp(wibs_datetime[p],ft_midtime,FL2_thresh) && FL1_280 < interp(wibs_datetime[p],ft_midtime,FL1_thresh) && FL2_370 < interp(wibs_datetime[p],ft_midtime,FL3_thresh) && gp==2

extract/o/d fl2_370, B_Fl3Clust2, FL2_280 > interp(wibs_datetime[p],ft_midtime,FL2_thresh) && FL1_280 < interp(wibs_datetime[p],ft_midtime,FL1_thresh) && FL2_370 < interp(wibs_datetime[p],ft_midtime,FL3_thresh) && gp==2

extract/o/d wibs_datetime, B_datetimeClust2, FL2_280 > interp(wibs_datetime[p],ft_midtime,FL2_thresh) && FL1_280 < interp(wibs_datetime[p],ft_midtime,FL1_thresh) && FL2_370 < interp(wibs_datetime[p],ft_midtime,FL3_thresh) && gp==2

extract/o/d size_cal, B_sizeClust3,FL2_280 > interp(wibs_datetime[p],ft_midtime,FL2_thresh) && FL1_280 < interp(wibs_datetime[p],ft_midtime,FL1_thresh) && FL2_370 < interp(wibs_datetime[p],ft_midtime,FL3_thresh) && gp==3

extract/o/d AF, B_AFClust3, FL2_280 > interp(wibs_datetime[p],ft_midtime,FL2_thresh) && FL1_280 < interp(wibs_datetime[p],ft_midtime,FL1_thresh) && FL2_370 < interp(wibs_datetime[p],ft_midtime,FL3_thresh) && gp==3

extract/o/d fl1_280, B_Fl1Clust3, FL2_280 > interp(wibs_datetime[p],ft_midtime,FL2_thresh) && FL1_280 < interp(wibs_datetime[p],ft_midtime,FL1_thresh) && FL2_370 < interp(wibs_datetime[p],ft_midtime,FL3_thresh) && gp==3
extract/o/d fl2_280, B_Fl2Clust3, FL2_280 > interp(wibs_datetime[p],ft_midtime,FL2_thresh) && FL1_280 < interp(wibs_datetime[p],ft_midtime,FL1_thresh) && FL2_370 < interp(wibs_datetime[p],ft_midtime,FL3_thresh) && gp==3

extract/o/d fl2_370, B_Fl3Clust3, FL2_280 > interp(wibs_datetime[p],ft_midtime,FL2_thresh) && FL1_280 < interp(wibs_datetime[p],ft_midtime,FL1_thresh) && FL2_370 < interp(wibs_datetime[p],ft_midtime,FL3_thresh)&& gp==3

extract/o/d wibs_datetime, B_datetimeClust3, FL2_280 > interp(wibs_datetime[p],ft_midtime,FL2_thresh) && FL1_280 < interp(wibs_datetime[p],ft_midtime,FL1_thresh) && FL2_370 < interp(wibs_datetime[p],ft_midtime,FL3_thresh)&& gp==3

extract/o/d size_cal, B_sizeClust4,FL2_280 > interp(wibs_datetime[p],ft_midtime,FL2_thresh) && FL1_280 < interp(wibs_datetime[p],ft_midtime,FL1_thresh) && FL2_370 < interp(wibs_datetime[p],ft_midtime,FL3_thresh) && gp==4

extract/o/d AF, B_AFClust4, FL2_280 > interp(wibs_datetime[p],ft_midtime,FL2_thresh) && FL1_280 < interp(wibs_datetime[p],ft_midtime,FL1_thresh) && FL2_370 < interp(wibs_datetime[p],ft_midtime,FL3_thresh) && gp==4

extract/o/d fl1_280, B_Fl1Clust4, FL2_280 > interp(wibs_datetime[p],ft_midtime,FL2_thresh) && FL1_280 < interp(wibs_datetime[p],ft_midtime,FL1_thresh) && FL2_370 < interp(wibs_datetime[p],ft_midtime,FL3_thresh) && gp==4

extract/o/d fl2_280, B_Fl2Clust4, FL2_280 > interp(wibs_datetime[p],ft_midtime,FL2_thresh) && FL1_280 < interp(wibs_datetime[p],ft_midtime,FL1_thresh) && FL2_370 < interp(wibs_datetime[p],ft_midtime,FL3_thresh) && gp==4

extract/o/d fl2_370, B_Fl3Clust4, FL2_280 > interp(wibs_datetime[p],ft_midtime,FL2_thresh) && FL1_280 < interp(wibs_datetime[p],ft_midtime,FL1_thresh) && FL2_370 < interp(wibs_datetime[p],ft_midtime,FL3_thresh)&& gp==4
extract/o/d wibs_datetime, B_datetimeClust4, FL2_280 > interp(wibs_datetime[p],ft_midtime,FL2_thresh) && FL1_280 < interp(wibs_datetime[p],ft_midtime,FL1_thresh) && FL2_370 < interp(wibs_datetime[p],ft_midtime,FL3_thresh)&& gp==4

 //C
extract/o/d size_cal, C_sizeClust1,FL2_370 > interp(wibs_datetime[p],ft_midtime,FL3_thresh) && FL2_280 < interp(wibs_datetime[p],ft_midtime,FL2_thresh) && FL1_280 < interp(wibs_datetime[p],ft_midtime,FL1_thresh) && gp==1

extract/o/d AF, C_AFClust1, FL2_370 > interp(wibs_datetime[p],ft_midtime,FL3_thresh) && FL2_280 < interp(wibs_datetime[p],ft_midtime,FL2_thresh) && FL1_280 < interp(wibs_datetime[p],ft_midtime,FL1_thresh) && gp==1

extract/o/d fl1_280, C_Fl1Clust1, FL2_370 > interp(wibs_datetime[p],ft_midtime,FL3_thresh) && FL2_280 < interp(wibs_datetime[p],ft_midtime,FL2_thresh) && FL1_280 < interp(wibs_datetime[p],ft_midtime,FL1_thresh) && gp==1

extract/o/d fl2_280, C_Fl2Clust1, FL2_370 > interp(wibs_datetime[p],ft_midtime,FL3_thresh) && FL2_280 < interp(wibs_datetime[p],ft_midtime,FL2_thresh) && FL1_280 < interp(wibs_datetime[p],ft_midtime,FL1_thresh) && gp==1

extract/o/d fl2_370, C_Fl3Clust1, FL2_370 > interp(wibs_datetime[p],ft_midtime,FL3_thresh) && FL2_280 < interp(wibs_datetime[p],ft_midtime,FL2_thresh) && FL1_280 < interp(wibs_datetime[p],ft_midtime,FL1_thresh) && gp==1

extract/o/d wibs_datetime, C_datetimeClust1, FL2_370 > interp(wibs_datetime[p],ft_midtime,FL3_thresh) && FL2_280 < interp(wibs_datetime[p],ft_midtime,FL2_thresh) && FL1_280 < interp(wibs_datetime[p],ft_midtime,FL1_thresh) && gp==1

extract/o/d size_cal, C_sizeClust2, FL2_370 > interp(wibs_datetime[p],ft_midtime,FL3_thresh) && FL2_280 < interp(wibs_datetime[p],ft_midtime,FL2_thresh) && FL1_280 < interp(wibs_datetime[p],ft_midtime,FL1_thresh) && gp==2
extract/o/d AF, C_AFClust2, FL2_370 > interp(wibs_datetime[p],ft_midtime,FL3_thresh) && FL2_280 < interp(wibs_datetime[p],ft_midtime,FL2_thresh) && FL1_280 < interp(wibs_datetime[p],ft_midtime,FL1_thresh) && gp==2

extract/o/d fl1_280, C_Fl1Clust2, FL2_370 > interp(wibs_datetime[p],ft_midtime,FL3_thresh) && FL2_280 < interp(wibs_datetime[p],ft_midtime,FL2_thresh) && FL1_280 < interp(wibs_datetime[p],ft_midtime,FL1_thresh) && gp==2

extract/o/d fl2_280, C_Fl2Clust2, FL2_370 > interp(wibs_datetime[p],ft_midtime,FL3_thresh) && FL2_280 < interp(wibs_datetime[p],ft_midtime,FL2_thresh) && FL1_280 < interp(wibs_datetime[p],ft_midtime,FL1_thresh) && gp==2

extract/o/d fl2_370, C_Fl3Clust2, FL2_370 > interp(wibs_datetime[p],ft_midtime,FL3_thresh) && FL2_280 < interp(wibs_datetime[p],ft_midtime,FL2_thresh) && FL1_280 < interp(wibs_datetime[p],ft_midtime,FL1_thresh)&& gp==2

extract/o/d wibs_datetime, C_datetimeClust2, FL2_370 > interp(wibs_datetime[p],ft_midtime,FL3_thresh) && FL2_280 < interp(wibs_datetime[p],ft_midtime,FL2_thresh) && FL1_280 < interp(wibs_datetime[p],ft_midtime,FL1_thresh)&& gp==2

extract/o/d size_cal, C_sizeClust3,FL2_370 > interp(wibs_datetime[p],ft_midtime,FL3_thresh) && FL2_280 < interp(wibs_datetime[p],ft_midtime,FL2_thresh) && FL1_280 < interp(wibs_datetime[p],ft_midtime,FL1_thresh) && gp==3

extract/o/d AF, C_AFClust3, FL2_370 > interp(wibs_datetime[p],ft_midtime,FL3_thresh) && FL2_280 < interp(wibs_datetime[p],ft_midtime,FL2_thresh) && FL1_280 < interp(wibs_datetime[p],ft_midtime,FL1_thresh) && gp==3

extract/o/d fl1_280, C_Fl1Clust3, FL2_370 > interp(wibs_datetime[p],ft_midtime,FL3_thresh) && FL2_280 < interp(wibs_datetime[p],ft_midtime,FL2_thresh) && FL1_280 < interp(wibs_datetime[p],ft_midtime,FL1_thresh) && gp==3
extract/o/d fl2_280, C_Fl2Clust3, FL2_370 > interp(wibs_datetime[p],ft_midtime,FL3_thresh) && FL2_280 < interp(wibs_datetime[p],ft_midtime,FL2_thresh) && FL1_280 < interp(wibs_datetime[p],ft_midtime,FL1_thresh) && gp==3

extract/o/d fl2_370, C_Fl3Clust3, FL2_370 > interp(wibs_datetime[p],ft_midtime,FL3_thresh) && FL2_280 < interp(wibs_datetime[p],ft_midtime,FL2_thresh) && FL1_280 < interp(wibs_datetime[p],ft_midtime,FL1_thresh) && gp==3

extract/o/d wibs_datetime, C_datetimeClust3, FL2_370 > interp(wibs_datetime[p],ft_midtime,FL3_thresh) && FL2_280 < interp(wibs_datetime[p],ft_midtime,FL2_thresh) && FL1_280 < interp(wibs_datetime[p],ft_midtime,FL1_thresh) && gp==3

extract/o/d size_cal, C_sizeClust4,FL2_370 > interp(wibs_datetime[p],ft_midtime,FL3_thresh) && FL2_280 < interp(wibs_datetime[p],ft_midtime,FL2_thresh) && FL1_280 < interp(wibs_datetime[p],ft_midtime,FL1_thresh) && gp==4

extract/o/d AF, C_AFClust4, FL2_370 > interp(wibs_datetime[p],ft_midtime,FL3_thresh) && FL2_280 < interp(wibs_datetime[p],ft_midtime,FL2_thresh) && FL1_280 < interp(wibs_datetime[p],ft_midtime,FL1_thresh) && gp==4

extract/o/d fl1_280, C_Fl1Clust4, FL2_370 > interp(wibs_datetime[p],ft_midtime,FL3_thresh) && FL2_280 <
interp(wibs_datetime[p],ft_midtime,FL2_thresh) && FL1_280 < interp(wibs_datetime[p],ft_midtime,FL1_thresh) && gp==4

extract/o/d fl2_280, C_Fl2Clust4, FL2_370 > interp(wibs_datetime[p],ft_midtime,FL3_thresh) && FL2_280 <
interp(wibs_datetime[p],ft_midtime,FL2_thresh) && FL1_280 < interp(wibs_datetime[p],ft_midtime,FL1_thresh) && gp==4

extract/o/d fl2_370, C_Fl3Clust4, FL2_370 > interp(wibs_datetime[p],ft_midtime,FL3_thresh) && FL2_280 <
interp(wibs_datetime[p],ft_midtime,FL2_thresh) && FL1_280 < interp(wibs_datetime[p],ft_midtime,FL1_thresh) && gp==4
extract/o/d wibs_datetime, C_datetimeClust4, FL2_370 > interp(wibs_datetime[p],ft_midtime,FL3_thresh) && FL2_280 <
interp(wibs_datetime[p],ft_midtime,FL2_thresh) && FL1_280 < interp(wibs_datetime[p],ft_midtime,FL1_thresh) && gp==4

 //AB
extract/o/d size_cal, AB_sizeClust1,FL2_370 < interp(wibs_datetime[p],ft_midtime,FL3_thresh) && FL1_280 >
interp(wibs_datetime[p],ft_midtime,FL1_thresh) && FL2_280 > interp(wibs_datetime[p],ft_midtime,FL2_thresh) && gp==1

extract/o/d AF, AB_AFClust1, FL2_370 < interp(wibs_datetime[p],ft_midtime,FL3_thresh) && FL1_280 >
interp(wibs_datetime[p],ft_midtime,FL1_thresh) && FL2_280 > interp(wibs_datetime[p],ft_midtime,FL2_thresh) && gp==1

extract/o/d fl1_280, AB_Fl1Clust1, FL2_370 < interp(wibs_datetime[p],ft_midtime,FL3_thresh) && FL1_280 >
interp(wibs_datetime[p],ft_midtime,FL1_thresh) && FL2_280 > interp(wibs_datetime[p],ft_midtime,FL2_thresh) && gp==1

extract/o/d fl2_280, AB_Fl2Clust1, FL2_370 < interp(wibs_datetime[p],ft_midtime,FL3_thresh) && FL1_280 >
interp(wibs_datetime[p],ft_midtime,FL1_thresh) && FL2_280 > interp(wibs_datetime[p],ft_midtime,FL2_thresh) && gp==1

extract/o/d fl2_370, AB_Fl3Clust1, FL2_370 < interp(wibs_datetime[p],ft_midtime,FL3_thresh) && FL1_280 >
interp(wibs_datetime[p],ft_midtime,FL1_thresh) && FL2_280 > interp(wibs_datetime[p],ft_midtime,FL2_thresh) && gp==1

extract/o/d wibs_Datetime, AB_datetimeClust1, FL2_370 < interp(wibs_datetime[p],ft_midtime,FL3_thresh) && FL1_280 >
interp(wibs_datetime[p],ft_midtime,FL1_thresh) && FL2_280 > interp(wibs_datetime[p],ft_midtime,FL2_thresh) && gp==1

extract/o/d size_cal, AB_sizeClust2, FL2_370 < interp(wibs_datetime[p],ft_midtime,FL3_thresh) && FL1_280 >
interp(wibs_datetime[p],ft_midtime,FL1_thresh) && FL2_280 > interp(wibs_datetime[p],ft_midtime,FL2_thresh) && gp==2
 extract/o/d AF, AB_AFClust2, FL2_370 < interp(wibs_datetime[p],ft_midtime,FL3_thresh) && FL1_280 >
interp(wibs_datetime[p],ft_midtime,FL1_thresh) && FL2_280 > interp(wibs_datetime[p],ft_midtime,FL2_thresh) && gp==2

extract/o/d fl1_280, AB_Fl1Clust2, FL2_370 < interp(wibs_datetime[p],ft_midtime,FL3_thresh) && FL1_280 >
interp(wibs_datetime[p],ft_midtime,FL1_thresh) && FL2_280 > interp(wibs_datetime[p],ft_midtime,FL2_thresh) && gp==2

extract/o/d fl2_280, AB_Fl2Clust2, FL2_370 < interp(wibs_datetime[p],ft_midtime,FL3_thresh) && FL1_280 >
interp(wibs_datetime[p],ft_midtime,FL1_thresh) && FL2_280 > interp(wibs_datetime[p],ft_midtime,FL2_thresh) && gp==2

extract/o/d fl2_370, AB_Fl3Clust2, FL2_370 < interp(wibs_datetime[p],ft_midtime,FL3_thresh) && FL1_280 >
interp(wibs_datetime[p],ft_midtime,FL1_thresh) && FL2_280 > interp(wibs_datetime[p],ft_midtime,FL2_thresh) && gp==2

extract/o/d wibs_datetime, AB_datetimeClust2, FL2_370 < interp(wibs_datetime[p],ft_midtime,FL3_thresh) && FL1_280 >
interp(wibs_datetime[p],ft_midtime,FL1_thresh) && FL2_280 > interp(wibs_datetime[p],ft_midtime,FL2_thresh) && gp==2

extract/o/d size_cal, AB_sizeClust3, FL2_370 < interp(wibs_datetime[p],ft_midtime,FL3_thresh) && FL1_280 >
interp(wibs_datetime[p],ft_midtime,FL1_thresh) && FL2_280 > interp(wibs_datetime[p],ft_midtime,FL2_thresh) && gp==3

extract/o/d AF, AB_AFClust3, FL2_370 < interp(wibs_datetime[p],ft_midtime,FL3_thresh) && FL1_280 >
interp(wibs_datetime[p],ft_midtime,FL1_thresh) && FL2_280 > interp(wibs_datetime[p],ft_midtime,FL2_thresh) && gp==3

extract/o/d fl1_280, AB_Fl1Clust3, FL2_370 < interp(wibs_datetime[p],ft_midtime,FL3_thresh) && FL1_280 >
interp(wibs_datetime[p],ft_midtime,FL1_thresh) && FL2_280 > interp(wibs_datetime[p],ft_midtime,FL2_thresh) && gp==3
extract/o/d fl2_280, AB_Fl2Clust3, FL2_370 < interp(wibs_datetime[p],ft_midtime,FL3_thresh) && FL1_280 >
interp(wibs_datetime[p],ft_midtime,FL1_thresh) && FL2_280 > interp(wibs_datetime[p],ft_midtime,FL2_thresh) && gp==3

extract/o/d fl2_370, AB_Fl3Clust3, FL2_370 < interp(wibs_datetime[p],ft_midtime,FL3_thresh) && FL1_280 >
interp(wibs_datetime[p],ft_midtime,FL1_thresh) && FL2_280 > interp(wibs_datetime[p],ft_midtime,FL2_thresh) && gp==3

extract/o/d wibs_datetime, AB_datetimeClust3, FL2_370 < interp(wibs_datetime[p],ft_midtime,FL3_thresh) && FL1_280 >
interp(wibs_datetime[p],ft_midtime,FL1_thresh) && FL2_280 > interp(wibs_datetime[p],ft_midtime,FL2_thresh) && gp==3

extract/o/d size_cal, AB_sizeClust4, FL2_370 < interp(wibs_datetime[p],ft_midtime,FL3_thresh) && FL1_280 > interp(wibs_datetime[p],ft_midtime,FL1_thresh) && FL2_280 > interp(wibs_datetime[p],ft_midtime,FL2_thresh) && gp==4

extract/o/d AF, AB_AFClust4, FL2_370 < interp(wibs_datetime[p],ft_midtime,FL3_thresh) && FL1_280 > interp(wibs_datetime[p],ft_midtime,FL1_thresh) && FL2_280 > interp(wibs_datetime[p],ft_midtime,FL2_thresh) && gp==4

extract/o/d fl1_280, AB_Fl1Clust4, FL2_370 < interp(wibs_datetime[p],ft_midtime,FL3_thresh) && FL1_280 > interp(wibs_datetime[p],ft_midtime,FL1_thresh) && FL2_280 > interp(wibs_datetime[p],ft_midtime,FL2_thresh) && gp==4

extract/o/d fl2_280, AB_Fl2Clust4, FL2_370 < interp(wibs_datetime[p],ft_midtime,FL3_thresh) && FL1_280 > interp(wibs_datetime[p],ft_midtime,FL1_thresh) && FL2_280 > interp(wibs_datetime[p],ft_midtime,FL2_thresh) && gp==4

extract/o/d fl2_370, AB_Fl3Clust4, FL2_370 < interp(wibs_datetime[p],ft_midtime,FL3_thresh) && FL1_280 > interp(wibs_datetime[p],ft_midtime,FL1_thresh) && FL2_280 > interp(wibs_datetime[p],ft_midtime,FL2_thresh) && gp==4
extract/o/d wibs_datetime, AB_datetimeClust4, FL2_370 < interp(wibs_datetime[p],ft_midtime,FL3_thresh) && FL1_280 > interp(wibs_datetime[p],ft_midtime,FL1_thresh) && FL2_280 > interp(wibs_datetime[p],ft_midtime,FL2_thresh) && gp==4

 //AC
extract/o/d size_cal, AC_sizeClust1, FL2_370 > interp(wibs_datetime[p],ft_midtime,FL3_thresh) && FL1_280 > interp(wibs_datetime[p],ft_midtime,FL1_thresh) && FL2_280 < interp(wibs_datetime[p],ft_midtime,FL2_thresh) && gp==1

extract/o/d AF, AC_AFClust1, FL2_370 > interp(wibs_datetime[p],ft_midtime,FL3_thresh) && FL1_280 > interp(wibs_datetime[p],ft_midtime,FL1_thresh) && FL2_280 < interp(wibs_datetime[p],ft_midtime,FL2_thresh) && gp==1

extract/o/d fl1_280, AC_Fl1Clust1, FL2_370 > interp(wibs_datetime[p],ft_midtime,FL3_thresh) && FL1_280 > interp(wibs_datetime[p],ft_midtime,FL1_thresh) && FL2_280 < interp(wibs_datetime[p],ft_midtime,FL2_thresh) && gp==1

extract/o/d fl2_280, AC_Fl2Clust1, FL2_370 > interp(wibs_datetime[p],ft_midtime,FL3_thresh) && FL1_280 > interp(wibs_datetime[p],ft_midtime,FL1_thresh) && FL2_280 < interp(wibs_datetime[p],ft_midtime,FL2_thresh) && gp==1

extract/o/d fl2_370, AC_Fl3Clust1, FL2_370 > interp(wibs_datetime[p],ft_midtime,FL3_thresh) && FL1_280 > interp(wibs_datetime[p],ft_midtime,FL1_thresh) && FL2_280 < interp(wibs_datetime[p],ft_midtime,FL2_thresh) && gp==1

extract/o/d wibs_Datetime, AC_datetimeClust1, FL2_370 > interp(wibs_datetime[p],ft_midtime,FL3_thresh) && FL1_280 > interp(wibs_datetime[p],ft_midtime,FL1_thresh) && FL2_280 < interp(wibs_datetime[p],ft_midtime,FL2_thresh) && gp==1

extract/o/d size_cal, AC_sizeClust2, FL2_370 > interp(wibs_datetime[p],ft_midtime,FL3_thresh) && FL1_280 > interp(wibs_datetime[p],ft_midtime,FL1_thresh) && FL2_280 < interp(wibs_datetime[p],ft_midtime,FL2_thresh)&& gp==2
extract/o/d AF, AC_AFClust2, FL2_370 > interp(wibs_datetime[p],ft_midtime,FL3_thresh) && FL1_280 > interp(wibs_datetime[p],ft_midtime,FL1_thresh) && FL2_280 < interp(wibs_datetime[p],ft_midtime,FL2_thresh) && gp==2

extract/o/d fl1_280, AC_Fl1Clust2, FL2_370 > interp(wibs_datetime[p],ft_midtime,FL3_thresh) && FL1_280 > interp(wibs_datetime[p],ft_midtime,FL1_thresh) && FL2_280 < interp(wibs_datetime[p],ft_midtime,FL2_thresh) && gp==2

extract/o/d fl2_280, AC_Fl2Clust2, FL2_370 > interp(wibs_datetime[p],ft_midtime,FL3_thresh) && FL1_280 > interp(wibs_datetime[p],ft_midtime,FL1_thresh) && FL2_280 < interp(wibs_datetime[p],ft_midtime,FL2_thresh) && gp==2

extract/o/d fl2_370, AC_Fl3Clust2, FL2_370 > interp(wibs_datetime[p],ft_midtime,FL3_thresh) && FL1_280 > interp(wibs_datetime[p],ft_midtime,FL1_thresh) && FL2_280 < interp(wibs_datetime[p],ft_midtime,FL2_thresh) && gp==2

extract/o/d wibs_datetime, AC_datetimeClust2, FL2_370 > interp(wibs_datetime[p],ft_midtime,FL3_thresh) && FL1_280 > interp(wibs_datetime[p],ft_midtime,FL1_thresh) && FL2_280 < interp(wibs_datetime[p],ft_midtime,FL2_thresh) && gp==2

extract/o/d size_cal, AC_sizeClust3, FL2_370 > interp(wibs_datetime[p],ft_midtime,FL3_thresh) && FL1_280 > interp(wibs_datetime[p],ft_midtime,FL1_thresh) && FL2_280 < interp(wibs_datetime[p],ft_midtime,FL2_thresh) && gp==3

extract/o/d AF, AC_AFClust3, FL2_370 > interp(wibs_datetime[p],ft_midtime,FL3_thresh) && FL1_280 > interp(wibs_datetime[p],ft_midtime,FL1_thresh) && FL2_280 < interp(wibs_datetime[p],ft_midtime,FL2_thresh) && gp==3

extract/o/d fl1_280, AC_Fl1Clust3, FL2_370 > interp(wibs_datetime[p],ft_midtime,FL3_thresh) && FL1_280 > interp(wibs_datetime[p],ft_midtime,FL1_thresh) && FL2_280 < interp(wibs_datetime[p],ft_midtime,FL2_thresh) && gp==3

164

extract/o/d fl2_280, AC_Fl2Clust3, FL2_370 > interp(wibs_datetime[p],ft_midtime,FL3_thresh) && FL1_280 > interp(wibs_datetime[p],ft_midtime,FL1_thresh) && FL2_280 < interp(wibs_datetime[p],ft_midtime,FL2_thresh) && gp==3

extract/o/d fl2_370, AC_Fl3Clust3, FL2_370 > interp(wibs_datetime[p],ft_midtime,FL3_thresh) && FL1_280 > interp(wibs_datetime[p],ft_midtime,FL1_thresh) && FL2_280 < interp(wibs_datetime[p],ft_midtime,FL2_thresh) && gp==3

extract/o/d wibs_datetime, AC_datetimeClust3, FL2_370 > interp(wibs_datetime[p],ft_midtime,FL3_thresh) && FL1_280 > interp(wibs_datetime[p],ft_midtime,FL1_thresh) && FL2_280 < interp(wibs_datetime[p],ft_midtime,FL2_thresh) && gp==3

extract/o/d size_cal, AC_sizeClust4, FL2_370 > interp(wibs_datetime[p],ft_midtime,FL3_thresh) && FL1_280 > interp(wibs_datetime[p],ft_midtime,FL1_thresh) && FL2_280 < interp(wibs_datetime[p],ft_midtime,FL2_thresh) && gp==4

extract/o/d AF, AC_AFClust4, FL2_370 > interp(wibs_datetime[p],ft_midtime,FL3_thresh) && FL1_280 > interp(wibs_datetime[p],ft_midtime,FL1_thresh) && FL2_280 < interp(wibs_datetime[p],ft_midtime,FL2_thresh) && gp==4

extract/o/d fl1_280, AC_Fl1Clust4, FL2_370 > interp(wibs_datetime[p],ft_midtime,FL3_thresh) && FL1_280 > interp(wibs_datetime[p],ft_midtime,FL1_thresh) && FL2_280 < interp(wibs_datetime[p],ft_midtime,FL2_thresh) && gp==4

extract/o/d fl2_280, AC_Fl2Clust4, FL2_370 > interp(wibs_datetime[p],ft_midtime,FL3_thresh) && FL1_280 > interp(wibs_datetime[p],ft_midtime,FL1_thresh) && FL2_280 < interp(wibs_datetime[p],ft_midtime,FL2_thresh) && gp==4

extract/o/d fl2_370, AC_Fl3Clust4, FL2_370 > interp(wibs_datetime[p],ft_midtime,FL3_thresh) && FL1_280 > interp(wibs_datetime[p],ft_midtime,FL1_thresh) && FL2_280 < interp(wibs_datetime[p],ft_midtime,FL2_thresh) && gp==4
extract/o/d wibs_datetime, AC_datetimeClust4, FL2_370 > interp(wibs_datetime[p],ft_midtime,FL3_thresh) && FL1_280 > interp(wibs_datetime[p],ft_midtime,FL1_thresh) && FL2_280 < interp(wibs_datetime[p],ft_midtime,FL2_thresh) && gp==4

//BC
extract/o/d size_cal, BC_sizeClust1, FL2_370 > interp(wibs_datetime[p],ft_midtime,FL3_thresh) && FL1_280 < interp(wibs_datetime[p],ft_midtime,FL1_thresh) && FL2_280 > interp(wibs_datetime[p],ft_midtime,FL2_thresh) && gp==1

extract/o/d AF, BC_AFClust1, FL2_370 > interp(wibs_datetime[p],ft_midtime,FL3_thresh) && FL1_280 < interp(wibs_datetime[p],ft_midtime,FL1_thresh) && FL2_280 > interp(wibs_datetime[p],ft_midtime,FL2_thresh) && gp==1

extract/o/d fl1_280, BC_Fl1Clust1, FL2_370 > interp(wibs_datetime[p],ft_midtime,FL3_thresh) && FL1_280 < interp(wibs_datetime[p],ft_midtime,FL1_thresh) && FL2_280 > interp(wibs_datetime[p],ft_midtime,FL2_thresh) && gp==1

extract/o/d fl2_280, BC_Fl2Clust1, FL2_370 > interp(wibs_datetime[p],ft_midtime,FL3_thresh) && FL1_280 < interp(wibs_datetime[p],ft_midtime,FL1_thresh) && FL2_280 > interp(wibs_datetime[p],ft_midtime,FL2_thresh) && gp==1

extract/o/d fl2_370, BC_Fl3Clust1, FL2_370 > interp(wibs_datetime[p],ft_midtime,FL3_thresh) && FL1_280 < interp(wibs_datetime[p],ft_midtime,FL1_thresh) && FL2_280 > interp(wibs_datetime[p],ft_midtime,FL2_thresh) && gp==1

extract/o/d wibs_datetime, BC_datetimeClust1, FL2_370 > interp(wibs_datetime[p],ft_midtime,FL3_thresh) && FL1_280 < interp(wibs_datetime[p],ft_midtime,FL1_thresh) && FL2_280 > interp(wibs_datetime[p],ft_midtime,FL2_thresh) && gp==1

extract/o/d size_cal, BC_sizeClust2, FL2_370 > interp(wibs_datetime[p],ft_midtime,FL3_thresh) && FL1_280 < interp(wibs_datetime[p],ft_midtime,FL1_thresh) && FL2_280 > interp(wibs_datetime[p],ft_midtime,FL2_thresh) && gp==2
extract/o/d AF, BC_AFClust2, FL2_370 > interp(wibs_datetime[p],ft_midtime,FL3_thresh) && FL1_280 < interp(wibs_datetime[p],ft_midtime,FL1_thresh) && FL2_280 > interp(wibs_datetime[p],ft_midtime,FL2_thresh) && gp==2

extract/o/d fl1_280, BC_Fl1Clust2, FL2_370 > interp(wibs_datetime[p],ft_midtime,FL3_thresh) && FL1_280 < interp(wibs_datetime[p],ft_midtime,FL1_thresh) && FL2_280 > interp(wibs_datetime[p],ft_midtime,FL2_thresh) && gp==2

extract/o/d fl2_280, BC_Fl2Clust2, FL2_370 > interp(wibs_datetime[p],ft_midtime,FL3_thresh) && FL1_280 < interp(wibs_datetime[p],ft_midtime,FL1_thresh) && FL2_280 > interp(wibs_datetime[p],ft_midtime,FL2_thresh) && gp==2

extract/o/d fl2_370, BC_Fl3Clust2, FL2_370 > interp(wibs_datetime[p],ft_midtime,FL3_thresh) && FL1_280 < interp(wibs_datetime[p],ft_midtime,FL1_thresh) && FL2_280 > interp(wibs_datetime[p],ft_midtime,FL2_thresh) && gp==2

extract/o/d wibs_datetime, BC_datetimeClust2, FL2_370 > interp(wibs_datetime[p],ft_midtime,FL3_thresh) && FL1_280 < interp(wibs_datetime[p],ft_midtime,FL1_thresh) && FL2_280 > interp(wibs_datetime[p],ft_midtime,FL2_thresh) && gp==2

165

extract/o/d size_cal, BC_sizeClust3, FL2_370 > interp(wibs_datetime[p],ft_midtime,FL3_thresh) && FL1_280 < interp(wibs_datetime[p],ft_midtime,FL1_thresh) && FL2_280 > interp(wibs_datetime[p],ft_midtime,FL2_thresh) && gp==3

extract/o/d AF, BC_AFClust3, FL2_370 > interp(wibs_datetime[p],ft_midtime,FL3_thresh) && FL1_280 < interp(wibs_datetime[p],ft_midtime,FL1_thresh) && FL2_280 > interp(wibs_datetime[p],ft_midtime,FL2_thresh) && gp==3

extract/o/d fl1_280, BC_Fl1Clust3, FL2_370 > interp(wibs_datetime[p],ft_midtime,FL3_thresh) && FL1_280 < interp(wibs_datetime[p],ft_midtime,FL1_thresh) && FL2_280 > interp(wibs_datetime[p],ft_midtime,FL2_thresh) && gp==3

extract/o/d fl2_280, BC_Fl2Clust3, FL2_370 > interp(wibs_datetime[p],ft_midtime,FL3_thresh) && FL1_280 < interp(wibs_datetime[p],ft_midtime,FL1_thresh) && FL2_280 > interp(wibs_datetime[p],ft_midtime,FL2_thresh) && gp==3

extract/o/d fl2_370, BC_Fl3Clust3, FL2_370 > interp(wibs_datetime[p],ft_midtime,FL3_thresh) && FL1_280 < interp(wibs_datetime[p],ft_midtime,FL1_thresh) && FL2_280 > interp(wibs_datetime[p],ft_midtime,FL2_thresh) && gp==3

extract/o/d wibs_datetime, BC_datetimeClust3, FL2_370 > interp(wibs_datetime[p],ft_midtime,FL3_thresh) && FL1_280 < interp(wibs_datetime[p],ft_midtime,FL1_thresh) && FL2_280 > interp(wibs_datetime[p],ft_midtime,FL2_thresh) && gp==3

extract/o/d size_cal, BC_sizeClust4, FL2_370 > interp(wibs_datetime[p],ft_midtime,FL3_thresh) && FL1_280 < interp(wibs_datetime[p],ft_midtime,FL1_thresh) && FL2_280 > interp(wibs_datetime[p],ft_midtime,FL2_thresh) && gp==4

extract/o/d AF, BC_AFClust4, FL2_370 > interp(wibs_datetime[p],ft_midtime,FL3_thresh) && FL1_280 < interp(wibs_datetime[p],ft_midtime,FL1_thresh) && FL2_280 > interp(wibs_datetime[p],ft_midtime,FL2_thresh) && gp==4

extract/o/d fl1_280, BC_Fl1Clust4, FL2_370 > interp(wibs_datetime[p],ft_midtime,FL3_thresh) && FL1_280 < interp(wibs_datetime[p],ft_midtime,FL1_thresh) && FL2_280 > interp(wibs_datetime[p],ft_midtime,FL2_thresh) && gp==4

extract/o/d fl2_280, BC_Fl2Clust4, FL2_370 > interp(wibs_datetime[p],ft_midtime,FL3_thresh) && FL1_280 < interp(wibs_datetime[p],ft_midtime,FL1_thresh) && FL2_280 > interp(wibs_datetime[p],ft_midtime,FL2_thresh) && gp==4

extract/o/d fl2_370, BC_Fl3Clust4, FL2_370 > interp(wibs_datetime[p],ft_midtime,FL3_thresh) && FL1_280 < interp(wibs_datetime[p],ft_midtime,FL1_thresh) && FL2_280 > interp(wibs_datetime[p],ft_midtime,FL2_thresh) && gp==4
extract/o/d wibs_datetime, BC_datetimeClust4, FL2_370 > interp(wibs_datetime[p],ft_midtime,FL3_thresh) && FL1_280 < interp(wibs_datetime[p],ft_midtime,FL1_thresh) && FL2_280 > interp(wibs_datetime[p],ft_midtime,FL2_thresh) && gp==4

 //ABC
extract/o/d size_cal, ABC_sizeClust1, FL2_370 > interp(wibs_datetime[p],ft_midtime,FL3_thresh) && FL1_280 > interp(wibs_datetime[p],ft_midtime,FL1_thresh) && FL2_280 > interp(wibs_datetime[p],ft_midtime,FL2_thresh) && gp==1

extract/o/d AF, ABC_AFClust1, FL2_370 > interp(wibs_datetime[p],ft_midtime,FL3_thresh) && FL1_280 > interp(wibs_datetime[p],ft_midtime,FL1_thresh) && FL2_280 > interp(wibs_datetime[p],ft_midtime,FL2_thresh) && gp==1

extract/o/d fl1_280, ABC_Fl1Clust1, FL2_370 > interp(wibs_datetime[p],ft_midtime,FL3_thresh) && FL1_280 > interp(wibs_datetime[p],ft_midtime,FL1_thresh) && FL2_280 > interp(wibs_datetime[p],ft_midtime,FL2_thresh) && gp==1

extract/o/d fl2_280, ABC_Fl2Clust1, FL2_370 > interp(wibs_datetime[p],ft_midtime,FL3_thresh) && FL1_280 > interp(wibs_datetime[p],ft_midtime,FL1_thresh) && FL2_280 > interp(wibs_datetime[p],ft_midtime,FL2_thresh) && gp==1

extract/o/d fl2_370, ABC_Fl3Clust1, FL2_370 > interp(wibs_datetime[p],ft_midtime,FL3_thresh) && FL1_280 > interp(wibs_datetime[p],ft_midtime,FL1_thresh) && FL2_280 > interp(wibs_datetime[p],ft_midtime,FL2_thresh) && gp==1

extract/o/d wibs_datetime, ABC_datetimeClust1, FL2_370 > interp(wibs_datetime[p],ft_midtime,FL3_thresh) && FL1_280 > interp(wibs_datetime[p],ft_midtime,FL1_thresh) && FL2_280 > interp(wibs_datetime[p],ft_midtime,FL2_thresh) && gp==1

extract/o/d size_cal, ABC_sizeClust2, FL2_370 > interp(wibs_datetime[p],ft_midtime,FL3_thresh) && FL1_280 > interp(wibs_datetime[p],ft_midtime,FL1_thresh) && FL2_280 > interp(wibs_datetime[p],ft_midtime,FL2_thresh) && gp==2
extract/o/d AF, ABC_AFClust2, FL2_370 > interp(wibs_datetime[p],ft_midtime,FL3_thresh) && FL1_280 > interp(wibs_datetime[p],ft_midtime,FL1_thresh) && FL2_280 > interp(wibs_datetime[p],ft_midtime,FL2_thresh) && gp==2

extract/o/d fl1_280, ABC_Fl1Clust2, FL2_370 > interp(wibs_datetime[p],ft_midtime,FL3_thresh) && FL1_280 > interp(wibs_datetime[p],ft_midtime,FL1_thresh) && FL2_280 > interp(wibs_datetime[p],ft_midtime,FL2_thresh) && gp==2

extract/o/d fl2_280, ABC_Fl2Clust2, FL2_370 > interp(wibs_datetime[p],ft_midtime,FL3_thresh) && FL1_280 > interp(wibs_datetime[p],ft_midtime,FL1_thresh) && FL2_280 > interp(wibs_datetime[p],ft_midtime,FL2_thresh) && gp==2

extract/o/d fl2_370, ABC_Fl3Clust2, FL2_370 > interp(wibs_datetime[p],ft_midtime,FL3_thresh) && FL1_280 > interp(wibs_datetime[p],ft_midtime,FL1_thresh) && FL2_280 > interp(wibs_datetime[p],ft_midtime,FL2_thresh) && gp==2

extract/o/d wibs_datetime, ABC_datetimeClust2, FL2_370 > interp(wibs_datetime[p],ft_midtime,FL3_thresh) && FL1_280 > interp(wibs_datetime[p],ft_midtime,FL1_thresh) && FL2_280 > interp(wibs_datetime[p],ft_midtime,FL2_thresh) && gp==2

extract/o/d size_cal, ABC_sizeClust3, FL2_370 > interp(wibs_datetime[p],ft_midtime,FL3_thresh) && FL1_280 > interp(wibs_datetime[p],ft_midtime,FL1_thresh) && FL2_280 > interp(wibs_datetime[p],ft_midtime,FL2_thresh) && gp==3

extract/o/d AF, ABC_AFClust3, FL2_370 > interp(wibs_datetime[p],ft_midtime,FL3_thresh) && FL1_280 > interp(wibs_datetime[p],ft_midtime,FL1_thresh) && FL2_280 > interp(wibs_datetime[p],ft_midtime,FL2_thresh) && gp==3

extract/o/d fl1_280, ABC_Fl1Clust3, FL2_370 > interp(wibs_datetime[p],ft_midtime,FL3_thresh) && FL1_280 > interp(wibs_datetime[p],ft_midtime,FL1_thresh) && FL2_280 > interp(wibs_datetime[p],ft_midtime,FL2_thresh) && gp==3
extract/o/d fl2_280, ABC_Fl2Clust3, FL2_370 > interp(wibs_datetime[p],ft_midtime,FL3_thresh) && FL1_280 > interp(wibs_datetime[p],ft_midtime,FL1_thresh) && FL2_280 > interp(wibs_datetime[p],ft_midtime,FL2_thresh) && gp==3

extract/o/d fl2_370, ABC_Fl3Clust3, FL2_370 > interp(wibs_datetime[p],ft_midtime,FL3_thresh) && FL1_280 > interp(wibs_datetime[p],ft_midtime,FL1_thresh) && FL2_280 > interp(wibs_datetime[p],ft_midtime,FL2_thresh) && gp==3

extract/o/d wibs_datetime, ABC_datetimeClust3, FL2_370 > interp(wibs_datetime[p],ft_midtime,FL3_thresh) && FL1_280 > interp(wibs_datetime[p],ft_midtime,FL1_thresh) && FL2_280 > interp(wibs_datetime[p],ft_midtime,FL2_thresh) && gp==3

extract/o/d size_cal, ABC_sizeClust4, FL2_370 > interp(wibs_datetime[p],ft_midtime,FL3_thresh) && FL1_280 > interp(wibs_datetime[p],ft_midtime,FL1_thresh) && FL2_280 > interp(wibs_datetime[p],ft_midtime,FL2_thresh) && gp==4

extract/o/d AF, ABC_AFClust4, FL2_370 > interp(wibs_datetime[p],ft_midtime,FL3_thresh) && FL1_280 > interp(wibs_datetime[p],ft_midtime,FL1_thresh) && FL2_280 > interp(wibs_datetime[p],ft_midtime,FL2_thresh) && gp==4

extract/o/d fl1_280, ABC_Fl1Clust4, FL2_370 > interp(wibs_datetime[p],ft_midtime,FL3_thresh) && FL1_280 > interp(wibs_datetime[p],ft_midtime,FL1_thresh) && FL2_280 > interp(wibs_datetime[p],ft_midtime,FL2_thresh) && gp==4

extract/o/d fl2_280, ABC_Fl2Clust4, FL2_370 > interp(wibs_datetime[p],ft_midtime,FL3_thresh) && FL1_280 > interp(wibs_datetime[p],ft_midtime,FL1_thresh) && FL2_280 > interp(wibs_datetime[p],ft_midtime,FL2_thresh) && gp==4

extract/o/d fl2_370, ABC_Fl3Clust4, FL2_370 > interp(wibs_datetime[p],ft_midtime,FL3_thresh) && FL1_280 > interp(wibs_datetime[p],ft_midtime,FL1_thresh) && FL2_280 > interp(wibs_datetime[p],ft_midtime,FL2_thresh) && gp==4
extract/o/d wibs_datetime, ABC_datetimeClust4, FL2_370 > interp(wibs_datetime[p],ft_midtime,FL3_thresh) && FL1_280 > interp(wibs_datetime[p],ft_midtime,FL1_thresh) && FL2_280 > interp(wibs_datetime[p],ft_midtime,FL2_thresh) && gp==4

End

///
Description of function: StackedCats() function should be used after Categories() function, it creates stacked type size distributions for each particle type.

Function StackedCats()

nvar numbin = root:numSDbins
nvar/z dsec=root:avgtimeint
nvar/z flowrate=root:flowrate
nvar dlogdp = root:dlogdp
variable numlim = numbin + 1
variable i, a, b

make/o/n=(numlim) d_lim = 0.5*10^(p*dlogdp)

//NonFl
wave non_sizeClust1, non_sizeClust2, non_sizeClust3, non_sizeClust4

//clust1
duplicate/o NON_sizeClust1 NON_sizeClust1_sort
Sort NON_sizeClust1_sort, NON_sizeClust1_sort

167

```
Make/o/n=(numpnts(d_lim)) nonFl_clust1_Sizedist
for(i=0;i<numlim-1;i+=1)
a = BinarySearch(NON_sizeClust1_sort ,d_lim[i])
b = BinarySearch(NON_sizeClust1_sort ,d_lim[i+1])
if(b>a)
nonFl_clust1_Sizedist[i] = (b-(a))
elseif (a==-1 && b==-2)//added by NS, if there is only one particle in category this condition forces to bin particle
nonFl_clust1_Sizedist[i] =1
elseif (a==b)// added by NS- if there are no particles in bin then a will equal b
nonFl_clust1_Sizedist[i] =0
elseif   (a>b && b==-2&&a>0) // forces to count particles that don't have an upper bin
make/o/n=(1,0) remain
remain=((numpnts(NON_sizeClust1_sort))-a)-1
nonFl_clust1_Sizedist[i]=remain

endif
endfor

//Clust2
duplicate/o NON_sizeClust2 NON_sizeClust2_sort
Sort NON_sizeClust2_sort, NON_sizeClust2_sort
Make/o/n=(numpnts(d_lim)) nonFl_clust2_Sizedist
for(i=0;i<numlim-1;i+=1)
a = BinarySearch(NON_sizeClust2_sort ,d_lim[i])
b = BinarySearch(NON_sizeClust2_sort ,d_lim[i+1])
if(b>a)
nonFl_clust2_Sizedist[i] = (b-(a))
elseif (a==-1 && b==-2)//added by NS, if there is only one particle in category this condition forces to bin particle
nonFl_clust2_Sizedist[i] =1
elseif (a==b)// added by NS- if there are no particles in bin then a will equal b
nonFl_clust2_Sizedist[i] =0
elseif   (a>b && b==-2&&a>0) // forces to count particles that don't have an upper bin
make/o/n=(1,0) remain
remain=((numpnts(NON_sizeClust2_sort))-a)-1
nonFl_clust2_Sizedist[i]=remain

endif
endfor

//clust3
duplicate/o NON_sizeClust3 NON_sizeClust3_sort
Sort NON_sizeClust3_sort, NON_sizeClust3_sort
Make/o/n=(numpnts(d_lim)) nonFl_clust3_Sizedist
for(i=0;i<numlim-1;i+=1)
a = BinarySearch(NON_sizeClust3_sort ,d_lim[i])
b = BinarySearch(NON_sizeClust3_sort ,d_lim[i+1])
if(b>a)
nonFl_clust3_Sizedist[i] = (b-(a))
elseif (a==-1 && b==-2)//added by NS, if there is only one particle in category this condition forces to bin particle
nonFl_clust3_Sizedist[i] =1
elseif (a==b)// added by NS- if there are no particles in bin then a will equal b
nonFl_clust3_Sizedist[i] =0
elseif   (a>b && b==-2&&a>0) // forces to count particles that don't have an upper bin
make/o/n=(1,0) remain
remain=((numpnts(NON_sizeClust3_sort))-a)-1
nonFl_clust3_Sizedist[i]=remain

endif
endfor

//Clust4
duplicate/o NON_sizeClust4 NON_sizeClust4_sort
Sort NON_sizeClust4_sort, NON_sizeClust4_sort
Make/o/n=(numpnts(d_lim)) nonFl_clust4_Sizedist
```

168

```
for(i=0;i<numlim-1;i+=1)
a = BinarySearch(NON_sizeClust4_sort ,d_lim[i])
b = BinarySearch(NON_sizeClust4_sort ,d_lim[i+1])
if(b>a)
nonFl_clust4_Sizedist[i] = (b-(a))
elseif (a==-1 && b==-2)//added by NS, if there is only one particle in category this condition forces to bin particle
nonFl_clust4_Sizedist[i] =1
elseif (a==b)// added by NS- if there are no particles in bin then a will equal b
nonFl_clust4_Sizedist[i] =0
elseif   (a>b && b==-2&&a>0) // forces to count particles that don't have an upper bin
make/o/n=(1,0) remain
remain=((numpnts(NON_sizeClust4_sort))-a)-1
nonFl_clust4_Sizedist[i]=remain

endif
endfor

//A

wave A_sizeClust1, A_sizeClust2,  A_sizeClust3, A_sizeClust4

//clust1
duplicate/o A_sizeClust1 A_sizeClust1_sort
Sort A_sizeClust1_sort, A_sizeClust1_sort
Make/o/n=(numpnts(d_lim)) A_clust1_Sizedist
for(i=0;i<numlim-1;i+=1)
a = BinarySearch(A_sizeClust1_sort ,d_lim[i])
b = BinarySearch(A_sizeClust1_sort ,d_lim[i+1])
if(b>a)
A_clust1_Sizedist[i] = (b-(a))
elseif (a==-1 && b==-2)//added by NS, if there is only one particle in category this condition forces to bin particle
A_clust1_Sizedist[i] =1
elseif (a==b)// added by NS- if there are no particles in bin then a will equal b
A_clust1_Sizedist[i] =0
elseif   (a>b && b==-2&&a>0) // forces to count particles that don't have an upper bin
make/o/n=(1,0) remain
remain=((numpnts(A_sizeClust1_sort))-a)-1
A_clust1_Sizedist[i]=remain

endif
endfor

//Clust2

duplicate/o A_sizeClust2 A_sizeClust2_sort
Sort A_sizeClust2_sort, A_sizeClust2_sort
Make/o/n=(numpnts(d_lim)) A_clust2_Sizedist
for(i=0;i<numlim-1;i+=1)
a = BinarySearch(A_sizeClust2_sort ,d_lim[i])
b = BinarySearch(A_sizeClust2_sort ,d_lim[i+1])
if(b>a)
A_clust2_Sizedist[i] = (b-(a))
elseif (a==-1 && b==-2)//added by NS, if there is only one particle in category this condition forces to bin particle
A_clust2_Sizedist[i] =1
elseif (a==b)// added by NS- if there are no particles in bin then a will equal b
A_clust2_Sizedist[i] =0
elseif   (a>b && b==-2&&a>0) // forces to count particles that don't have an upper bin
make/o/n=(1,0) remain
remain=((numpnts(A_sizeClust2_sort))-a)-1
A_clust2_Sizedist[i]=remain

endif
endfor
```

```
//Clust 3
duplicate/o A_sizeClust3 A_sizeClust3_sort
Sort A_sizeClust3_sort, A_sizeClust3_sort
Make/o/n=(numpnts(d_lim)) A_clust3_Sizedist
for(i=0;i<numlim-1;i+=1)
a = BinarySearch(A_sizeClust3_sort ,d_lim[i])
b = BinarySearch(A_sizeClust3_sort ,d_lim[i+1])
if(b>a)
A_clust3_Sizedist[i] = (b-(a))
elseif (a==-1 && b==-2)//added by NS, if there is only one particle in category this condition forces to bin particle
A_clust3_Sizedist[i] =1
elseif (a==b)// added by NS- if there are no particles in bin then a will equal b
A_clust3_Sizedist[i] =0
elseif   (a>b && b==-2&&a>0) // forces to count particles that don't have an upper bin
make/o/n=(1,0) remain
remain=((numpnts(A_sizeClust3_sort))-a)-1
A_clust3_Sizedist[i]=remain

endif
endfor

//Clust 4

duplicate/o A_sizeClust4 A_sizeClust4_sort
Sort A_sizeClust4_sort, A_sizeClust4_sort
Make/o/n=(numpnts(d_lim)) A_clust4_Sizedist
for(i=0;i<numlim-1;i+=1)
a = BinarySearch(A_sizeClust4_sort ,d_lim[i])
b = BinarySearch(A_sizeClust4_sort ,d_lim[i+1])
if(b>a)
A_clust4_Sizedist[i] = (b-(a))
elseif (a==-1 && b==-2)//added by NS, if there is only one particle in category this condition forces to bin particle
A_clust4_Sizedist[i] =1
elseif (a==b)// added by NS- if there are no particles in bin then a will equal b
A_clust4_Sizedist[i] =0
elseif   (a>b && b==-2&&a>0) // forces to count particles that don't have an upper bin
make/o/n=(1,0) remain
remain=((numpnts(A_sizeClust4_sort))-a)-1
A_clust4_Sizedist[i]=remain

endif
endfor

//B

wave B_sizeClust1, B_sizeClust2, B_sizeClust3, B_sizeClust4
//clust1
duplicate/o B_sizeClust1 B_sizeClust1_sort
Sort B_sizeClust1_sort, B_sizeClust1_sort
Make/o/n=(numpnts(d_lim)) B_clust1_Sizedist
for(i=0;i<numlim-1;i+=1)
a = BinarySearch(B_sizeClust1_sort ,d_lim[i])
b = BinarySearch(B_sizeClust1_sort ,d_lim[i+1])
if(b>a)
B_clust1_Sizedist[i] = (b-(a))
elseif (a==-1 && b==-2)//added by NS, if there is only one particle in category this condition forces to bin particle
B_clust1_Sizedist[i] =1
elseif (a==b)// added by NS- if there are no particles in bin then a will equal b
B_clust1_Sizedist[i] =0
elseif   (a>b && b==-2&&a>0) // forces to count particles that don't have an upper bin
make/o/n=(1,0) remain
remain=((numpnts(B_sizeClust1_sort))-a)-1
B_clust1_Sizedist[i]=remain
```

```
endif
endfor

//Clust2

duplicate/o B_sizeClust2 B_sizeClust2_sort
Sort B_sizeClust2_sort, B_sizeClust2_sort
Make/o/n=(numpnts(d_lim)) B_clust2_Sizedist
for(i=0;i<numlim-1;i+=1)
a = BinarySearch(B_sizeClust2_sort ,d_lim[i])
b = BinarySearch(B_sizeClust2_sort ,d_lim[i+1])
if(b>a)
B_clust2_Sizedist[i] = (b-(a))
elseif (a==-1 && b==-2)//added by NS, if there is only one particle in category this condition forces to bin particle
B_clust2_Sizedist[i] =1
elseif (a==b)// added by NS- if there are no particles in bin then a will equal b
B_clust2_Sizedist[i] =0
elseif   (a>b && b==-2&&a>0) // forces to count particles that don't have an upper bin
make/o/n=(1,0) remain
remain=((numpnts(B_sizeClust2_sort))-a)-1
B_clust2_Sizedist[i]=remain

endif
endfor

//clust3

duplicate/o B_sizeClust3 B_sizeClust3_sort
Sort B_sizeClust3_sort, B_sizeClust3_sort
Make/o/n=(numpnts(d_lim)) B_clust3_Sizedist
for(i=0;i<numlim-1;i+=1)
a = BinarySearch(B_sizeClust3_sort ,d_lim[i])
b = BinarySearch(B_sizeClust3_sort ,d_lim[i+1])
if(b>a)
B_clust3_Sizedist[i] = (b-(a))
elseif (a==-1 && b==-2)//added by NS, if there is only one particle in category this condition forces to bin particle
B_clust3_Sizedist[i] =1
elseif (a==b)// added by NS- if there are no particles in bin then a will equal b
B_clust3_Sizedist[i] =0
elseif   (a>b && b==-2&&a>0) // forces to count particles that don't have an upper bin
make/o/n=(1,0) remain
remain=((numpnts(B_sizeClust3_sort))-a)-1
B_clust3_Sizedist[i]=remain

endif
endfor

//Clust4
duplicate/o B_sizeClust4 B_sizeClust4_sort
Sort B_sizeClust4_sort, B_sizeClust4_sort
Make/o/n=(numpnts(d_lim)) B_clust4_Sizedist
for(i=0;i<numlim-1;i+=1)
a = BinarySearch(B_sizeClust4_sort ,d_lim[i])
b = BinarySearch(B_sizeClust4_sort ,d_lim[i+1])
if(b>a)
B_clust4_Sizedist[i] = (b-(a))
elseif (a==-1 && b==-2)//added by NS, if there is only one particle in category this condition forces to bin particle
B_clust4_Sizedist[i] =1
elseif (a==b)// added by NS- if there are no particles in bin then a will equal b
B_clust4_Sizedist[i] =0
elseif   (a>b && b==-2&&a>0) // forces to count particles that don't have an upper bin
make/o/n=(1,0) remain
remain=((numpnts(B_sizeClust4_sort))-a)-1
B_clust4_Sizedist[i]=remain
```

171

```
endif
endfor

//C

wave C_sizeClust1, C_sizeClust2, C_sizeClust3, C_sizeClust4
//clust1
duplicate/o C_sizeClust1 C_sizeClust1_sort
Sort C_sizeClust1_sort, C_sizeClust1_sort
Make/o/n=(numpnts(d_lim)) C_clust1_Sizedist
for(i=0;i<numlim-1;i+=1)
a = BinarySearch(C_sizeClust1_sort ,d_lim[i])
b = BinarySearch(C_sizeClust1_sort ,d_lim[i+1])
if(b>a)
C_clust1_Sizedist[i] = (b-(a))
elseif (a==-1 && b==-2)//added by NS, if there is only one particle in category this condition forces to bin particle
C_clust1_Sizedist[i] =1
elseif (a==b)// added by NS- if there are no particles in bin then a will equal b
C_clust1_Sizedist[i] =0
elseif   (a>b && b==-2&&a>0) // forces to count particles that don't have an upper bin
make/o/n=(1,0) remain
remain=((numpnts(C_sizeClust1_sort))-a)-1
C_clust1_Sizedist[i]=remain

endif
endfor

//Clust2

duplicate/o C_sizeClust2 C_sizeClust2_sort
Sort C_sizeClust2_sort, C_sizeClust2_sort
Make/o/n=(numpnts(d_lim)) C_clust2_Sizedist
for(i=0;i<numlim-1;i+=1)
a = BinarySearch(C_sizeClust2_sort ,d_lim[i])
b = BinarySearch(C_sizeClust2_sort ,d_lim[i+1])
if(b>a)
C_clust2_Sizedist[i] = (b-(a))
elseif (a==-1 && b==-2)//added by NS, if there is only one particle in category this condition forces to bin particle
C_clust2_Sizedist[i] =1
elseif (a==b)// added by NS- if there are no particles in bin then a will equal b
C_clust2_Sizedist[i] =0
elseif   (a>b && b==-2&&a>0) // forces to count particles that don't have an upper bin
make/o/n=(1,0) remain
remain=((numpnts(C_sizeClust2_sort))-a)-1
C_clust2_Sizedist[i]=remain

endif
endfor

//clust3
duplicate/o C_sizeClust3 C_sizeClust3_sort
Sort C_sizeClust3_sort, C_sizeClust3_sort
Make/o/n=(numpnts(d_lim)) C_clust3_Sizedist
for(i=0;i<numlim-1;i+=1)
a = BinarySearch(C_sizeClust3_sort ,d_lim[i])
b = BinarySearch(C_sizeClust3_sort ,d_lim[i+1])
if(b>a)
C_clust3_Sizedist[i] = (b-(a))
elseif (a==-1 && b==-2)//added by NS, if there is only one particle in category this condition forces to bin particle
C_clust3_Sizedist[i] =1
elseif (a==b)// added by NS- if there are no particles in bin then a will equal b
C_clust3_Sizedist[i] =0
elseif   (a>b && b==-2&&a>0) // forces to count particles that don't have an upper bin
```

```
make/o/n=(1,0) remain
remain=((numpnts(C_sizeClust3_sort))-a)-1
C_clust3_Sizedist[i]=remain

endif
endfor

//clust4

duplicate/o C_sizeClust4 C_sizeClust4_sort
Sort C_sizeClust4_sort, C_sizeClust4_sort
Make/o/n=(numpnts(d_lim)) C_clust4_Sizedist
for(i=0;i<numlim-1;i+=1)
a = BinarySearch(C_sizeClust4_sort ,d_lim[i])
b = BinarySearch(C_sizeClust4_sort ,d_lim[i+1])
if(b>a)
C_clust4_Sizedist[i] = (b-(a))
elseif (a==-1 && b==-2)//added by NS, if there is only one particle in category this condition forces to bin particle
C_clust4_Sizedist[i] =1
elseif (a==b)// added by NS- if there are no particles in bin then a will equal b
C_clust4_Sizedist[i] =0
elseif   (a>b && b==-2&&a>0) // forces to count particles that don't have an upper bin
make/o/n=(1,0) remain
remain=((numpnts(C_sizeClust4_sort))-a)-1
C_clust4_Sizedist[i]=remain

endif
endfor

//AC

wave AC_sizeClust1, AC_sizeClust2, AC_sizeClust3, AC_sizeClust4
//clust1

duplicate/o AC_sizeClust1 AC_sizeClust1_sort
Sort AC_sizeClust1_sort, AC_sizeClust1_sort
Make/o/n=(numpnts(d_lim)) AC_clust1_Sizedist
for(i=0;i<numlim-1;i+=1)
a = BinarySearch(AC_sizeClust1_sort ,d_lim[i])
b = BinarySearch(AC_sizeClust1_sort ,d_lim[i+1])
if(b>a)
AC_clust1_Sizedist[i] = (b-(a))
elseif (a==-1 && b==-2)//added by NS, if there is only one particle in category this condition forces to bin particle
AC_clust1_Sizedist[i] =1
elseif (a==b)// added by NS- if there are no particles in bin then a will equal b
AC_clust1_Sizedist[i] =0
elseif   (a>b && b==-2&&a>0) // forces to count particles that don't have an upper bin
make/o/n=(1,0) remain
remain=((numpnts(AC_sizeClust1_sort))-a)-1
AC_clust1_Sizedist[i]=remain

endif
endfor

//Clust2

duplicate/o AC_sizeClust2 AC_sizeClust2_sort
Sort AC_sizeClust2_sort, AC_sizeClust2_sort
Make/o/n=(numpnts(d_lim)) AC_clust2_Sizedist
for(i=0;i<numlim-1;i+=1)
a = BinarySearch(AC_sizeClust2_sort ,d_lim[i])
b = BinarySearch(AC_sizeClust2_sort ,d_lim[i+1])
if(b>a)
AC_clust2_Sizedist[i] = (b-(a))
```

173

```
elseif (a==-1 && b==-2)//added by NS, if there is only one particle in category this condition forces to bin particle
AC_clust2_Sizedist[i] =1
elseif (a==b)// added by NS- if there are no particles in bin then a will equal b
AC_clust2_Sizedist[i] =0
elseif   (a>b && b==-2&&a>0) // forces to count particles that don't have an upper bin
make/o/n=(1,0) remain
remain=((numpnts(AC_sizeClust2_sort))-a)-1
AC_clust2_Sizedist[i]=remain

endif
endfor

//clust3

duplicate/o AC_sizeClust3 AC_sizeClust3_sort
Sort AC_sizeClust3_sort, AC_sizeClust3_sort
Make/o/n=(numpnts(d_lim)) AC_clust3_Sizedist
for(i=0;i<numlim-1;i+=1)
a = BinarySearch(AC_sizeClust3_sort ,d_lim[i])
b = BinarySearch(AC_sizeClust3_sort ,d_lim[i+1])
if(b>a)
AC_clust3_Sizedist[i] = (b-(a))
elseif (a==-1 && b==-2)//added by NS, if there is only one particle in category this condition forces to bin particle
AC_clust3_Sizedist[i] =1
elseif (a==b)// added by NS- if there are no particles in bin then a will equal b
AC_clust3_Sizedist[i] =0
elseif   (a>b && b==-2&&a>0) // forces to count particles that don't have an upper bin
make/o/n=(1,0) remain
remain=((numpnts(AC_sizeClust3_sort))-a)-1
AC_clust3_Sizedist[i]=remain

endif
endfor

//clust4

duplicate/o AC_sizeClust4 AC_sizeClust4_sort
Sort AC_sizeClust4_sort, AC_sizeClust4_sort
Make/o/n=(numpnts(d_lim)) AC_clust4_Sizedist
for(i=0;i<numlim-1;i+=1)
a = BinarySearch(AC_sizeClust4_sort ,d_lim[i])
b = BinarySearch(AC_sizeClust4_sort ,d_lim[i+1])
if(b>a)
AC_clust4_Sizedist[i] = (b-(a))
elseif (a==-1 && b==-2)//added by NS, if there is only one particle in category this condition forces to bin particle
AC_clust4_Sizedist[i] =1
elseif (a==b)// added by NS- if there are no particles in bin then a will equal b
AC_clust4_Sizedist[i] =0
elseif   (a>b && b==-2&&a>0) // forces to count particles that don't have an upper bin
make/o/n=(1,0) remain
remain=((numpnts(AC_sizeClust4_sort))-a)-1
AC_clust4_Sizedist[i]=remain

endif
endfor

//BC

wave BC_sizeClust1, BC_sizeClust2, BC_sizeClust3, BC_sizeClust4
//clust1
duplicate/o BC_sizeClust1 BC_sizeClust1_sort
Sort BC_sizeClust1_sort, BC_sizeClust1_sort
Make/o/n=(numpnts(d_lim)) BC_clust1_Sizedist
for(i=0;i<numlim-1;i+=1)
```

174

```
a = BinarySearch(BC_sizeClust1_sort ,d_lim[i])
b = BinarySearch(BC_sizeClust1_sort ,d_lim[i+1])
if(b>a)
BC_clust1_Sizedist[i] = (b-(a))
elseif (a==-1 && b==-2)//added by NS, if there is only one particle in category this condition forces to bin particle
BC_clust1_Sizedist[i] =1
elseif (a==b)// added by NS- if there are no particles in bin then a will equal b
BC_clust1_Sizedist[i] =0
elseif   (a>b && b==-2&&a>0) // forces to count particles that don't have an upper bin
make/o/n=(1,0) remain
remain=((numpnts(BC_sizeClust1_sort))-a)-1
BC_clust1_Sizedist[i]=remain

endif
endfor

//Clust2

duplicate/o BC_sizeClust2 BC_sizeClust2_sort
Sort BC_sizeClust2_sort, BC_sizeClust2_sort
Make/o/n=(numpnts(d_lim)) BC_clust2_Sizedist
for(i=0;i<numlim-1;i+=1)
a = BinarySearch(BC_sizeClust2_sort ,d_lim[i])
b = BinarySearch(BC_sizeClust2_sort ,d_lim[i+1])
if(b>a)
BC_clust2_Sizedist[i] = (b-(a))
elseif (a==-1 && b==-2)//added by NS, if there is only one particle in category this condition forces to bin particle
BC_clust2_Sizedist[i] =1
elseif (a==b)// added by NS- if there are no particles in bin then a will equal b
BC_clust2_Sizedist[i] =0
elseif   (a>b && b==-2&&a>0) // forces to count particles that don't have an upper bin
make/o/n=(1,0) remain
remain=((numpnts(BC_sizeClust2_sort))-a)-1
BC_clust2_Sizedist[i]=remain

endif
endfor

//Clust3

duplicate/o BC_sizeClust3 BC_sizeClust3_sort
Sort BC_sizeClust3_sort, BC_sizeClust3_sort
Make/o/n=(numpnts(d_lim)) BC_clust3_Sizedist
for(i=0;i<numlim-1;i+=1)
a = BinarySearch(BC_sizeClust3_sort ,d_lim[i])
b = BinarySearch(BC_sizeClust3_sort ,d_lim[i+1])
if(b>a)
BC_clust3_Sizedist[i] = (b-(a))
elseif (a==-1 && b==-2)//added by NS, if there is only one particle in category this condition forces to bin particle
BC_clust3_Sizedist[i] =1
elseif (a==b)// added by NS- if there are no particles in bin then a will equal b
BC_clust3_Sizedist[i] =0
elseif   (a>b && b==-2&&a>0) // forces to count particles that don't have an upper bin
make/o/n=(1,0) remain
remain=((numpnts(BC_sizeClust3_sort))-a)-1
BC_clust3_Sizedist[i]=remain

endif
endfor

//Clust4

duplicate/o BC_sizeClust4 BC_sizeClust4_sort
Sort BC_sizeClust4_sort, BC_sizeClust4_sort
```

175

```
Make/o/n=(numpnts(d_lim)) BC_clust4_Sizedist
for(i=0;i<numlim-1;i+=1)
a = BinarySearch(BC_sizeClust4_sort ,d_lim[i])
b = BinarySearch(BC_sizeClust4_sort ,d_lim[i+1])
if(b>a)
BC_clust4_Sizedist[i] = (b-(a))
elseif (a==-1 && b==-2)//added by NS, if there is only one particle in category this condition forces to bin particle
BC_clust4_Sizedist[i] =1
elseif (a==b)// added by NS- if there are no particles in bin then a will equal b
BC_clust4_Sizedist[i] =0
elseif   (a>b && b==-2&&a>0) // forces to count particles that don't have an upper bin
make/o/n=(1,0) remain
remain=((numpnts(BC_sizeClust4_sort))-a)-1
BC_clust4_Sizedist[i]=remain

endif
endfor

//AB

wave AB_sizeClust1, AB_sizeClust2, AB_sizeClust3, AB_sizeClust4
//clust1
duplicate/o AB_sizeClust1 AB_sizeClust1_sort
Sort AB_sizeClust1_sort, AB_sizeClust1_sort
Make/o/n=(numpnts(d_lim)) AB_clust1_Sizedist
for(i=0;i<numlim-1;i+=1)
a = BinarySearch(AB_sizeClust1_sort ,d_lim[i])
b = BinarySearch(AB_sizeClust1_sort ,d_lim[i+1])
if(b>a)
AB_clust1_Sizedist[i] = (b-(a))
elseif (a==-1 && b==-2)//added by NS, if there is only one particle in category this condition forces to bin particle
AB_clust1_Sizedist[i] =1
elseif (a==b)// added by NS- if there are no particles in bin then a will equal b
AB_clust1_Sizedist[i] =0
elseif   (a>b && b==-2&&a>0) // forces to count particles that don't have an upper bin
make/o/n=(1,0) remain
remain=((numpnts(AB_sizeClust1_sort))-a)-1
AB_clust1_Sizedist[i]=remain

endif
endfor

//Clust2

duplicate/o AB_sizeClust2 AB_sizeClust2_sort
Sort AB_sizeClust2_sort, AB_sizeClust2_sort
Make/o/n=(numpnts(d_lim)) AB_clust2_Sizedist
for(i=0;i<numlim-1;i+=1)
a = BinarySearch(AB_sizeClust2_sort ,d_lim[i])
b = BinarySearch(AB_sizeClust2_sort ,d_lim[i+1])
if(b>a)
AB_clust2_Sizedist[i] = (b-(a))
elseif (a==-1 && b==-2)//added by NS, if there is only one particle in category this condition forces to bin particle
AB_clust2_Sizedist[i] =1
elseif (a==b)// added by NS- if there are no particles in bin then a will equal b
AB_clust2_Sizedist[i] =0
elseif   (a>b && b==-2&&a>0) // forces to count particles that don't have an upper bin
make/o/n=(1,0) remain
remain=((numpnts(AB_sizeClust2_sort))-a)-1
AB_clust2_Sizedist[i]=remain


endif
endfor
```

176

```
//clust 3

duplicate/o AB_sizeClust3 AB_sizeClust3_sort
Sort AB_sizeClust3_sort, AB_sizeClust3_sort
Make/o/n=(numpnts(d_lim)) AB_clust3_Sizedist
for(i=0;i<numlim-1;i+=1)
a = BinarySearch(AB_sizeClust3_sort ,d_lim[i])
b = BinarySearch(AB_sizeClust3_sort ,d_lim[i+1])
if(b>a)
AB_clust3_Sizedist[i] = (b-(a))
elseif (a==-1 && b==-2)//added by NS, if there is only one particle in category this condition forces to bin particle
AB_clust3_Sizedist[i] =1
elseif (a==b)// added by NS- if there are no particles in bin then a will equal b
AB_clust3_Sizedist[i] =0
elseif   (a>b && b==-2&&a>0) // forces to count particles that don't have an upper bin
make/o/n=(1,0) remain
remain=((numpnts(AB_sizeClust3_sort))-a)-1
AB_clust3_Sizedist[i]=remain

endif
endfor

//clust 4

duplicate/o AB_sizeClust4 AB_sizeClust4_sort
Sort AB_sizeClust4_sort, AB_sizeClust4_sort
Make/o/n=(numpnts(d_lim)) AB_clust4_Sizedist
for(i=0;i<numlim-1;i+=1)
a = BinarySearch(AB_sizeClust4_sort ,d_lim[i])
b = BinarySearch(AB_sizeClust4_sort ,d_lim[i+1])
if(b>a)
AB_clust4_Sizedist[i] = (b-(a))
elseif (a==-1 && b==-2)//added by NS, if there is only one particle in category this condition forces to bin particle
AB_clust4_Sizedist[i] =1
elseif (a==b)// added by NS- if there are no particles in bin then a will equal b
AB_clust4_Sizedist[i] =0
elseif   (a>b && b==-2&&a>0) // forces to count particles that don't have an upper bin
make/o/n=(1,0) remain
remain=((numpnts(AB_sizeClust4_sort))-a)-1
AB_clust4_Sizedist[i]=remain

endif
endfor

//ABC

wave ABC_sizeClust1, ABC_sizeClust2, ABC_sizeClust3, ABC_sizeClust4
//clust1
duplicate/o ABC_sizeClust1 ABC_sizeClust1_sort
Sort ABC_sizeClust1_sort, ABC_sizeClust1_sort
Make/o/n=(numpnts(d_lim)) ABC_clust1_Sizedist
for(i=0;i<numlim-1;i+=1)
a = BinarySearch(ABC_sizeClust1_sort ,d_lim[i])
b = BinarySearch(ABC_sizeClust1_sort ,d_lim[i+1])
if(b>a)
ABC_clust1_Sizedist[i] = (b-(a))
elseif (a==-1 && b==-2)//added by NS, if there is only one particle in category this condition forces to bin particle
ABC_clust1_Sizedist[i] =1
elseif (a==b)// added by NS- if there are no particles in bin then a will equal b
ABC_clust1_Sizedist[i] =0
elseif   (a>b && b==-2&&a>0) // forces to count particles that don't have an upper bin
make/o/n=(1,0) remain
remain=((numpnts(ABC_sizeClust1_sort))-a)-1
```

177

ABC_clust1_Sizedist[i]=remain

endif
endfor

//Clust2

duplicate/o ABC_sizeClust2 ABC_sizeClust2_sort
Sort ABC_sizeClust2_sort, ABC_sizeClust2_sort
Make/o/n=(numpnts(d_lim)) ABC_clust2_Sizedist
for(i=0;i<numlim-1;i+=1)
a = BinarySearch(ABC_sizeClust2_sort ,d_lim[i])
b = BinarySearch(ABC_sizeClust2_sort ,d_lim[i+1])
if(b>a)
ABC_clust2_Sizedist[i] = (b-(a))
elseif (a==-1 && b==-2)//added by NS, if there is only one particle in category this condition forces to bin particle
ABC_clust2_Sizedist[i] =1
elseif (a==b)// added by NS- if there are no particles in bin then a will equal b
ABC_clust2_Sizedist[i] =0
elseif   (a>b && b==-2&&a>0) // forces to count particles that don't have an upper bin
make/o/n=(1,0) remain
remain=((numpnts(ABC_sizeClust2_sort))-a)-1
ABC_clust2_Sizedist[i]=remain

endif
endfor

//clust3

duplicate/o ABC_sizeClust3 ABC_sizeClust3_sort
Sort ABC_sizeClust3_sort, ABC_sizeClust3_sort
Make/o/n=(numpnts(d_lim)) ABC_clust3_Sizedist
for(i=0;i<numlim-1;i+=1)
a = BinarySearch(ABC_sizeClust3_sort ,d_lim[i])
b = BinarySearch(ABC_sizeClust3_sort ,d_lim[i+1])
if(b>a)
ABC_clust3_Sizedist[i] = (b-(a))
elseif (a==-1 && b==-2)//added by NS, if there is only one particle in category this condition forces to bin particle
ABC_clust3_Sizedist[i] =1
elseif (a==b)// added by NS- if there are no particles in bin then a will equal b
ABC_clust3_Sizedist[i] =0
elseif   (a>b && b==-2&&a>0) // forces to count particles that don't have an upper bin
make/o/n=(1,0) remain
remain=((numpnts(ABC_sizeClust3_sort))-a)-1
ABC_clust3_Sizedist[i]=remain

endif
endfor

//clust4

duplicate/o ABC_sizeClust4 ABC_sizeClust4_sort
Sort ABC_sizeClust4_sort, ABC_sizeClust4_sort
Make/o/n=(numpnts(d_lim)) ABC_clust4_Sizedist
for(i=0;i<numlim-1;i+=1)
a = BinarySearch(ABC_sizeClust4_sort ,d_lim[i])
b = BinarySearch(ABC_sizeClust4_sort ,d_lim[i+1])
if(b>a)
ABC_clust4_Sizedist[i] = (b-(a))
elseif (a==-1 && b==-2)//added by NS, if there is only one particle in category this condition forces to bin particle
ABC_clust4_Sizedist[i] =1
elseif (a==b)// added by NS- if there are no particles in bin then a will equal b
ABC_clust4_Sizedist[i] =0
elseif   (a>b && b==-2&&a>0) // forces to count particles that don't have an upper bin

178

```
make/o/n=(1,0) remain
remain=((numpnts(ABC_sizeClust4_sort))-a)-1
ABC_clust4_Sizedist[i]=remain

endif
endfor

//TOT

wave TOT_sizeClust1, TOT_sizeClust2, TOT_sizeClust3, Tot_sizeClust4
//clust1
duplicate/o TOT_sizeClust1 TOT_sizeClust1_sort
Sort TOT_sizeClust1_sort,TOT_sizeClust1_sort
Make/o/n=(numpnts(d_lim)) TOT_clust1_Sizedist
for(i=0;i<numlim-1;i+=1)
a = BinarySearch(TOT_sizeClust1_sort ,d_lim[i])
b = BinarySearch(TOT_sizeClust1_sort ,d_lim[i+1])
if(b>a)
TOT_clust1_Sizedist[i] = (b-(a))
elseif (a==-1 && b==-2)//added by NS, if there is only one particle in category this condition forces to bin particle
TOT_clust1_Sizedist[i] =1
elseif (a==b)// added by NS- if there are no particles in bin then a will equal b
TOT_clust1_Sizedist[i] =0
elseif   (a>b && b==-2&&a>0) // forces to count particles that don't have an upper bin
make/o/n=(1,0) remain
remain=((numpnts(TOT_sizeClust1_sort))-a)-1
TOT_clust1_Sizedist[i]=remain

endif
endfor

//Clust2

duplicate/o TOT_sizeClust2 TOT_sizeClust2_sort
Sort TOT_sizeClust2_sort, TOT_sizeClust2_sort
Make/o/n=(numpnts(d_lim)) TOT_clust2_Sizedist
for(i=0;i<numlim-1;i+=1)
a = BinarySearch(TOT_sizeClust2_sort ,d_lim[i])
b = BinarySearch(TOT_sizeClust2_sort ,d_lim[i+1])
if(b>a)
TOT_clust2_Sizedist[i] = (b-(a))
elseif (a==-1 && b==-2)//added by NS, if there is only one particle in category this condition forces to bin particle
TOT_clust2_Sizedist[i] =1
elseif (a==b)// added by NS- if there are no particles in bin then a will equal b
TOT_clust2_Sizedist[i] =0
elseif   (a>b && b==-2&&a>0) // forces to count particles that don't have an upper bin
make/o/n=(1,0) remain
remain=((numpnts(TOT_sizeClust2_sort))-a)-1
TOT_clust2_Sizedist[i]=remain

endif
endfor

//Clust3

duplicate/o TOT_sizeClust3 TOT_sizeClust3_sort
Sort TOT_sizeClust3_sort, TOT_sizeClust3_sort
Make/o/n=(numpnts(d_lim)) TOT_clust3_Sizedist
for(i=0;i<numlim-1;i+=1)
a = BinarySearch(TOT_sizeClust3_sort ,d_lim[i])
b = BinarySearch(TOT_sizeClust3_sort ,d_lim[i+1])
if(b>a)
TOT_clust3_Sizedist[i] = (b-(a))
elseif (a==-1 && b==-2)//added by NS, if there is only one particle in category this condition forces to bin particle
```

179

```
TOT_clust3_Sizedist[i] =1
elseif (a==b)// added by NS- if there are no particles in bin then a will equal b
TOT_clust3_Sizedist[i] =0
elseif   (a>b && b==-2&&a>0) // forces to count particles that don't have an upper bin
make/o/n=(1,0) remain
remain=((numpnts(TOT_sizeClust3_sort))-a)-1
TOT_clust3_Sizedist[i]=remain

endif
endfor
//Clust4

duplicate/o TOT_sizeClust4 TOT_sizeClust4_sort
Sort TOT_sizeClust4_sort, TOT_sizeClust4_sort
Make/o/n=(numpnts(d_lim)) TOT_clust4_Sizedist
for(i=0;i<numlim-1;i+=1)
a = BinarySearch(TOT_sizeClust4_sort ,d_lim[i])
b = BinarySearch(TOT_sizeClust4_sort ,d_lim[i+1])
if(b>a)
TOT_clust4_Sizedist[i] = (b-(a))
elseif (a==-1 && b==-2)//added by NS, if there is only one particle in category this condition forces to bin particle
TOT_clust4_Sizedist[i] =1
elseif (a==b)// added by NS- if there are no particles in bin then a will equal b
TOT_clust4_Sizedist[i] =0
elseif   (a>b && b==-2&&a>0) // forces to count particles that don't have an upper bin
make/o/n=(1,0) remain
remain=((numpnts(TOT_sizeClust4_sort))-a)-1
TOT_clust4_Sizedist[i]=remain

endif
endfor

//Plot stacked category plots

Display /W=(24,117.5,777,591.5) ABC_clust2_Sizedist,BC_clust2_Sizedist,AC_clust2_Sizedist vs d_lim
AppendToGraph AB_clust2_Sizedist,C_clust2_Sizedist,B_clust2_Sizedist,A_clust2_Sizedist vs d_lim
AppendToGraph nonFl_clust2_Sizedist,TOT_clust2_Sizedist vs d_lim
ModifyGraph mode(ABC_clust2_Sizedist)=7,mode(BC_clust2_Sizedist)=7,mode(AC_clust2_Sizedist)=7
ModifyGraph mode(AB_clust2_Sizedist)=7,mode(C_clust2_Sizedist)=7,mode(B_clust2_Sizedist)=7
ModifyGraph mode(A_clust2_Sizedist)=7,mode(nonFl_clust2_Sizedist)=7,mode(TOT_clust2_Sizedist)=4
ModifyGraph marker(TOT_clust2_Sizedist)=19
ModifyGraph rgb(ABC_clust2_Sizedist)=(16384,48896,65280),rgb(BC_clust2_Sizedist)=(36864,14592,58880)
ModifyGraph rgb(AC_clust2_Sizedist)=(65280,32768,45824),rgb(AB_clust2_Sizedist)=(0,39168,0)
ModifyGraph rgb(C_clust2_Sizedist)=(65280,43520,0),rgb(B_clust2_Sizedist)=(0,0,52224)
ModifyGraph rgb(nonFl_clust2_Sizedist)=(34816,34816,34816),rgb(TOT_clust2_Sizedist)=(0,0,0)
ModifyGraph mrkThick(TOT_clust2_Sizedist)=2
ModifyGraph hbFill(ABC_clust2_Sizedist)=2,hbFill(BC_clust2_Sizedist)=2,hbFill(AC_clust2_Sizedist)=2
ModifyGraph hbFill(AB_clust2_Sizedist)=2,hbFill(C_clust2_Sizedist)=2,hbFill(B_clust2_Sizedist)=2
ModifyGraph hbFill(A_clust2_Sizedist)=2,hbFill(nonFl_clust2_Sizedist)=2
ModifyGraph hBarNegFill(AB_clust2_Sizedist)=2
ModifyGraph toMode(ABC_clust2_Sizedist)=3,toMode(BC_clust2_Sizedist)=3,toMode(AC_clust2_Sizedist)=3
ModifyGraph toMode(AB_clust2_Sizedist)=3,toMode(C_clust2_Sizedist)=3,toMode(B_clust2_Sizedist)=3
ModifyGraph toMode(A_clust2_Sizedist)=3
ModifyGraph log(bottom)=1
Label left "Counts"
Label bottom "Size (um)"
TextBox/C/N=text0/F=0/A=MC/X=43.10/Y=44.00 "Cluster 2"


Display /W=(24,117.5,777,591.5) ABC_clust1_Sizedist,BC_clust1_Sizedist,AC_clust1_Sizedist vs d_lim
AppendToGraph AB_clust1_Sizedist,C_clust1_Sizedist,B_clust1_Sizedist,A_clust1_Sizedist vs d_lim
AppendToGraph nonFl_clust1_Sizedist vs d_lim
AppendToGraph TOT_clust1_Sizedist vs d_lim
ModifyGraph mode(ABC_clust1_Sizedist)=7,mode(BC_clust1_Sizedist)=7,mode(AC_clust1_Sizedist)=7
```

180

ModifyGraph mode(AB_clust1_Sizedist)=7,mode(C_clust1_Sizedist)=7,mode(B_clust1_Sizedist)=7
ModifyGraph mode(A_clust1_Sizedist)=7,mode(nonFl_clust1_Sizedist)=7,mode(TOT_clust1_Sizedist)=4
ModifyGraph marker(TOT_clust1_Sizedist)=19
ModifyGraph rgb(ABC_clust1_Sizedist)=(16384,48896,65280),rgb(BC_clust1_Sizedist)=(36864,14592,58880)
ModifyGraph rgb(AC_clust1_Sizedist)=(65280,32768,45824),rgb(AB_clust1_Sizedist)=(0,39168,0)
ModifyGraph rgb(C_clust1_Sizedist)=(65280,43520,0),rgb(B_clust1_Sizedist)=(0,0,52224)
ModifyGraph rgb(nonFl_clust1_Sizedist)=(34816,34816,34816),rgb(TOT_clust1_Sizedist)=(0,0,0)
ModifyGraph mrkThick(TOT_clust1_Sizedist)=2
ModifyGraph hbFill(ABC_clust1_Sizedist)=2,hbFill(BC_clust1_Sizedist)=2,hbFill(AC_clust1_Sizedist)=2
ModifyGraph hbFill(AB_clust1_Sizedist)=2,hbFill(C_clust1_Sizedist)=2,hbFill(B_clust1_Sizedist)=2
ModifyGraph hbFill(A_clust1_Sizedist)=2,hbFill(nonFl_clust1_Sizedist)=2
ModifyGraph toMode(ABC_clust1_Sizedist)=3,toMode(BC_clust1_Sizedist)=3,toMode(AC_clust1_Sizedist)=3
ModifyGraph toMode(AB_clust1_Sizedist)=3,toMode(C_clust1_Sizedist)=3,toMode(B_clust1_Sizedist)=3
ModifyGraph toMode(A_clust1_Sizedist)=3
ModifyGraph log(bottom)=1
Label left "Counts"
Label bottom "Size (um)"
TextBox/C/N=text0/F=0/A=MC/X=43.10/Y=44.00 "Cluster 1"

Display /W=(24,117.5,777,591.5) ABC_clust3_Sizedist,BC_clust3_Sizedist,AC_clust3_Sizedist vs d_lim
AppendToGraph AB_clust3_Sizedist,C_clust3_Sizedist,B_clust3_Sizedist,A_clust3_Sizedist vs d_lim
AppendToGraph nonFl_clust3_Sizedist vs d_lim
AppendToGraph TOT_clust3_Sizedist vs d_lim
ModifyGraph mode(ABC_clust3_Sizedist)=7,mode(BC_clust3_Sizedist)=7,mode(AC_clust3_Sizedist)=7
ModifyGraph mode(AB_clust3_Sizedist)=7,mode(C_clust3_Sizedist)=7,mode(B_clust3_Sizedist)=7
ModifyGraph mode(A_clust3_Sizedist)=7,mode(nonFl_clust3_Sizedist)=7,mode(TOT_clust3_Sizedist)=4
ModifyGraph marker(TOT_clust3_Sizedist)=19
ModifyGraph rgb(ABC_clust3_Sizedist)=(16384,48896,65280),rgb(BC_clust3_Sizedist)=(36864,14592,58880)
ModifyGraph rgb(AC_clust3_Sizedist)=(65280,32768,45824),rgb(AB_clust3_Sizedist)=(0,39168,0)
ModifyGraph rgb(C_clust3_Sizedist)=(65280,43520,0),rgb(B_clust3_Sizedist)=(0,0,52224)
ModifyGraph rgb(nonFl_clust3_Sizedist)=(34816,34816,34816),rgb(TOT_clust3_Sizedist)=(0,0,0)
ModifyGraph mrkThick(TOT_clust3_Sizedist)=2
ModifyGraph hbFill(ABC_clust3_Sizedist)=2,hbFill(BC_clust3_Sizedist)=2,hbFill(AC_clust3_Sizedist)=2
ModifyGraph hbFill(AB_clust3_Sizedist)=2,hbFill(C_clust3_Sizedist)=2,hbFill(B_clust3_Sizedist)=2
ModifyGraph hbFill(A_clust3_Sizedist)=2,hbFill(nonFl_clust3_Sizedist)=2
ModifyGraph toMode(ABC_clust3_Sizedist)=3,toMode(BC_clust3_Sizedist)=3,toMode(AC_clust3_Sizedist)=3
ModifyGraph toMode(AB_clust3_Sizedist)=3,toMode(C_clust3_Sizedist)=3,toMode(B_clust3_Sizedist)=3
ModifyGraph toMode(A_clust3_Sizedist)=3
ModifyGraph log(bottom)=1
Label left "Counts"
Label bottom "Size (um)"
TextBox/C/N=text0/F=0/A=MC/X=43.10/Y=44.00 "Cluster 3"

Display /W=(24,117.5,777,591.5) ABC_clust4_Sizedist,BC_clust4_Sizedist,AC_clust4_Sizedist vs d_lim
AppendToGraph AB_clust4_Sizedist,C_clust4_Sizedist,B_clust4_Sizedist,A_clust4_Sizedist vs d_lim
AppendToGraph nonFl_clust4_Sizedist vs d_lim
AppendToGraph TOT_clust4_Sizedist vs d_lim
ModifyGraph mode(ABC_clust4_Sizedist)=7,mode(BC_clust4_Sizedist)=7,mode(AC_clust4_Sizedist)=7
ModifyGraph mode(AB_clust4_Sizedist)=7,mode(C_clust4_Sizedist)=7,mode(B_clust4_Sizedist)=7
ModifyGraph mode(A_clust4_Sizedist)=7,mode(nonFl_clust4_Sizedist)=7,mode(TOT_clust4_Sizedist)=4
ModifyGraph marker(TOT_clust4_Sizedist)=19
ModifyGraph rgb(ABC_clust4_Sizedist)=(16384,48896,65280),rgb(BC_clust4_Sizedist)=(36864,14592,58880)
ModifyGraph rgb(AC_clust4_Sizedist)=(65280,32768,45824),rgb(AB_clust4_Sizedist)=(0,39168,0)
ModifyGraph rgb(C_clust4_Sizedist)=(65280,43520,0),rgb(B_clust4_Sizedist)=(0,0,52224)
ModifyGraph rgb(nonFl_clust4_Sizedist)=(34816,34816,34816),rgb(TOT_clust4_Sizedist)=(0,0,0)
ModifyGraph mrkThick(TOT_clust4_Sizedist)=2
ModifyGraph hbFill(ABC_clust4_Sizedist)=2,hbFill(BC_clust4_Sizedist)=2,hbFill(AC_clust4_Sizedist)=2
ModifyGraph hbFill(AB_clust4_Sizedist)=2,hbFill(C_clust4_Sizedist)=2,hbFill(B_clust4_Sizedist)=2
ModifyGraph hbFill(A_clust4_Sizedist)=2,hbFill(nonFl_clust4_Sizedist)=2
ModifyGraph toMode(ABC_clust4_Sizedist)=3,toMode(BC_clust4_Sizedist)=3,toMode(AC_clust4_Sizedist)=3
ModifyGraph toMode(AB_clust4_Sizedist)=3,toMode(C_clust4_Sizedist)=3,toMode(B_clust4_Sizedist)=3
ModifyGraph toMode(A_clust4_Sizedist)=3
ModifyGraph log(bottom)=1
Label left "Counts"

181

Label bottom "Size (um)"
TextBox/C/N=text0/F=0/A=MC/X=43.10/Y=44.00 "Cluster 4"

End